River-Aquifer Interactions in Kosi Basin using Hydrological Models and Remote Sensing Inputs

Thesis submitted in partial fulfilment of the requirements for the award of the degree of

Doctor of Philosophy

in

Civil Engineering

by

LAVETI N. V. SATISH

under the supervision of

Prof. Subashisa Dutta

Dr. Suresh A. Kartha

Department of Civil Engineering
Indian Institute of Technology Guwahati
Guwahati – 781039, Assam, India
August, 2020

River-Aquifer Interactions in Kosi Basin using Hydrological Models and Remote Sensing Inputs

Thesis submitted in partial fulfilment of the requirements for the award of the degree of

Doctor of Philosophy

in

Civil Engineering

by

LAVETI N. V. SATISH

under the supervision of

Prof. Subashisa Dutta

Dr. Suresh A. Kartha

Department of Civil Engineering
Indian Institute of Technology Guwahati
Guwahati – 781039, Assam, India
August, 2020

Dedicated to

My Mother and Father

ACKNOWLEDGEMENTS

This thesis is not only just work, also it is a milestone achievement in one of the fruitful and remarkable periods of my life time. In this wonderful phase, I learnt many new things and also encountered tough situations which turned me stronger. I would like to thank all for their support, affection and friendship during this beautiful journey.

First and foremost, I would like to express my deep sense of gratitude to my supervisor, **Prof. Subashisa Dutta**, Former Head, Department of Civil Engineering and my co-supervisor, **Dr. Suresh A. Kartha**, Associate Professor, Department of Civil Engineering, Indian Institute of Technology Guwahati, for their meticulous guidance, consistent support, valuable suggestions and patience throughout my learning phase of research. I am always grateful and respectful for their kind support during all critical phases of this most important journey of my life. Also, due thanks to Doctoral Committee members Prof. Arup Kumar Sarma, Prof. Bimlesh Kumar of Department of Civil Engineering, Prof. Anugrah Singh, Department of Chemical Engineering, Dr Archana M Nair of Department of Civil Engineering and Dipankar Narayan Basu of Department of Mechanical Engineering, Indian Institute of Technology Guwahati, for their valuable suggestions in the enhancement of my research work. Furthermore I would like to extend my sincere thanks to Prof. V. Jothiprakash of Department of Civil Engineering, Indian Institute of Technology, Bombay and Prof. Sudhanshu Panda of Department of GIS/Environmental Science, University of North Georgia for evaluating my thesis and providing valuable suggestions to improve it. I am also thankful to technical staff (Jonali Saikia Madam, Juri Madam, Priyananda Saikia bhayya) and non-technical staff (Susanta Sir) of Department of Civil Engineering, IIT Guwahati for their continuous support throughout this phase.

I am also thankful to my beloved friends Dr. Varma, Dr. Dhamu, Dr. Ranga, Dr. Sachin, Dr. Satish, Sravani with whom I have shared all my happiness, problems, scholarly interactions. I never forget their friendship, affection and support at all stages of this phase. Without their support, I don't think so that I can able to complete this journey.

I am very much thankful to all my Water Resource Engineering group members. Specially, I am extremely thankful to Dr. Suman for providing unconditional support and timely help throughout this crucial phase of my research. Dr. Shreedevi, I am so much thankful for your support and friendship in every stage of this wonderful journey. Mr. Rajeev Gandhi, I like to thank you for support and help at my critical phase of my research period. Vinay, I am very much thankful to your help in difficult times and, thanks a lot for being here as younger brother. Anjaneyulu, thank you so much for the discussions and suggestions in many aspects of research. Bazal da, I am really thankful to you for the help in all the works, especially in experimental part of my study. Thanks to the extended family, Dr. Arpit, Dr. Amit, Dr. Someswaran, Dr. Debraj, Jayshree, Chandan, Suresh, Reddick, Ketan, Bhuvana, Mamata, Rupasree, Piya, Lasya, Ashes.

Also, thanks to my best friends Lalitha, Satish, Sriram, Ravindra, Krishna Chaitanya, Vinay, Kapil, Srinivasulu, Dasta Giri, Maharshi for their true friendship and affection towards me. Special thanks to Amrutha, Aparmita, Sagarika, Shiva, Sindhu, Divu, Punitha, Giri, Mahato, Nitin, Abhijit, Harathi, Pvr, Yogi, Srikanth, Sajjad, Ashok, Sudheer for your friendly support. Finally, Thanks to family members Tatayya garu, Ammamma, Annayya, Vadina, Attayya, Akka, Baavagaru, Pinni, Chinnannagaru, Baavagaru, Lakshmi Akka, Praba annayya, Swarupa Vadina, Nani Mavayya, Alekhya, Sunitha,Venu, Sarat, Nisitha, Ravi, Sudha, Teja, Manu, Shanmu, Sai, Shiva, Aahanavi, Jhanavi and all my relatives for their unconditional love and support throughout this phase.

*****

DECLARATION

I, **Laveti N. V. Satish**, author of the Ph. D. thesis "**River-Aquifer Interactions in Kosi Basin using Hydrological Models and Remote Sensing Inputs**" would like to certify that

- The work presented in this thesis is original research work carried out by me.
- The research work has not been submitted for any degree or diploma or any other qualification either in this institute or in any other university.
- Whenever I have used resources [theory, concepts, texts, data, graphs, figures or any other similar nature] from other sources, a due credit by citing in the text of the thesis is clearly made.
- The work presented here is free from plagiarism and I take the responsibility for any issues.
- I also affirm that thesis supervisor(s) is not responsible for any possible instance of plagiarism within this submitted work.

L. N. V. Satish

Date: 26-08-2020 LAVETI N. V. SATISH

Place: Guwahati

Indian Institute of Technology Guwahati

Department of Civil Engineering, Guwahati, Assam 781039

Dr. Subashisa Dutta

Professor and Former Head

Email: subashisa@iitg.ac.in

Dr. Suresh A. Kartha

Associate Professor

Email: kartha@iitg.ac.in

CERTIFICATE

This is to certify that thesis entitled "**River-Aquifer Interactions in Kosi Basin using Hydrological Models and Remote Sensing Inputs**" submitted by **Laveti N. V. Satish**, in partial fulfilment of the requirements for the award of degree of Doctor of Philosophy, to Indian Institute of Technology Guwahati, Assam, India, is a record of the bonafide research work carried out by him under my guidance and supervision at the Department of Civil Engineering, Indian Institute of Technology Guwahati, Assam, India. To the best of my knowledge, no part of the work reported in this thesis has been presented for the award of any degree at any other institution.

Date: 26-08-2020

Place: Guwahati

Prof. Subashisa Dutta

Dr. Suresh A. Kartha

ABSTRACT

River-Aquifer Interaction is a complex phenomenon that occurs through the sediment-water interface in the hyporheic zone. The interactions vary spatially and temporally along the river reach depending on topography and geology. Understanding the mechanism as well as quantification is an important aspect of the hydrological cycle for sustainable water management. The thesis aims to understand and quantify the river-aquifer interaction process in an agriculturally dominated basin of Kosi River, India.

Many recent studies that focused on the assessment of river-aquifer interactions used field, lab and modelling techniques. Among all, mathematical models to a certain extent utilize the physical processes to understand and quantify the interaction. However, for the better assessment of river-aquifer interaction, mathematical models need accurate inputs (recharge, evapotranspiration) and parameters (riverbed and aquifer properties). Groundwater models are also suitable to study river aquifer interactions and it consists of some essential parameters like recharge and riverbed conductivities. In this study, prominence is given in accurately estimating recharge and riverbed hydraulic conductivity prior to groundwater modelling.

As groundwater recharge is an important component, the present study estimates monthly groundwater recharge at sub-basin scale using semi-distributed surface water hydrological modelling (SWAT- Soil Water and Assessment Tool) and Soil Water Balance (SWB) method. Whereas, seasonal groundwater recharge was estimated at sub-basin scale using Water Table Fluctuation (WTF) and Rainfall Infiltration Factor (RIF). The results of the study showed that monsoonal recharge estimated using WTF and RIF methods did not capture the wet and dry year effects. In addition, monthly groundwater recharge estimated using a well-calibrated and validated semi-distributed model (SWAT) with observed discharge, over-predicted the recharge. Also it is not able to capture the effects of wet and

dry years on recharge due to the under-prediction of simulated Actual Evapotranspiration (38% of observed AET). While SWB method improved the monthly groundwater recharge estimations and also captured wet and dry effects on groundwater recharge in the study zone. However, these monthly groundwater recharge values (estimated using SWAT and SWB methods) were further utilized in groundwater modelling to reconfirm the suitable method for recharge estimation of Kosi river basin.

Another important component of groundwater modelling is riverbed hydraulic conductivity, which can significantly influence the river-aquifer interaction process. In this study, heat was used as a natural tracer to estimate the fluid flux and riverbed hydraulic conductivity. For this purpose, a series of laboratory-based experiments were conducted in a sandbox with four different scenarios (soil combinations) and conditions (temperature gradients and ponding depths). Initially, temperature profiles were measured in a soil column at different depths and these variations were further analyzed to estimate fluid fluxes using analytical solutions of Hatch and Kerry (Amplitude Ratio (AR) and Phase Difference (PD)) methods. The results showed that fluid fluxes estimated using the Keery AR method were found to have a good agreement with the seepage velocity. These fluxes were further utilized to estimate the hydraulic conductivity of different soil layers using Darcy's law. Finally, effective hydraulic conductivity of a soil column for all different scenarios was calculated from the estimated hydraulic conductivities and further utilized for calculating riverbed conductance for groundwater modelling purpose.

Later, using these estimated groundwater recharge and riverbed hydraulic conductivity along with other input parameters (evapotranspiration, ground top elevations and aquifer characteristics), groundwater modelling of Kosi river basin was carried out for two different cases. In the first case, modelling was carried out with recharge estimated using SWAT model whereas in the second case, the modelling was performed with recharge estimated using SWB method. The results showed that monthly groundwater levels simulated using SWAT recharge-based groundwater flow modelling (case I) has less correlation with observed groundwater levels. Also the model was not able to capture the wet and dry year effects. Whereas, simulated groundwater levels in the model using SWB based recharge were having a better agreement with the observed groundwater levels and also found to capture the effects of wet and dry years. It was also noted that the model was able to capture the effects of wet and dry years on the river-aquifer exchange process. Three different interaction zones were identified from upstream (Kosi barrage) to downstream

(conferencing point with Ganga river) in the study reach. It is observed that the river always loses water to the aquifer (as influent) in Zone I (80 km from upstream) and the river mostly gains water from the aquifer (as effluent) in Zone III (40 km above downstream). Whereas, in the middle reaches (Zone II), the river has a combination of both influent and effluent natures. At the upstream, the river always loses water to the aquifer and mostly gains water from the aquifer at downstream during wet and dry years indicates the significant influence of topography on river-aquifer exchange flux. The results obtained in case II modelling with different riverbed conductance values of different scenarios (soil combinations) indicate that the river-aquifer interactions are highly sensitive to the riverbed conductance

Overall, this inter-comparison of groundwater modelling results indicates, remote sensing inputs (recharge and evapotranspiration used in SWB method for estimating recharge) along with estimated riverbed conductance values can improve the assessment and understanding of the river-aquifer interaction process in an alluvial River Basin.

*****

Contents

LIST OF FIGURES

LIST OF TABLES

LIST OF SYMBOLS

Symbol	Description
μ	Mean
σ	Standard Deviation
K	Thermal Conductivity
D	Thermal Diffusivity
β	Thermal Dispersivity
C	Bulk Heat Capacity of Saturated Sediment
c_f	Heat Capacity of Fluid
ρ	Bulk Density of Saturated Sediment
ρ_f	Density of Fluid
G	Specific Gravity
n	Porosity
D_{50}	Representative Diameter
C_u	Coefficient of Uniformity
C_c	Coefficient of Curvature
R_e	Groundwater Recharge
A_r	Amplitude Ratio
D_p	Phase Difference
V_f	Fluid Flux
V_{Ar}	Thermal Frontal Velocity using Amplitude Ration Method
$V_{f.Ar}$	Fluid Flux using Amplitude Ratio Method
V_{DP}	Thermal Frontal Velocity using Phase Difference Method
$V_{f.DP}$	Fluid Flux using Phase Difference Method
K_{eff}	Effective Hydraulic Conductivity
K_{eff-10}	10 percentile of K_{eff}
K_{eff-50}	50 percentile of K_{eff}
K_{eff-90}	50 percentile of K_{eff}

LIST OF ABBREVIATIONS

Terms	Description
APHRODITE	Asian Precipitation-Highly-Resolved Observational Data Integration Towards Evaluation of Water Resources
PGF	Princeton Global Forcing Data
MODIS	Moderate Resolution Imaging Spectroradiometer
NBSS & LUP	National Bureau of Soil Survey and Land Use Planning
USGS	United States of Geological Survey
SRTM	Shuttle Radar Topography Mission
CWC	Central Water Commission
CGWB	Central Groundwater Board
GLDAS VIC	Variable Infiltration Capacity model in Global Land Data Assimilation System
NOAA	National Oceanic and Atmospheric Administration
ORNL DAAC	Oak Ridge National Laboratory Distributed Active Archive Center
GMS MODFLOW	Modular Three-Dimensional Finite Difference Groundwater Flow Model in Groundwater Modelling System
MODFLOW-RIV	River Package in MODFLOW model
SWAT	Soil and Water Assessment Tool

1

INTRODUCTION

Water is a unique substance and exists as a solid, liquid or gas [Young and Haveman, 1985; Harlen and Holroyd, 1997]. On the earth, approximately one billion cubic kilometres of water is available and covers nearly three fourth of the earth's surface [Biswas, 1996; Bhat, 2014]. In fact, less than only one percent of its total quantity is fresh and usable and is found in groundwater, lakes, ponds, and rivers [Gleick, 1996]. This quantity is quite enough to meet the needs of five to ten times the existing world population. But, due to the lack of proper management of water resources, scarcity problems come into attack [Almas and Scholz, 2006; Jain, 2019]. In this modern era, Integrated River Basin Management (IRBM) has become a practice in general [McNally and Tognetti, 2002; Evers, 2016]. Assessment of River-Aquifer Interactions will play a major role in providing valuable information for sustainable planning and management of water resources [Sophocleous, 2002]. From the ecological point of view, low seasonal flow is playing a major role in the sustainability of aquatic species [Rolls et al., 2012; Rolls and Bond, 2017]. This low flow generally originates from the baseflow from the groundwater to a stream [Kendy and Bredehoeft, 2006]. In this aspect also, river-aquifer interaction plays a major role [Ivkovic, 2009]. Moreover, contaminants from groundwater may reach stream water which is a severe condition to the health of a river [Carter, 2000]. Understanding river-aquifer processes may help to attenuate the pollutants [Smith et al., 2009]. By keeping all these points in view, it is understood that river-aquifer interaction processes need to be focused in hydrological studies [Fleckenstein et al., 2010; Krause et al., 2014].

1.1 RIVER-AQUIFER INTERACTIONS

River-Aquifer interaction is a natural process and a complex phenomenon to understand its physical dynamic processes [Sophocleous, 2002; Rassam et al., 2008; Li et al., 2018; Manoj et al., 2019]. Investigation of these interactions are to be conducted at the river reach scale and generally classified as connected and disconnected systems [Winter et al., 1998; Fleckenstein et al., 2006; Zhang et al., 2012]. As shown in Figure 1.1, river-aquifer interactions can take place in three types A) water flux entering from aquifer to river (gaining stream/ effluent stream), B) water flux leaving from river to aquifer (losing stream/ influent stream) or, C) combinations of both and this nature of exchange will change in both spatial and temporal scales [Banks et al., 2011]. Due to differences in the total head of river water and groundwater, either a river loses water to the shallow aquifer or gains water from a shallow aquifer [Dawoud and Ismail, 2013]. This general condition for gaining and losing stream in aquifer is shown in Figure 1.1.

Extensive research works have been carried out on river-aquifer interactions globally by using various technologies like mathematical models and field studies for understanding the physical dynamic processes and quantifying river-aquifer exchange fluxes [Chitsazan et al., 2014; Tang et al., 2017; Vrzel et al. 2018; Sahoo and Sahoo, 2019]. Mathematical modelling involves adoption of numerical and analytical methods [Lautz and Siegel 2006; Baalousha, 2012; Bailey et al., 2016], whereas experimentations along with field investigations involve piezometric level measurements [Baxter et al., 2003], thermal profiling [Anibas et al., 2016], environmental tracer [Stellato et al., 2008] and isotopic studies [Zhao et al., 2018]. Some studies suggest that simple and cost-effective methods such as data-driven and tracing techniques approaches will not serve for better understanding of river-aquifer interactions as these methods do not concern with the physical processes that govern the exchange [Sophocleous, 2002; Krause et al., 2014]. Hence, at present, most of the researchers extensively use physical-based mathematical models [Kim et al., 2008; Izady et al., 2015] for quantifying the river-aquifer interaction process.

However, for the better assessment of river-aquifer interaction, numerical models need accurate inputs (such as recharge, evapotranspiration, etc.) and parameters (such as riverbed and aquifer properties [Brunner et al., 2017]. Direct measurement of a few components (especially groundwater recharge and riverbed hydraulic conductivity) is extremely difficult and has to be estimated indirectly [Sharma, 1986; Wojnar, 2008].

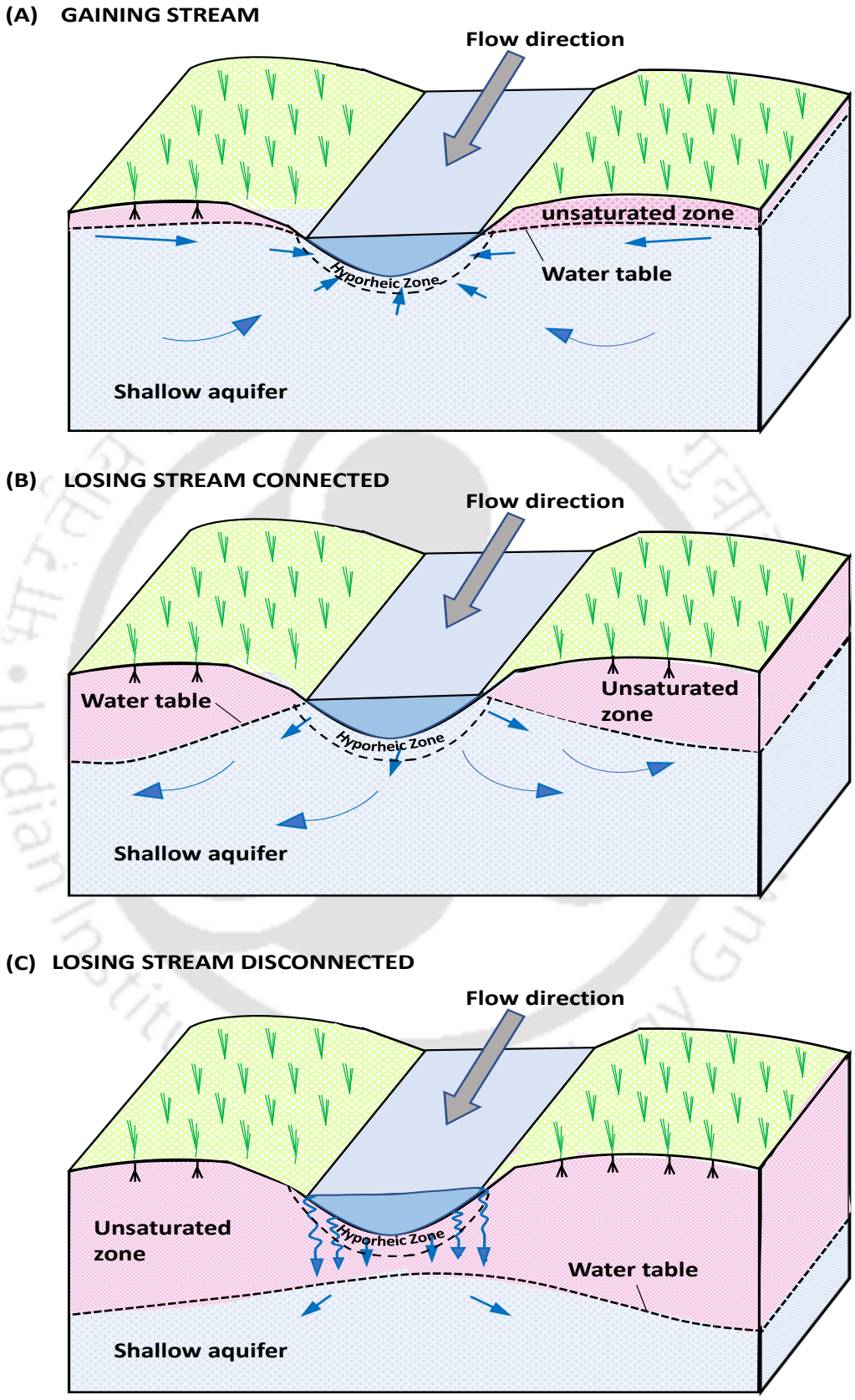

Figure 1.1: General Conditions for Gaining and Losing Streams in an Aquifer, after Winter et al. [1998]

Several studies have been carried out to estimate these components using different methodologies and techniques [Naganna et al., 2017; Walker et al., 2019]. Among various methods, selecting a suitable method for estimation these components is an important consideration for any river basin [Jassas and Merkel, 2014]. But, in developing countries like India, ground-based observations are not available for most of the river basins and this may become a constraint to make use of existing sophisticated methods for any hydrological study [Wakode et al., 2018]. The use of remote sensing data is an alternative approach to address such ground-based data deficiency issues and also provides many practical benefits in hydrological studies [Andersen et al., 2002].

Also, it is important to focus on the factors that influence the river-aquifer interaction process [Winter, 1995]. Anthropogenic activities such as groundwater extraction and landuse practices are among the main factors influencing the river-aquifer interaction and these activities are subjected to region-specific [Zhu et al., 2019]. Extensive groundwater extractions for agricultural practices and other purposes can lower down the groundwater table and alter the relationship between river stage and groundwater. Further, this may cause flow variability in the river and effects the equilibrium of river basin system [Kumar and Nagaraj, 2018]. Hence, a detail investigation is required in such basins (where anthropogenic activities take place) for understanding the river-aquifer interaction process.

1.2 MOTIVATION AND SCOPE OF THE STUDY

At present, developing countries like India are facing severe water crises due to over-exploitation of groundwater for multiple purposes (drinking and industrial), particularly for irrigation needs in areas where extensive agricultural activities are practicing [Tiwari et al., 2017]. In order to address this critical issue, assessment of primary components of hydrological cycle needs to be focused for effective groundwater management. Hence, the present study aims for an integrated approach for identifying and quantifying river-aquifer interaction exchange process in an agricultural dominated river basin system. For this purpose, Himalayan originated and agricultural dominated, Kosi river basin, India is selected for the study through experimental and modelling techniques. This river basin characterizes with agricultural lands and relies on a groundwater-based irrigation system. In this study, groundwater recharge estimation techniques using remote sensing inputs, tracer techniques using heat flux measurements and, sub-surface hydrological models are used for achieving the objectives. For this purpose, the entire river

basin is considered for surface hydrological modelling. Whereas plain parts of the river basin is selected for recharge estimation and sub-surface hydrological modelling due to non-availability of data in the hilly region of the basin. This understanding and quantifying of river-aquifer interaction of the river basin can contribute to the effective groundwater management in agricultural dominated river systems.

1.3 GOAL AND OBJECTIVES

Considering the research needs with emphasis for understanding, assessment of river-aquifer interactions and management, the following objectives are outlined for the present research study.

- Estimation of monthly groundwater recharge in Kosi basin using surface water hydrological model, soil water balance method, water table fluctuation method, and rainfall infiltration factor method.
- To conduct a series of sandbox experiments for estimating seepage velocity and hydraulic conductivity for different soil layer stratifications
- To assess monthly river-aquifer interactions of the Kosi river using subsurface hydrological model and remote sensing inputs.

1.4 RESEARCH HYPOTHESIS

It is hypothesized that hydrological models along with high resolution remote sensing inputs may improve the understanding and assessment of river-aquifer interaction in an alluvial channel. To test the hypothesis, monthly sub-surface hydrological modelling is simulated in an agriculturally dominated, Kosi basin. For this model, groundwater recharge and riverbed hydraulic conductivity are two major input parameters which are not available for the study area. Hence, estimation of these parameters are focused initially. To select suitable method, groundwater recharge is estimated using four different methods. Whereas, heat is used as a natural tracer to estimate the riverbed hydraulic conductivity.

1.5 ORGANISATION OF THESIS

The research work in this thesis is presented in six chapters. The thesis focuses on understanding and assessment of river-aquifer interaction process in the Kosi River through laboratory and modeling-based techniques. The thesis is divided between chapters based on the objectives of the present study. Initially, the estimation of groundwater recharge using remote sensing inputs is studied. This is followed by a laboratory-based experimental

study for estimating the fluid flux and hydraulic conductivity in a soil column. Finally, distributed groundwater modeling is carried out to quantify the rive-aquifer interaction using remote sensing inputs. The chapter-wise description of the thesis is

- *Chapter 1* discussed the overview of the river-aquifer interaction process and its significance followed by the aims and scope of the thesis.
- *Chapter 2* reports the review of literature carried on the theory of groundwater recharge estimation, fluid flux estimation using heat as a tracer and river-aquifer interaction assessment using numerical modelling necessary for the present research.
- *Chapter 3* deals with groundwater recharge estimation methods using four different methods with remote sensing inputs.
- *Chapter 4* deals with fluid flux and hydraulic conductivity estimation through sediment-water interface using heat as a tracer based on laboratory experiments in a sandbox.
- *Chapter 5* studies the assessment of river-aquifer interactions using estimated groundwater recharge and riverbed conductance.
- *Chapter 6* summarizes the present research and suggests the future scope of the present work.

2

REVIEW OF LITERATURE

River-aquifer interaction is one of the important components of the hydrological cycle and its direct estimation is extremely difficult. Understanding of river-aquifer process and mechanics through the field, lab, and modeling-based studies can be beneficial for the effective management of water resources. In order to assess river-aquifer interaction at different spatio-temporal scale through physical-based numerical modelling, use of accurate inputs (such as recharge and evapotranspiration etc.) and aquifer parameters (such as hydraulic conductivity of riverbed and aquifer etc.) have become an important implication. In this chapter, a review of research works on groundwater recharge estimation methods and riverbed hydraulic conductivity estimation techniques and river-aquifer interaction assessment through modeling and other techniques are highlighted. A synoptic understanding of river-aquifer interactions is discussed here.

2.1 GROUNDWATER RECHARGE ESTIMATION METHODS

Spatio-temporal fluctuations in the groundwater table and river stage are one of the important factors that influence the river-aquifer interaction process. There are many factors for the fluctuations in groundwater levels and among all, groundwater recharge is an important factor for these variations. Therefore, the assessment of spatio-temporal variation of groundwater recharge is the primary requirement of any groundwater modelling for identifying and quantifying river-aquifer interaction exchange process. Direct measurement of recharge is a challenging task at the field level but it can be estimated indirectly. Various techniques and methods have been practicing by many researchers for recharge estimation. Among all, selecting a suitable method or technique

plays a vital role in any river basin for effective management of water resources. The following sub-sections discuss the review of the previous works on various recharge estimation methods.

2.1.1 Conventional Methods

(a) Use of Lysimeter

Chapman and Malone [2002] tested the performance of recharge estimation models (13 single store and two-store) against using 11-year daily field observations measured from a weighing lysimeter 2.4 m deep at Coshocton, OH. This study concluded that five models performed well to capture the spatial variability in groundwater recharge but did not perform well to simulate the total soil water in the column especially during high evapotranspiration periods. Also, many other researchers used lysimeters to compare the recharge estimations of several models [White et al., 2003; Chen et al., 2008]. However, the installation of lysimeters is not only difficult, also expensive and only provides point recharge estimates [Moyer et al., 1996].

(b) Water Table Fluctuation Method

The water table fluctuation method is mainly derived on an event basis. It generally determines recharge from precipitation and water table measurements for a particular event. In 2004, Moon et al. used this method to estimate groundwater recharge in South Korea. To implement this methodology, they carried out the statistical analysis of hydrographs and water-table fluctuation. From which, they established a new relationship between the cumulative WTF and corresponding precipitation records. On the other hand, Crosbie et al. [2005] introduced a new multi-event time series concept to evaluate groundwater recharge from long-term water table and precipitation records using WTF. They have considered new variables, specific yield derived from soil moisture retention curve. It had a great advantage in recharge estimation even though there was no water table rise. It was concluded that WTF works good in gross recharge estimation and sensitive to time step size and specific yield.

Again Delin et al. [2007] carried out a comparative study to compute the ground-water recharge estimation in Minnesota, USA using three local-scale methods (unsaturated-zone water balance, Water Table Fluctuations (WTF) and age dating of groundwater). Finally, they observed that the WTF method was the simplest and easiest to estimate the

groundwater recharge. This method performed well in estimating recharge also in the semi-arid region, reported by Sibanda et al. [2009]. WTF was used to get the recharge in Nyamandhlovu area, Zimbabwe. Apart from this, a remote sensing and GIS-based WTF method has been tried for quantitative computation of groundwater recharge in hard-rock areas [Szucs et al., 2009]. To develop this model, they conducted an integrated assessment of infiltration capacity, normal rainfall and its cumulative frequency. Additionally, WTF method was employed to assess the natural recharge and its relation with aquifer parameters in Tamilnadu, India [Rangarajan et al., 2009]. The seasonal influence of groundwater fluctuations with reference to the rainfall was evaluated using WTF [Khadri and Moharir, 2015]. WTF has made possible to determine the groundwater depletion levels [Prasad and Rao, 2018]. Along with a decrease in groundwater levels, they found out its causes and reported detailed groundwater balance studies of Kandivalasa River Sub Basin, Andhra Pradesh, India.

(c) Water Balance Method

The soil water balance method is a very reliable approach for recharge estimation as it incorporates the actual representation of crop type and soil conditions. Soil water balance method exhibited well-accepted results in natural groundwater recharge estimation than any other methods such as zero flux plane method, inverse modeling technique, hybrid water fluctuation method, groundwater balance method, isotope and solute profile techniques [Amitha, 2000].

The potential of SWB in recharge estimation has been reported by Ragab et al. [1997], Allen et al. [1998], Finch [2001]. Also, Kendy et al. [2003] have expressed the valuable insights into the recharge estimation through soil water balance models. While on the other hand, Eilers et al. [2007] developed a single store (single layer) mass water balance model suitable for semi-arid areas. They considered the major hydrological processes taking place at or near the soil-vegetation surface including runoff. The results referred that temporal distribution of daily rainfall and the magnitude of the antecedent (pre-season) soil moisture deficit were the most vital hydrologic features in case of deep drainage at a particular site in a particular time. Also, they concluded that the annual rainfall total was not the main influencing factor for annual recharge. The spatial variation of potential recharge mainly depends on deep drainage and thus the water holding capacity and rooting depth. Whereas, Mileham et al. [2009] utilized precipitation and temperature data from the regional climate model (RCM) and developed a semi-distributed soil

moisture balance model (SMBM) in order to assess the various impacts of climate change on groundwater recharge and runoff for a medium-sized catchment (2,098 km^2) in tropical region of southwestern Uganda. Chung et al. [2016] worked on a comparative study on existing methods on groundwater recharge, specifically emphasized for semi-arid and humid regions of Africa. There were different methodologies available for the recharge estimation of Africa. Out of these, they found the water balance methods and the streamflow method using groundwater level data performed very well in the evaluation of recharge in semi-arid and humid regions of Africa.

(d) Rainfall Infiltration Factor Method

The seasonal groundwater recharge can also be calculated through Rainfall Infiltration Factor (RIF). Very limited studies are demonstrated in this method of estimating recharge however, it performed well in some study sites. Bhuiyan et al. [2009] used RIF method along with WTF method and their study revealed that the difference between the recharge estimated using WTF and RIF was small and also RIF method was able to compute recharge for even weekly and monthly rainfall data. Chandra et al. [2018] have performed this method to determine groundwater utilization status and time-series water level trends.

2.1.2 Modelling Techniques

Many hydrological models are available for recharge estimation such as one-dimensional semi-distributed numerical models and one-dimensional lumped parametric models. Arnold et al. [2000] estimated groundwater recharge and discharge of Upper Mississippi river basin using SWAT model and from daily stream flow data. Recharge estimated using this techniques showed largest discrepancies between these methods but general trends were evident. In 2005, Sun and Cornish estimated groundwater recharge in the headwaters of Liverpool plains in NSW, Australia using a physically-based semi-distributed watershed model (SWAT). The study indicated that the model overestimated the overall annual runoff during dry years which instigated uncertainty in the recharge estimations of the model. Hence, the study suggested further improvement in modelling to bypass flow modelling under dry conditions. Gebreyohannes [2008] used one-dimensional semi-distributed model, SWAP (Soil-Water-Atmosphere-Plant system) and one-dimensional lumped parameter model, EARTH (Extended model for Aquifer Recharge and soil moisture Transport through the unsaturated Hardrock) models to simulate groundwater

levels and found both the models were able to capture natural groundwater level fluctuations However, this study concluded that these models were not able to capture the groundwater level fluctuations due to man-induced abstractions. In both the models, such artificial influences were not included. Groundwater recharge values were obtained from both the models captured the vegetation effects on groundwater recharge of the study area. In 2010, Al-Dousari et al. used SWAT model to estimated groundwater recharge in Raudatain watershed in northern Kuwait using remote sensing inputs. They demonstrated the use of hydrological models as alternative approaches where the traditional data required to understand the hydrologic systems are absent for sustainable management of water resources.

Jimenez-Martinez et al. [2009] demonstrated a root zone modelling approach for estimating groundwater recharge from the irrigated area in a semi-arid region where return flow of irrigation accounts for substantial potential recharge. For this purpose, they used 1-D Hydrus model and the model was calibrated with field data measured within the plot area. This study suggested that although the root zone modelling approach was a promising method for recharge estimation, the modelling approach involved extensive data requirements and several crop-and soil specific parameters in comparison with other modelling methods.

Touhami et al. [2012] used a hydrological lumped model, HYDOBAL to estimate groundwater recharge and found the model provided reliable groundwater recharge estimates with an average recharge of the Ventós-Castellar system at approximately 10% of annual rainfall. In 2013, Baker and Miller used SWAT model to assess the landuse impact on water resources in East African watershed. The results their study showed that change in landuse caused increase in runoff and decrease in groundwater recharge. Whereas, Awan and Ismaeel [2014] demonstrated, use of a semi-distributed hydrological model, SWAT to estimate groundwater recharge under climate change conditions. This study concluded that the use of remote sensing data and SWAT model was able to estimate groundwater recharge at high spatial and temporal resolutions. On the other hand, Gyamfi et al. [2017] presented their study to investigate groundwater recharge dynamics of the Olifants river basin to landuse changes. The results of the study indicated declination in groundwater recharge in the study period. They concluded that SWAT model was capable as a decision support tool to asses groundwater recharge for large river basins.

2.1.3 Tracer, Empirical and other Methods

Tracer methods have been widely practicing tool for the estimation of groundwater recharge. Among many, isotope tracer techniques and chloride mass balance method (CMB) are a few of the well-known techniques. Gaye and Edmunds [1996] discussed the use of chloride, stable isotopes (deuterium, oxygen-18) and tritium to estimate groundwater recharge in deep sand profiles. This study suggested that chloride and tritium tracers provided a good agreement of recharge estimates in the site. Whereas, Subyani [2004] used CMB method and environmental isotopes to evaluate groundwater recharge in Wadi Tharad sub-basin, Saudi Arabia. In their study, they identified recharge zones and found that 11% of effective rainfall contributed to aquifer as recharge using CMB method. Stable isotopes can be used for quantitative assessment of recharge. However, using tracers such as tritium requires professional specialist for sampling and analysis.

Chaturvedi in 1936, derived an empirical equation to obtain a relation between rainfall and recharge using rainfall events and the water level fluctuations in Ganga-Yamuna doab and it was later modified further work at U.P. Irrigation Research Institute, India in 1973 [Chaturvedi, 1973; Kumar and Seethapathi, 2002]. While many other researchers developed empirical equations for developing relations between rainfall and recharge [Hearne and Dewey, 1988; Waltemeyer, 2001; Kambhammettu et al., 2011]. However, the application of these methods is often constraint to estimate the recharge for the study zone considered as they have been developed for specific regions with particular landuse, climate and hydrogeological conditions [Gemitzi et al., 2017].

Few other methods have been using by researchers for estimating recharge include baseflow separation methods and streamflow recession analysis [Frohlich et al., 1994; Wittenberg and Sivapalan, 1999; Lee et al. 2006; Partington et al., 2012]. Although the application of these methods is simple and uses available streamflow-discharge records, uncertainty associated with streamflow-discharge records may provide unreliable recharge estimates [Halford and Mayer, 2000].

2.2 ESTIMATION OF FLUID FLUX AND HYDRAULIC CONDUCTIVITY

River water and groundwater connect through an active ecotone called hyporheic zone and in this zone, water exchange is the fundamental interest of energy transport. Distribution of hydraulic head between river and aquifer as well as hydraulic conductivity of the riverbed are major important factors that influence this exchange rate [Doppler et al.,

2007]. Estimation of fluid flux and hydraulic bed conductivity play a key role in quantifying river-aquifer interaction exchange and helps for effective sustainable water management [Kalbus et al., 2006; Ivkovic, 2009; Naganna et al., 2017].

2.2.1 Fluid Flux Estimation

Several methods and techniques have been employed by various researchers for the estimation of fluid flux through Sediment-Water Interface (SWI). Direct seepage measurements [Rosenberry, 2008; Brodie et al., 2009], analytical modelling techniques [Lautz and Siegel 2006; Cho et al., 2010; Baalousha, 2012], numerical modelling techniques [Brunner et al., 2010; Sun et al., 2015; Semiromi and Koch, 2019] and application of environmental isotopes [Kumar et al., 2008; Gao et al., 2010; Paces and Wurster, 2014; Zhao et al., 2018] are widely used.

Direct determination of fluid flux through filed approaches has many challenges. However, using heat as a tracer to estimate fluid flux is an alternative approach [Constantz, 2008]. Scientific interest has increased on the application of heat as an environmental tracer to identify and quantify the river-aquifer exchange flux in hyporheic zone [Baskaran et al., 2009; Bartsch et al., 2014; Zhang et al., 2018]. Heat tracer technique is a cost-effective methodology for quantifying the interaction exchange at both spatial and temporal scales [Anderson, 2005].

Anibas et al. [2009] presented steady-state and transient simulations of 1D-fluid-heat transport equation for quantifying groundwater-surface water exchange fluxes. In their study, they measured temperature timer series data over a year in surface water and at different depths below a river in two different field sites, Aa river in Belgium and Lake 77 in Eastern Germany. They demonstrated both steady-state and transient simulations with two numerical codes, FEMME (Flexible Environment for Mathematically Modelling the Environment) and VS2DH. From the simulation results, they hypothesized that at certain times of the year, transient influences were negligible such that the distribution of vertical temperature variations were approximated as steady-state simulations. But, these steady-state simulations were not absolute values rather provided as first quantitative estimate of groundwater-surface water fluxes.

For quantification of seasonally distributed groundwater-surface water exchange flux, Anibas et al. [2011] suggested a simple and fast thermal mapping method that detects indirectly the moment of water in subsurface zone by using heat as a tracer. For this

purpose, spatially distributed temperature profiles were measured in the hyporheic zone of Aa river, Belgium in two seasons (summer and winter). They estimated advective vertical fluxes with the application of inverse modelling of thermal steady-state one-dimensional heat transport equation using a numerical model (STRIVE) and analytical model [Arriga and Leap, 2006] and compared with volumetric flux obtained from piezometer measurements. From the results, they found that higher flux and more heterogeneity were observed in upper reaches when compared to lower reaches, which highlighted the importance of local geomorphology. It was recommended that for initial stages of field investigations of river-aquifer interactions, the use of this thermal method was simple, fast and cost-effective to identify the zone of interest. Figure 2.1 shows the scheme for measuring temperature profiles in the riverbed of the Aa.

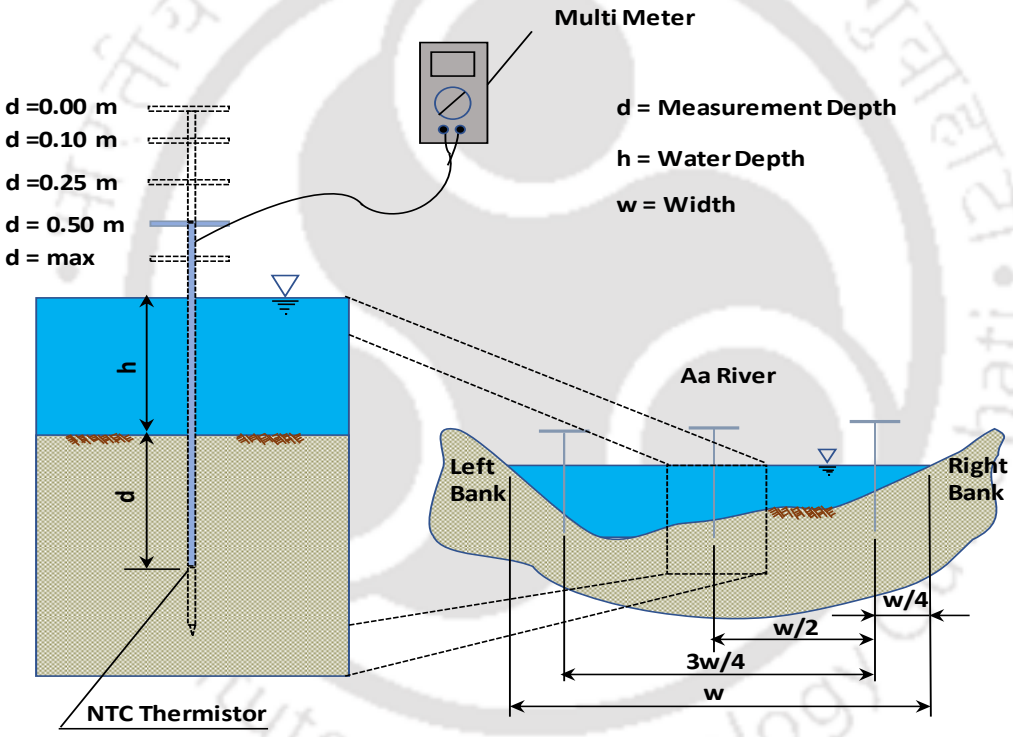

Figure 2.1: Scheme for measuring temperature profiles in the riverbed of the Aa with the T-stick instrument, after Anibas et al. [2011]

Irvine et al. [2015a] used synthetic streambed temperature data (generated by numerical flow and transport simulations) along with 1-D analytical solutions for quantifying and mapping high-resolution fluid fluxes. While Lu et.al [2017] identified the spatial patterns of hyporheic flux exchanges across a river transect in China by measuring temperature time series at high spatial resolution using a one-dimensional conduction-advection-dispersion model (VFLUX).

Various researchers proposed different approaches to solve the heat transport equation to estimate fluid fluxes from temperature time series data [Bredehoeft and Papaopulos, 1965; Stallman, 1965; Turcotte and Schubert, 2002]. In 2006, Hatch et al. presented the application of a new method by quantifying changes in phase and amplitude of temperature time series data from Pajaro river, Central coastal. The results of this study provided reliable range of streambed seepage rates of at least ±10 m d^{-1} and revealed that at low flow rates, amplitude variations being most sensitive whereas at higher rates, phase variations retained sensitivity. This new method simplified the use of thermal records for improved understanding of the complex dynamics of the river-aquifer interaction exchange process.

While Keery et al. [2007] presented another new method based on previously derived solutions of one-dimensional heat flow problems. They adopted a relatively new digital signal processing technique for extracting the 24 h component of temperature time series data from two or more depths. They applied this new method in a lowland UK river and the results of the study showed that estimated fluxes from the temperature series had a good agreement with the fluxes derived from seepage meter and flow gauging surveys.

But, few studies have been carried out to estimate fluid flux through experimental thermal measurements in a representative field soil column. In order to evaluate the influence of temperature probe design on the accuracy of vertical water flux estimation, Munz et al. [2011] conducted sandbox experiments. For this purpose, Multi-Level Temperature Stick (MLTS) was used to install the temperature probes into the sediment for measuring vertical temperature profiles. In their study, Keery's analytical solution was used to solve 1-D heat transport equation and found that fluxes estimated with amplitude ratios showed a good agreement with measured flow velocities. Their study suggested to use MLTS setup for accurate estimations of fluid flow fluxes.

McCallum et al. [2012] also utilized both amplitude ratio and phase difference methods of pairs of temperature series for estimating Darcy velocity through the surface water-groundwater interface. For this purpose, they presented a novel 1-D analytical method in which there was neither necessity to specify effective thermal diffusivity nor its need for iteration routines. They also illustrated the application of this novel method using the riverbed temperature data from Murray Darling Basin, Australia. The results showed

that at low river flows, reliable Darcy velocities of the riverbed were obtained using this method. However, they found this method had limitations under transient flow conditions.

Irvine et al. [2015b] evaluated the application of amplitude, phase and combined methods for the determination of water flux and thermal diffusivity. For this purpose, they measured vertical temperature profiles through experiments conducted in a sand column. These measured time series data further utilized for fluid flux estimation using phase and amplitude methods using VFLUX 2 program routine which includes Hatch et al. [2006] and Keery et.al [2007] analytical solutions. Their study suggested that amplitude and phase methods performed well during steady-state conditions however, the use of amplitude method provided better estimations of fluid flux during transient flow conditions.

In addition, Ren et al. [2018] characterized the dynamics of water flow and heat transport in riparian zones using heat as tracer through laboratory-based experiments conducted in a sand tank. They investigated the effect of hydraulic head (with two different heads - 25 cm and 45 cm), radiation temperatures (with no radiation and 22°C) and water temperature (with three different temperatures - 4°C, 6°C, and 9.5°C) on water flow and heat transport through experimental approaches as well as 2-D Hydrus Model. The results of the study showed that a good agreement of the predicted and observed thermal dynamics variation of the 2-D sand tank and also indicated that hydraulic head was the major mechanism for water flow and thermal dynamics variation. Also, the sensitivity analysis of this study results illustrated that the model was most sensitive to hydraulic head (H), followed by Van Genuchten parameter (α), permeability coefficient (K_s), water temperature (T), Van Genuchten parameter (n), residual moisture content (θ_r), and saturated moisture content (θ_s).

2.2.2 Hydraulic Conductivity Estimation

Riverbed hydraulic conductivity is one important characteristics of riverbed which influences the fluid flux that passing through sediment-water interface [Kalbus et al., 2009; Naganna et al., 2017]. Hence, it is necessary to estimate the spatial heterogeneity of riverbed hydraulic conductivity for the accurate assessment of river-aquifer interaction exchange. But, estimation of riverbed hydraulic conductivity is a challenging task for conceptualizing riverbeds in numerical models to quantify the river-aquifer exchange flux [Brunner et al., 2017].

Over past few years, various research studies have been employed to estimate the riverbed hydraulic conductivity using different methods and techniques include field approaches such as use of seepage meter [Isiorho and Meyer, 1999]; in-situ permeameter [Rosenberry, 2000; Landon et al., 2001]; slug tests [Landon et al., 2001; Baxter et al., 2003], laboratory measurements, [Cai et al., 2015] numerical and analytical modelling techniques [Mutiti and Levy, 2010; Pozdniakov et al., 2016]. Table 2.1 shows some of the studies carried out for the estimation of riverbed hydraulic conductivity using different methodologies and techniques. In recent years, research interest has been increased on using environmental tracers such as heat for fluid flux estimations in hyporheic zone [Anderson, 2005; Duque et al., 2010; Engeler et al., 2011; Ravazzani et al., 2016].

Table 2.1: Few studies carried out for the estimation of riverbed hydraulic conductivity using different methodologies and techniques.

Researcher	Year	Work	Method/Approach/Technique	Major Observations or Findings
Chen	2000	Measurement of streambed hydraulic conductivity	Using L-shaped standpipes directly to streambeds	Hydraulic conductivities measurements in horizontal, vertical and also in oblique directions
Chen	2004	Measurement of streambed hydraulic conductivity for rivers in South Central Nebraska	Using extend permeameter	The anisotropy of channel sediments can be determined from streambed tests of similar sediment volumes
Cheng and Chen	2007	Evaluation of methods of determination of hydraulic properties in an aquifer-aquitard system	Using the inverse modelling approach with MODFLOW	The combination of permeameter and direct push technique is less expensive than pumping tests
Cheong et al.	2008	Estimation of hydraulic conductivity in a riverside alluvial system in South Korea	Using grain-size analysis, pumping and slug tests and numerical modelling	Hydraulic conductivities estimated from pumping test and grain size analysis are found to higher than the estimations of slug test
Wojnar et al.	2013	Investigation of the ability of geophysical profiling techniques to determine hydraulic conductivity	Using seepage meter, slug test and heat-flow modelling	Geophysical methods cannot be used alone to assess appropriate vertical hydraulic conductivity ranges
Shamsuddin et al.	2019	Determination of vertical hydraulic conductivity at Muda River riverbank filtration site, Malaysia	Using rain size, pumping test and in situ falling head standpipe permeability tests.	Grain size data provided reliable estimates of hydraulic conductivity than pumping and permeability tests

Using heat transport modelling is an accurate and cost-effective technique [Lautz, 2010] and recent studies focused on using heat as a tracer for the assessment of riverbed hydraulic conductivity [Woodbury and Smith, 1988; Bravo et al., 2002; Niswonger, 2003]. While Mutiti and Levy [2010] used heat flow model for investigating the variability of riverbed hydraulic conductivity during storm events along the Great Miami River in Southwest Ohio. In their study, the response of variation in hydraulic conductivity for the storm event's rising limb was correlated.

However, the error in the estimation of fluid flux can propagate the error in streambed hydraulic conductivity estimations which can strongly influence the river-aquifer interaction process [Kalbus et al., 2009; Irvine et al., 2015; Tang et al., 2017]. Hence, it is necessary to understand the reliability of water flux estimations for heterogeneity streambed conditions using heat transport model in real field conditions. But, an assessment of the actual impacts of heterogeneity in a real field situation using heat transport models is somewhat difficult, and accurate representation of real heterogeneity in a model remains challenging and numerical instabilities may arise [Schornberg et al., 2010]. The heterogeneous streambed hydraulic conductivities can be determined using Darcy relations with the fluid fluxes in the soil. The fluid fluxes in the soil can be empirically related with temperature variations [Kalbus et al., 2009]. Hence using representative field soils in laboratory and measuring temperature variations using thermal sensors, fluid fluxes are first estimated. Thereafter, the streambed hydraulic conductivity is obtained by parameter estimation technique in the Darcy flow equation.

2.3 ASSESSMENT OF RIVER-AQUIFER INTERACTIONS

River and groundwater are important components of the hydrological cycle and interaction between river water and groundwater occurs in and across the hyporheic zone [Chitsazan et al., 2014; Anibas et al., 2016]. Understanding and quantifying this interaction plays a major role in the sustainable basin management [Smith et al., 2008; Kahil et al., 2016]. Significant research efforts have increased recently for understanding the mechanics of the interactions process and its quantification.

2.3.1 Tracer Techniques

The state of connection of the river-aquifer not only changes along river reaches, also changes concurrently at the same location in both space and time. This was demonstrated by Banks et al. [2011] by discussing the methods for regional-scale

assessment of spatial and temporal river-aquifer connectivity by the use of hydraulic, hydrochemical and tracer-based techniques. In their study, it was investigated that the state of connectivity of river-aquifer from catchment headwaters to sea in the pristine Rocky river in South Australia. It was found that there was no connection between river and aquifer in regional scale with the discharge data, water level data, together with salinity and stable isotope results. They hypothesized that the state of river-aquifer connection was controlled by native vegetation. It was understood from this study that determination of the type of connection between river and aquifer and the effect of change in landuse play an important role to understand river-aquifer interactions processes.

Bartsch et al. [2014] investigated the dynamics of river-aquifer interactions that were affected by monsoon precipitation events and resulting variability in discharge using heat as a tracer. For this purpose, this study was carried out in Haean-myun catchment, located in South Korea using a fully integrated HydroGeosphere numerical model to simulate for river-aquifer exchange fluxes. The model was well calibrated with measured temperature data and total head data. They discussed the river-aquifer potential that affects biogeochemical transformation by collecting river water and groundwater samples to analyse for dissolved organic carbon (DOC), nitrate (NO_3) and dissolved oxygen saturation (DO_{sat}). It was concluded from the results of the study that intense monsoon precipitations caused high spatiotemporal variation of river-aquifer fluxes by reflecting flow reversals and these flow reversals pushed high DOC into nitrate-rich groundwater under the stream, facilitated and increased natural attenuation of nitrate in the shallow aquifer.

Xie et al. [2016] examined the uncertainty of several natural tracers in quantifying the river-aquifer interaction in the Heihe River of northwest China. This study identified the applicability of the different tracer methods (temperature profile, radon profile, river temperature and river chemistry methods) to large rivers for estimating river-aquifer interaction at the point as well as at region scales. Results of their study showed that both the temperature profile method and the radon-222 profile method provided useful estimates of river-aquifer interactions at the point scale whereas the river chemistry method performed better than river temperature method at the regional scale.

2.3.2 Other Alternative Approaches

River-aquifer interaction processes are complex and their physical mechanisms are not fully understood. Many techniques such as numerical and analytical models were

employed to understand this phenomenon which may require significant time and cost. Ivkovic [2009] suggested an alternate data-driven (top-down) approach in which data patterns were assessed and processes were inferred from the data to characterize river-aquifer water interaction processes without being concerned about physical processes. In his study, the river reaches in semi-arid Namoi river catchments in Australia were characterized based on three levels of information (presence of river-aquifer of hydraulic connection, the dominant direction of flux and potential for groundwater extraction). The methods to characterize the river reaches were also discussed and a map was prepared to indicate river-aquifer connectivity and the dominant direction of flux. It was understood from this study that the use of the top-down approach will give a quick overview of large-scale river-aquifer interaction process as wide range of hydrometric data are available for most of the catchments.

Mohanty et al. [2010] investigated river-aquifer interactions along with hydrologic and hydrogeologic investigations in Kathajodi River basin of Orissa. For this purpose, they carried out stream flow analysis, pumping tests and hydrogeologic investigations. It was found from the streamflow analysis that river flow was highly seasonal and reduced to almost zero during the lean period (summer). It was noticed that the study area was dominated by a confined aquifer system with medium to coarse sand. From the analysis of pumping tests, it was found that aquifer is heterogonous with hydraulic conductivity varying 11.25-96.80 m/day. Correlation analysis was carried for groundwater levels with river stage and groundwater levels with rainfall. From the results of this correlation analysis, it was found that correlation value of groundwater level with river stage (R = 0.67-0.89) was higher than correlation value of groundwater levels with rainfall (R = 0.33-0.66). From this, they concluded that there were strong river-aquifer interactions in the study area. Table 2.2 shows various research works carried out using different technologies to quantify river-aquifer interaction.

Table 2.2: Few studies carried out for the estimation of river-aquifer interaction using different methodologies and techniques.

Researcher	Year	Work	Method/Approach/Technique	Major Observations or Findings
Baxter et al.	2003	Measurement of Groundwater-Surface water exchange	Installment of minipiezometers	Cost-efficient way for determining groundwater and stream water interaction at multi-scale approach
Schmidt et al.	2007	Quantification of groundwater discharge in Pine River, Angus, Ontario, Canada	Using mapped streambed temperatures	Analytical solution underestimate high fluxes however, sensitivity analysis of possible model inputs showed the solution
Brunner et al.	2010	Assessment of river-aquifer interactions with MODFLOW	Comparing MODFLOW simulations with Hydrogeosphere	Examination of accuracy of MODLFLOW to simulate surface water-groundwater interaction
Sanz et al.	2011	Modelling river-aquifer interactions in the Mancha Oriental System	Using 3-D large-scale numerical groundwater flow model (MODFLOW)	Showed potential use of remote sensing and GIS in mathematical modelling of aquifers
Partington et al.	2012	Evaluation of outputs from automated baseflow separation methods against simulated baseflow	Comparing Automated baseflow separation technique with Hydrogeosphere model simulation	Baseflow separation methods were not universally applicable
Xu et al.	2017	Investigation of river-aquifer interaction in Nalenggele River basin, Qinghai province	Using Multi tracers such as environmental ions, stable and radiogenic isotopes and heat	Inconsistency and uncertainty still exist even though multiple methods were used
Zhang et al.	2018	Quantification of spatial Variations of hyporheic water exchange in the Weihe River, China	Using Thermal method	Identified topography as the primary driver to influence the distribution of river tributaries

2.3.3 Modelling Approaches

Assessment of river-aquifer interaction can be investigated using many approaches. Among all, physically-based numerical modelling approaches can improve the interaction estimations at the reach scale. In their study, Fleckenstein et al. [2006] assessed how river seepage and low flows were affected with textural heterogeneity of an alluvial system in the Cosumnes River, California. For this purpose, low flows were tested for six realizations of aquifer heterogeneity and homogeneity by incorporating geostatistical simulation of hydrofacies using transient groundwater modelling (MODFLOW). It was found that net annual seepages were similar among these models. But, a significant difference was observed among these heterogeneity models to seepage spatial distribution, groundwater table configuration, local level connection and disconnection between river and aquifer. This study demonstrated consideration of incorporating geologic heterogeneity on the hydrofacies scale in river-aquifer models for simulating river-aquifer exchange and resulting low flows.

In 2009, Kalbus et al. investigated the influence of streambed heterogeneity on the distribution of groundwater fluxes through the streambed. For this purpose, the effect of heterogeneous hydraulic conductivity (with four different scenarios) within streambed and adjacent aquifer was examined by simulating 2-D groundwater flow and heat transport. The results of this study showed that the spatial distributions of groundwater fluxes were strongly influenced by the aquifer than that of streambed.

On the other hand, Baalousha [2012] characterized groundwater-surface water interaction using field measurements and numerical modelling in the Ruataniwha basin in NewZealand. In this, groundwater-surface water interaction was simulated using the finite difference based MODFLOW model using historical river flow data. The results of the model were calibrated with six runs of recent concurrent gauging data. The results of this study showed that relation between river and aquifer varied spatially from one location to another location. I was also identified that in the study reach the river gained much more water from aquifer than what they lose to aquifer.

Pérez-Martín et al. [2014] demonstrated river aquifer interactions using a new conceptual model PATRICAL. The behavior of groundwater and surface water and their interactions were included in this conceptual model. They applied the concept to a large river basin, Jucar River Basin District, Spain. The model was well calibrated with stream

flows, groundwater levels and river aquifer interactions. Using model parameters, the behavior of river and aquifer interactions was obtained with satisfactory findings. It was found that in the last 30 years, due to the changes occurred in precipitation and the impact of pumping, the groundwater level in the aquifer zone was reduced by 200 m.

Maheswaran et al. [2016] presented regional scale ground modelling of Ganga river basin using Visual MODFLOW. In this study, transient groundwater modelling was carried out with a single homogenous aquifer and the model was calibrated for quantifying surface-water groundwater interactions along the reaches of the river. They calibrated the model for 4 years and found simulated water levels were seen reasonable agreement with observed water levels. The results of this study showed that most of the river stretches had become losing or gaining much lesser water from the aquifer due to over-exploitation of groundwater in the study zone. This study suggested that the incorporation of multilayered aquifer system as well as heterogeneous groundwater transport system for representing reality can improve the model performance.

On the other hand, Kumar and Nagaraj [2018] assessed interactions between river and aquifer in Gowri-hole sub-catchment using numerical modelling. For this purpose, they used RIVER package of MODFLOW and the calibrated the model with the available seasonal observation well. They concluded that Gowri whole catchment acted as a gaining river during monsoon season and acted as loosing river during post monsoon season. The results of this study revealed the ability of MODFLOW model in assessing the spatio-temporal variations of river-aquifer interactions.

Although, the physical processes are considered in modelling approaches, the uncertainty with input data of aquifer and streambed properties leads to inaccurate assessment of river-aquifer interaction by the subsurface models. Hence, providing precise inputs is a primary need of any sub-surface hydrological model for a better understanding of the interaction process [Lu et al., 2011; Doble and Crosbie, 2017]. However, lack of ground-based observed data in arid semi-arid developing countries become a major constraint to the groundwater models. In such situations, the use of remote sensing is an alternative to some extent for improving the assessment of river-aquifer interactions, although all the inputs needed for subsurface modelling cannot be obtained from remote sensing techniques [Lekula and Lubczynski, 2019].

2.4 CHAPTER SUMMARY

The literature review on groundwater recharge estimation revealed that while investigating recharge estimation approaches, previous studies provided many sophisticated methods. However, for selecting a suitable method, it is necessary for any river basin to use multiple methods and compare for accurate recharge estimations. The literature on fluid flux and hydraulic conductivity estimation focused on new methods and techniques and revealed that using heat as a tracer is promising as well as cost-effective technique. However, the applicability of heat transport models along with one-dimensional analytical solutions for real field conditions remains challenging for the determination of hydraulic conductivity of heterogeneous streambeds. The literature review on river-aquifer interactions reveal the necessity of use of precise input parameters for accurate groundwater modelling to improve the understanding of river aquifer interactions along the river reach.

3

ESTIMATION OF GROUNDWATER RECHARGE

3.1 INTRODUCTION

In dense populated countries like India, groundwater is one of the major sources for drinking, agricultural, industrial, and domestic purposes in both rural and urban areas [Kaur et al., 2017]. With the growing demands, proper attention has to be given for the effective management of groundwater sources [Al-Bassam and Al-Rumikhani, 2003]. Groundwater recharge is one of the most important components of any river basin and its accurate estimation or quantification helps for groundwater modelling studies to manage groundwater [Yagbasan, 2016; Prasad and Rao, 2018]. Direct measurement of groundwater recharge is nearly impossible and it has to be estimated [Islam et al., 2015].

Over past few decades, many researchers have proposed various methodologies for estimating groundwater recharge at different scales [Simmers 1988; Van Tonder and Kirchner, 1990; Scanlon et al., 2002; Walker et al., 2019]. Penman's [1948] conventional method of recharge estimation was based on effective rainfall. Water table fluctuation method is a commonly used technique for recharge estimation by utilizing measured groundwater levels [Penman, 1948; Gerhart 1986; Rai and Singh, 1995; Healy and Cook, 2002; Varni et al., 2013; King et al. 2017]. The simplest way for recharge estimation is rainfall infiltration factor method where normal rainfall of long time series is multiplied with pre-determined infiltration factor [Bhuiyan et al. 2009; Chandra et al., 2018]. Soil water balance method has been widely recognized and used by many researchers for estimation of groundwater recharge at daily, monthly, seasonal and annual scale [Finch,

1998; Kendy et al., 2003; Dripps and Bradbury, 2007; Chung et al., 2016]. Hydrological modelling tools based on the water balancing approach are also used in various studies to estimate groundwater recharge at different spatio-temporal scales [Batelaan et al., 1996; Zhang et al., 1999; Sun and Cornish, 2005]. However, groundwater recharge estimated using a water balance approach requires accurate components of the hydrological cycle, particularly evapotranspiration [Rushton and Ward, 1979; Van Tonder and Kirchner, 1990]. Uncertainty in evapotranspiration can lead to inaccurate assessment of groundwater recharge that further affects the effective groundwater management. Some alternative methods such as base flow separation [Frohlich et al., 1994; Wittenberg and Sivapalan, 1999], empirical equations [Chaturvedi, 1973; Oke et al. 2015; Ali et al., 2017], non-reactive or conservative chloride mass balance [Bazuhair and Wood, 1996; Ting et al., 1998; Crosbie et al., 2017], isotope tracer techniques [Gaye and Edmunds, 1996; Bajjali, 2006; Koeniger et al., 2016] are also used depending on suitability and availability of information.

Among various methods, selecting a suitable method of groundwater recharge estimation is a necessary requirement of any river basin. Hence, it is recommended the use of multiple methods to improve the understanding and estimation of recharge at a study area considered [Healy and Cook, 2002; Walker et al., 2019]. Also, it is important to understand and analyze the hydrological components (rainfall, evapotranspiration, landuse/landcover etc.) which can affect groundwater recharge estimations [Rukundo and Doğan, 2019]. At present, many developing countries (like India) are facing severe water crises due to over-exploitation of groundwater for multiple purposes, particularly for irrigation needs [Tiwari et al., 2017]. Groundwater recharge is one of the important components of hydrological cycle and its estimation can help groundwater managers for better planning and management in the regions particularly agriculturally dominated and groundwater-based irrigation systems.

The present study focuses on the Kosi river basin (plain parts of the basin falls in Bihar state, India) is mostly covered with agricultural lands (90%). The agricultural lands are dependent on irrigation in which 60% of the area relies on groundwater [Najmuddin et al., 2018] that indicates extensive groundwater extraction in the study zone. The objectives of this chapter include (a) estimation of groundwater recharge using four different methods, i.e. Water Table Fluctuation (WTF), Soil Water Balance (SWB), Rainfall Infiltration Factor (RIF), and semi-distributed surface water hydrological modelling (SWAT)) (b) inter-

comparison of the groundwater recharge estimated using these methods. The last two methods estimate groundwater recharge at seasonal scale while the first two methods estimate groundwater recharge at a monthly scale, which is essential for effective groundwater management studies.

3.2 STUDY AREA AND DATASETS

3.2.1 Study Area

The Kosi river is one of the major tributaries of the Ganga that originates from the Himalayan region [Chen et al., 2013; Pradhan et al., 2018] (Figure 3.1). The study area lies between 85° 19' to 88° 56' East and 25° 18' to 29° 8' North and has a catchment area of 86,000 km^2 which includes parts of Nepal (45%), Tibet (32%) and India (23%) [Rajbhandari et al. 2017]. The basin has a complex geological structure covering six different zones namely Tibetan plateau, the Himalayas, the Himalayan mid-hill belt, the Mahabharat Range, the Siwalik Hills and the Terai [Sinha et al., 2005; Chen et al., 2013]. The basin has a diverse topography with high elevations at upper catchment (Himalayan hilly region) and low elevations at lower catchments (Indian flood plain regions) with a wide range of up to 8642 m above MSL. Two of the world's highest peaks Mount Everest (8848 m) and Kanchenjunga (8586 m) falls in the Kosi basin [Chen et al., 2013; Rai et al., 2018]. The river basin is confined by steep boundaries separating it from Yarlung Zangbo river in the north, Mahananda river in the east, Gandak on the west and the Ganga to the south [Rai et al., 2018]. The Kosi river originates from the foothills of Himalayas and joins the Ganga at Kursela in Katihar district, Bihar, India [Kumar et al., 2018]. The channel length is of 730 km and flowing through various districts of Bihar state (Supaul, Saharsa, Araria, Khagaria, Bhagalpur, Madhepura and Purnia) in Indian part of the catchment area [Sinha and Friend, 1994; Rai et al., 2018].

The basin falls under the sub-tropical belt and therefore experiences a humid climate towards low river valleys in the south and cold and arid climate on the mountainous region in the north [Shreshta et al., 2017]. The basin receives an average annual rainfall of 1000 mm and more than 80% of annual rainfall takes place during monsoon season [Rajbhandari et al. 2017; Shrestha, 2000]. The basin experiences a wide range of spatial temperature variations and generally decreasing from south (Bihar state, India) to north (Himalayan region) and the highest temperature records in June and lowest in December

or January [Agarwal et al., 2016]. Due to the complex topography and precipitation pattern, the Kosi river basin experiences frequent floods. In north Bihar, the river Kosi is called "the river of sorrow" because of its devastating floods, massive siltation, and dynamic morphological changes [Reddy et al., 2008; Kumar et al., 2018]. Hilly region of the basin is covered with forest and snow whereas plain parts of the basin are covered with agricultural lands (90%) predominantly used for rice cultivation during the month of June [Siddiq, 2006]. Although the basin receives reasonably high rainfall (~1200 mm per year), more than 80% of the irrigation demand in the plain regions (north Bihar) is met by groundwater resources [Sinha et al., 2018]. These groundwater extractions in the study area has a significant effect on river-aquifer interactions.

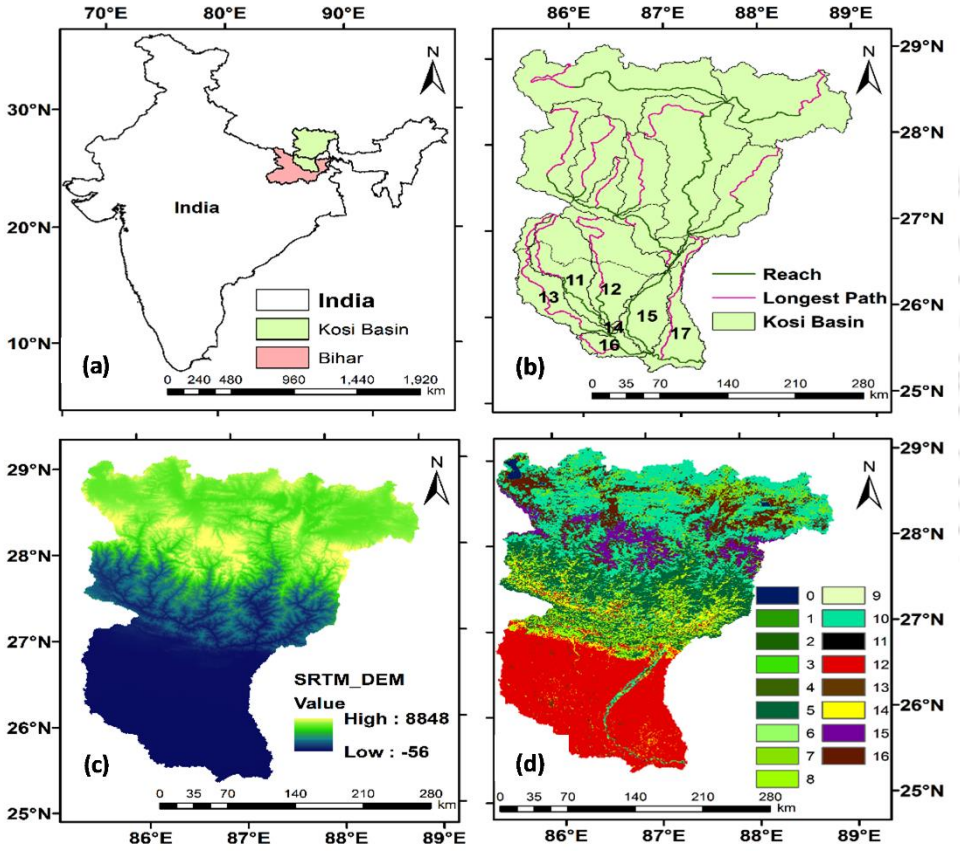

Figure 3.1: (a) Location of the study area (b) Drainage and sub-basin map (c) Topography map (d) Landuse/landcover map (MODIS-2000) of the study area

Note: LULC class 0: Water; 1: Evergreen Needle leaf forest; 2: Evergreen Broadleaf forest; 3: Deciduous Needle leaf forest; 4: Deciduous Broadleaf forest; 5: Mixed forest; 6: Closed shrublands; 7: Open shrublands; 8: Woody savannas; 9: Savannas; 10: Grasslands; 11: Permanent wetlands; 12: Croplands; 13: Urban and built-up; 14: Cropland/Natural vegetation mosaic; 15: Snow and ice; 16: Barren or sparsely vegetated)

Note: The numbers 11-17 in Figure 3.1(b) indicates sub-basin ID in the plain parts of the Kosi basin.

3.2.2 Data Sets

In the present study, four different methods were applied to estimate monthly and seasonal groundwater recharge at the sub-basin scale using the data (meteorological data, geospatial data, hydrological data, and aquifer parameters) obtained from different agencies Table 3.1 shows the data obtained from various agencies to estimate groundwater recharge using all four methods.

Table 3.1: Various data sources used in the study

Data	Source	Time Period	Resolution
Rainfall	APHRODITE	1970-2010	0.25°
Temperature	PGF	1970-2010	0.25°
Wind Speed	PGF	1970-2010	0.5°
Solar Radiation	PGF	1970-2010	0.5°
Relative Humidity	PGF	1970-2010	0.5°
Landuse/Landcover	MODIS	2000	1 km
Soil	NBSS & LUP		90 m
Topography	SRTM		90 m
Discharge	CWC	1980-2010	Daily
Groundwater Levels & Draft	CGWB	1996-2010	
Aquifer Characteristics	CGWB		
Soil Moisture	GLDAS VIC	1980-2010	0.5°
Evapotranspiration	NOAA	1982-2000	8 km
	MODIS	2001-2010	0.05°
Decadal Landuse/Landcover	ORNL DAAC	1985, 1995 & 2005	100 m

***Note:** In the present study, groundwater recharge was estimated for 1996-2010 due to the availability of the data of common time period of all four methods and the factors that affect recharge estimation such as rainfall, evapotranspiration and landuse/landcover were in consequence analyzed for the period 1982-2010. Whereas, SWAT modelling was carried out from 1970-2010 with a warm period of 9 years. All the web links of the various data sources are mentioned in the Web References section (Page 181).

The observed groundwater levels, groundwater draft and specific yield of the aquifer were obtained from Central Groundwater Board (CGWB), Patna and were used to estimate seasonal groundwater recharge using the WTF method. Satellite-based high-resolution rainfall data was used for RIF method and surface water hydrological modelling. Meteorological data (includes rainfall, temperature, wind speed, solar radiation, and relative humidity) and geospatial data (includes soil types, topography and

landuse/landcover data) were used in SWAT model for estimating monthly discharge and groundwater recharge at the sub-basin scale. The observed daily discharge time-series data obtained from Central Water Commission (CWC) was used to calibrate and validate the model. High-resolution satellite-based rainfall data, evapotranspiration data, soil moisture along with SWAT simulated discharge were used in SWB method to estimate monthly groundwater recharge at the sub-basin scale. In the present study, LULC change analysis was carried out using decadal landuse/landcover maps for the years 1985, 1995 and 2005.

3.3 METHODOLOGY

Previous works suggest different methods for estimation of groundwater recharge with different assumptions and limitations. In the present study, four different methods were used to estimate the monthly and seasonal groundwater recharge: (a) Water Table Fluctuation (WTF) Method (b) Rainfall Infiltration Factor (RIF) Method (c) Semi-distributed hydrological modelling and (d) Soil Water Balance Method (SWB). Figure 3.2 represents the flowchart discussing the methodology adopted for monthly groundwater recharge estimation in the study area.

(a) Water Table Fluctuation Method

Water Table Fluctuation (WTF) is a simple and widely used recharge estimation method in India. This method accounts for the inflows (recharge through rainfall and other sources) and outflows (pumping through wells and other sources) in a groundwater system for recharge estimation. The groundwater recharge can be estimated using WTF method by analyzing the fluctuations occurring in the observation wells [GEC, 1997; Crosbie et al., 2005; Delin et al., 2007; Bhuiyan et al. 2009; Chandra et al., 2018]. In this method, it is assumed that the rise in the water table level in the shallow observation well is due to the addition of water across the phreatic table. This method gives spatially averaged groundwater recharge at a seasonal scale. The monsoon recharge is computed as the sum of groundwater draft during monsoon season and the change in storage between pre and post-monsoon period multiplied with the area of assessment and specific yield. The mathematical equation used for monsoon recharge is expressed as

$$R_e = (A.\delta h.S_y) + D_g \qquad (3.1)$$

where

R_e = Recharge during Monsoon (ha-m)

D_g = Groundwater draft during monsoon (ha-m)

δh = Rise in water table during monsoon season (m)

S_y = Specific Yield and

A = Areas of assessment (ha)

(b) Rainfall Infiltration Factor Method

Rainfall Infiltration Factor (RIF) is an easy and indirect method based on normal rainfall (obtained using long term series of rainfall data) to estimate monsoon recharge [Bhuiyan et al. 2009]. It is an alternative method when adequate information on groundwater level between pre-monsoon and post-monsoon may not be available for estimating recharge using WTF method. RIF is the ratio of total recharge to the total rainfall during the monsoon or non-monsoon period. The Monsoonal groundwater recharge at the sub-basin scale is estimated as follows

$$R_e = f \cdot A \cdot \text{Normal rainfall in monsoon season} \qquad (3.2)$$

where,

A = Area of computation for recharge, ha

f = Rainfall Infiltration Factor

In the present study, normal rainfall during monsoon season is calculated based on the recent 29 years of rainfall data and the infiltration factor is collected from the previous literature which is 0.22 for Indo Gangetic and Inland alluvial area [Chandra et al., 2018].

(c) Semi-distributed Hydrological Model

A semi-distributed model, Soil and Water Assessment Tool (SWAT) is used to estimate monthly groundwater recharge at the sub-basin scale. It is a river basin or watershed scale model developed by Dr. Jeff Arnold for the USDA Agricultural Research Service (ARS) that is used to predict the impact of land management practices on water, sediment and agricultural chemical yields in large complex watersheds with varying soils, land use and management conditions over long periods of time. SWAT divides a basin into sub-basins for analyzing purpose and each sub-basin is connected through stream channel and further divided into Hydrologic Response Unit (HRU). HRU is a unique combination of soil and vegetation type in a sub-watershed.

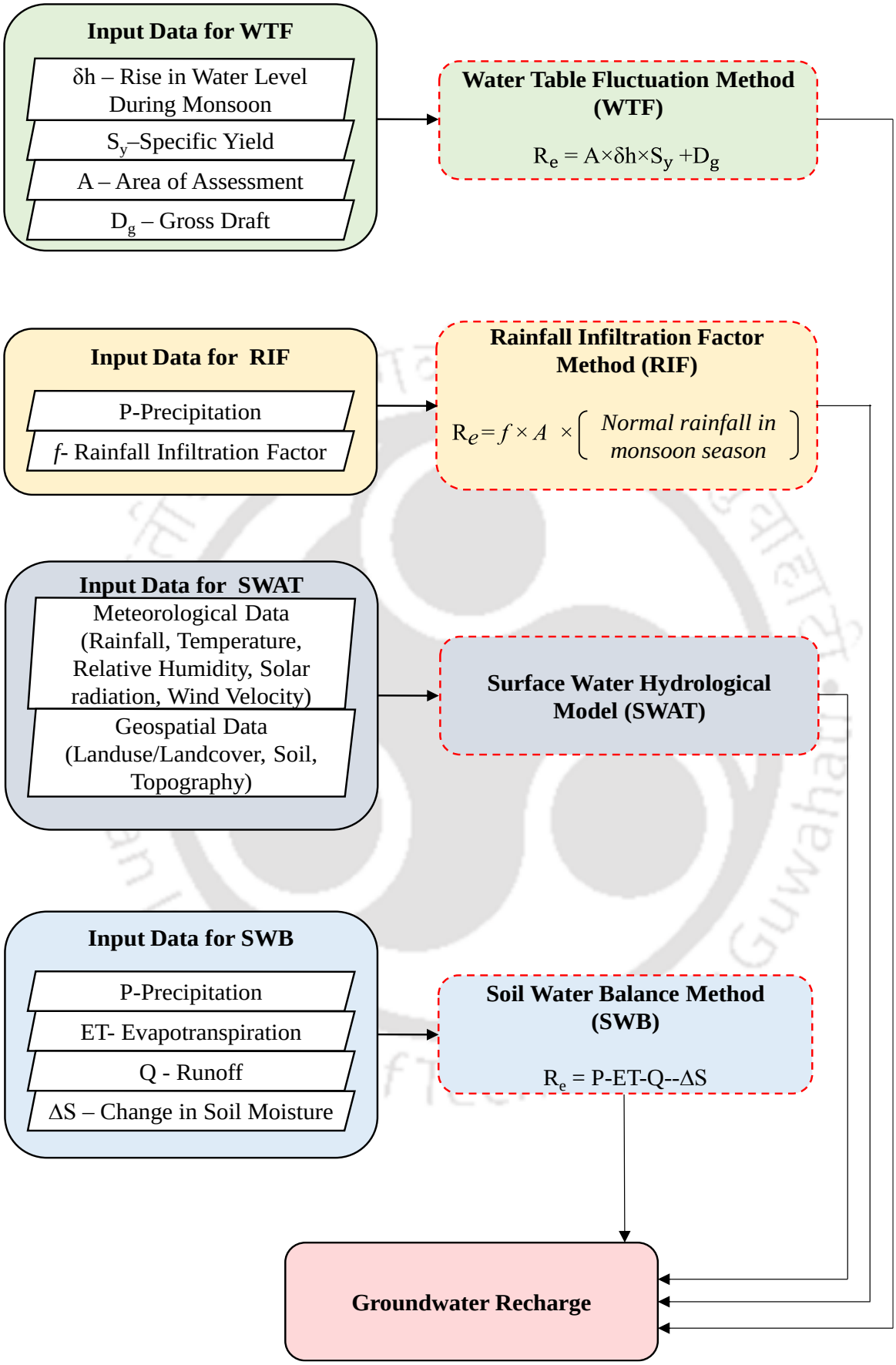

Figure 3.2: Methodology for monthly groundwater estimation at each sub-basin of Kosi

SWAT simulates hydrology, vegetation growth, and management practices at the HRU level. The model is developed to simulate the hydrologic components of the hydrological cycle such as surface runoff, evapotranspiration, groundwater recharge, return flow, percolation, lateral flow, etc. The concept and description of components of this model can be found in the literature [Arnold et al. 1998, Srinivasan et al. 1998, Neitsch et al. 2002]. The governing equations of water balance and runoff computation used in the model are presented in Appendix A.

The aquifer recharge equation used in the SWAT model is formulated as [Venetis, 1969; Sangrey et al., 1984]

$$W_{rchrg,i} = \left\{ W_{seep} \cdot \left(1\text{-}\exp\left[\frac{-1}{\delta_{gw}} \right] \right) + W_{rchrg,i-1} \cdot \exp\left[\frac{-1}{\delta_{gw}} \right] \right\} \qquad (3.3)$$

where,

$W_{rchrg,i}$ is the amount of recharge entering the aquifer on day i (mm H_2O).

W_{seep} is the total amount of water exiting the bottom of the soil profile on day i (mm H_2O),

δ_{gw} is the delay time or drainage time of overlying geologic formations (days)

$W_{rchrg,i-1}$.is the amount of recharge entering the aquifers on day i-1 (mm H_2O)

(d) Soil Water Balance Method

Thornthwaite [1948] developed the soil water balance method to estimate groundwater recharge which is later revised by Thornthwaite and Mather [1955]. It is a lumped model approach in which entire watershed is considered as a single unit and the status of soil water is tracked with time [Dhungel and Fiedler, 2016]. The monthly recharge or groundwater extraction at the sub-basin scale can be estimated using the following equation

$$R_e = P - ET - Q - \Delta S \qquad (3.4)$$

where,

R_e = Monthly recharge or extraction (cm),

P = Monthly precipitation (cm),

ET = Monthly actual evapotranspiration (cm),

Q = Monthly Runoff (cm),

ΔS = Change in soil moisture storage during the month (cm).

SWB method requires large and accurate initial data for monthly groundwater recharge estimations in the river basin [Van Tonder and Kirchner, 1990]. Accuracy of the estimated recharge using this method depends on the accuracy, spatial and temporal resolutions of water balance components. Particularly, accurate assessment of actual evapotranspiration (AET) may significantly influence the accuracy of the groundwater recharge estimations [Rushton and Ward, 1979]. In the present study, high-resolution satellite-based remotely sensed data of NOAA and MODIS AET products were utilized to estimate monthly recharge along with satellite-based precipitation, soil moisture and runoff at sub-basin scale. As monthly observed discharge time series data was not available at the sub-basin scale, simulated time series from a well calibrated and validated SWAT model was used to estimate the groundwater recharge at sub-basin scale.

Prior to groundwater recharge estimations, some of the major factors influencing the groundwater recharge such as rainfall, landuse/landcover and evapotranspiration were analyzed and discussed in the subsequent sections.

3.4 IDENTIFICATION OF WET AND DRY YEARS

A non-parametric Standard Precipitation Index (SPI) developed by McKee et al. [1995] was calculated to identify the wet and dry years during the analysis period (1982-2010). SPI index relies on representative parametric distribution function, whereas a non-parametric framework does not need assuming a representative parametric function [Solakova et al., 2014]. Based on SPI values, McKee et al. [1995] categorized rainfall into eight different classes ranging between extremely wet and dry as given in Table 3.2 [Aladaileh et al. 2019].

SPI used in this study is calculated as

$$\mathrm{SPI} = \frac{x_i - x_m}{\sigma} \qquad (3.5)$$

where x_i is annual, seasonal and monthly precipitation;

x_m is the long-term mean;

σ is its standard deviation.

Table 3.2: SPI values and different categories of wetness/dryness [McKee et al., 1995]

SPI Value	Category
2.00 or more	Extremely Wet
1.50 to 1.99	Severely Wet
1.00 to 1.49	Moderately Wet
0 to 0.99	Mildly Wet
-0.99 to 0	Mildly Dry
-1.49 to -1.00	Moderately Dry
-1.99 to -1.50	Severely Dry
-2.00 or less	Extremely Dry

SPI is a dimensionless index. The negative values indicating drought and positive values indicating wet conditions. To identify the wet and dry year variability across the sub-basin in the analyzing period, 12-monthly SPI was calculated. In order to represent the variability of hydrological components (rainfall, evapotranspiration and recharge) across the basin, there different sub-basins, i.e. sub-basin 11 (S-11), sub-basin 12 (S-14) and sub-basin 16 (S-16) were selected in the upper, middle and lower regions of the study area, respectively. Figure 3.3 shows 12-month non-parametric SPI index variation from 1982-2010 in S-11, S-14 and S-16. It was observed that there was an average of six-year cyclic period for the wet year and nine-year cyclic period for the dry year over the 29 years of the analysis period. An extremely wet year and dry year were observed to be different for sub-basin 11, 12 and 16. In sub-basin 11, 2007 and 1982 were found to be extremely wet and dry years having SPI value 2.17 and -2.17, while the years 1987 and 2005 for S-14 (SPI value 2.17 and -2.17) and the years 1987 and 2005 for S-16 with (SPI value 2.17 and -2.17) and years 1987 and 1982 for whole basin.

In the present study, groundwater recharge was estimated for the time period 1996-2010 at sub-basin scale. During this estimation period, wettest and driest years for S-11 were observed to be 2007 and 2009 (SPI value 2.17 and 1.74) (Figure 3.3a)), while 1998 and 2005 for S-14 (SPI value 1.05 and -2.17) (Figure 3.3b) and 2000 and 2005 for S-16 (SPI value 1.17 and -2.17) (Figure 3.3c), respectively. For the whole basin, wettest and driest years were found to be 1999 and 2005 (SPI value 1.74 and -1.74) (Figure 3.3d).

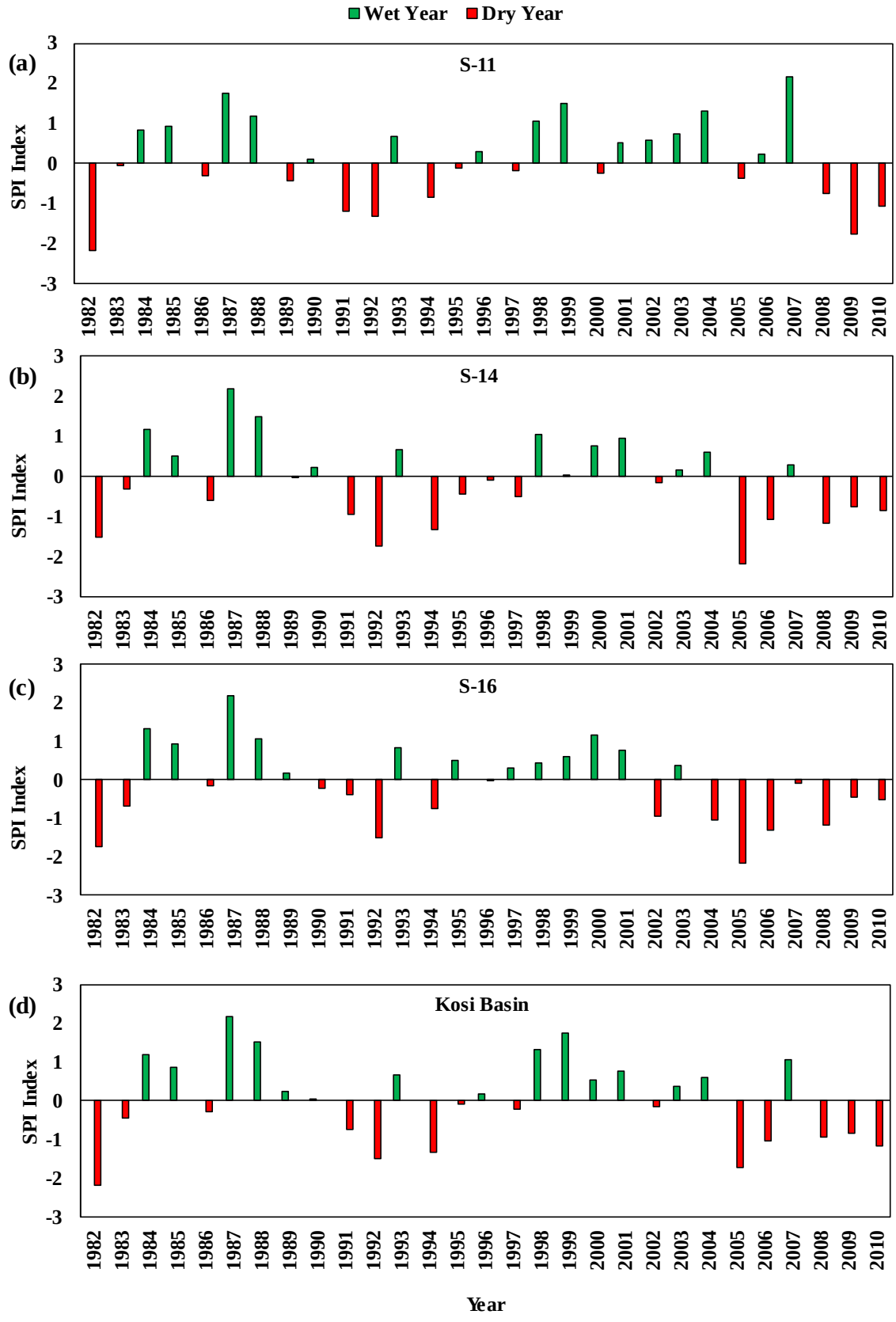

Figure 3.3: 12-month SPI Index for sub-basin (a) 11, (b) 14, (c) 16 and (d) whole study area

It is observed that sub-basin 11 received high rainfall compared to other sub-basins, whereas sub-basins 14 and 16 experienced more number of dry years during the estimation period (Figure 3.3(a-c)). Figure 3.3(d) indicated the basin experienced a wet cycle during 1996-2003 and dry cycle during the years 2004-2010.

In case of sub-basin 12 (S-12), sub-basin (S-13), sub-basin 15 (S-15) and sub-basin17 (S-17), variations of 12-month non-parametric SPI index are shown in Figure B.1 (Appendix). In the recharge estimation period, wettest and driest year were found to be 2007 and 2005 for S-12 with SPI index 1.49 and -1.49 (Figure B.1(a)), 2007 and 2009 for S-13 with SPI index 2.17 and -1.74 (Figure B.1(b)), 2001 and 2005 for S-15 with SPI index 1.74 and -2.17 (Figure B,1(c)), 1999 and 2005 for S-17 with SPI index 1.74 and -2.17 (Figure B.1(d)), respectively.

3.5 LANDUSE/LANDCOVER CHANGE ANALYSIS

Pre-classified decadal landuse/landcover (LULC) maps were utilized in order to study LULC changes observed in the analysis period (1982-2010). The study area was categorized into eight different LULC classes namely, croplands, built-up land, shrubland, fallow land, wasteland, water bodies, plantations, and permanent wetlands. Figures 4-6 show LULC maps for the years 1985, 1995, and 2005, while the LULC statistics are summarized for the years 1985, 1995 and 2005 in Table 3.3.

Decadal LULC covering eight different classes: cropland, built-up land, shrubland, fallow land, wasteland, water bodies, plantations, permanent wetlands of 1985, 1995 and 2005 are shown in Figure 3.4-3.6. The LULC maps indicated that in the year 1985, most of the basin area was covered with cropland, fallow land and plantations (93.44%) whereas built-up, shrub and wastelands covered about 2.43% of the area and water bodies and permanent wetlands covered about 4.13% of the area. On the other hand, in 1995 about 91.12% area was occupied with croplands, fallow and plantations which were found to be approximately the same in 1985 (93.44%). This indicated an insignificant change in the cultivation area. Built-up, shrub and wastelands covered 2.58% and water bodies and wetlands occupied with 4.44% also indicated insignificant changes in the study region from 1985 to 1995.

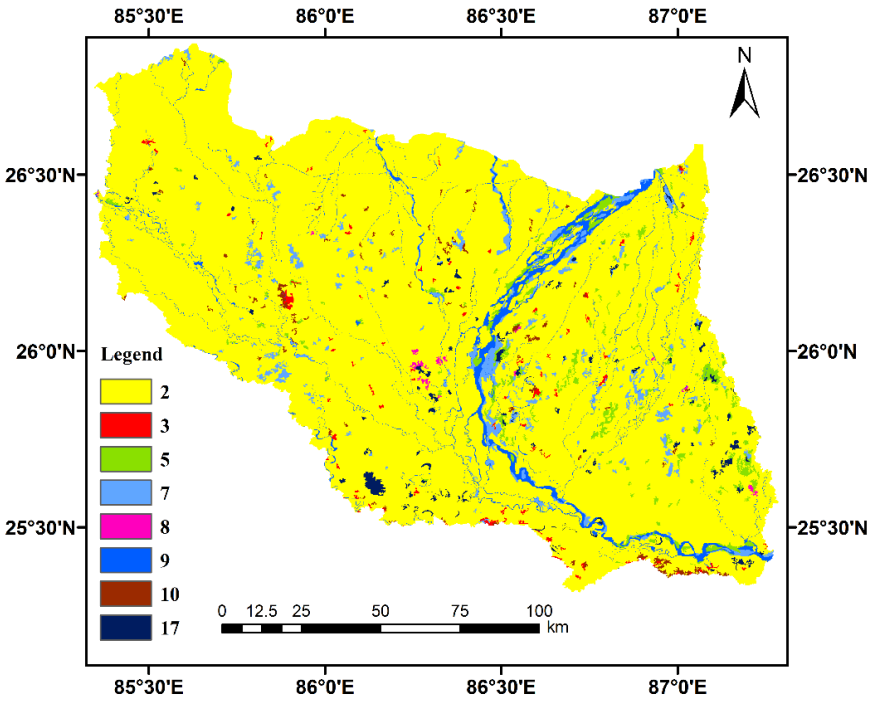

Figure 3.4: LULC map for 1985
***(*Note:** Legend numbers are explained in Table 3.3)*

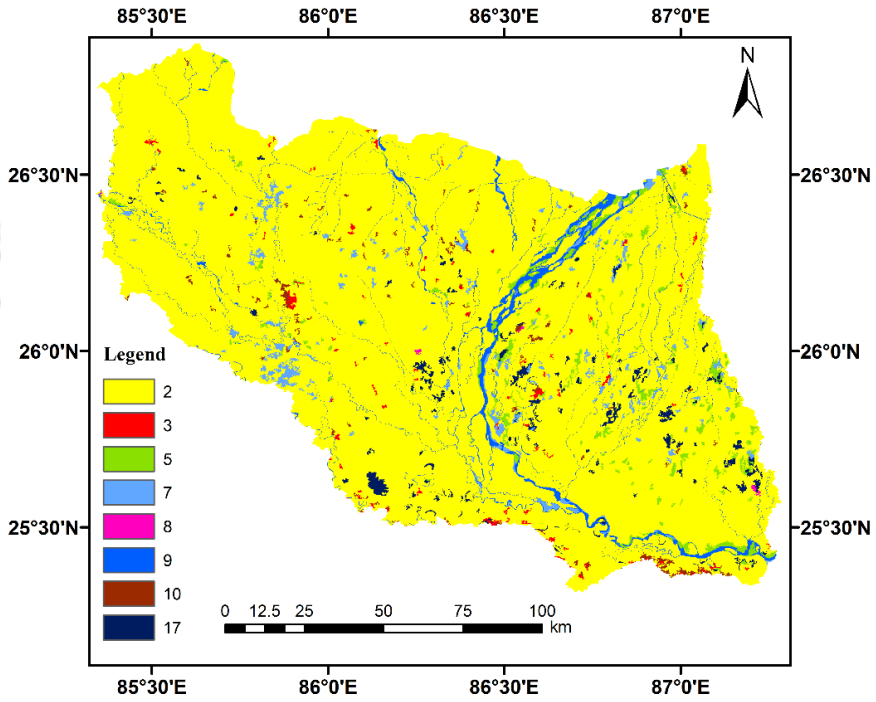

Figure 3.5: LULC map for 1995
***(*Note:** Legend numbers are explained in Table 3.3)*

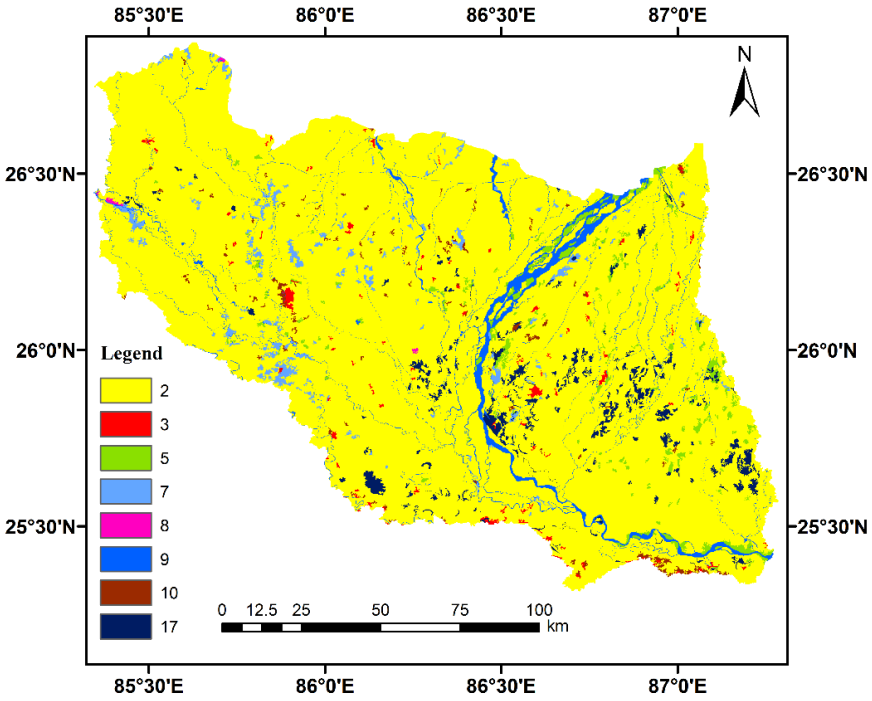

Figure 3.6: LULC map for 2005

(*Note: Legend numbers are explained in Table 3.3)

The decadal LULC map of 2005 indicated that more than 91% of the area is covered with cropland, fallow land and plantations. Not much change in cultivation land between 1995 and 2005 was observed in the study area. However, 2.5% of the area is covered with built-up, shrub, wastelands and 5.5% of the area is occupied by water bodies and wetlands indicating that there is insignificant LULC change over the decade.

Table 3.3: Landuse/Landcover Class Statistics

Class ID	Class Name	1985		1995		2005		Relative Change	
		Area (sq. km)	Area (%)	Area (sq. km)	Area (%)	Area (sq. km)	Area (%)	Area (sq. km)	Area (%)
2	Cropland	17232	90.09	17309	90.49	17145	89.63	-87	-0.46
3	Built-up Land	94	0.49	101	0.52	119	0.62	25	0.13
5	Shrub Land	345	1.80	385	2.01	351	1.84	6	0.04
7	Fallow Land	536	2.80	358	1.86	320	1.67	-216	-1.13
8	Wasteland	25	0.14	8	0.05	10	0.06	-16	-0.08
9	Water Bodies	627	3.27	579	3.04	649	3.39	23	0.12
10	Plantations	104	0.55	122	0.63	119	0.62	15	0.07
17	Permanent Wetlands	165	0.86	269	1.40	416	2.17	251	1.31

Table 3.3 shows the relative changes in the LULC classes which indicated that only 0.5% decrement in major LULC class (cropland) and less or insignificant decrement and increment of other classes in the study area over the two decades (1985-2005). This LULC change analysis indicates that there may not be much influence or effect of LULC on estimations of groundwater recharge in the study region due to insignificant changes observed in LULC maps.

3.6 SPATIO-TEMPORAL VARIATIONS IN EVAPOTRANSPIRATION TRENDS

Land evapotranspiration (ET) is a fundamental process in the climate system and terrestrial link among the water, energy, and carbon cycles. Global land ET returns about 60% of annual land precipitation to the atmosphere. It is one of the important components of the hydrological cycle and its accurate assessment helps to improve the groundwater recharge estimations. In this study, satellite-based Actual Evapotranspiration (AET) products of NOAA (1982-1999) and MODIS (2000-2010) were utilized to estimate the groundwater recharge in Soil Water Balance (SWB) method. These ET products of NOAA and MODIS were well-calibrated and validated with in-situ measurements for Indian sub-content [Mallick et al., 2009; Goroshi et al., 2017].

3.6.1 Monthly ET Spatio-Temporal variations during years 1982-83 (March to February)

In the present study, the period 1982-83 was selected to represent the spatio-temporal variations of monthly ET during the 1980s. Figure 3.7 presents the estimates of monthly average ET data of NOAA satellite product data from March to February. The maps show that ET values are varying spatially and seasonally throughout the river basin. In the pre-monsoon (March-May) period, ET has reached a peak in March followed by a decreasing trend in successive months. Whereas, in monsoon season (June-September), ET is observed to increase from June with the initiation of irrigation and, reached a peak in July followed by decreasing variability in August and September. During post monsoons season (October-February), this value again increased from September and, reached a peak in October over the river basin followed by a declining trend in succeeding months. These maps show that monthly average ET values are significantly varying across the catchment and seasons, showing a wide range from 1.16-3.78 mm/day.

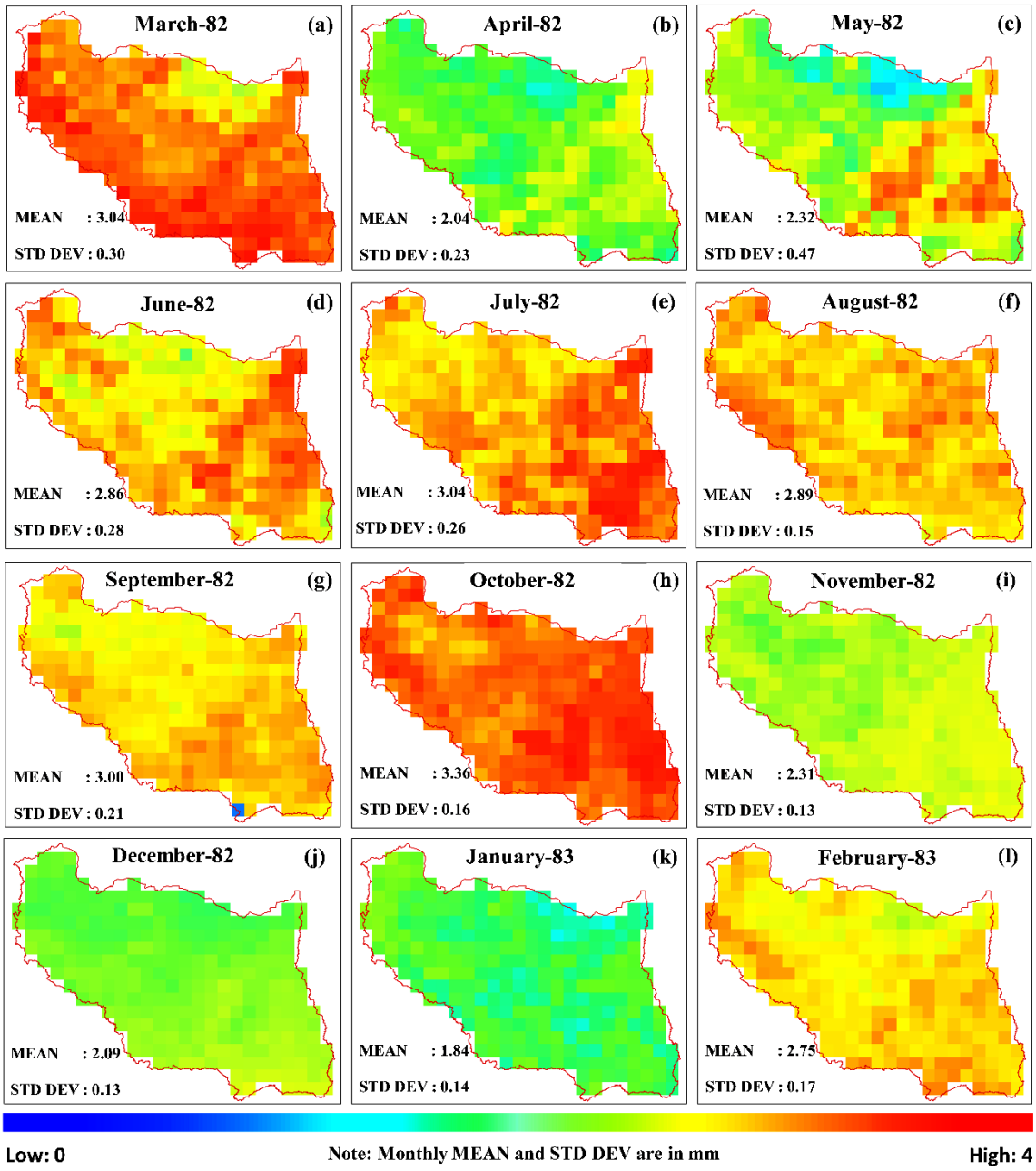

Figure 3.7: Spatial variations of monthly average ET (mm) for the year 1982-83 during (a) March (b) April (c) May (d) June (e) July (f) August, (g) September (h) October (i) November (j) December (k) January and (l) February.

The ET variations are observed to be high in the month of March, ranging between 2.1-3.78 mm/day (Figure 3.7(a)). The low variation may be due to less rainfall and groundwater extractions to meet irrigation requirements. In the succeeding months (April and May), the ET values gradually decreased comparatively to March ranging from 1.48 to 2.74 mm/day and 1.16 to 3.30 mm/day, respectively (Figures 3.7(b –c)). The basin experiences hot climate and the start of monsoonal rainfall causes the increase in ET values

during June (1.7-3.46 mm/day) and July (2.51-3.6 mm/day) (Figures 3.7(d-e)). This gradual increase might be due to irrigation in agricultural fields and this variation observed to be high in the Eastern parts of the study area. During August and September ET variations are observed to be moderate ranging from 2.51 to 3.62 mm/day and 2.32 to 3.27 mm/day, respectively (Figures 3.7(f-g)) and these variations are spatially distributed throughout the basin. Whereas, during October ET variations (2.91-3.71 mm/day) are high throughout the basin followed by a declining trend during November (1.93-2.58 mm/day) (Figures 3.7(h-i)). The monthly average ET maps presented in Figures 3.7(j) and 3.7(k) indicate that December followed by January month has low ET values ranging from 1.41 to 2.11 mm/day and 1.76 to 2.52 mm/day, respectively. These low values are resulted due to low temperature, less or no rainfall, less solar radiation and shine hours during winter. Whereas, ET begins to increase gradually from February month (2.18-3.09 mm/day) as the solar radiation sunshine hours and temperature increases slowly (Figure 3.7(l)). From these analyses, it is found that ET has high variations during March, July and October which indicated three major crop irrigations in these months during 1982-83.

3.6.2 Monthly ET Spatio-Temporal variations during years 1998-99 (March to February)

Monthly average ET variations for the period 1998-99 during March-February are shown in Figure 3.8. The seasonal and spatial variations of ET can be seen from the maps throughout the basin. The maps show that during the pre-monsoon period, ET has reached the peak value and followed a decreasing trend in June. During monsoon season, ET is observed to increase from June and reach the peak value in July. This is followed by a decreasing trend in August which is followed by again increasing trend in September. It continued a similar trend in ET during October and shown decreasing variability in the successive months during the post-monsoon period. It can be observed that during this period, ET values have both significant seasonal and spatial variations throughout the river basin having a dynamic range of 0.62-3.98 mm/day.

Figure 3.8(a) shows the medium range of monthly average ET variations (2.15-3.32 mm/day) in March followed by an increasing trend in succeeding months. The maps presented in Figures 3.8(b) and 3.8(c) show ET has high values varying throughout the basin during April (2.38-3.98 mm/day) and continued the similar trend in May (2.37-3.84 mm/day). This could be resulted due to low rainfall and high temperature during summer

and extensive groundwater irrigations throughout the basin to meet agricultural needs during these periods.

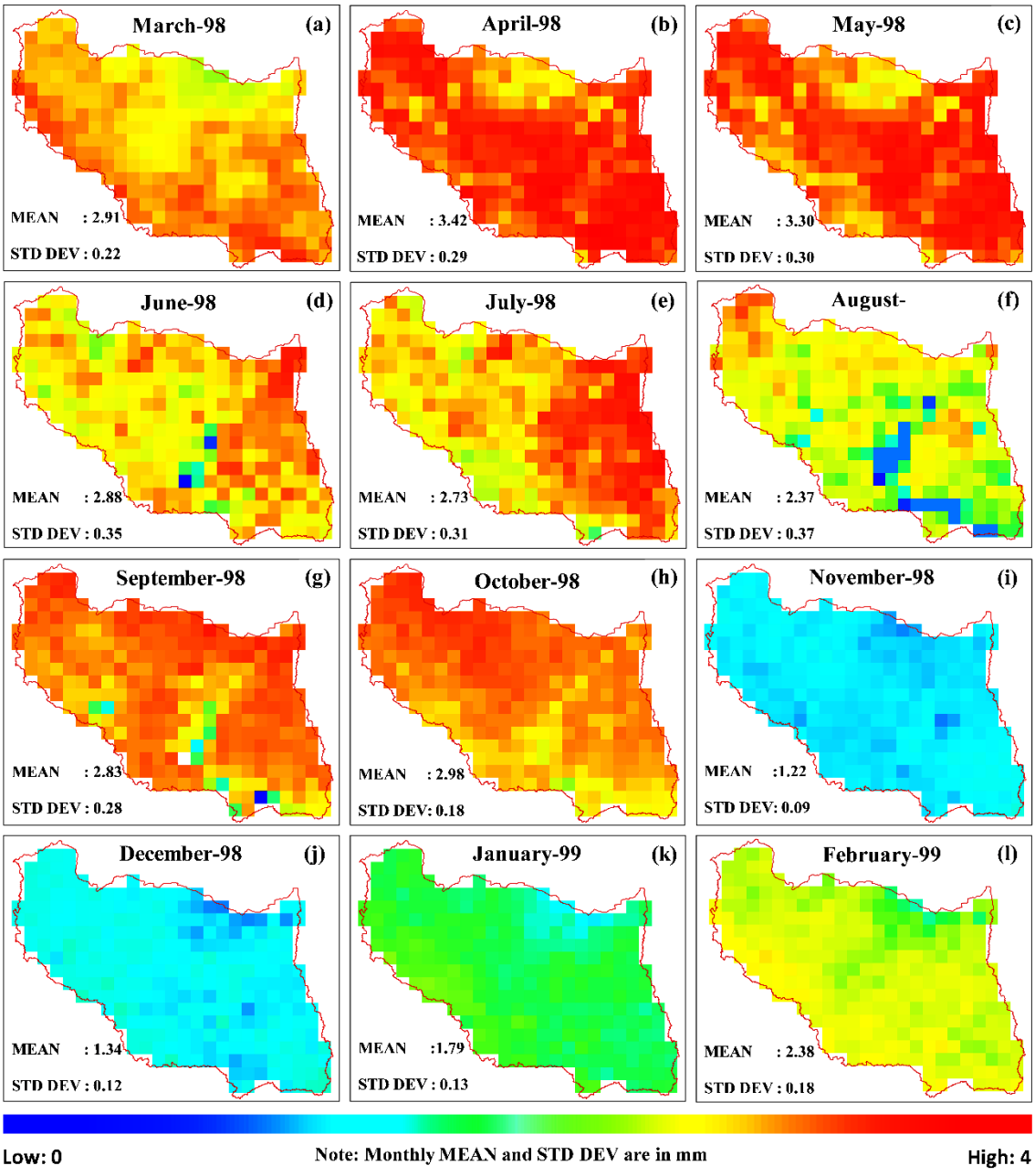

Figure 3.8: Spatial variations of monthly average ET (mm) for the year 1998-99 during (a) March (b) April (c) May (d) June (e) July (f) August, (g) September (h) October (i) November (j) December (k) January and (l) February.

Whereas, ET variations showed declining trend during June (0.78-3.47 mm/day) followed by increasing trend in July (1.82-3.78 mm/day) during monsoon season due to high rainfall and irrigations in the eastern part of the study area (Figures 3.8(d) and 3.8(e)). During August, low ET values (0.62-3.17 mm/day) can be observed in the basin against July

followed by increasing trend throughout the basin during September (1.2.3-3.59 mm/day) and continued the similar trend during October (2.12-3.34 mm/day) ((Figures 3.8(f-h)). This might be resulted due to less rainfall that increased groundwater extractions to meet agricultural requirements during this period whereas, during 1982-83, similar agricultural activities are observed to be initiated in the month of October. Figures 3.8(i-k) show during November, ET has declining trend (0.95-1.53 mm/day) and continued the similar trend in December (0.99-1.60 mm/day) and January (1.26-2.34 mm/day) due to less rainfall, temperature, solar radiation and sunshine hours during the winter season. Whereas Figure 3.8(l) shows ET has a medium range of variations (1.5- 2.7 mm/day) during February due to low rainfall and transition temperatures from winter to summer. From these analyses, it is noted that ET has high variations during April, July and September which indicated three major crops might be irrigated in the months during 1998-99. But, this trend is different and can be seen in March, July and October months from 1982-83. This analysis clearly indicated that there is a shift of one month in agricultural patterns from March to April and October to September during this study period.

Figure 3.9 depicts box plots of the monthly average of ET for Kosi basin for the analysis period 1982-2010. It shows the variations of ET between the 1st and 3rd quartile along with the median from January – December of all the 29 years. The plot shows that initially, ET has increased and then decreased on the monthly scale with maximum ET during August and minimum during December. It is observed that ET has high values during March, August, and October months with a median value of around 2.8 mm/day, whereas November and December months have minimum ET value with a median value of around 1.5 mm/day. Figure 3.9 indicated that during monsoon, particularly during June-August, ET is highly skewed, which might be to fluctuations between wet and dry cycles during the analysis period. However, ET is less skewed during other months, for example, January and December that maybe due to low fluctuations. The box plot shows that during summer- monsoon ET has maximum values whereas minimum during winter season as the temperature and rainfall variations are high during summer-monsoon and low during winter.

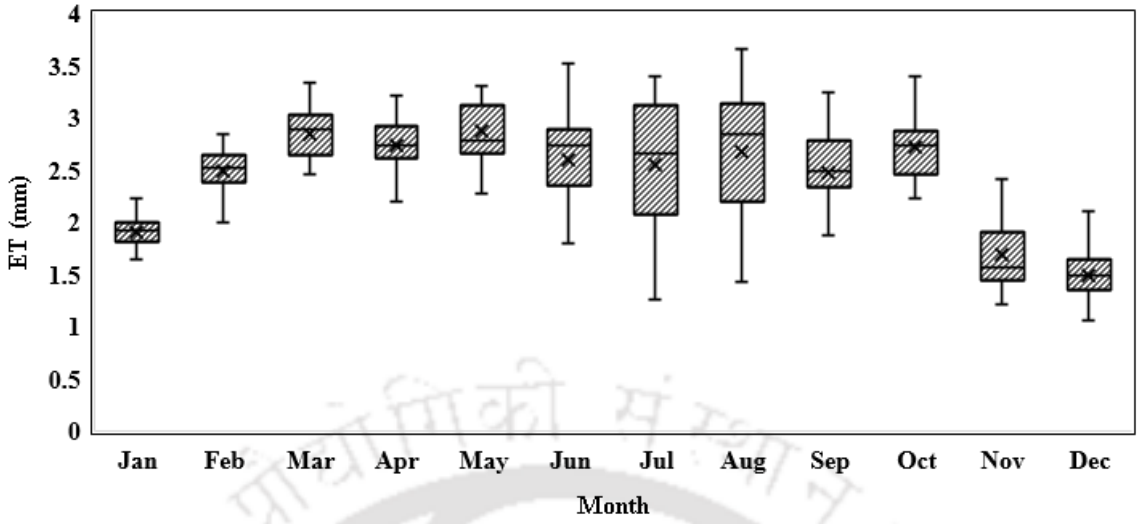

Figure 3.9: Box plots of monthly average ET of Kosi basin for the period 1982-2010

3.7 RESULTS AND DISCUSSION

In this study, groundwater recharge was estimated using four different methods that include Water Table Fluctuation method (WTF), Rainfall Infiltration Factor (RIF) method, a semi-distributed hydrological model, SWAT (Soil & Water Assessment Tool) and Soil Water Balance (SWB) methods. WTF and RIF estimate groundwater recharge at seasonal scale whereas SWAT and SWB estimate groundwater recharge at monthly scale. SWAT model categorized the study area into 17 sub-basins whereas, the study region (Indian part of the Kosi basin) consists of seven sub-basins (S-11, S-12, S-13, S-14, S-15, S-16 and S-17) in which groundwater recharge was estimated. As a representative of the basin, three sub-basins located at upper (S-11), middle (S-14) and lower (S-16) are selected. In these sub-basins, spatio-temporal variations of monthly groundwater recharge estimated using four different methods are presented in this section.

3.7.1 Estimation of Groundwater Recharge using WTF Method

Figure 3.10 shows the monsoonal groundwater recharge estimated using WTF method for sub-basins 11, 14 and 16 for the time period 1996-2010 using pre and post monsoonal groundwater levels. In S-11, monsoon groundwater recharge is observed to vary with a range of 29-38 cm, whereas these variations in S-14 and S-16 are found to vary similarly (25-38 cm). In S-11, during the extremely wet year (2007) and dry year (2009), the maximum and minimum recharge can be observed whereas the maximum and minimum values of recharge were not corresponding to the wettest and driest year in other

sub-basins (S-14 and S-16). In S-14 and S-16, the wettest year was found to be 1998 and 2000 whereas the maximum recharge values were observed to be found during 2001. Similarly, the driest year in S-14 and S-16 were observed to be 2005 whereas the minimum recharge was observed to be found during 1999 and 2005. These variations could be uncertainly associated with observed pre and post-monsoon groundwater levels and aquifer characteristics.

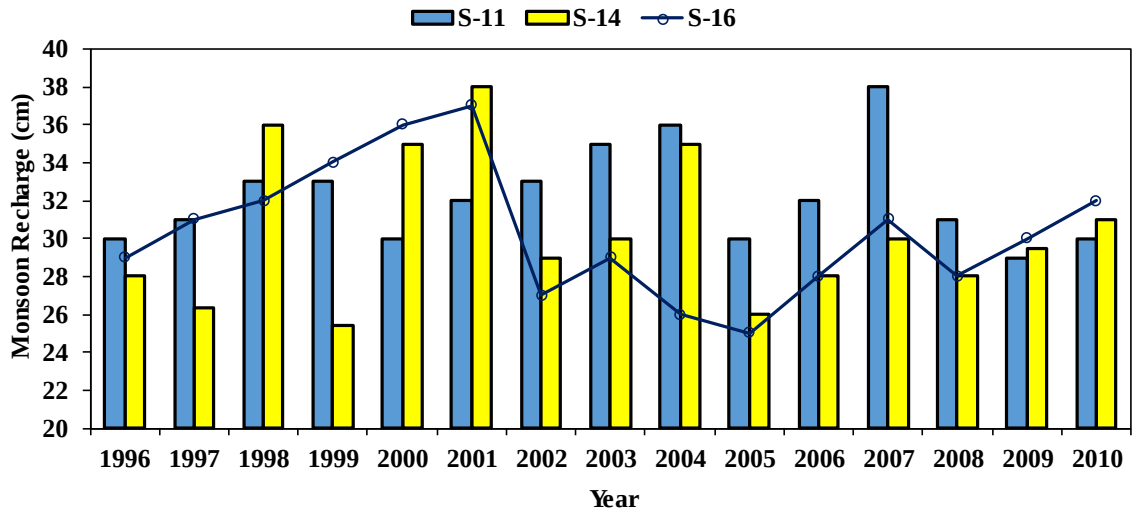

Figure 3.10: Estimated monsoonal groundwater recharge in (a) S-11 (b) S-14 (c) S-16 using WTF method for the year 1996-2010.

3.7.2 Estimation of recharge using Rainfall Infiltration Factor Method (RIF)

The recharge estimated at the sub-basin scale using RIF method is shown in Figure 3.11. Three sub-basin S-11, S-14 and S-16 are observed to show varying responses during the study period. In sub-basin (S-11), the recharge is observed to be in the range between 13-34 cm which is relatively higher compared to other basins S-14 and S-16. The recharge in sub-basins S-14 and S-16 is observed to be closely similar with a range of 10-22 cm and followed similar increasing and decreasing trends. Figure 3.3 shows the SPI values and respective wet and dry year classification during the analysis period. The sub-basin S-11 experiences two extremely wet years and one severely dry year while the other sub-basins (S-14 and S-16) experienced one extremely dry year and no extremely wet phase. This may suggest that the increase in recharge in the upper sub-basin (S-11) may be due to multiple wet years in the recharge estimation period.

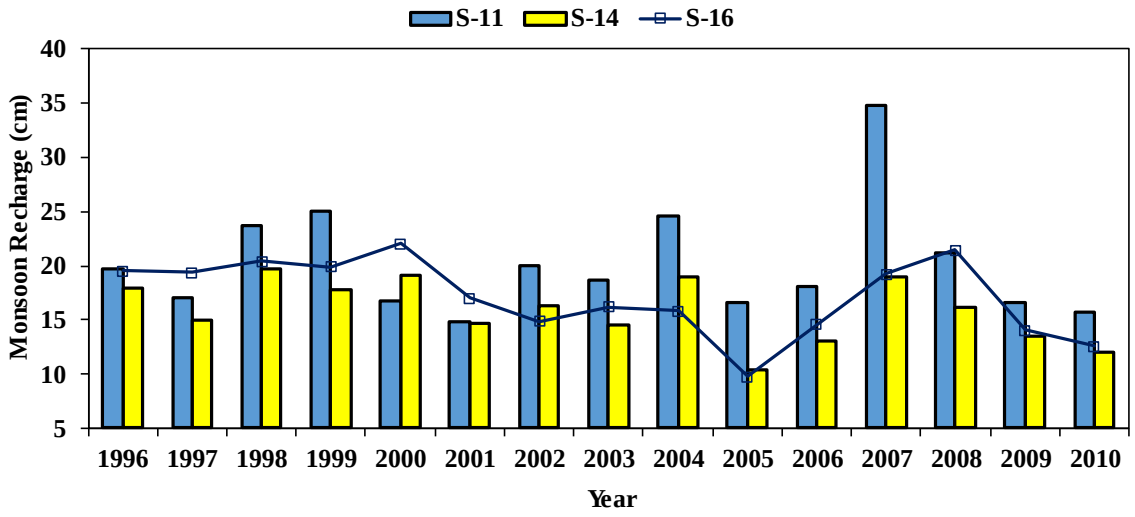

Figure 3.11: Estimated monsoonal groundwater recharge in (a) S-11 (b) S-14 (c) S-16 using RIF method for the year 1996-2010

3.7.3 Groundwater Recharge Estimation using A Semi-Distributed Hydrological Modelling (SWAT)

In order to predict monthly discharge as well as groundwater recharge at the sub-basin scale, SWAT modelling was carried out from 1970 to 2010 with a warm-up period of nine years. The development (Section A.1.3) and methodology flow chart (Figure A.1) of SWAT model can be found in appendix A. In this section, calibration and validation of the model, inter-comparison of simulated ET with observed ET and spatio-temporal variations of groundwater recharge are discussed.

3.7.3.1 Calibration and Validation

SWAT model was calibrated using the daily discharge data at Baltara gauging station for the time periods 1980-2010 and multiple simulations were carried out for successful model calibration. Groundwater Delay (GW_DELAY) and shallow groundwater storage (GWQMN) were found to be the most calibration parameters. Following the recommendation from previous works on similar basins [Haldar et al., 2014; Anand et al., 2018], the model simulations were performed at monthly scale. Figure 3.12(a) shows that the monthly discharge time series of measured and model-simulated values during the calibration period (1981-1990). It can be observed that general rising and falling trends are well captured by the model, however, over and underestimated the peaks for few years. The observations also show that the model performance is better estimated for the low flow period. The observed and simulated discharge values were compared and plotted

against each other for determining R^2, NSE and RMSE which is obtained as 0.85, 0.83 and 960 cumec respectively (Figure 3.12(c)).

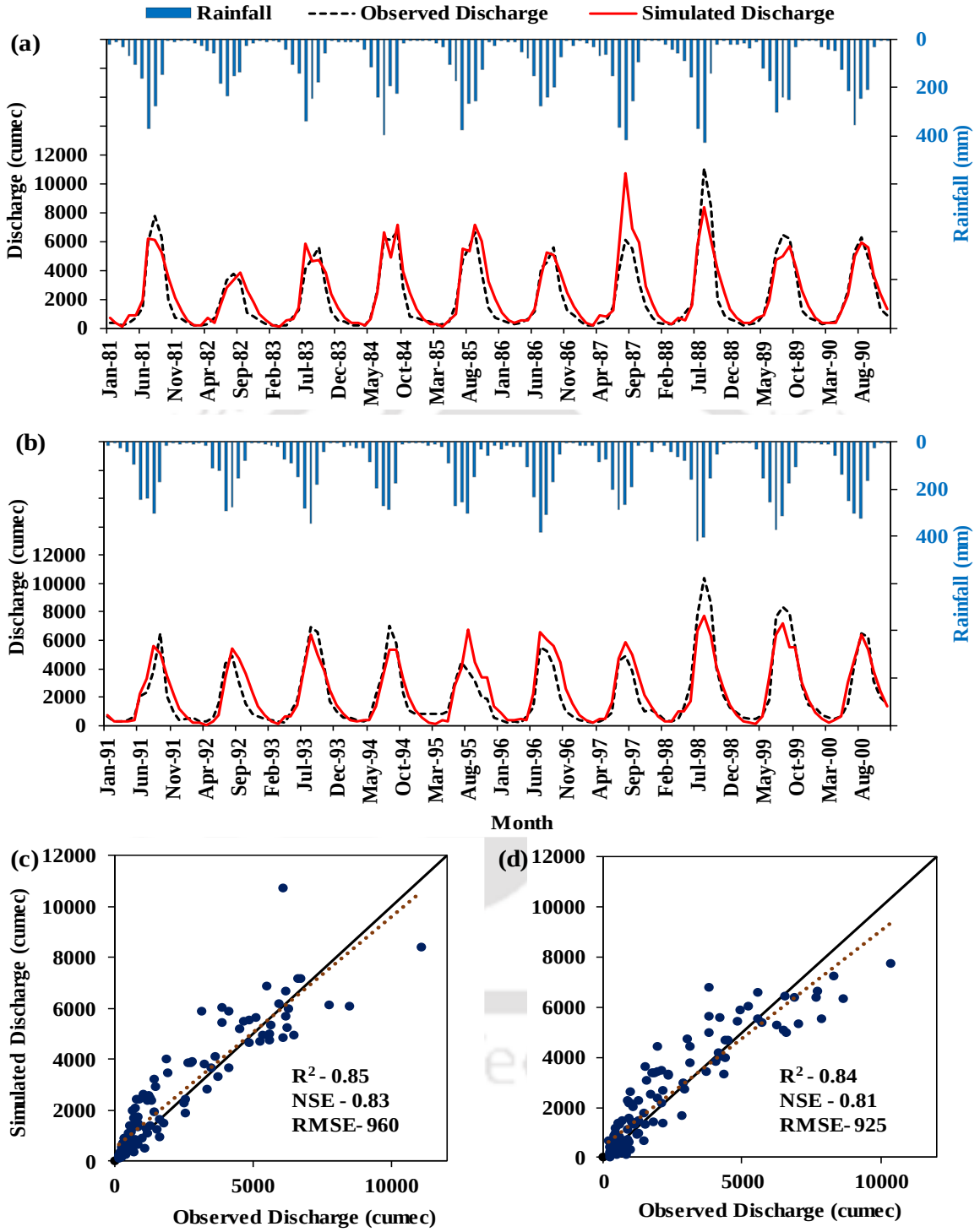

Figure 3.12: Comparison of observed and simulated discharge series for Kosi basin at Baltara gauging station during (a) calibration (1981-1990) and (b) validation period (1991-2000) (c) scatter plot during calibration period (d) scatter plot during the validation period

It is observed that the observed and simulated values are performed well for the discharge ranges from 0-2000 cumec and better for 2000-6000 cumec and poor correlation beyond 6000 cumec. These variations could be resulted from the uncertainty associated with the observed data. Further, the model was validated for the period 1991-2000 by comparing the measured and simulated monthly discharge values. Figure 3.12(b) and (d) show the inter-comparison and model performance of observed and simulated monthly discharge values. The analysis shows R^2, NSE, RMSE values of 0.84, 0.81, 925 cumec respectively which is found to be satisfactory.

3.7.3.2 Inter-Comparison of SWAT Simulated ET with Observed ET

Figure 3.13 shows box plots of observed satellite ET and simulated ET obtained using three available methods in SWAT model i.e. Penman Monteith (PM), Priestly-Taylor (PT) and Hargreaves methods (HG) in S-11, S-14 and S-16 for the period 1996-2010. In S-11, observed monthly ET has a minimum value of 31 mm whereas, SWAT simulated ET show highest deviations which reach up to 90% and this kind of similar ET simulated values can be observed in other sub-basins (S-14 and S-16) using all three methods. In the case of maximum value, the deviations of simulated ET from observed ET (113 mm) are 51% using PM, 40 % using PT and 29% using HG in sub-basin S-11. Whereas, these deviations are comparatively less i.e. 49, 31 and 31 % in S-14 and 49, 30 and 29% in S-16 using PM, PT and HG, respectively. It can also be observed that the basin has a median value of 71 mm (observed ET) whereas simulated ET has a range of 25-40 mm (43-64% deviations from the observed value) and these deviations are less in S-16 in comparison with other sub-basins. This analysis indicated that although HG method performed better than other methods, none of them yields better simulations to match with observed ET having high deviations in all sub-basins.

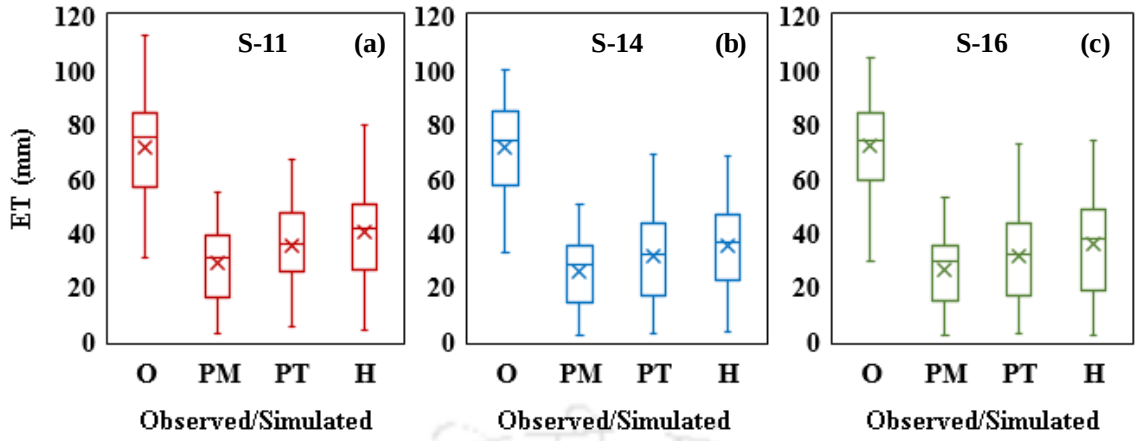

Figure 3.13: Box plots of monthly observed satellite ET and simulated ET using three available methods in SWAT model in (a) S-11; (b) S-14 and (c) S-16 for the period 1996-2010

***Note**:* O – Observed ET; PM – Simulated ET (Penman Monteith Method); PT – Simulated ET (Priestley-Taylor Method); H – Simulated ET (Hargreaves Method)

3.7.3.3 SWAT Simulated Recharge

Simulated SWAT monthly groundwater recharge variation for sub-basin 11 (S-11), sub-basin (S-14) and sub-basin (S-16) are shown in Figure 3.14. In order to understand the model behavior in predicting recharge, the monthly variation of recharge for a wet or dry year are compared with the monthly recharge variation of preceding year. In the case of S-11, 2007 was found to be extremely wet year and the preceding year (2006) was found to be mildly wet year. Similarly, 2009 was found to be a severely dry year and the preceding year (2008) was found to a mildly dry year respectively (section 3.4).

Figure 3.14(a) shows the monthly groundwater recharge variation in S-11, during 2006 (mildly wet year) and 2007 (extremely wet year). During September 2006, the maximum recharge is observed to be 20 cm which is around 50% of maximum rainfall (40 cm). Similarly, during July, 2007 the maximum recharge is observed to be 24 cm which is around 41% of maximum rainfall (59 cm) in 2007. This comparison is an indication of the over-prediction of modelled recharge during mildly wet year with respect to extremely wet year. The monsoonal recharge is noted to be 40 cm in mildly wet year (2006) which is 49% of monsoonal rainfall (82 cm) whereas in extremely wet year (2007), monsoon recharge is observed to be 61 cm which is 38% of monsoonal rainfall (158 cm). The comparison of monsoon recharge also clearly indicates the model has over-predicted the recharge in mildly wet year in compared to extremely wet year.

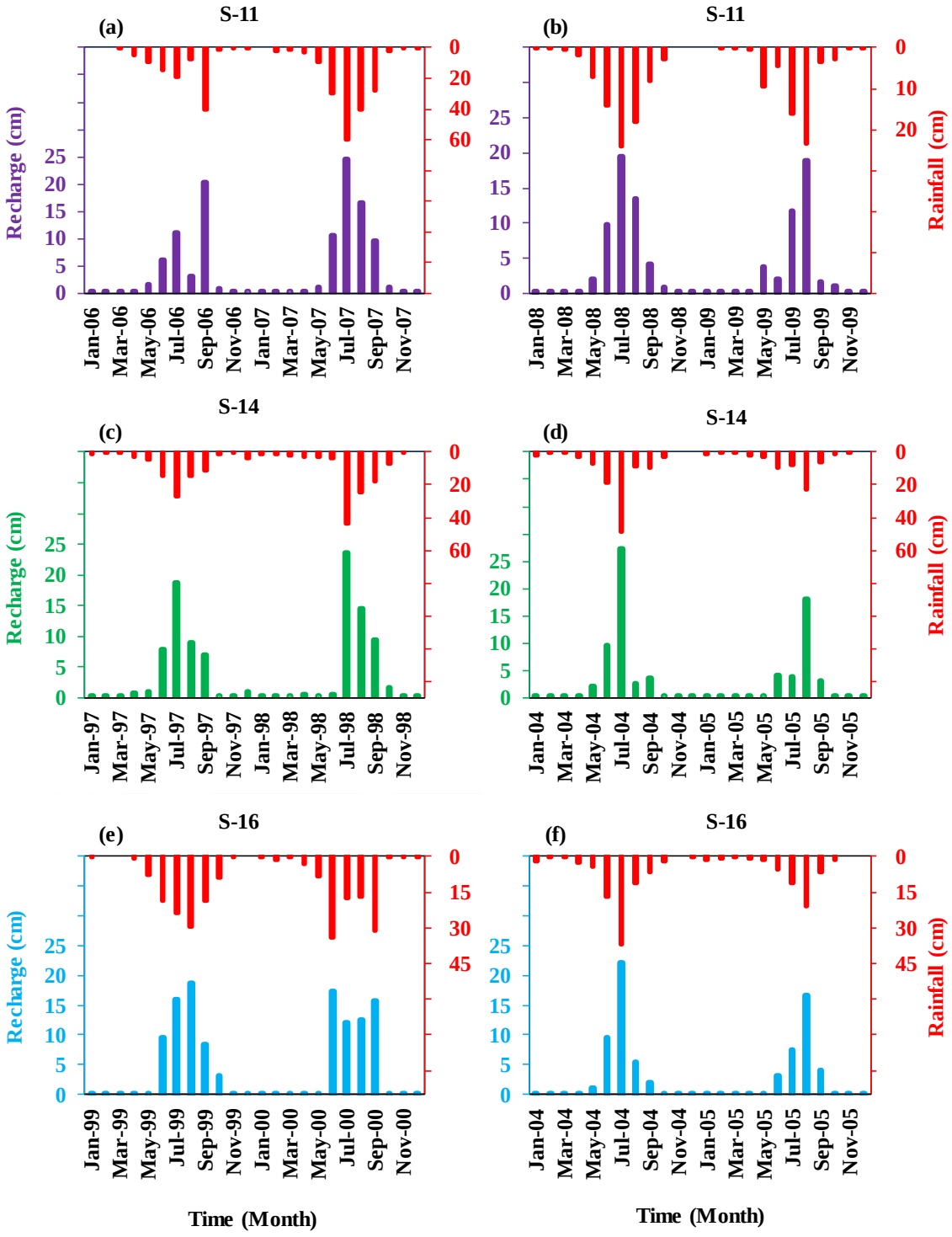

Figure 3.14: SWAT simulated monthly groundwater recharge in (a) S-11 (b) S-14 (c) S-16

Similarly, the monthly groundwater recharge variations for mildly dry year (2008) and severely dry year (2009) can be seen in Figure 3.14(b). In case of mildly dry year (2008), recharge has maximum value of 19 cm during June which is found be to 72% of maximum rainfall (24 cm). On the other hand, the maximum recharge value (18 cm) is

observed in August during severely dry year (2009) which is around 80% of maximum rainfall (23 cm). It indicates the over-prediction of recharge by the model during severely dry year over mildly dry year. In addition, monsoonal recharge is found be 46 cm in mildly dry year (2008) which is 72% of monsoonal rainfall (64 cm) whereas it is noted to be 34 cm which is 71% of monsoonal rainfall (47 cm). Monsoonal recharge comparison also clearly indicates the over-prediction of simulated recharge in severely dry year in compared to mildly dry year. This over-prediction of simulated recharge is resulted due to the under-prediction of actual evapotranspiration by the SWAT model (section 3.7.3.2).

Similar observations can be seen in case of sub-basin 14 (S-14) and sub-basin 16 (S-16) (Figure 3.4(c-f)). Table 3.4 shows the comparisons of maximum recharge and monsoonal recharge between wet or dry years along with the preceding year

Table 3.4: Sub-basin wise statistics of maximum and seasonal recharge

Sub-basin	**Sub-basin 14**		**Sub-basin 14**	
Year	**Mildly Dry Year (1997)**	**Moderately Wet Year (1998)**	**Mildly Wet Year (2004)**	**Extremely Dry Year (2005)**
Month	July	July	July	August
Rainfall (cm)	26	43	48	23
Recharge (cm)	18	23	27	18
Percentage of Rainfall as recharge (%)	69	53	56	78
Monsoon Rainfall (cm)	67	89	85	47
Monsoon Recharge (cm)	42	48	42	29
Percentage of Rainfall as recharge (%)	62	53	49	61
Sub-basin	**Sub-basin 16**		**Sub-basin 16**	
Year	**Mildly Dry Year (1997)**	**Moderately Wet Year (1998)**	**Mildly Wet Year (2004)**	**Extremely Dry Year (2005)**
Month	August	July	July	August
Rainfall (cm)	29	34	36	20
Recharge (cm)	18	17	22	16
Percentage of Rainfall as recharge (%)	62	50	61	80
Monsoon Rainfall (cm)	90	100	72	43
Monsoon Recharge (cm)	52	57	39	30
Percentage of Rainfall as recharge (%)	58	57	54	70

***Note:** Month corresponds to the maximum rainfall and recharge in a year and percentage of rainfall indicates how much rainfall is converted to recharge.

3.7.4 Estimation of recharge using SWB Method

Figure 3.15 shows the variability in different hydrological components of SWB method in different sub-basins for wet and dry years. In sub-basin 11 which is located in the upper side of the catchment, 2007 and 2009 are observed as wet and dry year. Figure 3.15(a-b) shows the variation of hydrological components in sub-basin 11 during wet and dry years. The cumulative values of ET are observed to be linearly increasing and relatively smooth as compared to rainfall values. In both wet and dry years although there is a significant difference in rainfall availability, the amount of ET is observed to be closely similar. Also, it is observed that during the low flow season of the year, the difference between rainfall and ET depth is not significantly varying for both dry and wet years where the difference is significant during monsoon season.

This infers that in the dry year the groundwater extractions are observed to be significantly high during the dry year for meeting the irrigation requirements. The total rainfall and ET are observed to be 150 and 70 cm for the extremely wet year whereas 80 and 80 cm for the dry year, while the total recharge for wet and dry year is observed to be 60 and 10 cm.

In S-14, 1998 and 2005 and in S-16, 2000 and 2005 are observed to be wet and dry years. In both the sub-basins, the total annual ET shows no significant change and remained closely same (85 cm). The relative difference in the rainfall availability during the dry year resulted in increased groundwater extraction to meet the irrigation demands. Figure 3.15(c-f) shows the changes in recharge due to the non-availability of sufficient rainfall during different seasons throughout the year. Also, it is observed that in comparison to the upper basin (S-11) the decrease in cumulative rainfall depth of middle (S-14) and lower basin (S-16) during dry years decreased the recharge, increased the groundwater extraction. The details of the recharge or extraction in the basin at various stretches, during various time period by different models is explained in section 3.8.

The results of the analysis show that while estimating the monthly groundwater recharge at the sub-basin scale, ET is observed to be one of the important components to be considered.

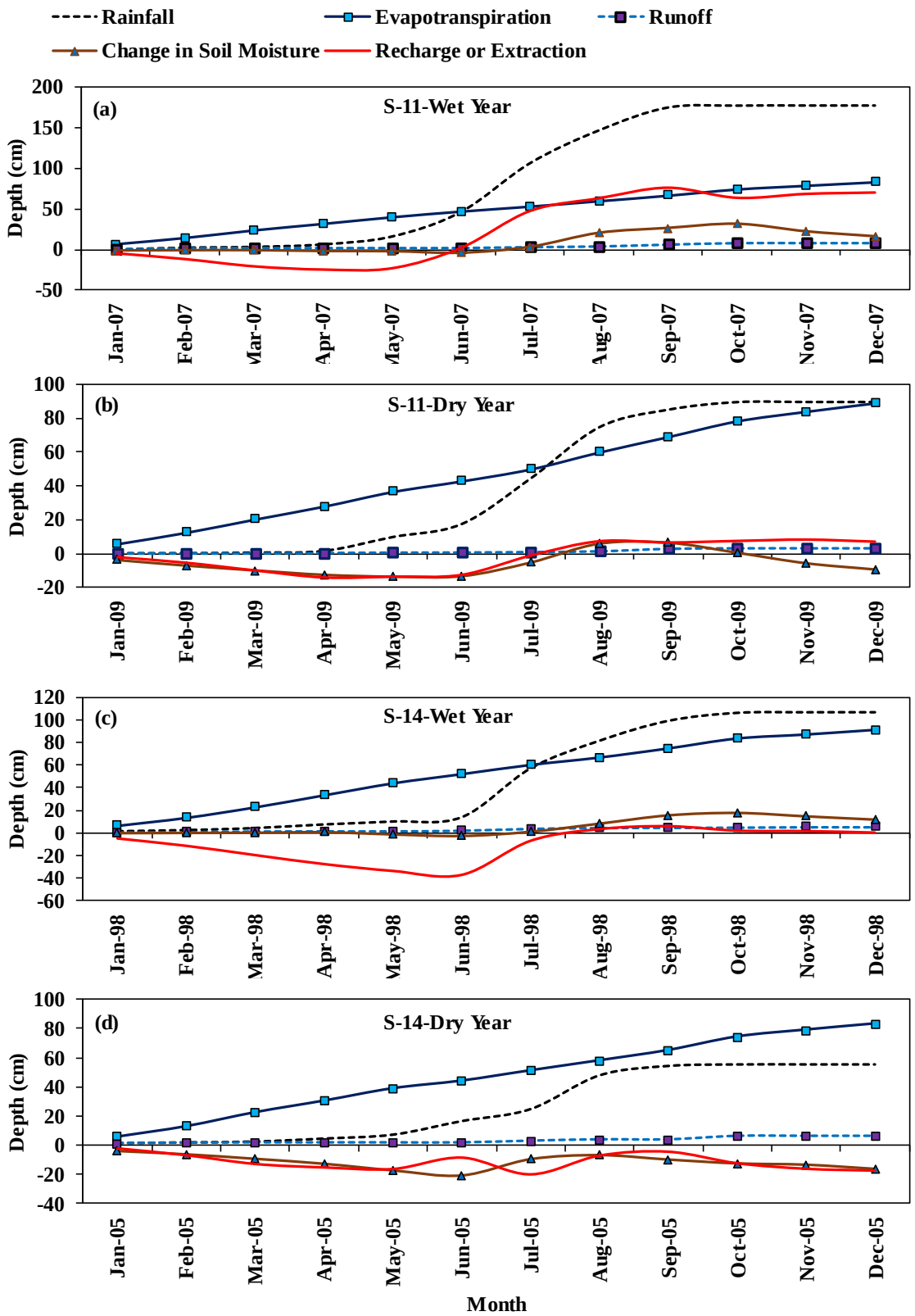
Rainfall
Evapotranspiration
Runoff
Change in Soil Moisture
Recharge or Extraction
(a)
S-11-Wet Year
(b)
S-11-Dry Year
(c)
S-14-Wet Year
(d)
S-14-Dry Year
Depth (cm)
Month
Jan-07
Feb-07
Mar-07
Apr-07
May-07
Jun-07
Jul-07
Aug-07
Sep-07
Oct-07
Nov-07
Dec-07
Jan-09
Feb-09
Mar-09
Apr-09
May-09
Jun-09
Jul-09
Aug-09
Sep-09
Oct-09
Nov-09
Dec-09
Jan-98
Feb-98
Mar-98
Apr-98
May-98
Jun-98
Jul-98
Aug-98
Sep-98
Oct-98
Nov-98
Dec-98
Jan-05
Feb-05
Mar-05
Apr-05
May-05
Jun-05
Jul-05
Aug-05
Sep-05
Oct-05
Nov-05
Dec-05

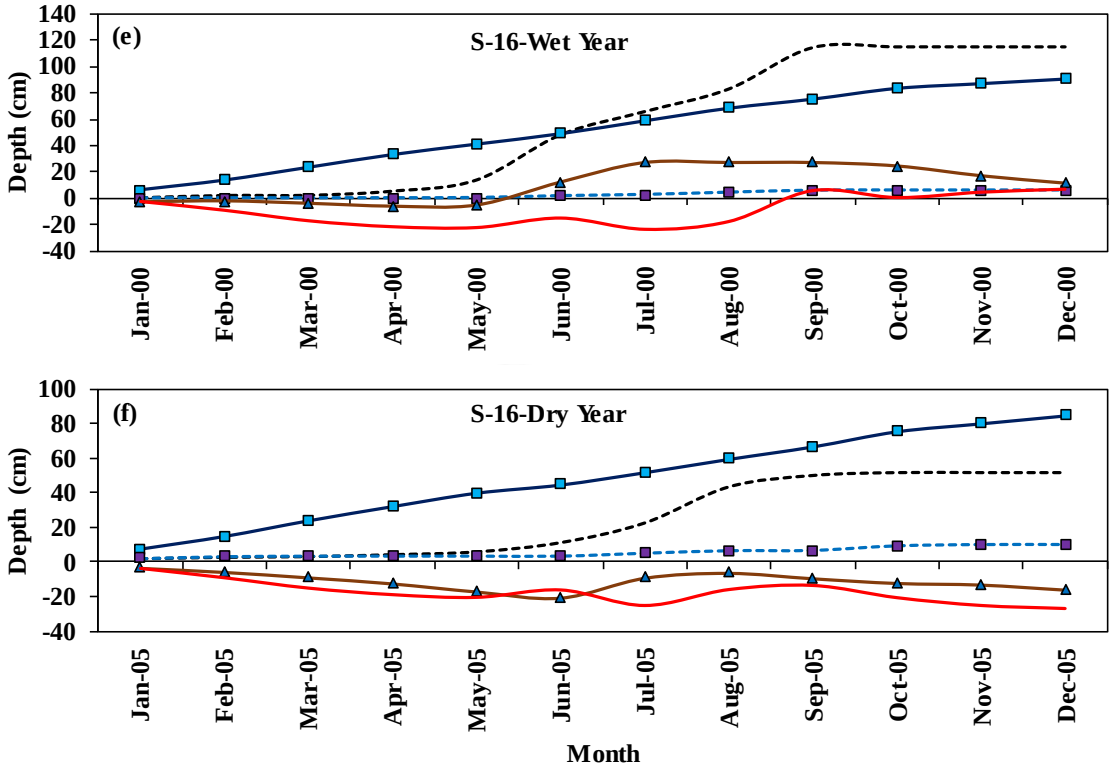

Figure 3.15: Cumulative plots of monthly rainfall, evapotranspiration, runoff, change in soil moisture and net recharge in S-11 during (a) wet year (b) dry year; in S-14 during (c) wet year (d) dry year; in S-16 during (e) wet year (f) dry year

3.8 COMPARISON OF ESTIMATED RECHARGE USING WTF, RIF, SWAT AND SWB

Figure 3.16 shows the monsoon recharge variability estimated using Water Table Fluctuation (WTF), Rainfall Infiltration Factor (RIF), Semi -distributed hydrological model (SWAT) and Soil water balance (SWB) methods. In the estimation period, it is observed that the maximum and minimum recharge estimated is 32 and 38 cm using WTF, 14 and 35 cm using RIF, 27 and 62 cm using SWAT and 14 and 98 cm using SWB method. It can be observed that there is no significant difference among the WTF computed recharge over the estimation period. Recharge estimated using RIF method followed a similar trend with rainfall observed over the basin. In S-11, 2007 and 2009 are observed as wet and dry years. In general, the maximum recharge corresponds to a wet year and minimum recharge corresponds to a dry year, which is observed true for WTF, RIF and SWB methods (Figure 3.16(a)). However, it is observed that SWAT estimated minimum and maximum recharge does not correspond to wet and dry years. In order to understand the agreement of estimated recharge with Central Groundwater Board (CGWB) computed recharge an inter-

comparison was carried out with the available CGWB data (for the years 2004 and 2009). This shows that recharge computed using WTF method closely resembles with CGWB computed recharge in 2009, RIF method in 2004 and SWB method in 2004. Whereas, no such close agreement is observed with SWAT.

Inter-comparison of estimated recharge using the four methods for sub-basins 14 and 16 shows similar observations as sub-basin 11 (Figure 3.16 (b-c)). In the case of sub-basin 14, wet and dry years are observed to be 1998 and 2005. The maximum recharge corresponds to the wet year and minimum recharge corresponds to dry year is observed true for RIF and SWB methods. Whereas, it is not followed the same behavior in case of WTF and SWAT estimated recharge. An inter-comparison carried out with the available CGWB data shows that recharge computed using WTF method closely resembles with CGWB computed recharge in 2004 and 2009 and SWB method in 2009. Whereas, no such close agreement is observed with RIF and SWAT estimated recharge. In the case of sub-basin 16, In S-16, 2000 and 2005 are observed as wet and dry years in the estimation period. It is observed that the maximum recharge corresponds to wet year and minimum recharge corresponds to dry year in case of RIF and SWB methods whereas WTF and SWAT estimated recharge does not show the maximum and minimum corresponds to wet and dry years. Inter-comparison of estimated recharge with the available CGWB data shows that recharge computed using WTF method closely resembles with CGWB computed recharge in 2004 and SWB method in 2009. Whereas, no such close agreement is observed with RIF and SWAT.

Figure 3.17 shows the comparative analysis of monthly recharge/extraction estimated using SWAT and SWB methods for wet and dry years. It can be observed that the general trend in SWAT computed recharge remained positive in any season of wet and dry year whereas, SWB method shows variability in recharge i.e. either positive (recharge) or negative (extraction) at different seasons depending on rainfall and other hydrological parameters. In SWB method, in wet year negative recharge or extraction is observed during non-monsoon periods, while in the dry year the extractions observed in both monsoon and non-monsoon periods may be resulting due to inadequate rainfall for meet the irrigation requirements. The analysis of recharge plots (Figure 3.17) shows that the peak value of recharge during the monsoon period corresponds to the peak value of the rainfall. In the case of SWAT simulated recharge, the peak value in recharge is observed to be between 12-25 cm in both wet and dry years irrespective of the rainfall pattern. Whereas, SWB

method shows the variability in recharge/extraction of in the range of 45 cm in wet years and -10 cm (extraction) in dry years depending on the availability of the rainfall.

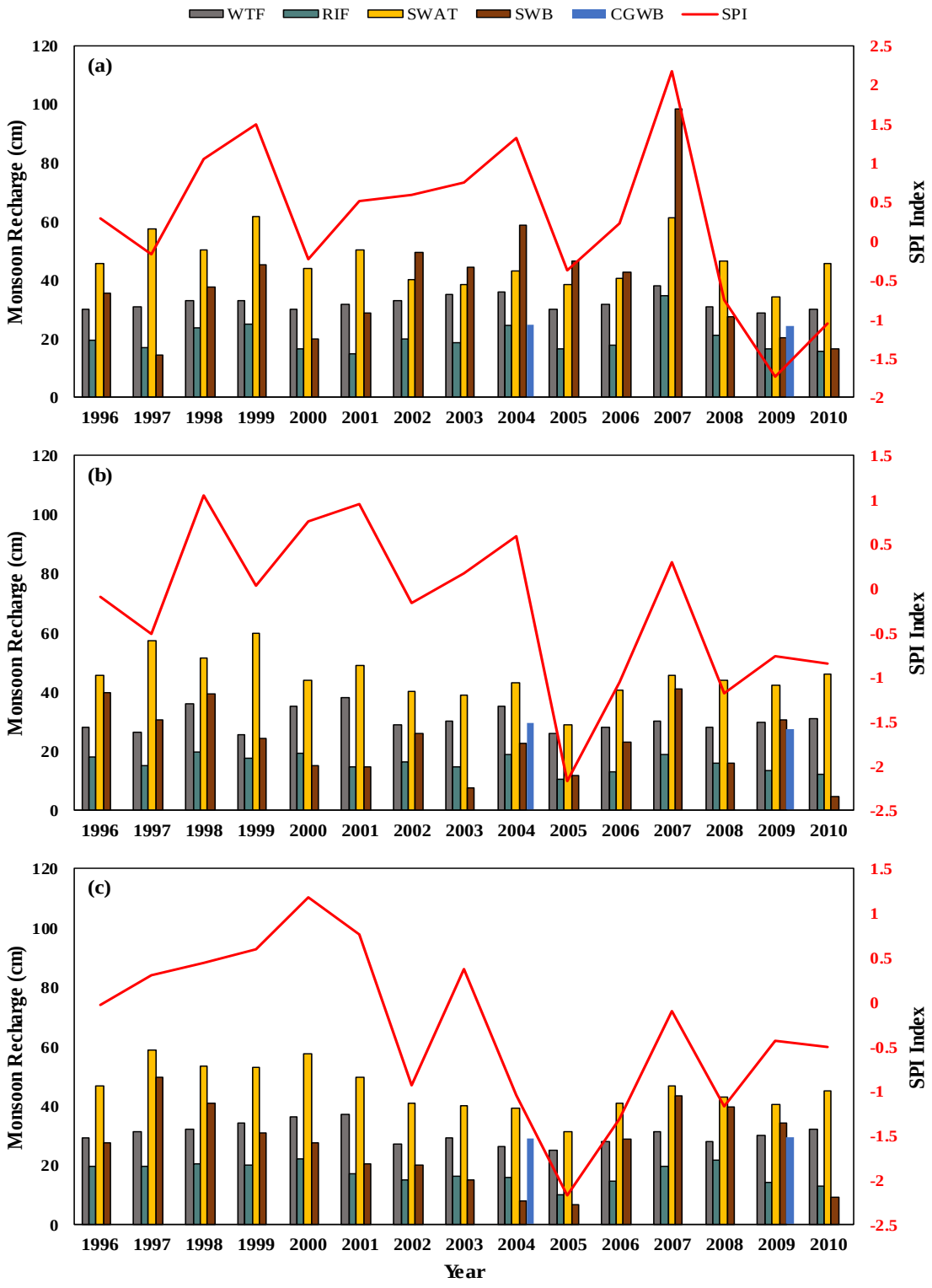

Figure 3.16: Monsoon Recharge estimated in (a) S-11 (b) S-14 (c) S-16 using WTF, RIF, SWAT, SWB and CGWB method along with SPI index of rainfall

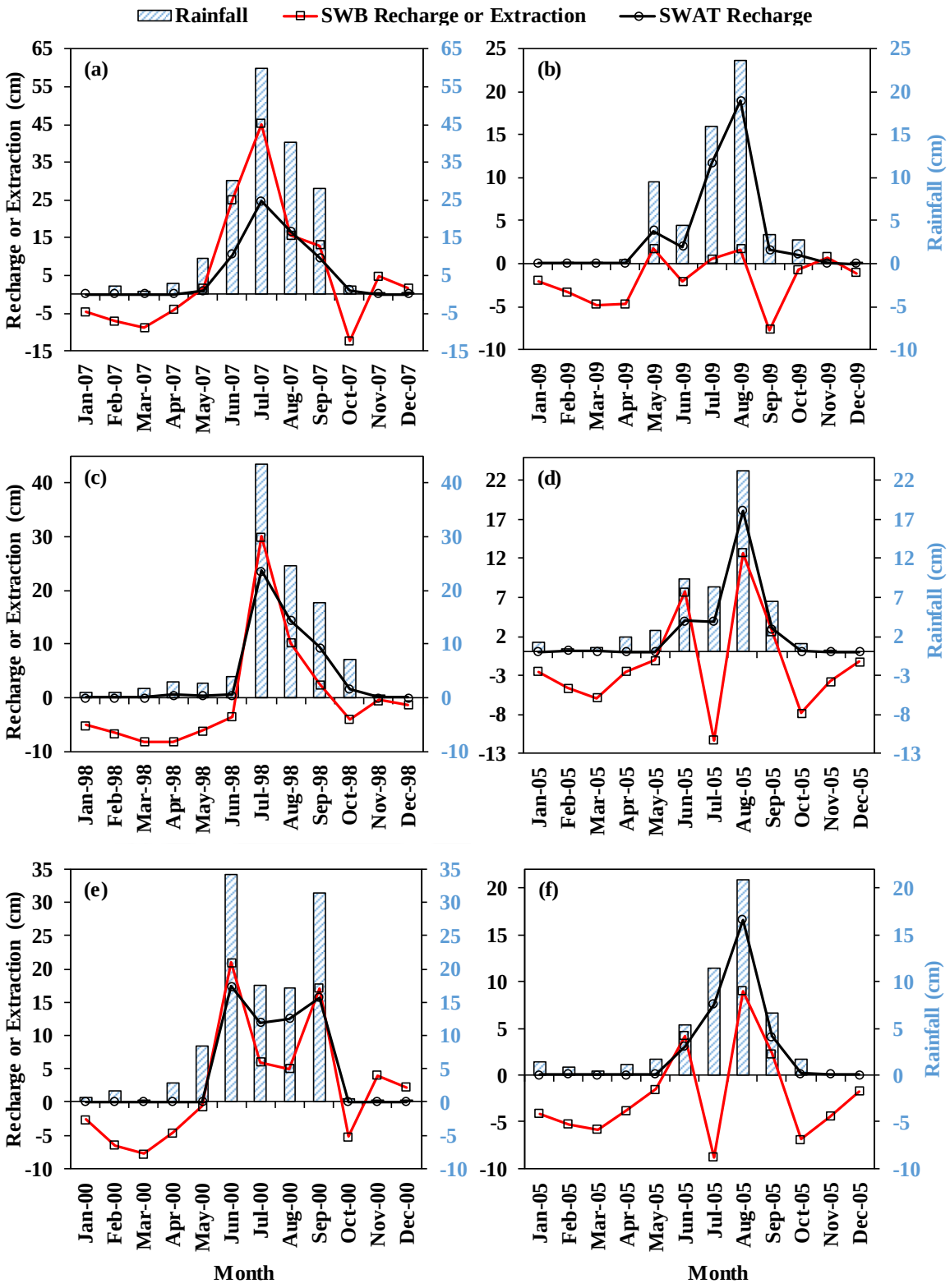

Figure 3.17: Monthly recharge or extraction using SWB and SWAT in S-11 during (a) extremely wet period (2007), (b) extremely dry period (2009); in S-14 during (c) extremely wet period (1998), (d) extremely dry period (2005); in S-16 during (e) extremely wet period (2000), (f) extremely dry period (2005)

3.9 CONCLUSIONS

In the present study, the monthly and seasonal groundwater recharge was estimated for Kosi river basin, India. Four different methods namely, Water Table Fluctuation (WTF) and Rainfall Infiltration Factor (RIF), Soil and Water Assessment Tool (SWAT) and Soil Water Balance (SWB) were used for seasonal as well as monthly groundwater recharge computations. The results provided insights in groundwater recharge estimation using different methods for effective groundwater management in highly irrigation dominated region. The results of the study lead to the following conclusion.

1) Prior to the estimation, the factors affecting groundwater recharge such as rainfall, landuse/landcover and evapotranspiration were analyzed. Analysis of rainfall variations indicated that there was an average of six-year cyclic period for the wet year and nine-year cyclic period for the dry year over the 29 years of the analysis period (1982-2010).
2) LULC change analysis for the year 1985-2005 indicated that there was no significant change in the LULC in the study region, which was mostly dominated by agricultural lands (90%).
3) Spatio-temporal variations of evapotranspiration (ET) derived from satellite data were analyzed from the year 1982-2010. It was observed that daily average ET varied from 1.16-3.78 mm/day and 0.62-3.98 mm/day during the year 1982-83 and 1998-99, respectively. It was observed that there was a shift of one month in the cropping pattern from October to September during the study period (1982-2010).
4) The seasonal groundwater estimation results showed that WTF method considered the fluctuations in groundwater levels whereas RIF method simply followed the rainfall patterns. But both the methods did not able to capture the wet and dry year impacts on groundwater recharge.
5) The surface water hydrological model (SWAT) was calibrated and validated with the observed monthly discharge time series to get the monthly groundwater recharge at the sub-basin scale. In the modelling study, it was found that groundwater delay and shallow groundwater storage were found to be the most sensitive calibration parameters.
6) The Actual Evapotranspiration (AET) obtained from SWAT model was compared with observed satellite ET data and it was observed that the model was under

predicted the AET i.e. 38% of observed AET. In order to do water balancing, SWAT model over-predicted monthly groundwater recharge at all the sub-basins.

7) A monthly Soil Water Balance (SWB) method was employed to estimate monthly groundwater recharge at sub-basin scale using remote sensing-based satellite datasets such as precipitation, evapotranspiration, soil moisture along with runoff obtained from SWAT model. Monthly groundwater recharge obtained from SWB method well-captured variations in the groundwater heads during wet and dry spells.
8) Inter-comparisons of monsoonal groundwater recharge estimations using four different methods reveals that maximum and minimum recharge corresponds to wet and dry years in case of RIF and SWB methods whereas, it is not followed the similar behavior in case of WTF and SWAT. Also, an inter-comparison carried out with the available CGWB data shows that recharge computed using WTF method closely resembles with CGWB computed recharge in 2004 and 2009 and SWB method in 2009. Whereas, no such agreement is observed with RIF and SWAT estimated recharge.

As the observed monthly groundwater recharge is not available at the sub-basin scale, the validation of recharge (estimated using SWAT model and SWB methods) for Kosi basin is attempted in further sections (section 5.7.1. and 5.7.2) using groundwater flow modelling.

4

ESTIMATION OF FLUID FLUX AND HYDRAULIC CONDUCTIVITY

4.1 INTRODUCTION

River-Aquifer interaction is a natural process and complex phenomenon which occurs in and across hyporheic zone [Winter et al., 1998; Boano et al., 2014; Anibas et al., 2016]. Major factors that influence this exchange rate are the distribution of hydraulic head between river and aquifer and the distribution of hydraulic conductivity of the riverbed [Doppler et al., 2007]. Determination of fluid flux and sediment hydraulic bed conductivity plays key role in understanding and quantifying river-aquifer interaction process and helps for effective sustainable water management [Winter, 1995; Kalbus et al., 2006; Keery et al, 2007; Ivkovic, 2009; Naganna et al., 2017; Shamsuddin et al., 2019].

Various methods and techniques have been reported by many researchers for the assessment of river-aquifer exchange flux at a different scale. Direct seepage measurements [Landon et al., 2001; Rosenberry, 2008; Brodie et al., 2009], analytical and numerical modelling techniques [Vasiliev, 1987; Workman et al., 1997; Lautz and Siegel 2006; Cho et al., 2010; Baalousha, 2012], numerical modelling techniques [Brunner et al., 2010; Sun et al., 2015; Semiromi and Koch, 2019] and application of environmental isotopes [Katz et al., 1997; Kumar et al., 2008; Gao et al., 2010; Paces and Wurster, 2014; Zhao et al., 2018] are widely used. Over past few decades, scientific interest has increased on the application of heat as environmental tracer to identify and quantify the river-aquifer exchange flux in hyporheic zone [Taniguchi, 1993; Johnson et al., 2005; Baskaran et al., 2009; Bartsch et al., 2014; Zhang et al., 2018]. Using heat as a tracer is an inexpensive but effective

methodology for determining the interaction exchange rate at different spatial and temporal scales [Anderson, 2005].

In order to quantify the river-aquifer exchange flux using riverbed temperature measurements, various methods have been employed for solving the coupled water and heat advection-dispersion equation [Suzuki, 1960; Bredehoeft and Papadopoulos, 1965; Schmidt et al., 2006]. Stallman [1965] proposed a one-dimensional solution to estimate seepage flux using streambed temperature measurements. In recent studies, Hatch et al. [2006] and Keery et al. [2007] followed Stallman's approach using amplitude ratio and phase difference methods.

Characterizing the physical environment of river-aquifer systems is an important aspect to be considered for the accurate assessment of river-aquifer estimation. Riverbed hydraulic conductivity is one among the riverbed characteristics that significantly influence the assessment of river-aquifer interaction process [Kalbus et al., 2009; Naganna et al., 2017]. Estimation of riverbed hydraulic conductivity is a challenging task for conceptualizing riverbeds in numerical models to quantify the river-aquifer exchange flux [Brunner et al., 2017].

In the present study, laboratory-based experiments were conducted in a soil column for measuring vertical thermal profiles at different depths in order to estimate fluid flux through Sediment-Water Interface (SWI) using analytical solutions of Keery and Hatch (amplitude ratio method and phase difference method). In order to understand the variation in fluid flux for different conditions, a series of experiments were conducted with four different scenarios (soil combinations, temperature gradients (gradient between hot water and normal water) and ponding depths. Riverbed hydraulic conductivity of different soil layers was determined using these estimated fluxes. Finally, effective hydraulic conductivity of the soil column was calculated from the estimated hydraulic conductivities of different soil layers and were further used for calculating riverbed conductance for groundwater modelling purpose (chapter 5).

4.2 MATERIALS AND METHODS

4.2.1 Laboratory Experimental Setup

A sandbox, having dimensions of 80 × 120 × 150 cm was designed and used for conducting experiments in a laboratory to measure vertical temperature profiles in a soil

column (Figure 4.1). The experimental setup is fully transparent and made up of acrylic sheet of thickness 1.2 cm and it is supported with frameworks around the walls. It has two separate inlets, provided on the right-side wall at a height of 20 and 22.5 cm from the top of the sandbox for injecting normal and hot water. An outlet is provided on the left side wall at a height of 10 cm from the bottom of the sandbox to allow seepage through soil column and up to this height, the sandbox is filled with coarse sand layer as filling material. Over this layer, a soil column of three different layers of varying thickness is placed in the sandbox in which temperature measurements are made at different vertical depths below the soil column while the fluid flux is passing through it. Fine Sand I (FS I), Fine Sand II (FS II) and Medium Sand (MS) are used to fill the soil layers in four different soil layer combinations or scenarios (Table 4.1). In all the four scenarios, it is maintained that the top and middle layers consist of 30 cm thick soil layer whereas the bottom layer consists of 50 cm thick soil layer. The entire soil column is made saturated and allowed water to be ponded to the required depth over the soil column before starting the experiment.

Table 4.1: Layer combinations of four different scenarios

Layer Position	Layer No	Scenario 1 (S1)	Scenario 2 (S2)	Scenario 3 (S3)	Scenario 4 (S4)
Top	Layer 1	Fine Sand I (FS I)	Fine Sand II (FS II)	Medium Sand (MS)	Medium Sand (MS)
Middle	Layer 2	Fine Sand II (FS II)	Fine Sand I (FS I)	Fine Sand I (FS I)	Fine Sand II (FS II)
Bottom	Layer 3	Medium Sand (MS)	Medium Sand (MS)	Fine Sand II (FS II)	Fine Sand I (FS I)

4.2.2 Temperature measurements using T-lance

Temperature profiles below the soil column are measured using the temperature measuring rod (T-lance) manufactured by Umwelt- und Ingenieurtechnik GmbH Dresden, Germany. It can measure temperature ranging between -20°C to 50°C, has a resolution of 0.004°C and typo accuracy +/- 0.07°C. The equipment is integrated with a data logger and GPRS/GSM data transmission unit. T-lance has a sensor rod of 3 cm diameter and 120 cm long, provided with a data logger of cable length of 500 cm. It consists of 8 temperature measuring sensors placed at different spacing as shown in (Figure 4.1).

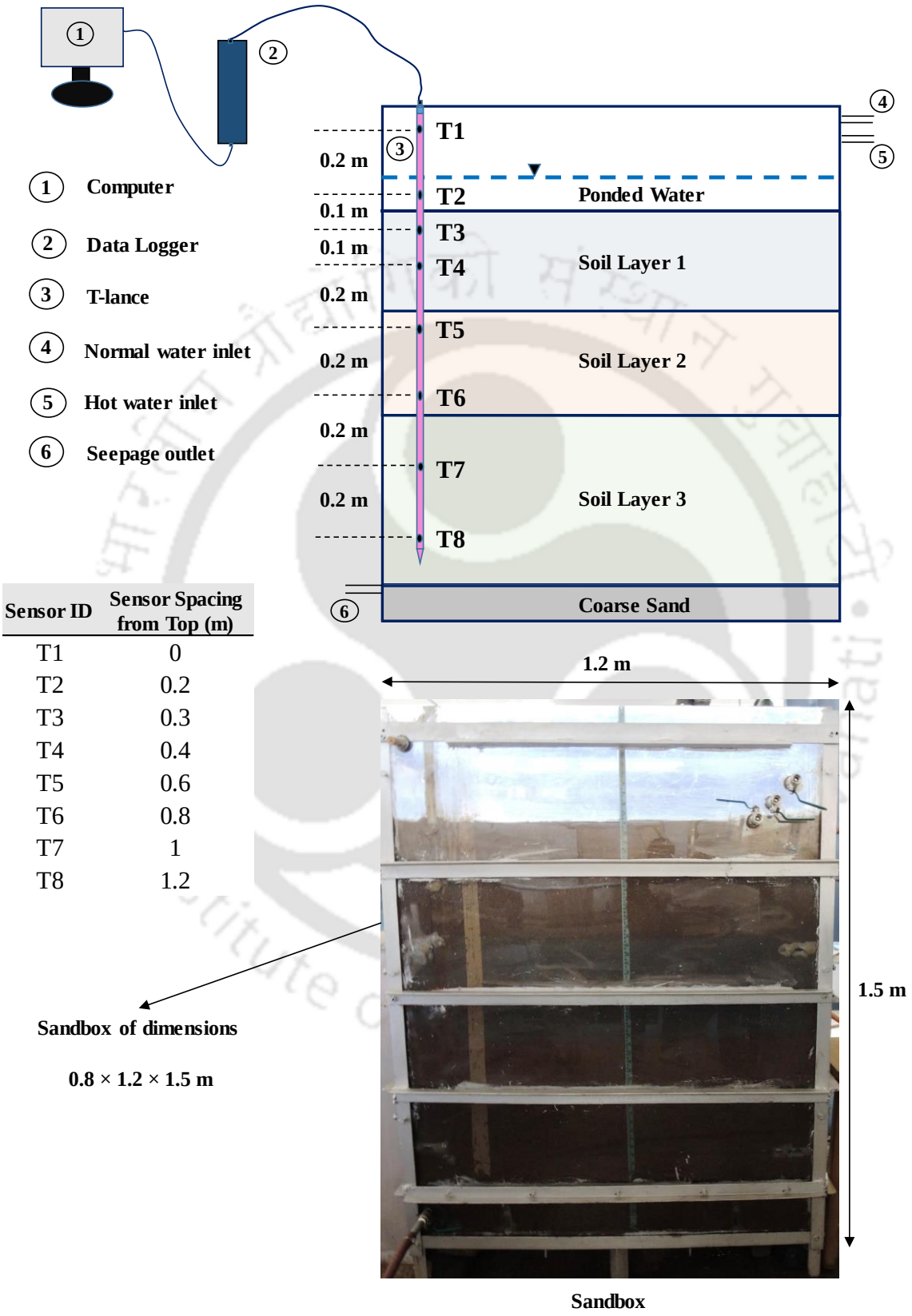

Sensor ID	Sensor Spacing from Top (m)
T1	0
T2	0.2
T3	0.3
T4	0.4
T5	0.6
T6	0.8
T7	1
T8	1.2

Figure 4.1: Experiment setup and T-lance instrument along with data logger (not to scale)

In all the experiments, T-lance is placed inside the soil column towards the left side wall, nearer to the outlet to ensure the one-dimensional vertical flow (in order to utilize the proposed analytical solutions (section 4.3)). The T-lance sensor rod is positioned vertically in the soil column such that its top sensor (T1) is positioned in air; second sensor (T2) is positioned 5 cm above the soil column (in ponding water) to measure the water temperature; third, (T3) and fourth sensor (T4) are positioned in top soil layer; fifth (T5) and sixth (T6) sensors are positioned in middle soil layer; seventh (T7) and eighth (T8) are positioned in bottom soil layer to measure soil temperatures (Figure 4.1). The SENSOlog software, provided with the T-lance instrument is used to extract the data (time-series data of measured temperature profiles at various sensors) transmitted through data logger.

4.2.3 Soil Layer Combinations or Scenarios

Sandbox experiments are conducted for four different soil layer combinations or scenarios. In Scenario 1, Fine Sand I, Fine Sand II and Medium Sand are placed in top (first), middle (second) and bottom (third) layers, respectively. Whereas, these top (FS I) and middle layers (FS II) are shuffled in Scenario 2 keeping the bottom layer (MS) unaltered. In Scenario 3, MS, FS I and FS II are used in the top, middle and bottom layers whereas the middle (FS I) and bottom (FS II) layers are shuffled keeping the top layer (MS) unaltered in Scenario 4. Total sixty-four experiments (sixteen experiments in each scenario) were conducted with varying ponding depths (10, 11, 12 and 13 cm) and temperature gradients (gradient between ponding water and hot water) of 2°.4°, 6° and 8°C (Table 4.2).

4.2.4 Soil Characteristics

Determination of river bed hydraulic conductivity is one of the important aspects of river-aquifer interaction studies for any watershed. Kosi river is chosen for this study and determination of its bed conductivity is aimed in this chapter from the fluid fluxes estimated using temperature profiles measured through sandbox experiments. As Kosi river bed material is composed of fine sands and medium sands with mean diameter (d_{50}) of 0.23 (Burele el al., 2014), a similar type of sands were used in the experimental study. However, actual representation of aquifer in a sandbox is very difficult. The aquifer is made up of distributed sample, but the soil characteristics/properties of the material used in the sand box represents well the aquifer, hence the error in the results would be minimal.

Three different soil layers i.e. Fine Sand I (FS I), Fine Sand II (FS II) and Medium Sand (MS) placed in the sandbox were obtained from two different soil categories having

d_{50} of 0.2 and 0.22. Fine Sand I and Medium Sand were obtained from one source whereas, Fine Sand II was obtained from the second source. Specific gravity, porosity and thermal properties of these sands are shown in Table 4.3. Whereas, particle size distribution curves and the soil properties of two soil sample sources can be seen in Figure B.2 and Table B.1 (Appendix B).

Table 4.2: Experimental plan for the four Scenarios

Set	Ponding Depth (cm)	Scenario 1	Scenario 2	Scenario 3	Scenario 4
A	10	S1-A1	S2-A1	S3-A1	S4-A1
		S1-A2	S2-A2	S3-A2	S4-A2
		S1-A3	S2-A3	S3-A3	S4-A3
		S1-A4	S2-A4	S3-A4	S4-A4
B	11	S1-B1	S2-B1	S3-B1	S4-B1
		S1-B2	S2-B2	S3-B2	S4-B2
		S1-B3	S2-B3	S3-B3	S4-B3
		S1-B4	S2-B4	S3-B4	S4-B4
C	12	S1-C1	S2-C1	S3-C1	S4-C1
		S1-C2	S2-C2	S3-C2	S4-C2
		S1-C3	S2-C3	S3-C3	S4-C3
		S1-C4	S2-C4	S3-C4	S4-C4
D	13	S1-D1	S2-D1	S3-D1	S4-D1
		S1-D2	S2-D2	S3-D2	S4-D2
		S1-D3	S2-D3	S3-D3	S4-D3
		S1-D4	S2-D4	S3-D4	S4-D4

Note: Temperature gradient between normal water and hot water in A1, B1, C1, D1 is 2°C; A2, B2, C2, D2 is 4°C; A3, B3, C3, D3 is 6°C and A4, B4, C4, D4 is 8°C

Table 4.3: Thermal and geotechnical properties of different sand layers and fluid

Soil Layer	K (W/mK)	D (mm^2/s)	C (J/kg◦C)	C_f (J/kg◦C)	ρ (kg/m^3)	ρ_f (kg/m^3)	G	n
Medium Sand (MS)	1.52	0.71	1159.87		2098.80		2.64	0.33-0.44
Fine Sand I (FS I)	1.57	0.61	1281.46	4186	2008.90	1000	2.68	0.42-0.44
Fine Sand II (FS II)	1.56	0.57	1415.91		1940.80		2.71	0.40-042

Note: **K**- Thermal conductivity; **D**- Thermal diffusivity; C -bulk heat capacity of saturated sediment; C_f - heat capacity of fluid; ρ -Bulk density of saturated sediment; ρ_f - density of fluid; **G**- Specific Gravity; **n** – Porosity.

4.2.5 Experiment Procedure

For all the experiments, the sandbox was filled with layers of the sand and saturated using normal water. A consistent ponding depth of h cm was maintained over the soil column by allowing the seepage through the outlet. At stage 1, hot water (T_0°C) was injected and continuous flow between the sand layers was maintained by allowing the seepage. The hot water supply was stopped as the temperature of ponding water reaches to the required temperature gradient. At stage 2, the normal water was injected continuously to maintain constant ponding depth by allowing outlet seepage throughout the experiment. Measured temperature time series data was extracted using SENSOlog software from the data logger and using analytical solutions of Hatch and Keery fluid fluxes were estimated (Hatch et al., 2006, Keery et al., 2007).

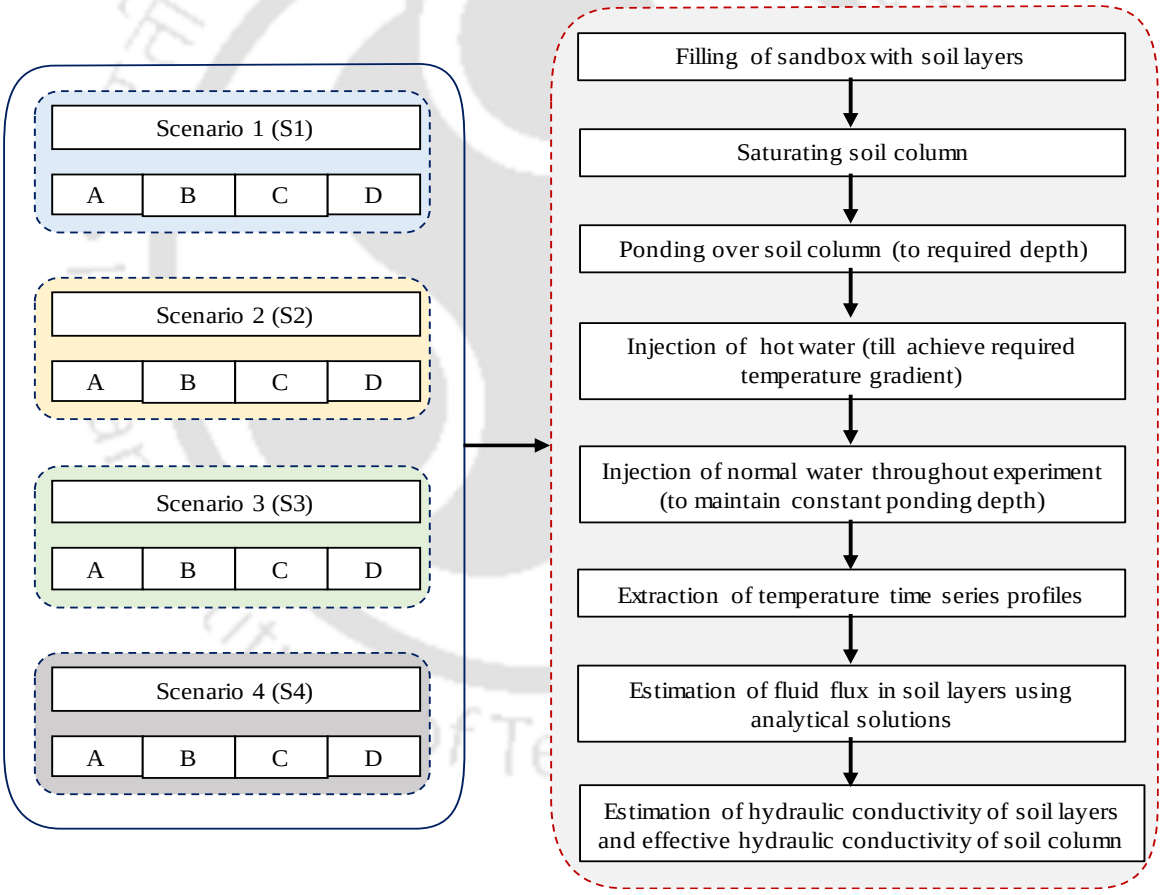

Figure 4.2: Experimental Scenarios and methodology used for fluid flux and hydraulic conductivity estimation

4.2.5.1 Initial Parameters to be Determined/Estimated

1) d_{50} value of sand particles was found by carrying sieve analysis of soil
2) Porosity (n) of all the soils was determined to calculate the void ratio.

3) Specific gravity of all the soil layers was determined using a density bottle method to determine the saturated bulk density of the soil column.
4) Thermal conductivity, specific heat, thermal diffusivity of all the soils were determined using KD2 probe.

4.3 ESTIMATION OF FLUID FLUX USING HATCH AND KEERY ANALYTICAL SOLUTIONS

In this study, two transient temperature profiles methods of Hatch and Keery [Hatch et al., 2006, Keery et al., 2007] were used to estimate the fluid flux through the SWI. Both these methods are derived from the analytical solutions of Stallman [1965]. He described the solutions along a one-dimensional half-space, transient temperature with a periodic temperature boundary condition at upper boundary or origin (Figure 4.3). Sediment underlying a waterbody could be utilized as half-space. SWI is considered as the origin of half-space where the time boundary condition is imposed. When water and its associated heat is transported through the subsurface, thermal fronts create along the SWI due to periodic temperature changes. The assumptions (provided by Stallman) included in this study can be found in the appendix (section B.4)

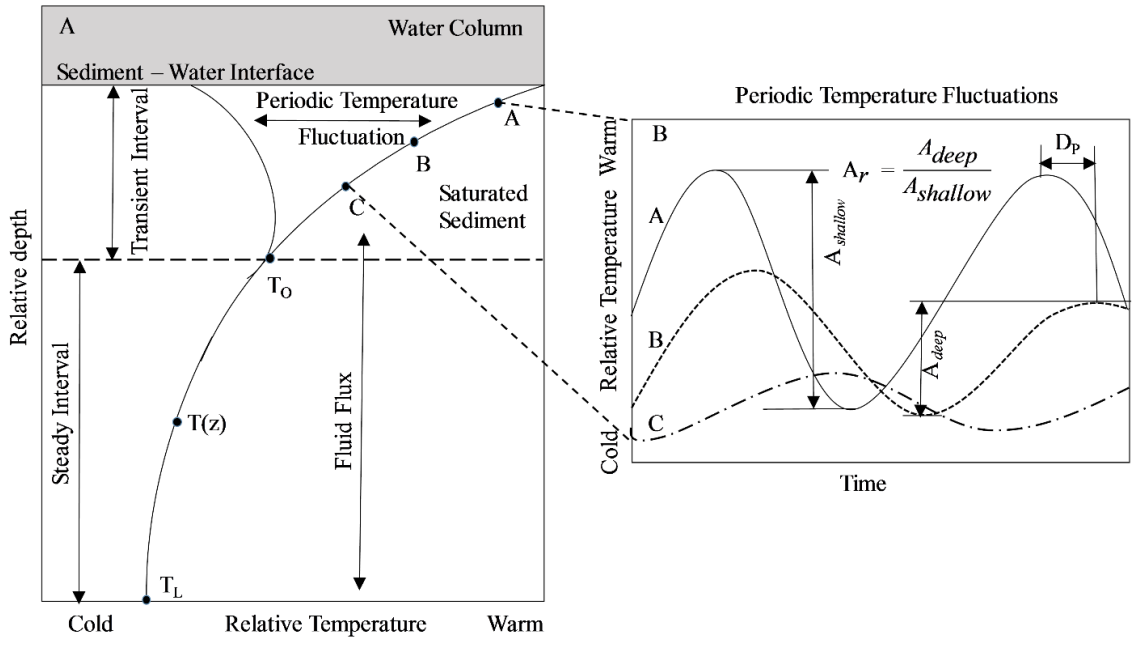

Figure 4.3: Conceptual model of thermal profile within saturated sediment underneath a surface water body experiencing a periodic temperature fluctuation and (B)conceptual temperature time series at three observation points (A, B, C) along the transient section of the thermal profile. Note*:* After Swanson and Cardenas [2011].

4.3.1 Hatch Amplitude Ratio (AR) and Phase Difference (PD) Method

Ratio of amplitude (A_r) and the difference in phase (D_p) of periodic temperature signals between two points are used to estimate the thermal frontal velocity (V_{Ar}). It is given as

$$V_{Ar} = \frac{2k_e}{\Delta z} \ln A_r + \sqrt{\frac{(V_{Ar}{}^4 + (8\pi k_e)^2)^{1/2} - V_{Ar}{}^2}{2}} \qquad (4.1)$$

where,

Δz is vertical sensor spacing (m);

A_r is the ratio of amplitudes of the temperature time series of deeper sensor divided by that of the shallow sensor;

P is the oscillation period (s);

k_e is the effective thermal diffusivity ($m^2 s^{-1}$).

Thermal diffusivity is given by

$$k_e = \frac{\lambda_e}{\rho c} = \frac{\lambda_o}{\rho c} + \beta |V_f| \qquad (4.2)$$

where,

λ_e is the effective thermal conductivity ($Wm^{-1} \circ C^{-1}$);

ρ is the bulk density of the saturated sediment system (kgm^{-3});

c is the bulk heat capacity the saturated sediment system ($Jkg^{-1} \circ C^{-1}$)

λ_o is the baseline thermal conductivity ($Wm^{-1} \circ C^{-1}$);

β is the thermal dispersivity (m)

V_f is the fluid flux (ms^{-1})

Based on Hatch AR method, fluid flux ($V_{f.Ar}$) is estimated as

$$V_{f.Ar} = V_{Ar}\, \gamma \qquad (4.3)$$

Where,

$V_{f.Ar}$ – Fluid flux using AR method (m s^{-1});

V_{Ar} - thermal frontal velocity (m s^{-1});

$$\gamma = \frac{\rho c}{\rho_f c_f}$$

ρ and ρ_f are the bulk density of saturated sediment and fluid (kgm^{-3})

c and c_f are the bulk heat capacity of saturated sediment and fluid (J $kg^{-1} \circ C^{-1}$)

Based on the Phase Difference (PD) method, the thermal front velocity is given by

$$V_{DP} = \sqrt{\left({V_{DP}}^4 + \left(\frac{8\pi k_e}{P} \right)^2 \right)^{1/2} - 2\left(\frac{D_p 4\pi k_e}{P\Delta z} \right)^2} \qquad (4.4)$$

where,

V_{DP} is the thermal front velocity (m s^{-1});

Similar to AR method, the fluid velocity (m s^{-1}) is calculated by

$$V_{f.DP} = V_{DP}\,\gamma \qquad (4.5)$$

A_r and D_P parameters are extracted from the temperature time series data at locations i by determining amplitude and phase for each location with nonlinear least-squares fit to the data with the model equation

$$T\left(z = z_{i,t}\right) = A_i \sin\left(\frac{2\pi t}{P} + B_i \right) + C_i \qquad (4.6)$$

where,

A_i is the amplitude of the periodic oscillation (◦C);

B_i is the phase (s);

C_i is the average temperature (◦C) over the period of analysis P (s)

After the determination of amplitude and phase for the locations i, Amplitude ratio (A_r) and Phase difference (D_p) are calculated using the below equations.

$$A_r = \frac{A_{deep}}{A_{shallow}} \quad (4.7)$$

$$D_P = \phi_{Deep} - \phi_{Shallow} \quad (4.8)$$

where,

A_{deep} and $A_{shallow}$ – Amplitude of temperature time series of deeper and shallow sensor

ϕ_{Deep} and $\phi_{Shallow}$ – Phase of temperature time series of deeper and shallow sensor

4.3.2 Keery Amplitude Ratio (AR) and Phase Difference (PD) Method

In the estimation of fluid flux, thermal-mechanical dispersity (β) term is not considered in Keery method. It is the main difference between Hatch and Keery Method (Swanson and Cardenas, 2011). Compare to Hatch method, Keery method is a more straightforward approach.

Fluid flux V_f (m s^{-1}) based on Keery AR method is given by

$$\left(\frac{H^3 \ln(A_r)}{4\Delta z}\right)V_f^3 + \left(5\left(\frac{H \ln(A_r)}{2\Delta z}\right)^2\right)V_f^2 + \left(2H\left(\frac{\ln(A_r)^3}{\Delta z}\right)\right)V_f + \left(\frac{\pi \rho c}{\lambda_e P}\right)^2 - \left(\frac{\ln(A_r)}{\Delta z}\right)^4 = 0 \quad (4.9)$$

where,

$$H = \frac{\rho_f c_f}{\lambda_e}$$

Based on Keery PD method, fluid flux V_f (m s^{-1}) is calculated by

$$V_f = \sqrt{\left(\frac{c \rho \Delta z}{D_p c_f \rho_f}\right)^2 + \left(\frac{4\pi D_p \lambda_e}{P \Delta z c_f \rho_f}\right)^2} \quad (4.10)$$

4.4 RESULTS AND DISCUSSION

In this section, variation of vertical temperature profiles (measured through the experiments conducted in sandbox); estimated fluid flux through Sediment Water Interface (SWI) using analytical solutions; calculated hydraulic conductivity of soil layers using estimated fluid fluxes and calculated effective thermal conductivity of Scenario 1 (S1), Scenario 2 (S2), Scenario 3 (S3) and Scenario 4 (S4) are presented and discussed.

4.4.1 Scenario 1 (FS I, FS II, MS)

In scenario 1 (S1), Fine Sand I (FS I), Fine Sand II (FS II) and Medium Sand (MS) were placed at top, middle and bottom layers in the sandbox and total sixteen experiments were conducted by varying ponding depths (10, 11, 12 and 13 cm) and temperature gradient between normal water and hot water (2°, 4°, 6° and 8°C). In this sub-section, experiments conducted for the cases S1-A1, S1-A2, S1-A3, S1-A4 (varying temperature gradient and constant ponding depth (10 cm); S1-A1, S1-B1, S1-C1, S1-D1 (varying ponding depth at constant temperature gradient (2°C)) are presented and discussed.

4.4.1.1 Variation of Vertical Temperature Profiles

Figure 4.4 shows the vertical variation of temperature profiles measured below the soil column in scenario 1 for different temperature gradients (2°, 4°, 6° and 8°C) at constant ponding depth (10 cm). It can be seen that the temporal variation of temperature profiles at each sensor followed the sinusoidal wave nature in all the experiments with a single peak. It can also be observed clearly that the temperature variations in the bottom layer are comparatively less with the soils at the middle and top layers. Furthermore, temperature amplitude is observed to be decreased and time to peak increased gradually as a function of soil depth with the heat flux passing through soil layers. In the case of S1-A1 (ponding depth 10 cm, temperature gradient of 2°C), the experimental results are presented in Figure 4.4(a). It can be noted that the time taken to attain the required temperature gradient (2°C) at sensor T2 is around 18 min. The sensors (T3 and T4) in the top soil layer (FS I) are close to Sediment-Water Interface (SWI) and their responses are quick and attained higher peaks (1.90° and 1.72°C) in 26 and 42 min, respectively. In the middle layer (FS II), the amplitudes (1.56 and 1.42°C) and time to peak (79 and 105 min) of sensors T5 and T6 are reduced and delayed gradually over the time. The amplitudes are further reduced and time to peak increased in the bottom layer MS (T7 and T8) 1.30° and 1.2°C and 116 and 124 min, respectively.

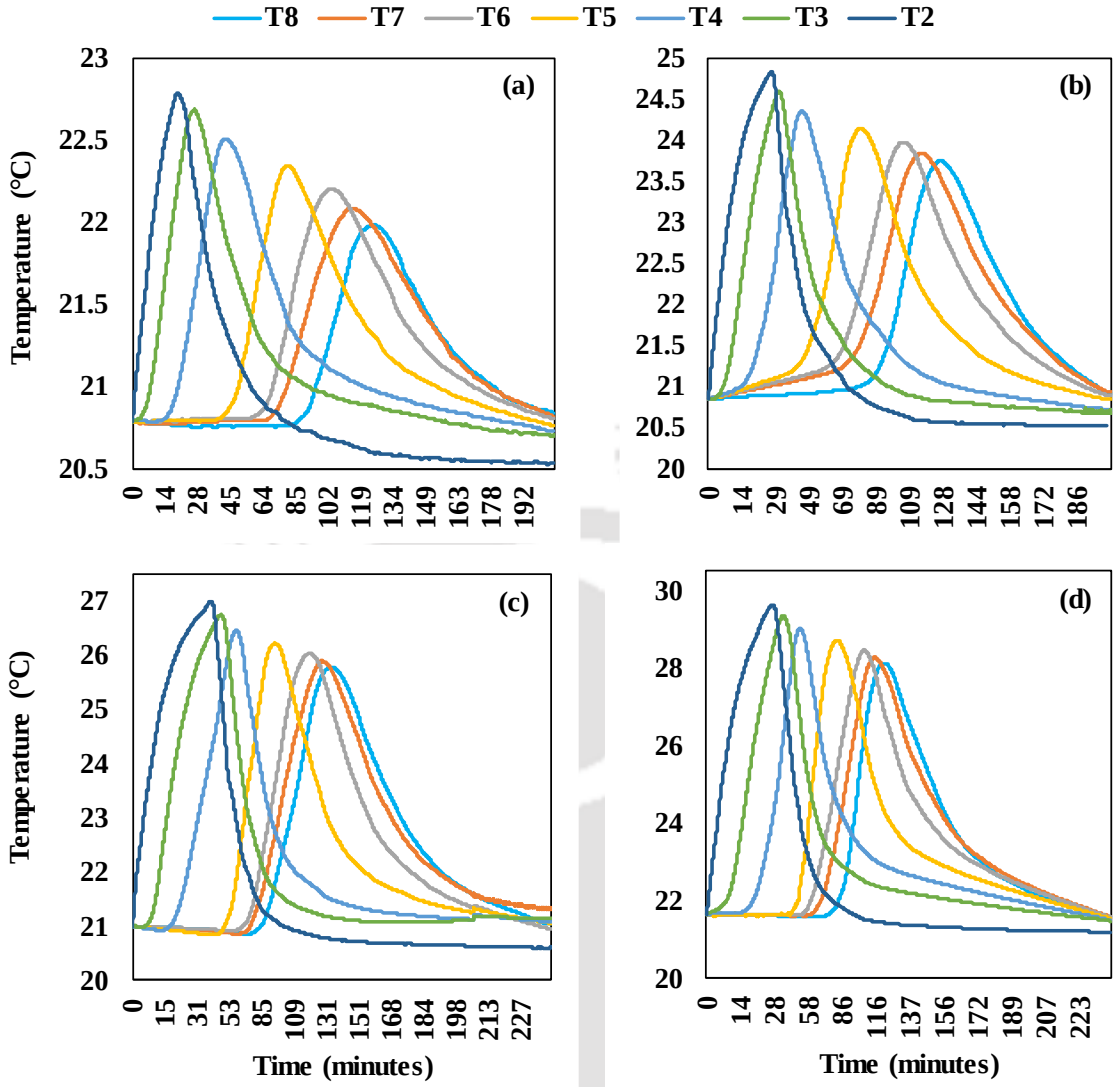

Figure 4.4: Variation of temperature profiles measured at different sensors in case of (a) S1-A1 (b) S1-A2 (c) S1-A3 (d) S1-A4

Figures 4.4(b-d) shows the temperature profile variation at different sensor positions in case of S1-A2 (ponding depth 10 cm, temperature gradient of 4°C), S1-A3 (ponding depth 10 cm, temperature gradient of 6°C) and S1-A4 (ponding depth 10 cm, temperature gradient of 8°C). It can be observed that the observations drawn from these cases are similar to S1-A1. The amplitudes and time to peak at different sensors for different experiments (change in temperature gradient) are presented in Table 4.4. It is observed that the time taken to attain the required temperature gradient at sensor T2 increased with increase in temperature gradient whereas, in-comparison to case 3 (S1-A3), the time taken to attain the required temperature gradient is less in case 4 (S1-A4), may be resulted due to higher temperature gradients. However, the time to peak at all sensors in the soil column

slightly decreased with the increase in temperature gradient. It indicated that the influence of change in temperature gradient on fluid flux passing through soil layers is gradual or not much significant.

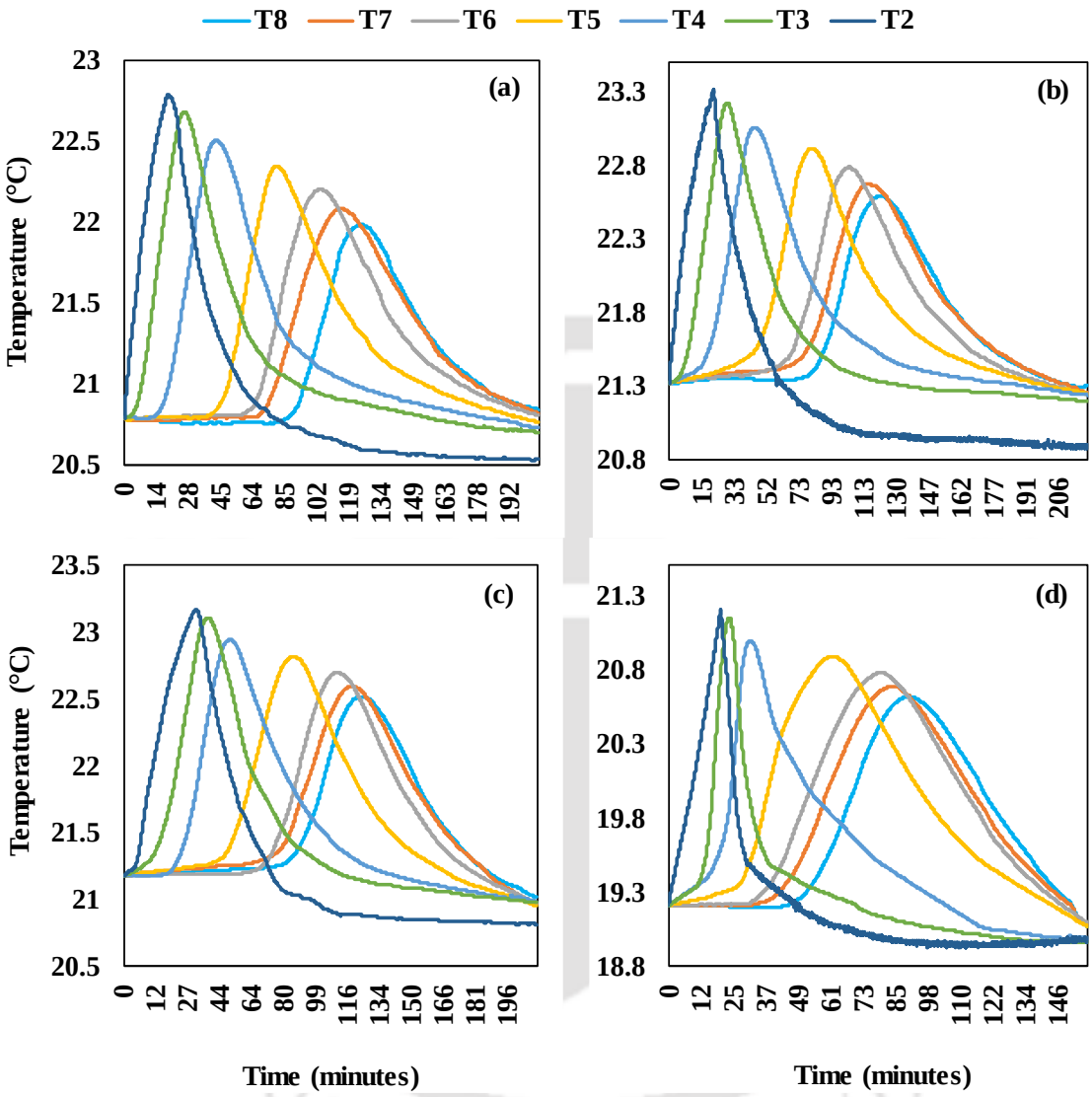

Figure 4.5: Variation of temperature profiles measured at different sensors in case of (a) S1-A1 (b) S1-B1 (c) S1-C1 (d) S1-D1

In order to observe the influence of ponding depth over temperature gradient, different experiments of various ponding depths at constant temperature gradient are compared. Figure 4.5 shows the variation of temperature profiles measured at different depths below the soil column in Scenario 1 for different ponding depths (10, 11, 12 and 13 cm) and temperature gradient of 2°C (S1-A1, S1-B1, S1-C1 and S1-D1). Figure 4.5(a-b) presents experimental results of case S1-A1 (depth 10 and temperature gradient of 2°C) and S1-B1 (ponding depth 11 cm and temperature gradient of 2°C). The time taken to attain the required temperature gradient (2°C) at sensor T2 for case S1-B1 is around 22 min

whereas 18 min for case S1-A1. As the top soil (FS I) is close to SWI, the responses of T3 and T4 sensors in case of S1-B1 are much quick and higher peaks (1.91° and 1.74°C) obtained against S1-A1 (1.90° and 1.72°C) whereas the time taken to attain peak temperature (29 and 44 min for T3 and T4) is increased with increase in ponding depth to 11 cm against S1-A1 (26 and 42 min). It is resulted due to increment in water depth from 10 to 11 cm, causing more time to attain peak. While the amplitudes of sensors T5 and T6 positioned in the middle layer (FS II) S1-B1 are reduced to 1.60° and 1.47°C as fluid flux passing through the soil column and this reduction is less as compared to S1-A1 (1.56° and 1.42°C). However, the time to peak is observed to be approximately the same for S1-A1 and S1-B1 at T5 and T6 sensors (80 and 105 min). It may be due to the increased ponding depth causing higher fluid flux. Further, the amplitudes of bottom layer (MS) sensors T7 and T8 are reduced (1.36° and 1.27°C) in case of S1-B1 and this variation is less against S1-A1 (1.3° and 1.2°C). It is noted that the time to peak at sensors T7 and T8 for S1-B1 are also further delayed (115 and 122 min), however, these values are close against S1-A1 (116 and 124 min).

In the case of S1-C1 (ponding depth 12 cm and temperature gradient of 2°C) and S1-D1 (ponding depth 13 cm and temperature gradient of 2°C), the temperature profile variation at different sensor depths are presented in Figures 4.5(c-d). It can be observed that the conclusions drawn from these cases are similar to S1-A1 (Figure 4.5a). Table 4.4 presents the amplitudes and time to peak at different sensors for different ponding depths at the constant temperature gradient (2°C). An increase in ponding depth increased the time to attain the required temperature gradient at sensor T2, which is less in S1-D1 against S1-C1. It may be resulted due to higher incoming discharges to maintain the constant ponding depth. However, the amplitude at each sensor is observed to be increased while the time to peak decreased significantly with the increase in ponding depth (Table 4.4) and it is clearly indicated that change in ponding depth has a significant influence on fluid flux over the change in temperature gradient.

Table 4.4: Temperature profile Amplitude and Time to peak at different sensors for different cases in Scenario 1

Variable	Case	Parameters	T2	T3	T4	T5	T6	T7	T8
(I) Ponding Depth (10 cm)	S1-A1	Amplitude (°C)	2.00	1.90	1.72	1.56	1.42	1.30	1.20
		Time to Peak (min)	18	26	42	79	105	116	124
	S1-A2	Amplitude (°C)	4.00	3.77	3.51	3.30	3.14	3.00	2.89
		Time to Peak (min)	27	34	49	85	110	120	126
	S1-A3	Amplitude (°C)	6.00	5.75	5.46	5.22	5.03	4.88	4.76
		Time to Peak (min)	38	45	60	95	119	128	134
	S1-A4	Amplitude (°C)	8.00	7.70	7.37	7.09	6.84	6.64	6.49
		Time to Peak (min)	27	33	47	82	106	115	120
(II) Temperature Gradient (2°C)	S1-A1	Amplitude (°C)	2.00	1.90	1.72	1.56	1.42	1.30	1.20
		Time to Peak (min)	18	26	42	79	105	116	124
	S1-B1	Amplitude (°C)	2.00	1.91	1.74	1.60	1.47	1.36	1.27
		Time to Peak (min)	22	29	44	80	105	115	122
	S1-C1	Amplitude (°C)	2.00	1.93	1.77	1.64	1.52	1.42	1.34
		Time to Peak (min)	31	37	51	86	110	118	123
	S1-D1	Amplitude (°C)	2.00	1.94	1.79	1.68	1.57	1.48	1.41
		Time to Peak (min)	24	27	37	69	90	95	100

Note:

(1) Amplitude is the difference between initial temperature and peak temperature; Time to peak is the time elapsed to reach the peak.

(2) I-Inter-comparison between experiments with constant ponding depth (10cm) and varying temperature gradient (2°, 4°, 6° and 8°C)

II- Inter-comparison between experiments with constant temperature gradient (2°C) and varying ponding depth (10, 11, 12 and 13 cm)

(3) T2 in ponding water; T3 and T4 in Fine Sand I (FS I); T5 and T6 in Fine Sand II (FS II); T7 and T8 in Medium Sand (MS)

4.4.1.2 Variation of Fluid Flux Profiles

The fluid fluxes in different soil layers were estimated through the temperature profiles obtained from sandbox experiments for different scenarios using analytical solutions reported by Keery et al. (2007) and Hatch et al. (2006). In this section, the estimated fluid flux variation of Scenario 1 is presented and discussed.

Inter-comparison of fluid fluxes estimated using Keery and Hatch Amplitude Ratio (AR) and Phase Difference (PD) methods in different cases (S1-A1, S1- A2, S1-A3 and S1-A4) of Scenario 1 having constant ponding depth (10 cm) and varying temperature gradient (2°, 4°, 6° and 8 °C) can be seen in Figures 4.6(a-d). It can be clearly observed that the fluid fluxes in the bottom layer (Medium Sand (MS)) are higher than the middle layer (Fine Sand II (FS II)) followed by top layer (Fine Sand I (FS I)). In-comparison of fluxes estimated with Keery AR and PD method, PD method estimations are observed to be more than AR method. Similar observations can be seen in the estimations of flux using Hatch AR and PD method. However, the maximum and minimum values of fluxes are observed to be estimated using Keery AR method and PD methods (Table 4). Figure 4.6(a) shows the fluid fluxes estimated using Keery AR method for the cases S1-A1 (ponding depth of 10 cm and temperature gradient of 2°C), S1-A2 (ponding depth of 10 cm and temperature gradient of 4°C), S1-A3 (ponding depth of 10 cm and temperature gradient of 6°C) and S1-A4 (ponding depth of 10 cm and temperature gradient of 8°C) in top (FS I), middle (FS II) and bottom (MS) soil layers. It can be noted that estimated fluxes slightly increased from 12.26 to 12.61 m/day in FS I; 14.71 to 15.13 m/day in FS II, 17.81 to 18.02 m/day in MS with an increment of temperature gradient by 2°C while the ponding depth remains constant (10 cm). Whereas, the fluxes estimated using Keery PD method are observed to be slightly increased from 27.84-28.14 m/day, 34.03-34.45 m/day, 37.87-38.33 m/day in FS I, FS II and MS layers respectively from case S1-A1 to S1-A4. Similar observations can also be seen in the case of fluxes estimated using Hatch AR and PD methods (Figures 4.6(c-d). However, in very few cases, this behavior is different. It can be observed that there is a slight decrement or not significant in fluid flux with the increase in temperature gradient. For example, fluxes estimated using Hatch AR method are observed to be decreased in the case of S1-A4 against S1-A3 in FS I layer (Table 4.5). It may be resulted due to the fluctuation in water level while maintaining constant ponding depth throughout the experiment. Table 4.5 shows the estimated fluid fluxes of various cases for Scenario 1 for different temperature gradients (2°, 4°, 6° and 8°C) at constant ponding depth (10 cm). It

is noted that fluid fluxes slightly increased with increase in temperature gradient while ponding depth remains constant and this increase is not much significant.

Figures 4.6(e-h) show the variation of fluxes estimated using Keery and Hatch analytical methods obtained in Scenario 1 for four different ponding depths (10, 11, 12 and 13 cm) and temperature gradient (2°C). Fluid fluxes estimated using Keery AR method in case of S1-A1 (ponding depth 10 cm and temperature gradient of 2°C), S1-B1 (ponding depth 11 cm and temperature gradient of 2°C), S1-C1 (ponding depth 12 cm and temperature gradient of 2°C) and S1-D1 (ponding depth 13 cm and temperature gradient of 2°C) are shown in Figure 6(e). It can be noted that fluid fluxes increased from 12.26 to 13.73 m/day, 14.71 to 16.25 m/day 17.81 to 19.46 m/day in top (FS I), middle (FS II) and bottom (MS) soil layers respectively with an increment of 1 cm ponding depth while the temperature gradient remains constant. However, fluxes estimated using Keery PD method are observed to be increased from 28.04 to 31.60 m/day, 34.03-36.88 m/day, 37.87 to 41.61 m/day in FS I, FS II and MS layers respectively from case S1-A1 to S1-D1. Similar observations can be noted in the case of fluxes estimated using Hatch AR and PD methods (Figures 4.6(g-h). The estimated fluid fluxes of various cases for Scenario 1 for different ponding depths (10, 11, 12 and 13 cm) and temperature gradient (2° C) are presented in Table 4.6. It can be observed that fluid fluxes significantly increased with the increase in ponding depth while the temperature gradient remains constant. However, it is clearly observed that change in ponding depth has a significant influence on fluid flux over the change in temperature gradient. Also, it can be noted that in all the experiments, the fluid fluxes are observed to be more in Medium Sand (MS) then Fine Sand II (FS II) followed by Fine Sand I (FS I) irrespective of method. Overall, it is clearly observed that Keery AR method provides good agreement with the measured seepage velocity at the bottom outlet than other three methods (Table 4.5 and 4.6). It might be due to the lack of consideration of the dispersion term in Keery analytical method and violating the one-dimensional assumption [Hatch et al., 2006; Keery et al., 2007].

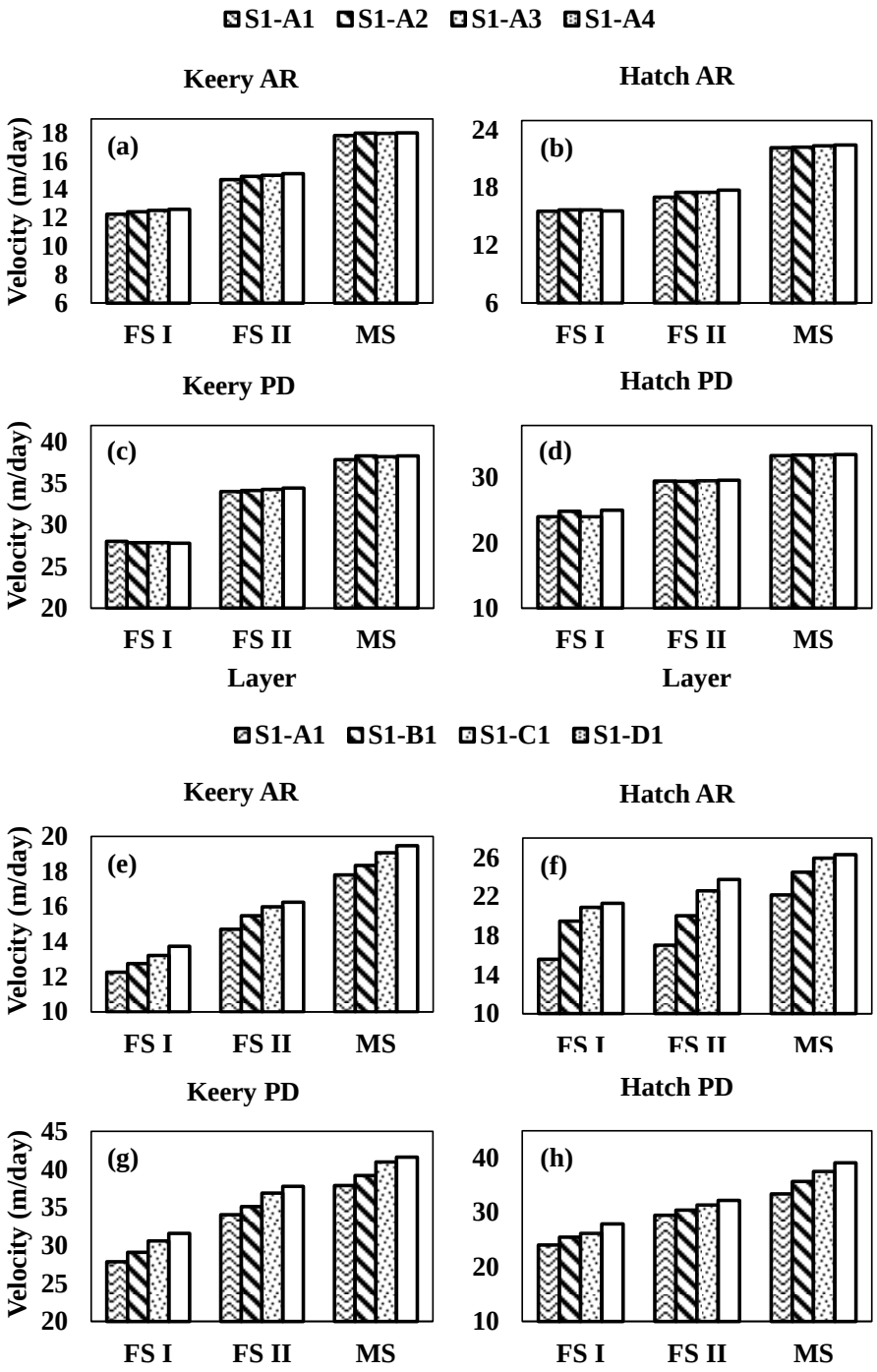

Figure 4.6: Fluid flux variation in different soil layers in Scenario 1 for the cases S1-A1, S1-A2, S1-A3 and S1-A4 using (a) Keery AR (b) Hatch AR (c) Keery PD (d) Hatch PD methods and for the cases S1-A1, S1-B1, S1-C1 and S1-D1 using (e) Keery AR (f) Hatch AR (g) Keery PD (h) Hatch PD methods

Table 4.5: Estimated fluid fluxes for different temperature gradients and ponding depth (10 cm) along with measured seepage velocities at the bottom outlet

Case	Soil Layer	Velocity (m/day)				Measured Velocity at outlet (m/day)
		Keery-AR	Keery-PD	Hatch-AR	Hatch-PD	
S1-A1	Fine Sand (FS I)	12.26	27.84	15.57	24.00	18.12
	Fine Sand II (FS II)	14.71	34.03	17.01	29.49	
	Medium Sand (MS)	17.81	37.87	22.16	33.39	
S1-A2	Fine Sand (FS I)	12.45	27.89	15.70	24.83	18.19
	Fine Sand II (FS II)	14.93	34.15	17.53	29.44	
	Medium Sand (MS)	17.98	38.32	22.24	33.45	
S1-A3	Fine Sand (FS I)	12.54	27.90	15.70	24.02	18.24
	Fine Sand II (FS II)	15.02	34.30	17.53	29.54	
	Medium Sand (MS)	17.97	38.25	22.38	33.45	
S1-A4	Fine Sand (FS I)	12.61	28.14	15.59	24.99	18.30
	Fine Sand II (FS II)	15.13	34.45	17.77	29.63	
	Medium Sand (MS)	18.02	38.33	22.46	33.53	

Table 4.6: Estimated fluid fluxes for different ponding depths and temperature gradient (2°C) along with measured seepage velocities at the bottom outlet

Case	Soil Layer	Velocity (m/day)				Measured Velocity at outlet (m/day)
		Keery-AR	Keery-PD	Hatch-AR	Hatch-PD	
S1-A1	Fine Sand (FS I)	12.26	27.84	15.57	24.00	18.12
	Fine Sand II (FS II)	14.71	34.03	17.01	29.49	
	Medium Sand (MS)	17.81	37.87	22.16	33.39	
S1-B1	Fine Sand (FS I)	12.75	29.11	19.48	25.47	18.51
	Fine Sand II (FS II)	15.47	35.10	20.04	30.44	
	Medium Sand (MS)	18.35	39.19	24.51	35.69	
S1-C1	Fine Sand (FS I)	13.21	30.59	20.90	26.17	18.93
	Fine Sand II (FS II)	15.99	36.88	22.60	31.38	
	Medium Sand (MS)	19.07	40.97	25.96	37.52	
S1-D1	Fine Sand (FS I)	13.73	31.60	21.31	27.89	19.35
	Fine Sand II (FS II)	16.25	37.78	23.76	32.20	
	Medium Sand (MS)	19.46	41.61	26.32	39.09	

4.4.1.3 Variation of Hydraulic Conductivity

As fluid fluxes estimated using Keery AR method showed good agreement with measured seepage velocity, these fluxes are further utilized to calculate hydraulic conductivities of soil layers (using Darcy' law [Darcy, 1856]) for different scenarios. In this section, the calculated hydraulic conductivity variation of different soil layers of various experiments of Scenario 1 are presented and discussed.

Figure 4.7 shows the hydraulic conductivity variation of soil layers calculated using the fluxes with Keery AR method for different cases of Scenario 1. It can be clearly observed that the hydraulic conductivity in the bottom layer (Medium Sand (MS)) are higher than the middle layer (Fine Sand II (FS II)) followed by top layer (Fine Sand I (FS I)). Inter-comparison of hydraulic conductivities for the cases S1-A1 (ponding depth of 10 cm and temperature gradient of 2°C), S1-A2 (ponding depth of 10 cm and temperature gradient of 4°C), S1-A3 (ponding depth of 10 cm and temperature gradient of 6°C) and S1-A4 (ponding depth of 10 cm and temperature gradient of 8°C) in top (FS I), middle (FS II), bottom (MS) soil layers are presented in Figure 4.7(a). It can be noted that calculated conductivity variation is insignificant and ranged from 3.21-3.25 m/day in FS I, 4.97-5.11 m/day in FS II, 5.31-5.37 m/day in MS layers respectively with an increment of temperature gradient by 2°C while the ponding depth remains constant (10 cm). Similar observations can also be seen in the cases of varying ponding depth (10 cm) at the constant temperature gradient (2°C). Figure 4.7(b) shows hydraulic conductivity variation of cases S1-A1 (ponding depth of 10 cm and temperature gradient of 2°C), S1-B1 (ponding depth of 11 cm and temperature gradient of 2°C), S1-C1 (ponding depth of 11 cm and temperature gradient of 2°C) and S1-D1 (ponding depth of 11 cm and temperature gradient of 2°C) in FS I, FS II and MS layers. Hydraulic conductivity value slightly increased and ranged from 3.21-3.25 m/day in FS I, 4.97-5.25 m/day in FS II, 5.31-5.65 m/day in MS layers respectively with an increment of ponding depth by 1 cm while the temperature gradient remains constant (2°C). However, these increases in conductivity values are insignificant or not much varied with change in ponding depth. Table 4.7 shows the calculated hydraulic conductivity values of different cases (varying ponding depths and varying temperature gradients) of Scenario 1. Inter-comparison of different cases of Scenario 1 reveals that there was not significant influence of ponding depth and temperature gradient on hydraulic conductivity.

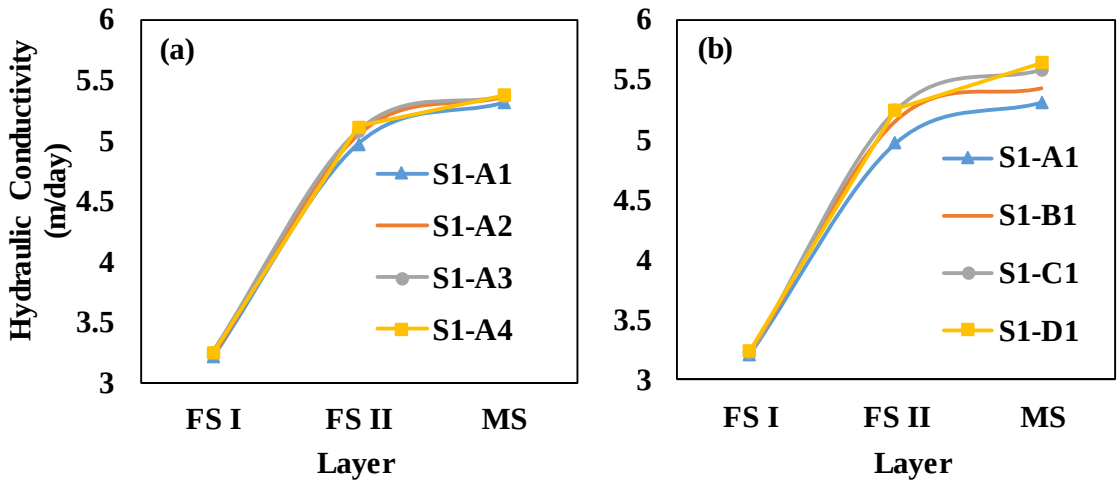

Figure 4.7: Hydraulic conductivity variation using Keery AR method in Scenario 1 for (a) S1-A1, S1-A2, S1-A3, S1-A4 (b) S1-A1, S1-B1, S1-C, S1-D1

Table 4.7: Calculated hydraulic conductivity of different soil layers for different temperature gradients at constant ponding depth (10 cm) in Scenario 1

Soil Layer	Case	Hydraulic Conductivity (m/day)	Case	Hydraulic Conductivity (m/day)
Fine Sand (FS I)		3.22		3.22
Fine Sand II (FS II)	S1-A1	4.98	S1-A1	4.98
Medium Sand (MS)		5.32		5.32
Fine Sand (FS I)		3.22		3.22
Fine Sand II (FS II)	S1-A2	5.05	S1-B1	5.16
Medium Sand (MS)		5.37		5.43
Fine Sand (FS I)		3.25		3.22
Fine Sand II (FS II)	S1-A3	5.08	S1-C1	5.25
Medium Sand (MS)		5.37		5.59
Fine Sand (FS I)		3.24		3.25
Fine Sand II (FS II)	S1-A4	5.12	S1-D1	5.26
Medium Sand (MS)		5.38		5.65

4.4.2 Scenario 2 (FS II, FS I, MS)

In scenario 2 (S2), Fine Sand II (FS II), Fine Sand I (FS I) and Medium Sand (MS) were placed at top, middle and bottom layers in the sandbox and total sixteen experiments were conducted in the sandbox by varying ponding depths (10, 11, 12 and 13 cm) and temperature gradient between normal water and hot water (2°, 4°, 6° and 8°C). In this sub-section, experiments conducted for the cases S2-A1, S2-A2, S2-A3, S2-A4 (varying temperature gradient and constant ponding depth (10 cm); S2-A1, S2-B1, S2-C1, S2-D1 (varying ponding depth and constant temperature gradient (2°C)) are presented and discussed.

4.4.2.1 Variation of Vertical Temperature Profiles

Vertical variation of temperature profiles measured below the soil column in scenario 2 for different temperature gradients (2, 4, 6 and 8°C) at constant ponding depth (10 cm) is shown in Figure 4.8. It can be noted that the observations drawn from Scenario (S2) such as sinusoidal wave nature of temperature profiles; less variation of temperature in bottom soil layers; timely decrease in temperature amplitudes and increase in time to attain peak temperature are similar to Scenario 1 (S1) as function of soil depth with the heat flux passing through soil layers. Figure 4.8(a) shows the temperature profile variation at each sensor in the case of S2-A1 (ponding depth 10 cm, temperature gradient of 2°C). The time taken to attain the required temperature gradient (2°C) at sensor T2 is around 27 min. The responses of sensors (T3 and T4) in top soil layer (FS II) are quick and attained higher peaks (1.94° and 1.78°C) in 30 and 42 min respectively. While the flux passing through the middle soil (FS I) layer, the amplitudes (1.60° and 1.40°C) and time to peak (59 and 77 min) of sensors T5 and T6 reduced and delayed gradually over the time. The amplitudes further reduced and time to peak increased in the bottom soil (MS) layer (T7 and T8) 1.18° and 0.94°C and 97 and 119 min respectively.

In Fig.4.8 (a), T2 probe is behaving differently than other probes and it is not reaching the common temperature even after longer time step. The reason for this different behavior can be explained from the observation made while conducting this particular experiment. Fig.4.8 (a) represents the temperature profiles measured for ponding depth of 10 cm and temperature gradient of 2°C. The initial temperature of normal water measured at T2 probe (ponding water temperature) was around 24°C and required temperature gradient was about 26°C. In order to achieve the required temperature, hot water of 26°C

was injected into ponding water. Once the required peak was attained at T2 probe 26°C, the incoming hot water supply was stopped and normal water of 24°C was injected through the experiment. But, it was noticed that after one hour or so, while injecting the normal water (after the required peak attained), there was heavy rain (for 20-30 minutes) outside due to which the incoming normal water temperature suddenly drops below 24°C (reduced to 23.6°C) and did not come to initial temperature (24°C) before finishing the experiment. The sudden drop of normal water temperature is also due to the season or date of experiment conduced. This particular experiment was conducted on 18th November, 2018 (during winter season) which caused sudden drop of water temperature. T2 probe only was able to capture this change as it was placed in water and others did not capture this sudden change as they were placed inside the soil and they behaved normally.

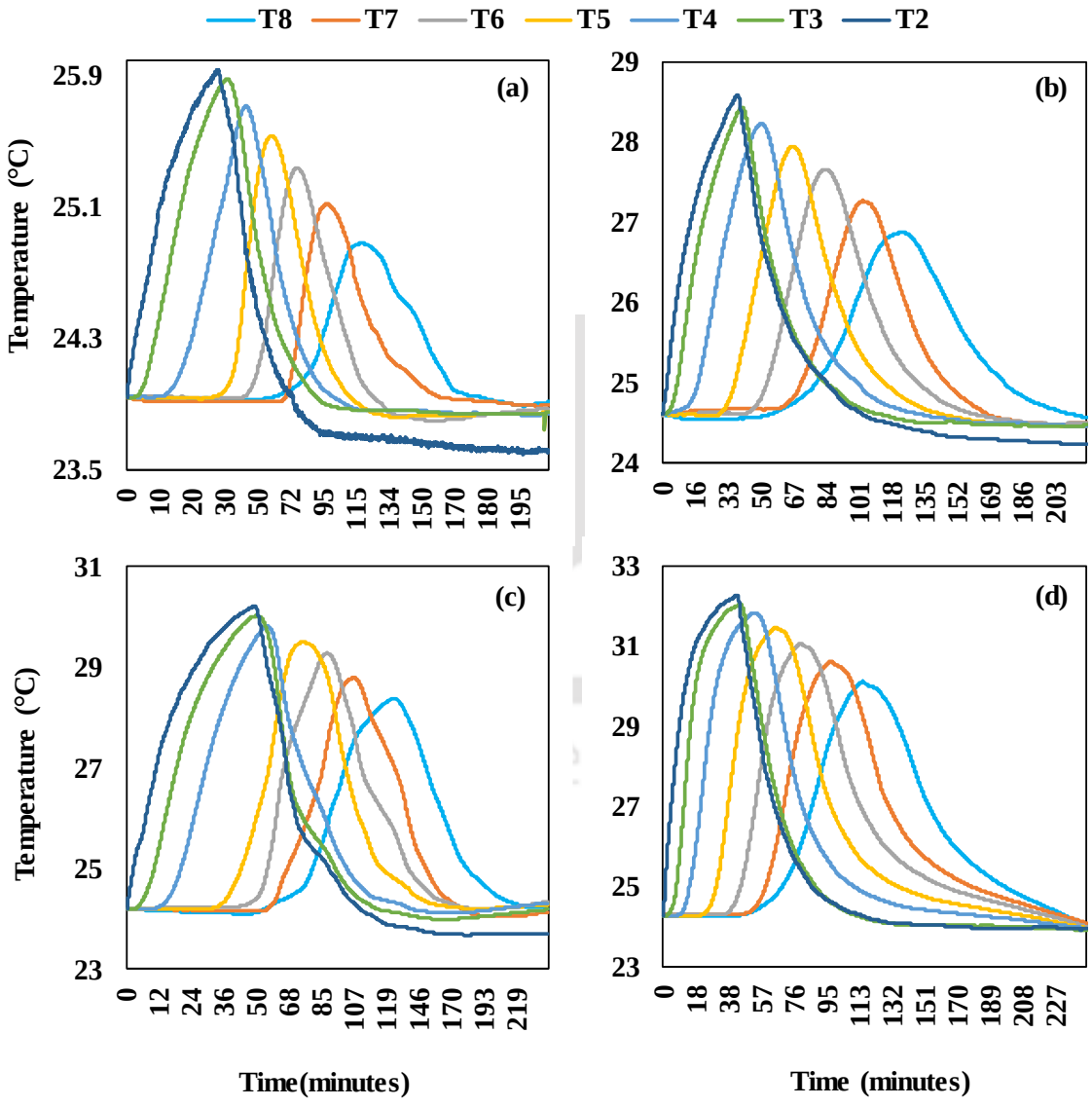

Figure 4.8: Variation of temperature profiles measured at different sensors in case of (a) S2-A1 (b) S2-A2 (c) S2-A3 (d) S2-A4

The temperature profile variation at different sensor positions in case of S2-A2 (ponding depth 10 cm, temperature gradient of 4°C), S2-A3 (ponding depth 10 cm, temperature gradient of 6°C) and S2-A4 (ponding depth 10 cm, temperature gradient of 8°C) are shown in Figures 4.8(b-d). Similar observations can be seen in these cases against S2-A1. Table 4.8 presents the amplitudes and time to peak at different sensors for different experiments (change in temperature gradient) are presented. The time taken to attain the required temperature gradient at sensor T2 increased with the increase in temperature gradient whereas, in-comparison to case 3 (S2-A3), the time taken to attain the required temperature gradient is less in case 4 (S2-A4) and it may be resulted due to higher temperature gradients. However, the time to peak at all sensors in the soil column slightly decreased with the increase in temperature gradient. Similar to S1, it can be observed that there is no significant influence of change in temperature gradient on fluid flux.

The variation of temperature profiles measured at different depths below the soil column in scenario 2 for different ponding depths (10, 11, 12 and 13 cm) and temperature gradient of 2°C (S2-A1, S2-B1, S2-C1 and S2-D1) are shown in Figure 4.9. The temperature profiles of case S2-A1 (depth 10 and temperature gradient of 2°C) and S2-B1 (ponding depth 11 cm and temperature gradient of 2°C) can be seen in Figure 4.9(a-b). It can be noted that the time taken to attain the required temperature gradient (2°C) at sensor T2 for case S1-B1 is around 29 min and this value is less in the case of S2-A1 (27 min). The responses of T3 and T4 sensors in case of S2-B1 are much quick and attained higher peaks (1.96° and 1.81°C) against S2-A1 (1.94° and 1.78°C) whereas the time taken to attain peak temperature (32 and 42 min for T3 and T4) increased with increase in ponding depth to 11 cm against S2-A1 (30 and 42 min).It may be resulted due to the increment in water depth from 10 to 11 cm might increase the velocity of flow. The amplitudes of sensors T5 and T6 positioned in the middle layer (FS I) reduced to 1.65 and 1.46°C (S2-B1) and this reduction is less compared to S2-A1 (1.60° and 1.40°C). However, the time to peak at T5 (58 min) and T6 (75 min) is observed to be approximately the same for S2-A1 and S2-B1 (59 and 77 min). Increased ponding depth may result in higher fluid flux due to which time

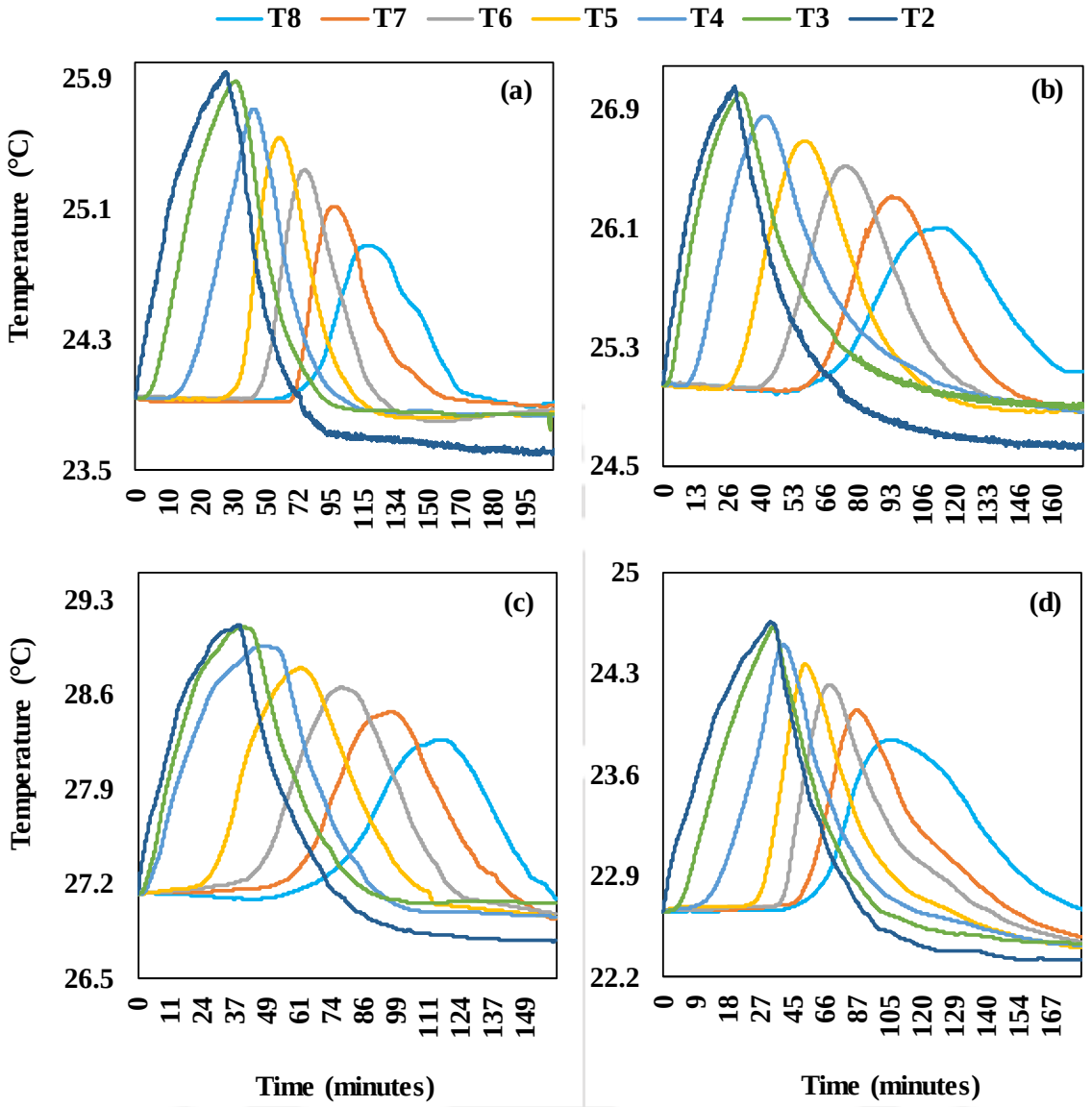

Figure 4.9: Variation of temperature profiles measured at different sensors in case of (a) S2-A1 (b) S2-B1 (c) S2-C1 (d) S2-D1

to peak is reduced. Further, the amplitudes of sensors T7 and T8 in the bottom (MS) layer are reduced (1.27° and 1.05°C) and this reduction is less against S2-A1 (1.18° and 0.94°C). The time to peak at sensors T7 and T8 also further delayed (94 and 115 min) in the case of S2-B1 and it is almost close to S2-A1 (97 and 119 min).

Figures 4.9(c-d) show the temperature profile variation at different sensor depths in the case of S2-C1 (ponding depth 12 cm and temperature gradient of 2°C) and S2-D1 (ponding depth 13 cm and temperature gradient of 2°C). It can be noted that the observations drawn from these cases are similar to S2-A1 (Figure 4.9(a)). The amplitudes and time to peak at different sensors for different ponding depths and constant temperature gradient (2°C) are presented in Table 4.8. The time to attain the required temperature

gradient at sensor T2 increased with the increase in ponding depth except for S2-D1 against S2-C1. It may be resulted due to higher incoming discharges to maintain the constant ponding depth. However, with the increase in ponding depth, the amplitude at each sensor is observed to be increased while the time to peak decreased significantly (Table 4.8). Similar to S1, in S2 it is clearly indicated that change in ponding depth has a significant influence on fluid flux over the change in temperature gradient. However, it can be observed that in Scenario 2, The reduction in temperature amplitude and increase in time to peak are more in comparison with Scenario 1 (Table 4.4 and 4.8).

Table 4.8: Temperature profile Amplitude and Time to peak at different sensors for different cases in Scenario 2

Variable	Case	Parameters	T2	T3	T4	T5	T6	T7	T8
(I) Ponding Depth (10 cm)	S2-A1	Amplitude (°C)	2.00	1.94	1.78	1.60	1.40	1.18	0.94
		Time to Peak (min)	27	30	42	59	77	97	119
	S2-A2	Amplitude (°C)	4.00	3.83	3.63	3.35	3.06	2.67	2.27
		Time to Peak (min)	39	41	51	67	84	104	124
	S2-A3	Amplitude (°C)	6.00	5.82	5.60	5.30	4.99	4.58	4.16
		Time to Peak (min)	48	50	59	73	88	107	127
	S2-A4	Amplitude (°C)	8.00	7.78	7.54	7.20	6.80	6.35	5.85
		Time to Peak (min)	42	44	52	65	79	97	115
(II) Temperature Gradient (2°C)	S2-A1	Amplitude (°C)	2.00	1.94	1.78	1.60	1.40	1.18	0.94
		Time to Peak (min)	27	30	42	59	77	97	119
	S2-B1	Amplitude (°C)	2.00	1.96	1.81	1.65	1.46	1.27	1.05
		Time to Peak (min)	29	32	42	58	75	94	115
	S2-C1	Amplitude (°C)	2.00	1.97	1.83	1.68	1.52	1.34	1.13
		Time to Peak (min)	38	40	47	62	78	97	117
	S2-D1	Amplitude (°C)	2.00	1.98	1.85	1.71	1.56	1.39	1.19
		Time to Peak (min)	33	34	40	54	69	87	106

Note:

(1) Amplitude is the difference between initial temperature and peak temperature; Time to peak is the time elapsed to reach the peak.

(2) I-Inter-comparison between experiments with constant ponding depth (10cm) and varying temperature gradient (2°, 4°, 6° and 8°C)

II- Inter-comparison between experiments with constant temperature gradient (2°C) and varying ponding depth (10, 11, 12 and 13 cm)

(3) T2 in ponding water; T3 and T4 in Fine Sand II (FS II); T5 and T6 in Fine Sand I (FS I); T7 and T8 in Medium Sand (MS)

4.4.2.2 Variation of Fluid Flux Profiles

In this section, estimated fluid flux (using Amplitude Ratio (AR) and Phase Difference (PD) methods) variation of Scenario 2 is presented and discussed. Figure 4.10(a-d) presents variation of fluid fluxes estimated using Keery and Hatch methods using Amplitude Ratio (AR) and Phase Difference (PD) for different cases (S2-A1, S2- A2, S2-A3 and S2-A4) of Scenario 2 (S2) with varying temperature gradient (2°, 4°, 6° and 8°C) while the ponding depth remains constant. Similar to S1. It can be seen that the fluid fluxes in the bottom layer Top layer (FS I) Medium Sand (MS)) are higher than middle layer (Fine Sand II (FS II)) and bottom layer (Medium Sand (MS)) whereas the estimated fluxes in bottom layer are observed to higher than middle layer followed by top layer in S1. Similar to S1, in-comparison of fluxes estimated with Keery, Hatch AR and PD methods and the maximum and minimum values of fluxes are observed to be estimated using Keery AR method and PD methods (Table 4.9). The fluid fluxes estimated using Keery AR method for the cases S2-A1 (ponding depth of 10 cm and temperature gradient of 2°C), S2-A2 (ponding depth of 10 cm and temperature gradient of 4°C), S2-A3 (ponding depth of 10 cm and temperature gradient of 6°C) and S2-A4 (ponding depth of 10 cm and temperature gradient of 8°C) in top (FS I), middle (FS II) and bottom (MS) soil layers are shown in Figure 4.10(a). The estimated fluxes slightly increased from 13.44 to 13.53 m/day in FS II, 11.60 to 11.92 m/day in FS I, 11.13 to 11.31 m/day with an increment of temperature gradient by 2°C while the ponding depth remains constant (10 cm). Whereas, the fluxes estimated using Keery PD method are observed to be slightly increased from 38.45-38.71 m/day, 37.10-38.03 m/day, 34.82-35.04 m/day in FS II, FS I and MS layers respectively from case S2-A1 to S2-A4 (Figure 10(b)). In Figure 10(c-d), similar observations can also be seen in the case of fluxes estimated using Hatch AR and PD methods. However, similar to S1, in very few cases, this behavior is different. For example, fluxes estimated using Keery PD method are observed to be decreased in the case of S2-A2 against S1-A1 in FS I layer (Table 4.9). It may be resulted due to the fluctuations in water level while maintaining the constant ponding depth throughout the experiment. The estimated fluid fluxes of various cases for Scenario 1 for different temperature gradients (2, 4, 6 and 8°C) at constant ponding depth (10 cm) are shown in Table 4.9. It can be noted that the increase in temperature gradient slightly increased the fluid fluxes with while ponding depth remains constant. However, this increase is not much significant similar to S1.

The variation of fluxes estimated using Keery and Hatch analytical methods obtained in Scenario 2 for four different ponding depths (10, 11, 12 and 13 cm) and temperature gradient (2°C) are shown in Figures 4.10(e-h). Fluid fluxes estimated using Keery AR method in case of S2-A1 (ponding depth 10 cm and temperature gradient of 2°C), S2-B1 (ponding depth 11 cm and temperature gradient of 2°C), S2-C1 (ponding depth 12 cm and temperature gradient of 2°C) and S2-D1 (ponding depth 13 cm and temperature gradient of 2°C) are shown in Figure 4.10(e). The fluid fluxes are noted to be increased from 13.44 to 15.19 m/day, 11.60 to 12.87 m/day, 11.13 to 12.44 m/day in top (FS I), middle (FS II) and bottom (MS) soil layers respectively with an increment of 1 cm ponding depth while the temperature gradient remains constant. Whereas, the fluxes estimated using Keery PD method are observed to be increased from 38.71 to 41.79 m/day, 37.10-40.05 m/day, 34.82 to 36.27 m/day in FS I, FS II and MS layers respectively from case S2-A1 to S2-D1 (Figure 10 (f)). Similar observations can be seen in the case of fluxes estimated using Hatch AR and PD methods also (Figures 4.10(g-h). Table 9 presents the estimated fluid fluxes of various cases for Scenario 2 for different ponding depths (10, 11, 12 and 13 cm) and temperature gradient (2° C). In S2 also, it was noted that fluid fluxes significantly increased with the increase in ponding depth while the temperature gradient remains constant. However, similar to S1, it is clearly observed that change in ponding depth has a significant influence on fluid flux over the change in temperature gradient. Also, it is noted that in all the experiments, the fluid fluxes are observed to be more in Fine Sand I (FS I) than Fine Sand II (FS II) followed by Medium Sand (MS) irrespective of method. Similar to S1, it can be observed that Keery AR method provides good agreement with measured seepage velocity than Kerry PD, Hatch AR and PD methods (Table 4.10). Also, it can be noted that the fluxes estimated in Scenario 1 are observed to be more in comparison with Scenario 2 (Table 4.5, 4.6, 4. 9 and 4.10).

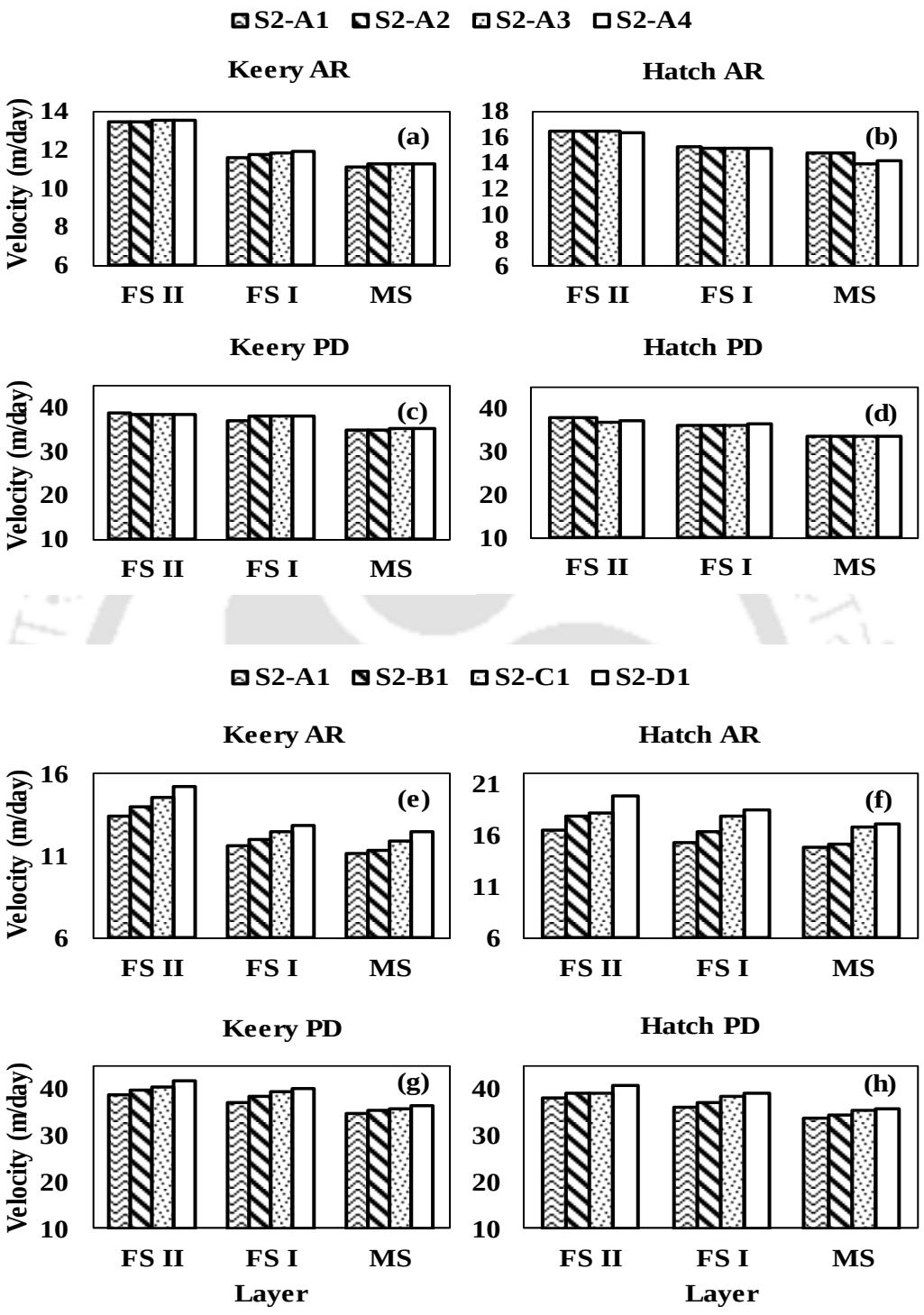

Figure 4.10: Fluid flux variation in different soil layers in Scenario 2 for the cases S2-A1, S2-A2, S2-A3 and S2-A4 using (a) Keery AR (b) Hatch AR (c) Keery PD (d) Hatch PD methods and for the cases S2-A1, S2-B1, S2-C1 and S2-D1 using (e) Keery AR (f) Hatch AR (g) Keery PD (h) Hatch PD methods

Table 4.9: Estimated fluid fluxes for different temperature gradients and ponding depth (10 cm) along with measured seepage velocities at bottom outlet

Case	Soil Layer	Velocity (m/day)				Measured Velocity at outlet (m/day)
		Keery-AR	Keery-PD	Hatch-AR	Hatch-PD	
S2-A1	Fine Sand II (FS II)	13.44	38.71	16.49	37.90	11.01
	Fine Sand (FS I)	11.60	37.10	15.24	36.07	
	Medium Sand (MS)	11.13	34.82	14.82	33.65	
S2-A2	Fine Sand II (FS II)	13.44	38.28	16.50	37.94	11.19
	Fine Sand (FS I)	11.76	37.95	15.19	36.26	
	Medium Sand (MS)	11.31	35.02	14.82	33.72	
S2-A3	Fine Sand II (FS II)	13.56	38.41	16.48	37.00	11.25
	Fine Sand (FS I)	11.86	38.04	15.20	36.14	
	Medium Sand (MS)	11.30	35.03	14.01	33.66	
S2-A4	Fine Sand II (FS II)	13.53	38.45	16.41	37.11	11.35
	Fine Sand (FS I)	11.92	38.03	15.19	36.53	
	Medium Sand (MS)	11.31	35.04	14.17	33.78	

Table 4.10: Estimated fluid fluxes for different temperature gradients and ponding depth (10 cm) along with measured seepage velocities at bottom outlet

Case	Soil Layer	Velocity (m/day)				Measured Velocity at outlet (m/day)
		Keery-AR	Keery-PD	Hatch-AR	Hatch-PD	
S2-A1	Fine Sand II (FS II)	13.44	38.71	16.49	37.90	11.01
	Fine Sand (FS I)	11.60	37.10	15.24	36.07	
	Medium Sand (MS)	11.13	34.82	14.82	33.65	
S2-B1	Fine Sand II (FS II)	13.99	39.56	17.94	38.87	11.26
	Fine Sand (FS I)	12.03	38.36	16.40	37.07	
	Medium Sand (MS)	11.39	35.24	15.20	34.46	
S2-C1	Fine Sand II (FS II)	14.53	40.22	18.22	39.05	11.83
	Fine Sand (FS I)	12.46	39.36	17.88	38.42	
	Medium Sand (MS)	11.94	35.79	16.81	35.19	
S2-D1	Fine Sand II (FS II)	15.19	41.79	19.83	40.62	12.32
	Fine Sand (FS I)	12.87	40.05	18.46	39.07	
	Medium Sand (MS)	12.44	36.27	17.20	35.84	

4.4.2.3 Variation of Hydraulic Conductivity

Similar to S1, fluid fluxes estimated using Keery AR method showed good agreement with measured seepage velocity in S2. These fluxes were used to calculate hydraulic conductivities of soil layers (using Darcy' law) for different scenarios. In this section, the calculated hydraulic conductivity variation of different soil layers along with effective hydraulic conductivities of various experiments of Scenario 2 are presented and discussed.

Variation of hydraulic conductivities of soil layers calculated using the fluxes with Keery AR method for different cases of Scenario 2 is shown in Figure 4.11. Although, the fluxes in top layer are observed to be more than middle and bottom layers, the hydraulic conductivity in the bottom layer (Medium Sand (MS)) is higher than middle layer (Fine Sand I (FS I)) followed by top layer (Fine Sand II (FS II)). However, these values are observed to be less in all soil layers in comparison with S1. Figure 4.11(a) shows the variation of hydraulic conductivities for the cases S2-A1 (ponding depth of 10 cm and temperature gradient of 2°C), S2-A2 (ponding depth of 10 cm and temperature gradient of 4°C), S2-A3 (ponding depth of 10 cm and temperature gradient of 6°C) and S2-A4 (ponding depth of 10 cm and temperature gradient of 8°C) in top (FS I), middle (FS II), bottom (MS) soil layers. It can be found that calculated conductivity variation is insignificant (or less variation) and ranged from 3.24-3.30 m/day in FS II, 4.12-4.24 m/day in FS I, 4.43-4.50 m/day in MS layers, respectively with an increment of temperature gradient by 2°C while the ponding depth remains constant (10 cm). It can be also noted that similar observations are seen in the cases of varying ponding depth (10 cm) at the constant temperature gradient (2°C). Hydraulic conductivity variation in case S1-A1 (ponding depth of 10 cm and temperature gradient of 2°C), S1-B1 (ponding depth of 11 cm and temperature gradient of 2°C), S1-C1 (ponding depth of 11 cm and temperature gradient of 2°C) and S1-D1 (ponding depth of 11 cm and temperature gradient of 2°C) in FS I, FS II and MS layers are shown in Figure 4.11(b). It can be noted that the hydraulic conductivity values slightly increased with an increment of ponding depth by 1 cm while the temperature gradient remains constant (2°C).and the values ranged from 3.24-3.26 m/day in FS II, 4.12-4.37 m/day in FS I, 4.43-4.82 m/day in MS layers respectively. However, it can be observed that this increase in conductivity values are insignificant or not much varied with increase in ponding depth. The calculated hydraulic conductivity values of different cases (varying ponding depth and varying temperature gradient).of Scenario 2 are shown in Table 4.11.

Similar to Scenario 1, inter-comparison of different cases of Scenario 2 reveals that ponding depth and temperature gradient are not significantly influenced hydraulic conductivity values of soil layers.

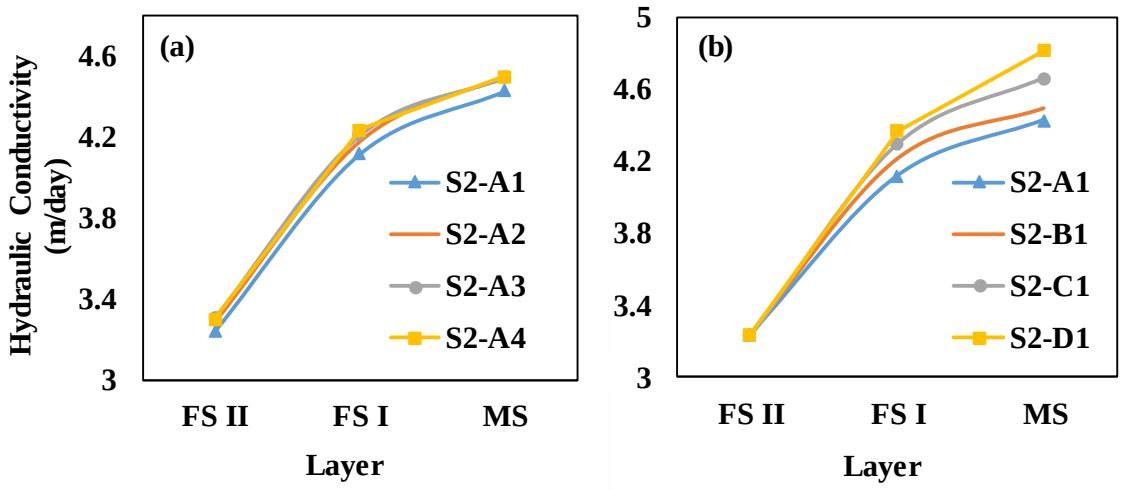

Figure 4.11: Hydraulic conductivity variation using Keery AR method in Scenario 2 for (a) S2-A1, S2-A2, S2-A3, S2-A4 (b) S2-A1, S2-B1, S2-C, S2-D1

Table 4.11: Calculated hydraulic conductivity of different soil layers for different temperature gradients at constant ponding depth (10 cm) in Scenario 2

Soil Layer	Case	Hydraulic Conductivity (m/day)	Case	Hydraulic Conductivity (m/day)
Fine Sand II (FS II)		3.24		3.24
Fine Sand (FS I)	S2-A1	4.12	S2-A1	4.12
Medium Sand (MS)		4.43		4.43
Fine Sand II (FS II)		3.29		3.26
Fine Sand (FS I)	S2-A2	4.18	S2-B1	4.21
Medium Sand (MS)		4.50		4.49
Fine Sand II (FS II)		3.31		3.25
Fine Sand (FS I)	S2-A3	4.21	S2-C1	4.30
Medium Sand (MS)		4.50		4.66
Fine Sand II (FS II)		3.30		3.24
Fine Sand (FS I)	S2-A4	4.24	S2-D1	4.37
Medium Sand (MS)		4.50		4.82

4.4.3 Scenario 3 (MS, FS I, FS II)

In scenario 3 (S3), Medium Sand (MS), Fine Sand I (FS I) and Fine Sand (FS II) were placed at top, middle and bottom layers in the sandbox and total sixteen experiments were conducted in the sandbox by varying ponding depths (10, 11, 12 and 13 cm) and temperature gradient between normal water and hot water (2°, 4°, 6° and 8°C). In this sub-section, experiments conducted for the cases S3-A1, S3-A2, S3-A3, S3-A4 (varying temperature gradient at constant ponding depth (10 cm); S3-A1, S3-B1, S3-C1, S3-D1 (varying ponding depth at constant temperature gradient (2°C)) are presented and discussed.

4.4.3.1 Variation of Vertical Temperature Profiles

Figure 4.12 shows the variation of temperature profiles measured at different sensor positions in scenario 3 for different temperature gradients (2°, 4°, 6° and 8°C) at constant ponding depth (10 cm). Similar to S1 and S2, the temperature profiles followed sinusoidal nature with a single peak in S3. The amplitudes of temperature profiles are observed to be decreased while the time to attain peak temperature increased with time. It was also noted that the variation of temperature at the bottom sensor is less comparative to sensors placed at the top. The vertical variation of temperature profile in the case of S3-A1 (ponding depth 10 cm, temperature gradient of 2°C) is shown in Figure 4.12(a). The time taken to attain the required temperature gradient (2°C) at sensor T2 is around 22 min. As the sensors (T3 and T4) in the top layer (MS) are nearer to SWI, the responses of these sensors are quick and attained higher peaks (1.87° and 1.67°C) in 31 and 51 min respectively. The amplitudes (1.42° and 1.15°C) and time to peak (93 and 143 min) of sensors T5 and T6 reduced and delayed with time in the middle layers (FS I). Whereas, in bottom layers (FS II), the amplitudes further reduced (0.90° and 0.70°C) and time to peaks increased (184 and 221 min) at sensors T7 and T8 respectively.

The variation of vertical temperature profile at different sensor positions in case of S3-A2 (ponding depth 10 cm, temperature gradient of 4°C), S3-A3 (ponding depth 10 cm, temperature gradient of 6°C) and S3-A4 (ponding depth 10 cm, temperature gradient of 8°C) are shown in Figures 4.12(b-d). The observations drawn from these cases are similar to the case against S3-A1. The amplitudes and time to peak at different sensors for different experiments (change in temperature gradient) are presented in Table 4.12. It can be observed that the time taken to attain the required temperature gradient at sensor T2

increased with increase in temperature gradient whereas, in-comparison to case 3, the time taken to attain the required temperature gradient is noted to be less in case 4 and it may be resulted due to higher temperature gradients. However, the time to peak at all sensors in the soil column slightly decreased with the increase in temperature gradient. Similar toS1 and S2, it can be noted that the influence of change in temperature gradient on fluid flux passing through soil layers is gradual or not much significant.

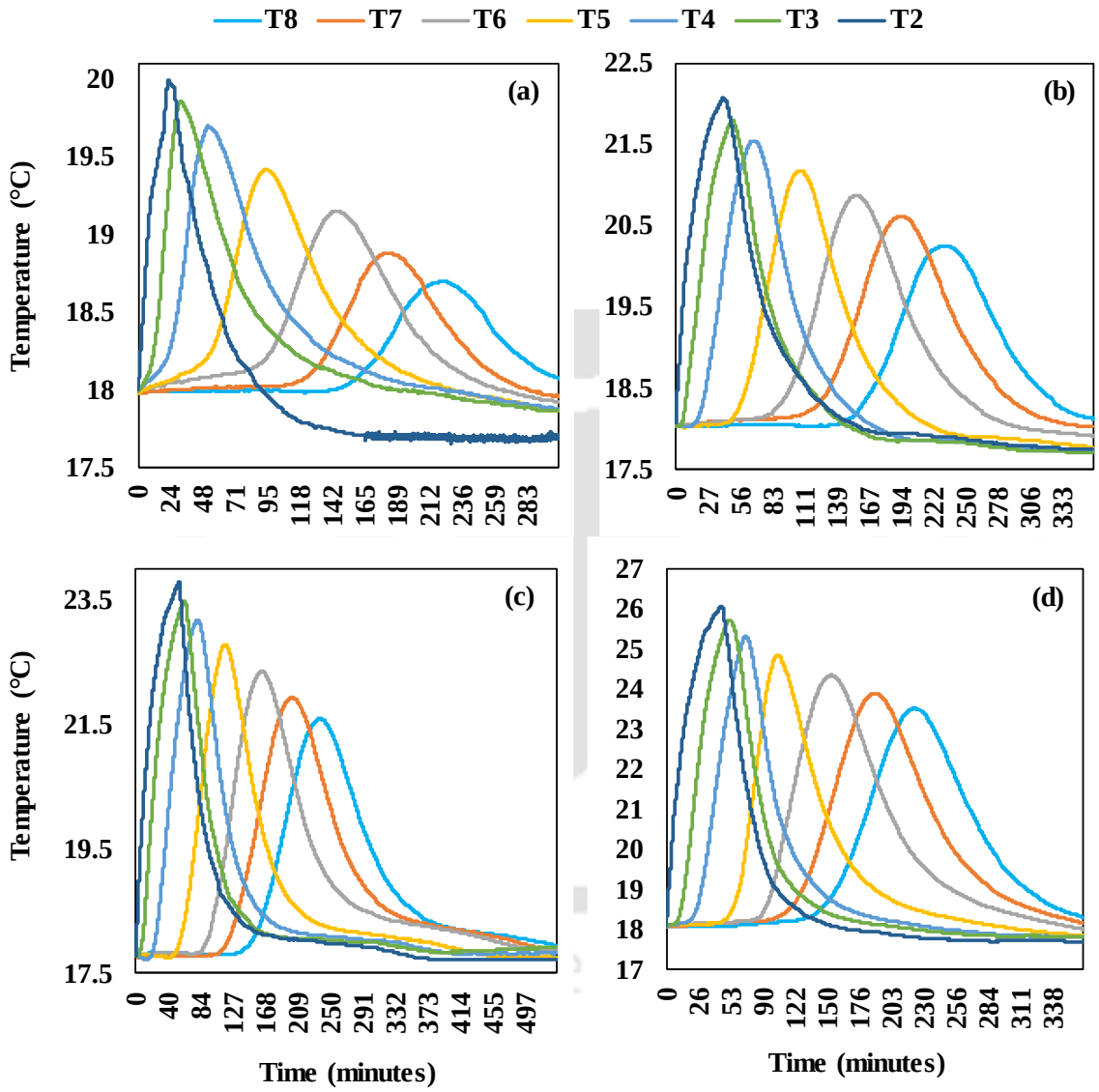

Figure 4.12: Variation of temperature profiles measured at different sensors in case of (a) S3-A1 (b) S3-A2 (c) S3-A3 (d) S3-A4

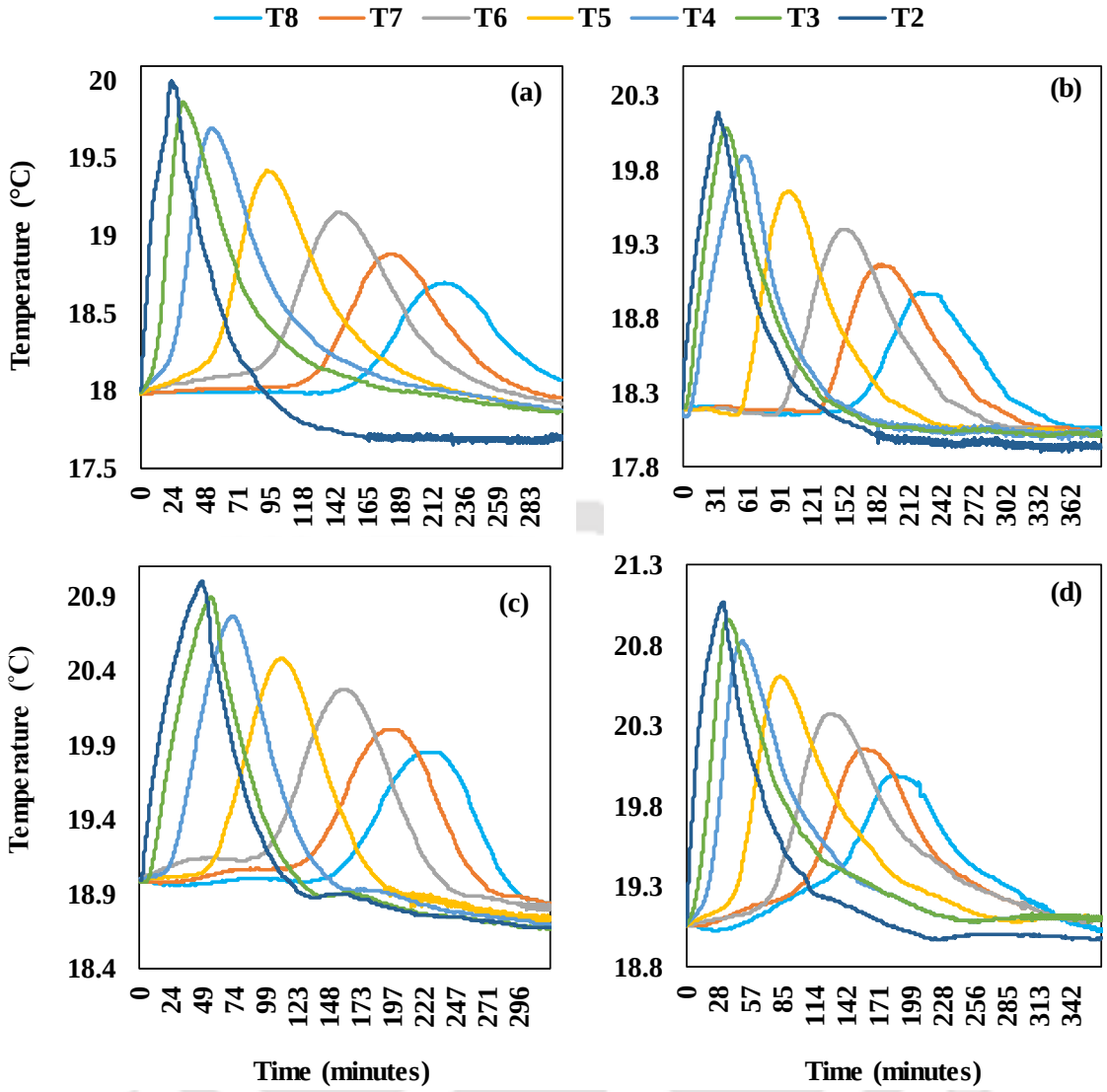

Figure 4.13: Variation of temperature profiles measured at different sensors in case of (a) S3-A1 (b) S3-B1 (c) S3-C1 (d) S3-D1

Figure 4.13 shows the variation of temperature profiles measured at different depths below the soil column in scenario 3 for different ponding depths (10, 11, 12 and 13 cm) and constant temperature gradient of 2°C (S3-A1, S3-B1, S3-C1 and S3-D1). The temperature profiles of case S3-A1 (depth 10 and temperature gradient of 2°C) and S3-B1 (ponding depth 11 cm and temperature gradient of 2°C) can be seen in Figure 4.13(a-b). It can be noted that the time taken to attain the required temperature gradient (2°C) at sensor T2 for case S3-B1 is around 34 min and this value is less in the case of S3-A1 (22 min). In the top layer, the responses of T3 and T4 sensors in case of S3-B1 are much quick and attained higher peaks (1.89° and 1.71°C) against S3-A1 (1.87° and 1.67°C) whereas the time taken to attain peak temperature (42 and 60 min for T3 and T4) increased with increase in ponding depth to 11 cm against S3-A1 (31 and 51 min). It may be resulted due to the

increment in water depth from 10 to 11 cm might increase the fluid flow flux. In the middle layers, the amplitudes of sensors T5 and T6 positioned (FS I) reduced to 1.47° and 1.21°C (S3-B1) and this reduction is less compared to S3-A1 (1.42° and 1.15°C). Whereas, the time to peak is observed to be 101 min and 150 min at T5 and T6 and these values are less for S3-B1 against S3-B1 (93 and 143 min). It is resulted due to the increase in ponding depth, increased fluid flow velocity. Further, in the bottom (MS) layer, the amplitudes of sensors T7 and T8 in the bottom (MS) layer reduced (0.97° and 0.78°C) and this reduction also observed to be more in case of S3-A1 (0.90° and 0.70°C) and the time to peak at sensors T7 and T8 further delayed (188 and 224 min) in case of S3-B1 whereas time to peak in case of S3-A1 are also observed to similar (184 and 221 min).

The temperature profile variation at different sensor depths in the case of S2-C1 (ponding depth 12 cm and temperature gradient of 2°C) and S2-D1 (ponding depth 13 cm and temperature gradient of 2°C) are shown in Figures 4.13(c-d). The observations drawn from these cases are similar to S3-A1 (Figure 4.13(a)). Table 4.12 presents the amplitudes and time to peak at different sensors for different ponding depths and constant temperature gradient (2°C). Similar to S1, and S2, in Scenario 3, the time to attain the required temperature gradient at sensor T2 increased with the increase in ponding depth except for S3-D1 against S3-C1. Higher incoming discharges might have resulted in this change. However, with the increase in ponding depth, the amplitude at each sensor observed to be increased while the time to peak decreased significantly (Table 4.12). It can be noted that the observations are similar to S1 and S2 and also it is clearly indicated that change in ponding depth has a significant influence on fluid flux over the change in temperature gradient. Similar to Scenario 2, the reduction in temperature amplitude and an increase in time to peak in Scenario 3 are observed to be more than S2 and S1.

Table 4.12: Temperature profile Amplitude and Time to peak at different sensors for different cases in Scenario 3

Variable	Case	Parameters	T2	T3	T4	T5	T6	T7	T8
(I) Ponding Depth (10 cm)	S3-A1	Amplitude (°C)	2.00	1.87	1.67	1.42	1.15	0.90	0.70
		Time to Peak (min)	22	31	51	93	143	184	221
	S3-A2	Amplitude (°C)	4.00	3.76	3.49	3.18	2.84	2.53	2.24
		Time to Peak (min)	41	49	67	107	156	195	231
	S3-A3	Amplitude (°C)	6.00	5.70	5.37	4.97	4.54	4.14	3.77
		Time to Peak (min)	54	61	78	117	165	202	236
	S3-A4	Amplitude (°C)	8.00	7.65	7.21	6.74	6.25	5.82	5.42
		Time to Peak (min)	46	53	69	107	153	189	222
(II) Temperature Gradient (2°C)	S3-A1	Amplitude (°C)	2.00	1.87	1.67	1.42	1.15	0.90	0.70
		Time to Peak (min)	22	31	51	93	143	184	221
	S3-B1	Amplitude (°C)	2.00	1.89	1.71	1.47	1.21	0.97	0.78
		Time to Peak (min)	34	42	60	101	150	188	224
	S3-C1	Amplitude (°C)	2.00	1.91	1.75	1.52	1.27	1.04	0.86
		Time to Peak (min)	48	55	72	111	158	194	228
	S3-D1	Amplitude (°C)	2.00	1.92	1.77	1.55	1.31	1.09	0.92
		Time to Peak (min)	33	37	50	84	127	158	183

Note:

(1) Amplitude is the difference between initial temperature and peak temperature; Time to peak is the time elapsed to reach the peak.

(2) I-Inter-comparison between experiments with constant ponding depth (10cm) and varying temperature gradient (2°, 4°, 6° and 8°C)

II- Inter-comparison between experiments with constant temperature gradient (2°C) and varying ponding depth (10, 11, 12 and 13 cm)

(3) T2 in ponding water; T3 and T4 in Medium Sand (MS); T5 and T6 in Fine Sand I (FS I); T7 and T8 in Fine Sand II (FS II)

4.4.3.2 Variation of Fluid Flux Profiles

In this section, estimated fluid flux (using Amplitude Ratio (AR) and Phase Difference (PD) methods) variation of Scenario 3 is presented and discussed. The variation of fluid fluxes estimated using Keery and Hatch Amplitude Ratio (AR) and Phase Difference (PD) methods in different cases (S3-A1, S3- A2, S3-A3 and S3-A4) in Scenario 3 (S3) with varying temperature gradient (2, 4, 6 and 8 °C) while the ponding depth remains constant can be seen in Figure 4.14(a-d)). It can be observed that the fluid fluxes in the bottom layer (Fine Sand II) are higher than top layer (Medium Sand) followed by Fine Sand I. Whereas, fluxes are more in bottom (Medium Sand) layer in Scenario 1, and in the top layer (Fine Sand II) in Scenario 2. Similar to S1 and S2, in-comparison of fluxes estimated with Keery, Hatch AR and PD methods and the maximum and minimum values of fluxes are observed to be estimated using Keery AR method and PD methods (Table 4.13). Figure 4.14(a) shows the fluid fluxes estimated using Keery AR method for the cases S3-A1 (ponding depth of 10 cm and temperature gradient of 2°C), S3-A2 (ponding depth of 10 cm and temperature gradient of 4°C), S3-A3 (ponding depth of 10 cm and temperature gradient of 6°C) and S3-A4 (ponding depth of 10 cm and temperature gradient of 8°C) in top (FS I), middle (FS II) and bottom (MS) soil layers. It can be noted that the estimated fluxes slightly increased from 11.05 to 11.32 m/day in MS, 10.32 to 10.38 m/day in FS I, 11.42 to 11.85 m/day with an increment of temperature gradient by 2°C while the ponding depth remains constant (10 cm). Whereas, the fluxes estimated using Keery PD method are observed to be slightly increased from 26.27-26.80 m/day, 24.71-25.07 m/day, 34.82-35.04 m/day in MS, FS I and FS II layers respectively from case S3-A1 to S3-A4 (Figure 4.14(b)). Similar observations can also be seen in the case of fluxes estimated using Hatch AR and PD methods (Figure 4.14(c-d). However, similar to S1 and S2, in very few cases, this behavior is different. For example, fluxes estimated using Hatch PD method are observed to be decreased in the case of S3-A2 against S3-A1 in FS II layer (Table 12). Water level fluctuations might have resulted this change. The estimated fluid fluxes of various cases for Scenario 3 for different temperature gradients (2, 4, 6 and 8°C) at constant ponding depth (10 cm) are shown in Table 4.14. It can be observed that the increase in temperature gradient slightly increased the fluid fluxes with while ponding depth remains constant. However, this increase is not much significant similar to S1 and S2.

Figures 4.14(e-h) shows the variation of fluxes estimated using Keery and Hatch analytical methods obtained in Scenario 3 for four different ponding depths (10, 11, 12 and

13 cm) and constant temperature gradient (2°C) Fluid fluxes estimated using Keery AR method in case of S3-A1 (ponding depth 10 cm and temperature gradient of 2°C), S3-B1 (ponding depth 11 cm and temperature gradient of 2°C), S3-C1 (ponding depth 12 cm and temperature gradient of 2°C) and S3-D1 (ponding depth 13 cm and temperature gradient of 2°C) are shown in Figure 4.14(e). The fluid fluxes increased from 11.05-12.72 m/day, 10.38-11.89 m/day, 11.42-12.92 m/day in the top (MS), middle (FS I) and bottom (FS II) soil layers respectively with an increment of 1 cm ponding depth while the temperature gradient remains constant. Whereas, the fluxes estimated using Keery PD method ae observed to be increased from 26.27 to 28.90 m/day 24.71-26.48, 27.02-28.90 m/day in MS, FS II and FS II layers respectively from case S3-A1 to S3-D1 (Figure 4.14(f)). The observations drawn from these cases are similar to S1 and S2 using Hatch and PD methods (Figure 4.14(g-h)). The estimated fluid fluxes of various cases for Scenario 3 for different ponding depths (10, 11, 12 and 13 cm) and temperature gradient (2° C) are shown in Table 4.14. It can be found that fluid fluxes significantly increased with the increase in ponding depth while temperature gradient remains constant similar to S1 and S2. Also, it is clearly observed that change in ponding depth has a significant influence on fluid flux over the change in temperature gradient. Also, it can be noted that in all the experiments, the fluid fluxes are observed to be more in Fine Sand II (FS II) than Medium Sand (MS) followed by Fine Sand I (FS I) irrespective of method. Similar to S1 and S2, it is observed that Keery AR method provides good agreement with measured seepage velocity than Kerry PD, Hatch AR and PD methods (Table 4.14). It is also noted that in comparison of fluxes estimated in S1 and S2 with S3 indicate that the fluxes are observed to less than S2 and S1.

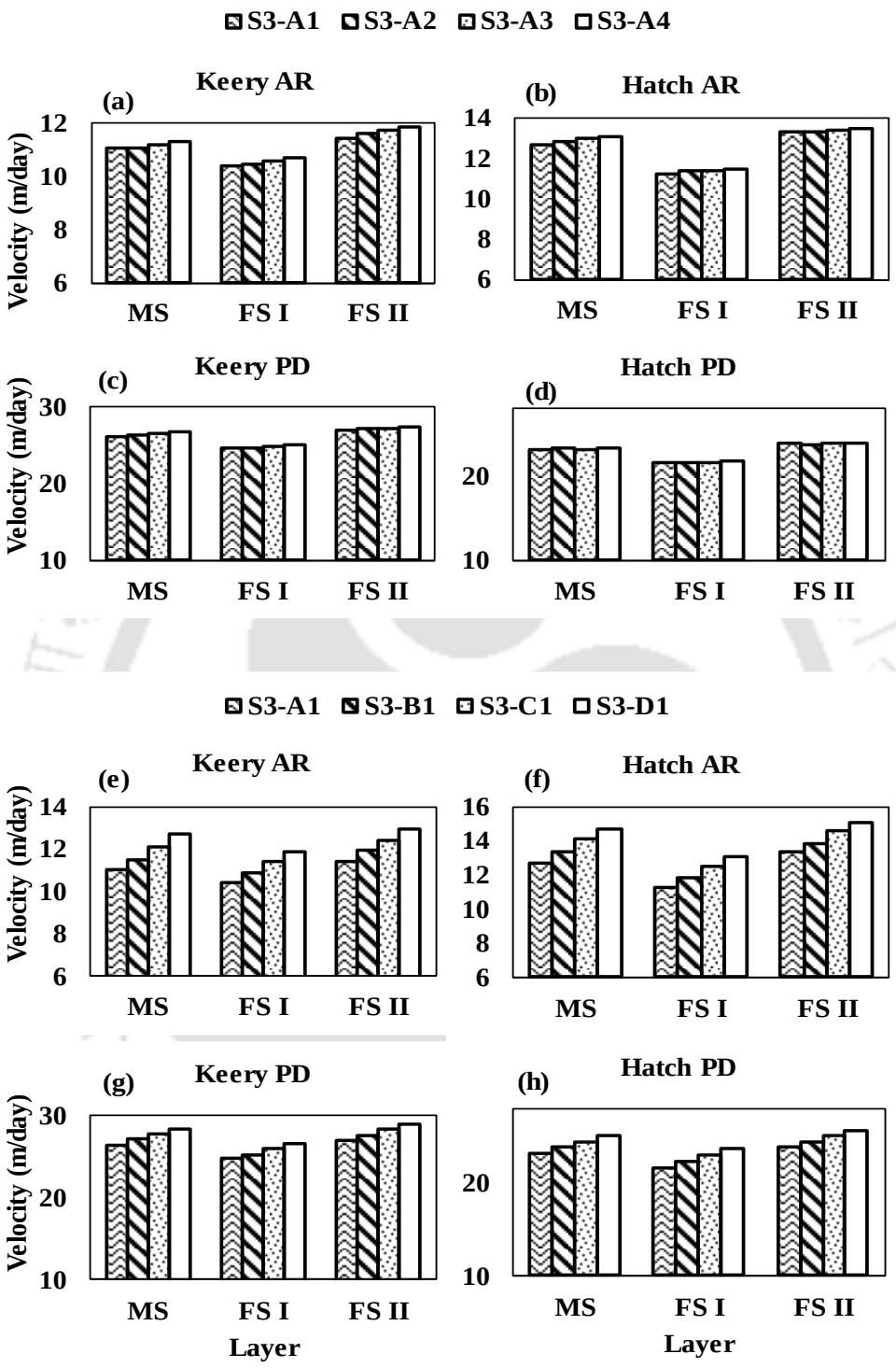

Figure 4.14: Fluid flux variation in different soil layers in Scenario 3 for the cases S3-A1, S3-A2, S3-A3 and S3-A4 using (a) Keery AR (b) Hatch AR (c) Keery PD (d) Hatch PD methods and for the cases S3-A1, S3-B1, S3-C1 and S3-D1 using (e) Keery AR (f) Hatch AR (g) Keery PD (h) Hatch PD methods

Table 4.13: Estimated fluid fluxes for different temperature gradients and ponding depth (10 cm) along with measured seepage velocities at bottom outlet

Case	Soil Layer	Velocity (m/day)				Measured Velocity at outlet (m/day)
		Keery-AR	Keery-PD	Hatch-AR	Hatch-PD	
S3-A1	Medium Sand (MS)	11.05	26.27	12.72	23.17	11.29
	Fine Sand (FS I)	10.38	24.71	11.24	21.62	
	Fine Sand II (FS II)	11.42	27.02	13.31	23.84	
S3-A2	Medium Sand (MS)	11.10	26.46	12.90	23.25	11.51
	Fine Sand (FS I)	10.49	24.76	11.45	21.61	
	Fine Sand II (FS II)	11.62	27.23	13.38	23.82	
S3-A3	Medium Sand (MS)	11.17	26.66	13.00	23.24	11.68
	Fine Sand (FS I)	10.59	24.99	11.44	21.70	
	Fine Sand II (FS II)	11.76	27.31	13.46	23.89	
S3-A4	Medium Sand (MS)	11.32	26.80	13.07	23.37	11.77
	Fine Sand (FS I)	10.72	25.07	11.51	21.88	
	Fine Sand II (FS II)	11.85	27.48	13.52	23.98	

Table 4.14: Estimated fluid fluxes for different ponding depths and temperature gradient (2°C) along with measured seepage velocities at bottom outlet

Case	Soil Layer	Velocity (m/day)				Measured Velocity at outlet (m/day)
		Keery-AR	Keery-PD	Hatch-AR	Hatch-PD	
S3-A1	Medium Sand (MS)	11.05	26.27	12.72	23.17	11.77
	Fine Sand (FS I)	10.38	24.71	11.24	21.62	
	Fine Sand II (FS II)	11.42	27.02	13.31	23.84	
S3-B1	Medium Sand (MS)	11.49	27.12	13.38	23.85	11.84
	Fine Sand (FS I)	10.86	25.16	11.81	22.33	
	Fine Sand II (FS II)	11.93	27.57	13.81	24.46	
S3-C1	Medium Sand (MS)	12.12	27.76	14.12	24.40	12.19
	Fine Sand (FS I)	11.41	25.87	12.50	23.02	
	Fine Sand II (FS II)	12.39	28.27	14.54	25.06	
S3-D1	Medium Sand (MS)	12.72	28.26	14.72	25.08	12.86
	Fine Sand (FS I)	11.89	26.48	13.09	23.70	
	Fine Sand II (FS II)	12.92	28.90	15.07	25.62	

4.4.3.3 Variation of Hydraulic Conductivity

Similar to S1 and S2, the fluid fluxes estimated using Keery AR method were in accordance with measured seepage velocity in S3. These fluxes were used to calculate hydraulic conductivities of soil layers (using Darcy' law) for different scenarios. In this section, the calculated hydraulic conductivity variation of different soil layers along with effective hydraulic conductivities of various experiments of Scenario 3 are presented and discussed.

Variation of hydraulic conductivities of soil layers calculated using the fluxes with Keery AR method for different cases of Scenario 3 is shown in Figure 4.15. Although, hydraulic conductivities of Medium Sand (MS) are more than other soil layers in S1 and S2, in the case of S3, the conductivities are more in Fine Sand II (bottom layer) followed by FS I and MS. The variation of hydraulic conductivities for the cases S3-A1 (ponding depth of 10 cm and temperature gradient of 2°C), S3-A2 (ponding depth of 10 cm and temperature gradient of 4°C), S3-A3 (ponding depth of 10 cm and temperature gradient of 6°C) and S3-A4 (ponding depth of 10 cm and temperature gradient of 8°C) in top (MS), middle (FS I), bottom (FS II) soil layers are shown in Figure 4.15(a). The calculated conductivity variation is insignificant (or less variation) and ranged from 2.72-3.30 m/day in MS, 3.86-4.23 m/day in FS I, 4.13-4.55 m/day in FS II layers respectively with an increment of temperature gradient by 2°C while the ponding depth remains constant (10 cm). Similar to S1 and S2, it can be also noted that similar observations are also seen in the cases of varying ponding depth (10 cm) at the constant temperature gradient (2°C). Hydraulic conductivity variation case S3-A1 (ponding depth of 10 cm and temperature gradient of 2°C), S3-B1 (ponding depth of 11 cm and temperature gradient of 2°C), S3-C1 (ponding depth of 11 cm and temperature gradient of 2°C) and S3-D1 (ponding depth of 11 cm and temperature gradient of 2°C) in MS, FS I and FS II layers are shown in Figure 4.15(b). The hydraulic conductivity values slightly increased with an increment of ponding depth by 1 cm while the temperature gradient remains constant (2°C) and the values ranged from 2.72-2.79 m/day in MS, 3.86-3.99 m/day in FS I, 3.86-4.29 m/day in FS II layers respectively. However, it can be observed that this increase in conductivity values is insignificant or not much varied with the increase in ponding depth. Table 4.15 shows the calculated hydraulic conductivity values of different cases (varying ponding depth and varying temperature gradient) of Scenario 3. Similar to Scenario 1 and 2, inter-comparison

of different cases of Scenario 3 reveals that varying ponding depth and temperature gradient is not significantly influenced hydraulic conductivity values of soil layers.

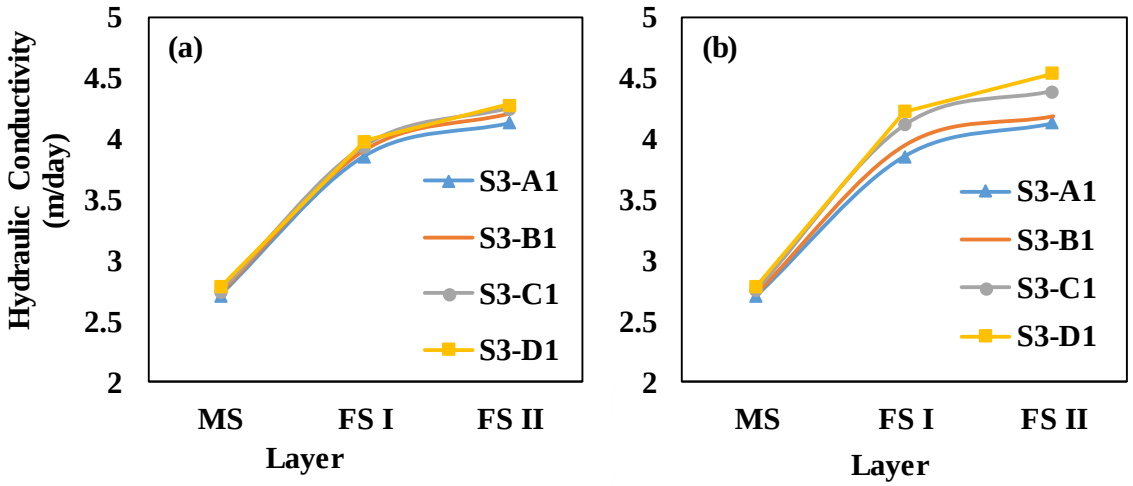

Figure 4.15: Hydraulic conductivity variation using Keery AR method in Scenario 3 for (a) S3-A1, S3-A2, S3-A3, S3-A4 (b) S3-A1, S3-B1, S3-C1, S3-D1

Table 4.15: Calculated hydraulic conductivity of different soil layers for different temperature gradients at constant ponding depth (10 cm) in Scenario 3

Soil Layer	Case	Hydraulic Conductivity (m/day)	Case	Hydraulic Conductivity (m/day)
Medium Sand (MS)		2.72		2.72
Fine Sand (FS I)	S3-A1	3.86	S3-A1	3.86
Fine Sand II (FS II)		4.13		4.13
Medium Sand (MS)		2.74		2.73
Fine Sand (FS I)	S3-A2	3.95	S3-B1	3.91
Fine Sand II (FS II)		4.18		4.21
Medium Sand (MS)		2.76		2.75
Fine Sand (FS I)	S3-A3	4.12	S3-C1	3.94
Fine Sand II (FS II)		4.40		4.25
Medium Sand (MS)		2.79		2.79
Fine Sand (FS I)	S3-A4	4.23	S3-D1	3.99
Fine Sand II (FS II)		4.55		4.29

4.4.4 Scenario 4 (MS, FS II, FS I)

In scenario 4 (S4), Medium Sand (MS), Fine Sand II (FS II) and Fine Sand I (FS I) were placed at top, middle and bottom layers in the sandbox and total sixteen experiments were conducted in the sandbox by varying ponding depths (10, 11, 12 and 13 cm) and temperature gradient between normal water and hot water (2, 4, 6 and 8 °C). In this sub-section, experiments conducted for the cases S4-A1, S4-A2, S4-A3, S4-A4 (varying temperature gradient at constant ponding depth (10 cm); S4-A1, S3-B1, S4-C1, S4-D1 (varying ponding depth at constant temperature gradient (2°C)) are presented and discussed.

4.4.4.1 Variation of Vertical Temperature Profiles

The variation of vertical temperature profiles measured at different sensor positions in Scenario 4 for different temperature gradients (2, 4, 6 and 8°C) at constant ponding depth (10 cm) is shown in Figure 4.16. In S4 also, the temperature profiles followed sinusoidal nature with single peak similar to S1, S2 and S3, the amplitudes of temperature profile decreased while the time to attain peak temperature increased with time and the variation of temperature at the bottom sensor is less comparative to sensors placed at the top. Figure 4.16(a) shows the variation of the temperature profiles in case of S4-A1 (ponding depth 10 cm, temperature gradient of 2°C). The time taken to attain the required temperature gradient (2°C) at sensor T2 is around 35 min and this time is observed to be more in comparison with other scenarios. The responses of T3 and T4 in the first layer (MS) are quick and attained higher peaks, the responses of these sensors are quick and attained higher peaks (1.8° and 1.6°C) in 62 and 100 min respectively. With passage of fluid flux, the amplitudes (1.36° and 1.10°C) and time to peak (145 and 200 min) of sensors T5 and T6 reduced and delayed with time in middle layers (FS II). Whereas, in bottom layers (FS I), the amplitudes further reduced (0.82° and 0.50°C) and time to peaks increased (293 and 396 min) at sensors T7 and T8 respectively.

Figures 4.16(b-d) present the variation of vertical temperature profile at different sensor positions in case of S3-A2 (ponding depth 10 cm, temperature gradient of 4°C), S3-A3 (ponding depth 10 cm, temperature gradient of 6°C) and S3-A4 (ponding depth 10 cm, temperature gradient of 8°C). The observations drawn from these cases are similar to the case against S4-A1. Table 15 shows the amplitudes and time to peak at different sensors for different experiments (change in temperature gradient). Similar other scenarios, in S4

also it can be observed that the time taken to attain the required temperature gradient at sensor T2 increased with the increase in temperature gradient whereas, in-comparison to case 3, the time taken to attain the required temperature gradient is less in case 4. It may be resulted due to higher temperature gradients. However, the time to peak at all sensors in the soil column slightly decreased with the increase in temperature gradient. Similar to S1, S2 and S3 it is observed that the influence of change in temperature gradient on fluid flux passing through soil layers is gradual or not much significant in S4.

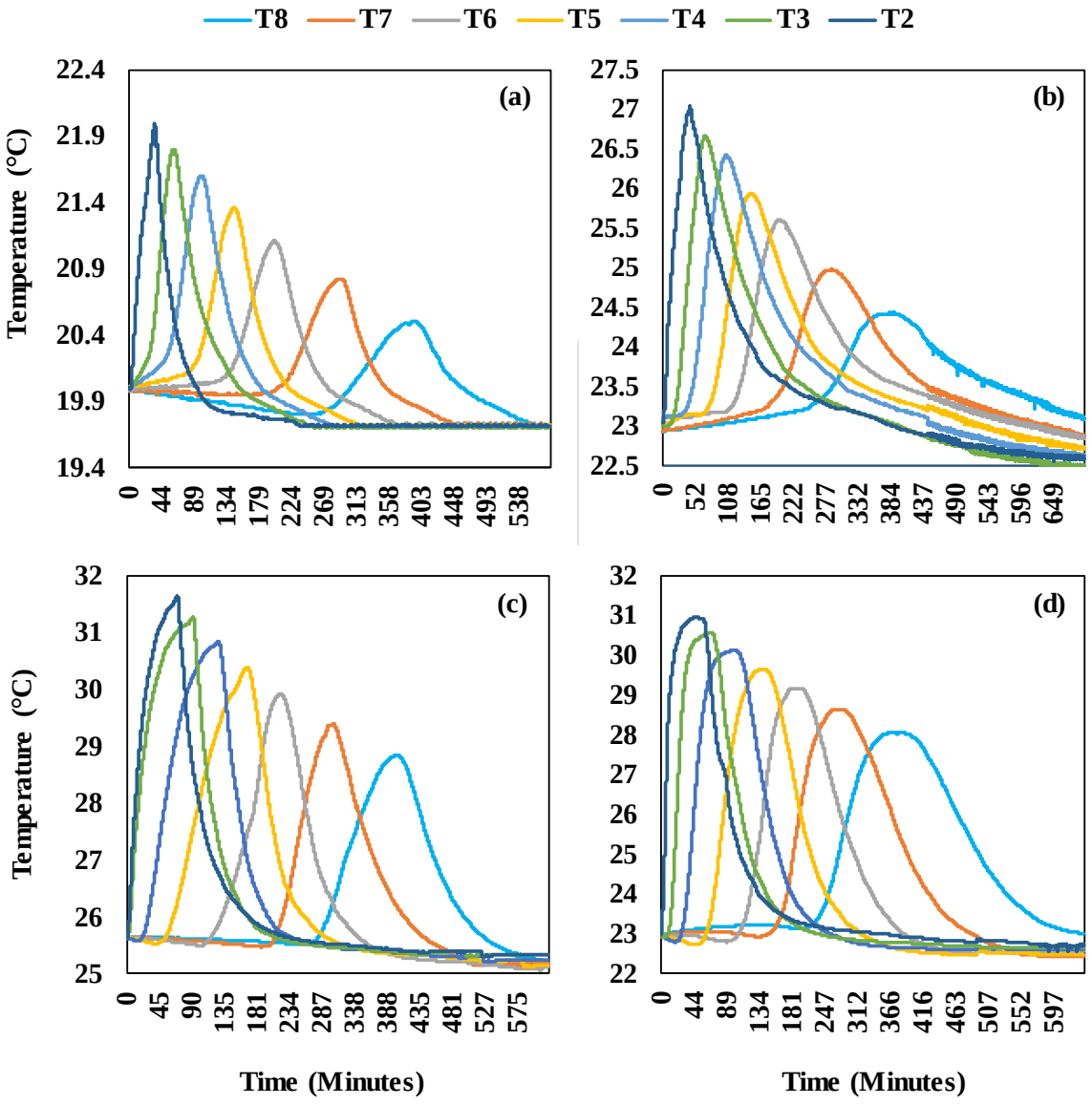

Figure 4.16: Variation of temperature profiles measured at different sensors in case of (a) S4-A1 (b) S4-A2 (c) S4-A3 (d) S4-A4

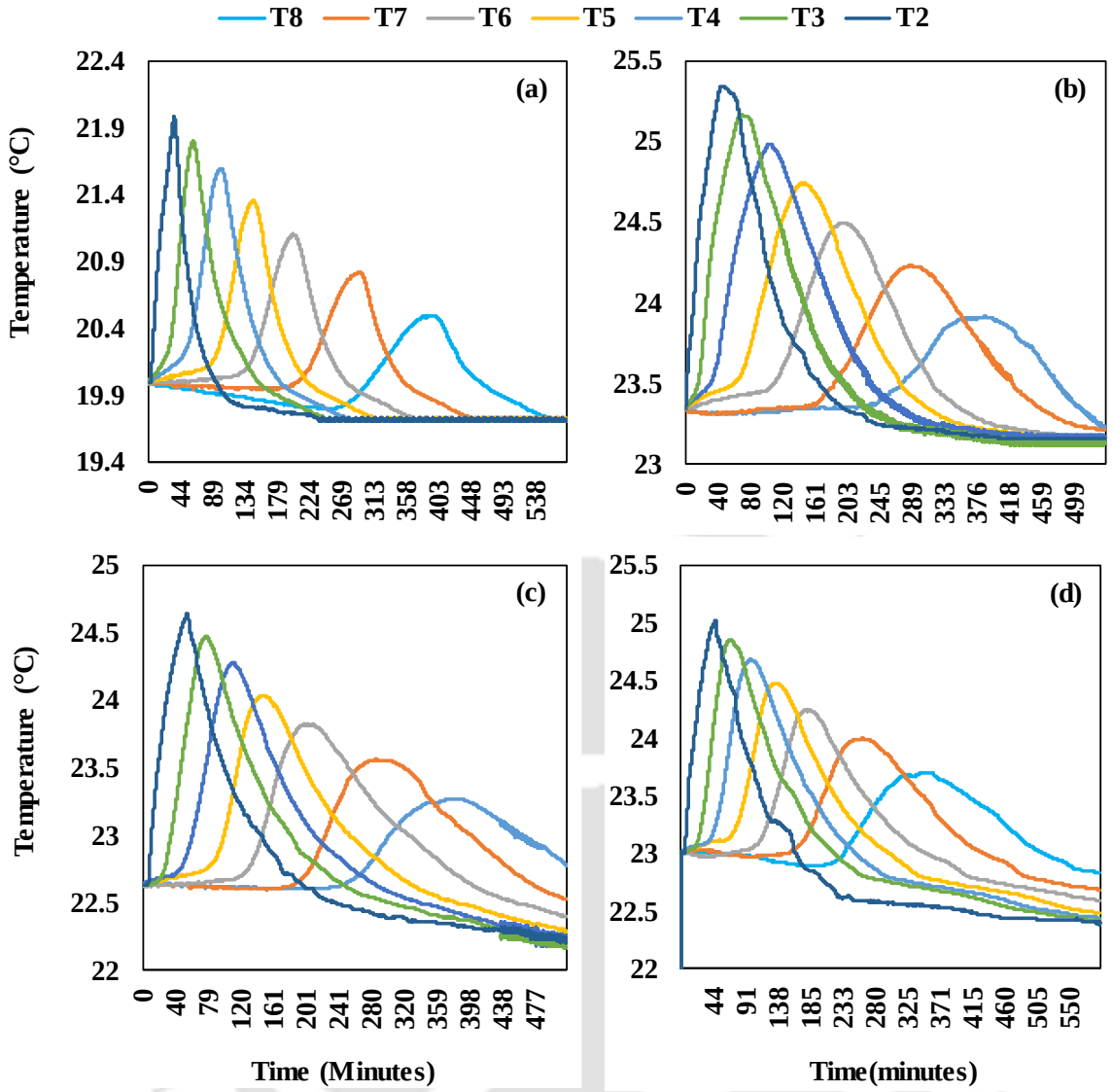

Figure 4.17: Variation of temperature profiles measured at different sensors in case of (a) S4-A1 (b) S4-B1 (c) S4-C1 (d) S4-D1

Figure 4.17 shows the variation of temperature profiles measured at different depths below the soil column in scenario 3 for different ponding depths (10, 11, 12 and 13 cm) and temperature gradient of 2°C (S4-A1, S4-B1, S4-C1 and S4-D1). Figure 4.17(a-b) presents the temperature profiles of case S4-A1 (depth 10 and temperature gradient of 2°C) and S4-B1 (ponding depth 11 cm and temperature gradient of 2°C). The time taken to attain the required temperature gradient (2°C) at sensor T2 for case S4-B1 is around 45 min and this value is noted to be less in case of S4-A1 (35 min). It can be observed that the responses of T3 and T4 sensors in top layer (MS) in case of S4-B1 are much quick and attained higher peaks (1.82° and 1.62°C) against S3-A1 (1.80° and 1.60°C) whereas the time taken to attain peak temperature (68 and 104 min for T3 and T4) was increased with increase in ponding depth to 11 cm against S4-A1 (62 and 100 min). It may be resulted due to the increment in

water depth from 10 to 11 cm might increase the fluid velocity. The amplitudes of sensors T5 and T6 positioned in the middle layer (FS II) are reduced to 1.40° and 1.15°C in S4-B1 and this reduction is found to be less compared to S4-A1 (1.36° and 1.10°C). Whereas, the time to peak at T5 (145 min) and T6 (200 min) is observed to be approximately the same for S4-A1 and S4-B1 (145 and 198 min). It is be resulted due to the increase in ponding depth might increase the fluid flux flow. Further, the amplitudes of sensors T7 and T8 in the bottom layer (FS I) reduced (0.88° and 0.57°C) and this reduction is also in case of S4-A1 (0.82° and 0.50°C) and the time to peak at sensors T7 and T8 further delayed (288 and 387 min) in case of S4-B1 whereas time to peak in case of S3-A1 also observed to be 293 and 396 min respectively.

Figures 4.17(c-d) present the vertical temperature profile variation at different sensor depths in case of S4-C1 (ponding depth 12 cm and temperature gradient of 2°C) and S4-D1 (ponding depth 13 cm and temperature gradient of 2°C). The observations drawn from these cases are similar to S4-A1 (Figure 4.17(a)). The amplitudes and time to peak at different sensors for different ponding depths at the constant temperature gradient (2°C) are presented in Table 4.12. Similar to S1, S2 and S3, the time to attain the required temperature gradient at sensor T2 increased with the increase in ponding depth except for S4-D1 against S4-C1 Higher incoming discharges might be caused this change. However, with the increase in ponding depth, the amplitude at each sensor observed to be increased while the time to peak decreased significantly (Table 4.16). It can be noted that the observations are similar to S1, S2 and S3. Also, it is clearly indicated that change in ponding depth has a significant influence on fluid flux over the change in temperature gradient. Similar to Scenario 3, the reduction in temperature amplitude and increase in time to peak in Scenario 3 is observed to be more than S3, S2 and S1.

Table 4.16: Temperature profile Amplitude and Time to peak at different sensors for different cases in Scenario 4

Variable	Case	Parameters	T2	T3	T4	T5	T6	T7	T8
(I) Ponding Depth (10 cm)	S4-A1	Amplitude (°C)	2.00	1.80	1.60	1.36	1.10	0.82	0.50
		Time to Peak (min)	35	62	100	145	200	293	396
	S4-A2	Amplitude (°C)	4.00	3.68	3.34	2.93	2.48	2.00	1.49
		Time to Peak (min)	45	70	106	149	202	291	391
	S4-A3	Amplitude (°C)	6.00	5.62	5.20	4.75	4.29	3.78	3.20
		Time to Peak (min)	70	93	127	167	219	305	403
	S4-A4	Amplitude (°C)	8.00	7.60	7.17	6.70	6.22	5.69	5.09
		Time to Peak (min)	48	69	101	140	189	273	370
(II) Temperature Gradient (2°C)	S4-A1	Amplitude (°C)	2.00	1.80	1.60	1.36	1.10	0.82	0.50
		Time to Peak (min)	35	62	100	145	200	293	396
	S4-B1	Amplitude (°C)	2.00	1.82	1.63	1.40	1.15	0.88	0.57
		Time to Peak (min)	45	68	104	145	198	288	387
	S4-C1	Amplitude (°C)	2.00	1.83	1.65	1.43	1.19	0.93	0.63
		Time to Peak (min)	54	75	108	148	199	286	382
	S4-D1	Amplitude (°C)	2.00	1.84	1.67	1.46	1.23	0.98	0.69
		Time to Peak (min)	48	67	98	135	183	262	357

Note:

(1) Amplitude is the difference between initial temperature and peak temperature; Time to peak is the time elapsed to reach the peak.

(2) I-Inter-comparison between experiments with constant ponding depth (10cm) and varying temperature gradient (2°, 4°, 6° and 8°C)

II- Inter-comparison between experiments with constant temperature gradient (2°C) and varying ponding depth (10, 11, 12 and 13 cm)

(3) T2 in ponding water; T3 and T4 in Medium Sand (MS); T5 and T6 in Fine Sand II (FS II); T7 and T8 in Fine Sand I (FS I)

4.4.4.2 Variation of Fluid Flux Profiles

In this section, estimated fluid flux (using Amplitude Ratio (AR) and Phase Difference (PD) methods) variation of Scenario 3 are presented and discussed. Figure 4.18(a-d) presents the variation of fluid fluxes estimated using Keery and Hatch Amplitude Ratio (AR) and Phase Difference (PD) methods in different cases (S4-A1, S4- A2, S4-A3 and S4-A4) in Scenario 4 (S4) with varying temperature gradient (2°, 4°, 6° and 8°C) while the ponding depth remains constant. It can be seen that the fluid fluxes in the top layer (Medium Sand) are higher than the middle layer (Fine Sand II) followed by Fine Sand II. Whereas, the fluxes are observed to be more in the bottom (Medium Sand) layer in Scenario 1, and in the top layer (Fine Sand II) in Scenario 2, in the bottom layer (Fine Sand II) in Scenario 3. Similar to S1, S2 and S3, in-comparison of fluxes estimated with Keery, Hatch AR and PD methods and the maximum and minimum values of fluxes are observed to be estimated using Keery AR method and PD methods (Table 4.17). The fluid fluxes estimated using Keery AR method for the cases S4-A1 (ponding depth of 10 cm and temperature gradient of 2°C), S4-A2 (ponding depth of 10 cm and temperature gradient of 4°C), S4-A3 (ponding depth of 10 cm and temperature gradient of 6°C) and S4-A4 (ponding depth of 10 cm and temperature gradient of 8°C) in top (FS I), middle (FS II) and bottom (MS) soil layers are shown in Figure 18 (a). It can be noted that the estimated fluxes slightly increased from 3.5 to 3.67 m/day in MS, 2.98 to 3.21 m/day in FS II, 2.64 to 2.8 m/day with an increment of temperature gradient by 2°C while the ponding depth remains constant (10 cm). Whereas, the fluxes estimated using Keery PD method are observed to be slightly increased from 4.61-4.80 m/day, 3.83-4.03 m/day, 3.42-3.53 m/day in MS, FS II and FS I layers respectively from case S4-A1 to S4-A4 (Figure 4.18(b)). Similar observations can also be seen in the case of fluxes estimated using Hatch AR and PD methods (Figure 4.18(c-d). However, similar to S1, S2 and S3, in very few cases, this behavior is different. For example, fluxes estimated using Keery PD method are observed to be decreased in the case of S4-A4 against S4-A3 in MS layer (Table 16). It may be due to the water level fluctuation while conducting the experiment. Table 16 shows the estimated fluid fluxes of various cases for Scenario 3 for different temperature gradients (2°, 4°, 6° and 8°C) at constant ponding depth (10 cm). It can be observed that the increase in temperature gradient slightly increased the fluid fluxes with while ponding depth remains constant. However, this increase is not much significant similar to S1, S2 and S3.

The variation of fluxes estimated using Keery and Hatch analytical methods obtained in Scenario 4 for four different ponding depths (10, 11, 12 and 13 cm) and temperature gradient (2°C) are shown in Figure 4.18(e-f). Figure 18 (e) shows the fluid fluxes estimated using Keery AR method in case of S3-A1 (ponding depth 10 cm and temperature gradient of 2°C), S3-B1 (ponding depth 11 cm and temperature gradient of 2°C), S3-C1 (ponding depth 12 cm and temperature gradient of 2°C) and S3-D1 (ponding depth 13 cm and temperature gradient of 2°C). It can be observed that the fluid fluxes increased from 3.50-4.63 m/day, 2.98-3.91 m/day, 2.64-3.59 m/day in top (MS), middle (FS II) and bottom (FS I) soil layers respectively with an increment of 1 cm ponding depth while the temperature gradient remains constant. Whereas, the fluxes estimated using Keery PD method are observed to be increased from 4.61-5.63 m/day, 3.83-4.77 m/day, 3.42-4.34 m/day in MS, FS II and FS I layers respectively from case S4-A1 to S4-D1 (Figure 4.18(f)). The observations drawn from these cases are similar to S1, S2 and S3 using Hatch and PD methods (Figure 418(g-h)). Table 4.18 shows the estimated fluid fluxes of various cases for Scenario 3 for different ponding depths (10, 11, 12 and 13 cm) and temperature gradient (2° C). It can be observed that fluid fluxes were significantly increased with the increase in ponding depth while temperature gradient remains constant similar to S1, S2 and S3. Also, it is clearly observed that change in ponding depth has a significant influence on fluid flux over the change in temperature gradient. Also, it can be noted that in all the experiments, the fluid fluxes are observed to be more in Medium sand (MS) than Fine Sand II (FS II) followed by Fine Sand I (FS I) irrespective of method. Similar to S1, S2 and S3, it can be found that Keery AR method provides good agreement with measured seepage velocity than Kerry PD, Hatch AR and PD methods (Table 4.18). It can also be observed that in comparison of fluxes estimated in S1, S2 and S3 with S4 indicates that the fluxes are observed to very less than S3, S2 and S1.

In the present study, it can be noted that Keery and Hatch methods showed disagreement with each other in all the scenarios considered and it might be due to the lack of consideration of dispersion term in Keery analytical method. It can also be observed that AR and PD methods (used both in Keery and Hatch methods) showed disagreement with each other. The differing sensitivities of these methods to input parameters might be a reason for this disagreement and also partly due to multidimensional (2D and 3D) nature of flow paths violating the one-dimensional assumption (Hatch et al., 2006; Keery et al., 2007). Overall, it is clearly observed that Keery AR methods provide good agreement with

measured seepage velocity at bottom outlet than other three methods (Tables 4.5, 4.6, 4.9, 4.10, 4.12, 4.13, 4.17 and 4.18).

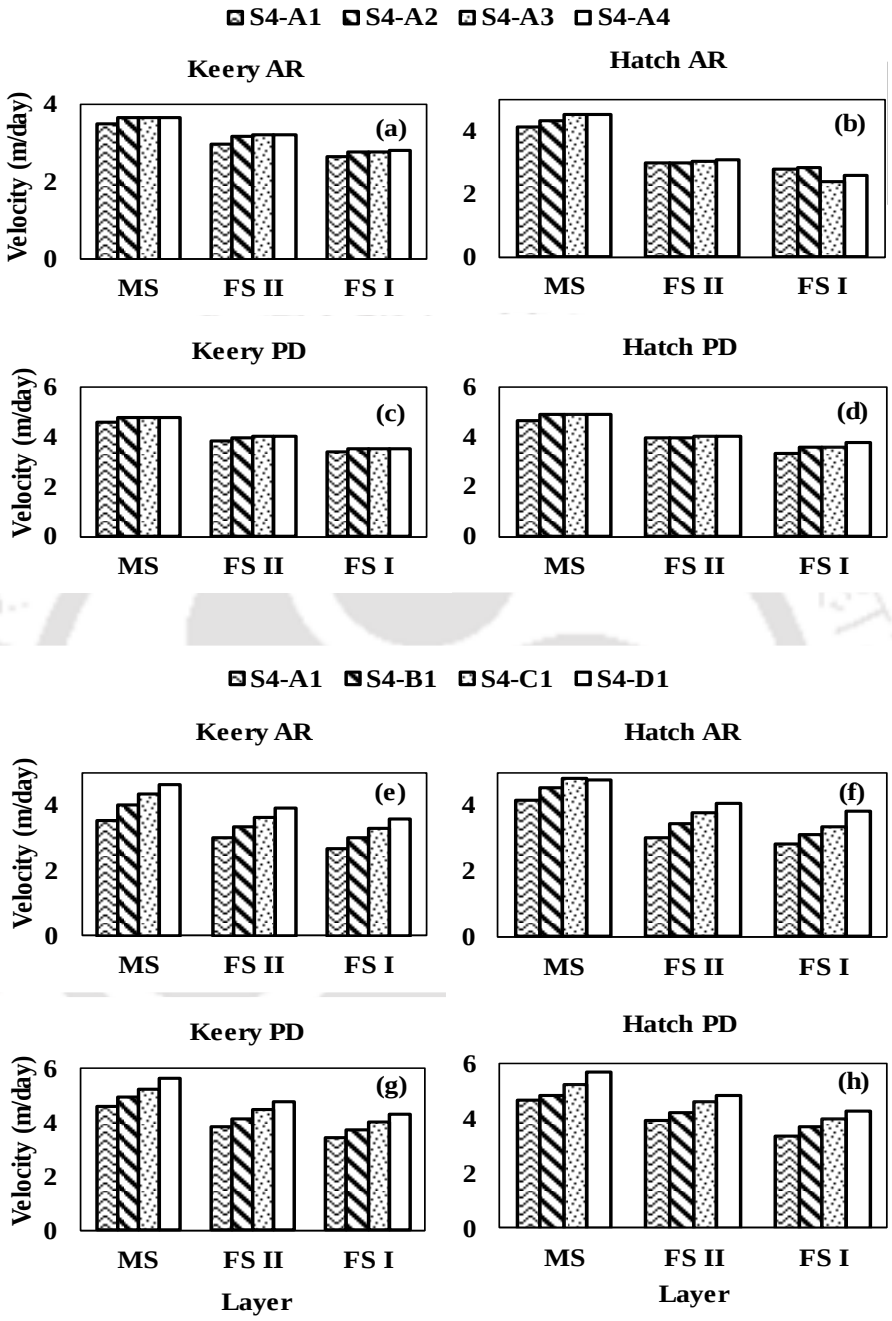

Figure 4.18: Fluid flux variation in different soil layers in Scenario 4 for the cases S4-A1, S4-A2, S4-A3 and S4-A4 using (a) Keery AR (b) Hatch AR (c) Keery PD (d) Hatch PD methods and for the cases S4-A1, S4-B1, S4-C1 and S4-D1 using (e) Keery AR (f) Hatch AR (g) Keery PD (h) Hatch PD methods

Table 4.17: Estimated fluid fluxes for different temperature gradients and ponding depth (10 cm) along with measured seepage velocities at the bottom outlet

Case	Soil Layer	Velocity (m/day)				Measured Velocity at outlet (m/day)
		Keery-AR	Keery-PD	Hatch-AR	Hatch-PD	
S4-A1	Medium Sand (MS)	3.50	4.61	4.17	4.67	2.48
	Fine Sand II (FS II)	2.98	3.83	3.01	3.94	
	Fine Sand I (FS I)	2.64	3.42	2.82	3.35	
S4-A2	Medium Sand (MS)	3.68	4.81	4.34	4.89	2.63
	Fine Sand II (FS II)	3.17	3.99	3.03	3.96	
	Fine Sand I (FS I)	2.78	3.50	2.84	3.60	
S4-A3	Medium Sand (MS)	3.68	4.81	4.54	4.90	2.71
	Fine Sand II (FS II)	3.22	4.05	3.04	4.01	
	Fine Sand I (FS I)	2.77	3.50	2.42	3.59	
S4-A4	Medium Sand (MS)	3.67	4.80	4.54	4.90	2.82
	Fine Sand II (FS II)	3.21	4.03	3.09	4.00	
	Fine Sand I (FS I)	2.80	3.53	2.63	3.76	

Table 4.18: Estimated fluid fluxes for different ponding depths and temperature gradient (2°C) along with measured seepage velocities at the bottom outlet

Case	Soil Layer	Velocity (m/day)				Measured Velocity at outlet (m/day)
		Keery-AR	Keery-PD	Hatch-AR	Hatch-PD	
S4-A1	Medium Sand (MS)	3.50	4.61	4.17	4.67	2.48
	Fine Sand II (FS II)	2.98	3.83	3.01	3.94	
	Fine Sand I (FS I)	2.64	3.42	2.82	3.35	
S4-B1	Medium Sand (MS)	4.02	4.93	4.54	4.85	2.89
	Fine Sand II (FS II)	3.33	4.15	3.43	4.20	
	Fine Sand I (FS I)	3.01	3.72	3.10	3.68	
S4-C1	Medium Sand (MS)	4.32	5.23	4.80	5.23	3.18
	Fine Sand II (FS II)	3.62	4.50	3.76	4.58	
	Fine Sand I (FS I)	3.29	4.04	3.32	3.98	
S4-D1	Medium Sand (MS)	4.63	5.63	4.75	5.67	3.48
	Fine Sand II (FS II)	3.91	4.77	4.05	4.84	
	Fine Sand I (FS I)	3.59	4.34	3.81	4.28	

4.4.4.3 Variation of Hydraulic Conductivity

Similar to S1, S2 and S3, the fluid fluxes estimated using Keery AR supported the results with measured seepage velocity in S4. These fluxes were used to calculate hydraulic conductivities of soil layers (using Darcy' law) for different scenarios. In this section, the calculated hydraulic conductivity variation of different soil layers of Scenario 4 is presented and discussed.

Figure 4.19 shows the variation of hydraulic conductivities of soil layers calculated using the fluxes with Keery AR method for different cases of Scenario 4. Although, hydraulic conductivities of Medium Sand (MS) are more than other soil layers in S1 and S2, whereas, similar to S3 the conductivities are more in Fine Sand I (bottom layer) followed by FS II and MS in case of S4. Figure 4.19(a) shows the variation of hydraulic conductivities for the cases S3-A1 (ponding depth of 10 cm and temperature gradient of 2°C), S3-A2 (ponding depth of 10 cm and temperature gradient of 4°C), S3-A3 (ponding depth of 10 cm and temperature gradient of 6°C) and S3-A4 (ponding depth of 10 cm and temperature gradient of 8°C) in top (MS), middle (FS I), bottom (FS II) soil layers. The calculated conductivity variation is insignificant (or less variation) and ranged from 0.69-0.73 m/day in MS, 1.01-1.09 m/day in FS II, 1.05-1.12 m/day in FS I layers respectively with an increment of temperature gradient by 2°C while the ponding depth remains constant (10 cm). Similar to S1, S2 and S3, it can be also noted that similar observations are also seen in the cases of varying ponding depth (10 cm) at constant temperature gradient (2°C). Figure 4.19(b) shows the hydraulic conductivity variation case S4-A1 (ponding depth of 10 cm and temperature gradient of 2°C), S4-B1 (ponding depth of 11 cm and temperature gradient of 2°C), S4-C1 (ponding depth of 11 cm and temperature gradient of 2°C) and S4-D1 (ponding depth of 11 cm and temperature gradient of 2°C) in MS, FS I and FS II layers. The hydraulic conductivity values slightly increased with an increment of ponding depth by 1 cm while the temperature gradient remains constant (2°C) and the values ranged from 0.69-0.82 m/day in MS, 1.01-1.26 m/day in FS II, 1.05-1.39 m/day in FS I layers respectively. However, it is observed that this increase in conductivity values are insignificant or not much varied with increase in ponding depth. The calculated hydraulic conductivity values of different cases (varying ponding depth and varying temperature gradient) of Scenario 4 are shown in Table 4.19. Similar to Scenario 1, 2 and 3, inter-comparison of different cases of Scenario 4 reveals that varying ponding depth and temperature gradient is not greatly influenced hydraulic conductivity values of soil layers.

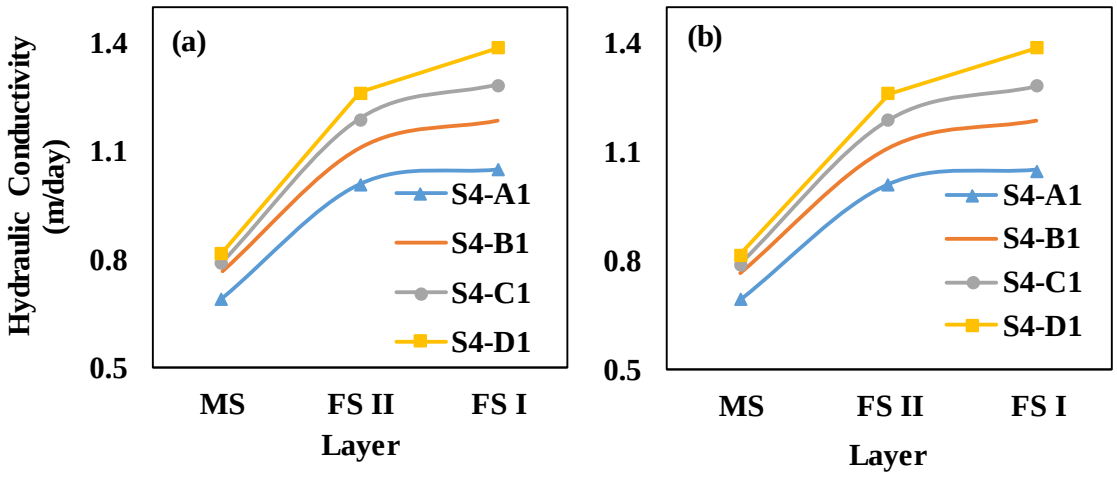

Figure 4.19: Hydraulic conductivity variation using Keery AR method in Scenario 4 for (a) S4-A1, S4-A2, S4-A3, S4-A4 (b) S4-A1, S4-B1, S4-C, S4-D1

Table 4.19: Calculated hydraulic conductivity of different soil layers for different temperature gradients at constant ponding depth (10 cm) in Scenario 4

Soil Layer	Case	Hydraulic Conductivity (m/day)	Case	Hydraulic Conductivity (m/day)
Medium Sand (MS)		0.69		0.69
Fine Sand II (FS II)	S4-A1	1.01	S4-A1	1.01
Fine Sand I (FS I)		1.05		1.05
Medium Sand (MS)		0.73		0.77
Fine Sand II (FS II)	S4-A2	1.07	S4-B1	1.11
Fine Sand I (FS I)		1.11		1.19
Medium Sand (MS)		0.73		0.79
Fine Sand II (FS II)	S4-A3	1.09	S4-C1	1.19
Fine Sand I (FS I)		1.10		1.28
Medium Sand (MS)		0.73		0.82
Fine Sand II (FS II)	S4-A4	1.09	S4-D1	1.26
Fine Sand I (FS I)		1.12		1.39

4.5 INTER-COMPARISON OF FLUID FLUXES OF DIFFERENT SCENARIOS

In order to understand the influence of stratified soils over fluid flux, comparisons between estimated fluid fluxes of the four Scenarios (S1, S2, S3 and S4) is made. Table 4.20 shows fluid fluxes estimated using Keery AR method between the Scenarios for case A1 (ponding depth 10 cm and Temperature gradient 2°C). In S1, less permeable soil layer (Fine Sand I (FS I)) was placed in top layer whereas moderately permeable (Fine Sand II (FS II)) and highly permeable (Medium Sand (MS)) were placed in middle and bottom layers respectively. In S1, fluid fluxes are found to be high in the bottom layer (MS) (17.81 m/day) followed by FS II (14.71 m/day) and FS I (12.26 m/day) which indicates less permeable soil (FS I) placed at top layer does not have any influence the fluxes in highly permeable soil (MS). Whereas, in S2, moderately permeable soil layer (FS II) was placed at top followed by less permeable soil layer was placed at the middle while highly permeable soil layer (MS) placed remained constant at the bottom. In S2, fluid fluxes are found to be high in FS II (13.44 m/day) followed by FS I (11.60 m/day) and MS (11.13 m/ day). It indicates less permeable soil (FS II) is placed over highly permeable (MS) soil has significant effect on fluxes in MS.

Similar observations can be drawn from the other two scenarios (S3 and S4). In S3 and S4, the top layers remain constant (MS), while the other two layers are shuffled. In S3, fluid fluxes are found to be high in the bottom layer (FS II) (11.42 m/day) followed by MS (11.04 m/day) and FS I (10.38 m/day) which indicates less permeable soil (FS I) placed at middle layer have less influence the fluxes in moderately permeable soil (FS II). Whereas, in S2, fluid fluxes are found to be high in MS (3.50 m/day) followed by FS II (2.98 m/day) and FS I (2.64 m/ day) which indicates highly significant influence of less permeable soil (FS II) on fluid fluxes in other layers.

Table 4.20: Estimated fluid fluxes in top, middle and bottom layers of Scenario 1, 2, 3 and 4

Layer Position	S1-A1		S2-A1		S3-A1		S4-A1	
	Layer	Velocity (m/day)	Layer	Velocity (m/day)	Layer	Velocity (m/day)	Layer	Velocity (m/day)
Top	FS I	12.26	FS II	13.44	MS	11.05	MS	3.50
Middle	FS II	14.71	FS I	11.60	FS I	10.38	FS II	2.98
Bottom	MS	17.81	MS	11.13	FS II	11.42	FS I	2.64

Note: Fluid fluxes estimated using Keery AR method are compared between Scenarios for the case A1 (Ponding depth 10 cm, Temperature gradient 2°C)

From this inter-comparison of fluid fluxes, it is understood that if highly permeable soils exist at the bottom layer, the influence of this soil cannot be seen in top layers and if less permeable exists at the bottom layer, highly significant influence can be seen on fluid fluxes in top layers.

4.6 STATISTICAL ANALYSIS OF FLUID FLUXES OF DIFFERENT SCENARIOS

Fluid flux values generated from varying ponding depth and constant temperature gradient were subjected to analysis of variance (ANOVA) and pairwise comparison using the Tukey-Kramer HSD test at $P \leq 0.05$. The results were analyzed using JMP Pro v. 14.0.0, SAS Institute Inc., Cary, NC [Varma et al., 2018].

The effect of changing ponding depth when temperature gradient remained constant with different scenarios 1, 2, 3 and 4 was found highly significantly different to the fluid flux. As depicted from the results of changing ponding depth from 10 cm to 13 cm, the fluid flux was increased gradually in all the scenarios. In contrast to the greater fluxes, the high significance effects were well supported by the statistical analysis and are presented in Table 4.21. Hence it can be concluded that the fluid fluxes projected using Keery AR method were in accordance with measured seepage velocity and corresponding fluxes calculated for hydraulic conductivities of soil layers using Darcy' law. However, the effect of ponding depth with the constant temperature gradient on fluid flux was not found significant throughout all the four scenarios. Hence, the significant flux values with respect to the changing pond depth can be used to explore the possible effects while changing the different ponding depths. Similarly, fluid fluxes generated from varying temperature gradient when ponding depth remained constant was also subjected to ANOVA Tukey-Kramer HSD test at $P \leq 0.05$. The effect of changing temperature gradient when ponding depth remained constant with different scenarios 1, 2, 3 and 4 was found not significantly different to the fluid flux and can be seen in Table 4.21. Therefore, from the statistical analysis it is evident that higher significance was found with the fluid fluxes by changing the ponding depth, but not varying temperature gradient.

Table 4.21: The significances of the ponding depth and temperature gradient on fluid flux

Scenario	Layer	Ponding Depth	Significant levels	Mean Flux value (m/day)	Temperature Gradient	Significant levels	Mean Flux value (m/day)
S1	FSI	10	C	12.47	2	A	12.99
		11	C	12.67	4	A	13.03
		12	B	13.29	6	A	13.10
		13	A	13.88	8	A	13.18
	FS II	10	C	14.95	2	A	15.61
		11	B	15.54	4	A	15.74
		12	A	16.24	6	A	15.85
		13	A	16.36	8	A	15.90
	MS	10	D	17.95	2	A	18.67
		11	C	18.55	4	A	18.76
		12	B	19.10	6	A	18.82
		13	A	19.54	8	A	18.89
S2	FS II	10	D	13.49	2	A	14.28
		11	C	14.14	4	A	14.37
		12	B	14.66	6	A	14.47
		13	A	15.32	8	A	14.48
	FS I	10	D	11.79	2	A	12.24
		11	C	12.11	4	A	12.35
		12	B	12.61	6	A	12.42
		13	A	13.05	8	A	12.51
	MS	10	C	11.26	2	A	11.73
		11	C	11.46	4	A	11.82
		12	B	12.12	6	A	11.90
		13	A	12.60	8	A	12.00

Scenario	Layer	Ponding Depth	Significant levels	Mean Flux value (m/day)	Temperature Gradient	Significant levels	Mean Flux value (m/day)
S3	MS	10	D	11.60	2	A	11.85
		11	C	11.64	4	A	11.96
		12	B	12.30	6	A	12.07
		13	A	12.85	8	A	12.08
	FS I	10	D	10.55	2	A	11.14
		11	C	10.99	4	A	11.22
		12	B	11.58	6	A	11.33
		13	A	12.00	8	A	11.44
	FS II	10	D	11.66	2	A	12.17
		11	C	12.07	4	A	12.29
		12	B	12.45	6	A	12.40
		13	A	13.16	8	A	12.49
S4	MS	10	C	3.63	2	A	4.12
		11	B	4.12	4	A	4.18
		12	A	4.48	6	A	4.23
		13	A	4.57	8	A	4.28
	FS II	10	D	3.15	2	A	3.46
		11	C	3.41	4	A	3.55
		12	B	3.67	6	A	3.59
		13	A	3.99	8	A	3.61
	FS I	10	C	2.75	2	A	3.13
		11	B	3.14	4	A	3.25
		12	B	3.29	6	A	3.25
		13	A	3.73	8	A	3.27

Note: Raw data was analyzed by the standard least squares fit model and compared by Tukey-Kramer HSD test and different letters (in each row) denote significantly different effect ($P \leq 0.05$).

4.7 VARIATION OF EFFECTIVE HYDRAULIC CONDUCTIVITY

In each scenario, Effective hydraulic conductivity (K_{eff}) of stratified soils were estimated using the concept of flow orthogonal to the plane of stratification (Appendix B) using the estimated hydraulic conductivities of all the three layers. K_{eff} of each case of all the four scenarios were calculated and presented in this section.

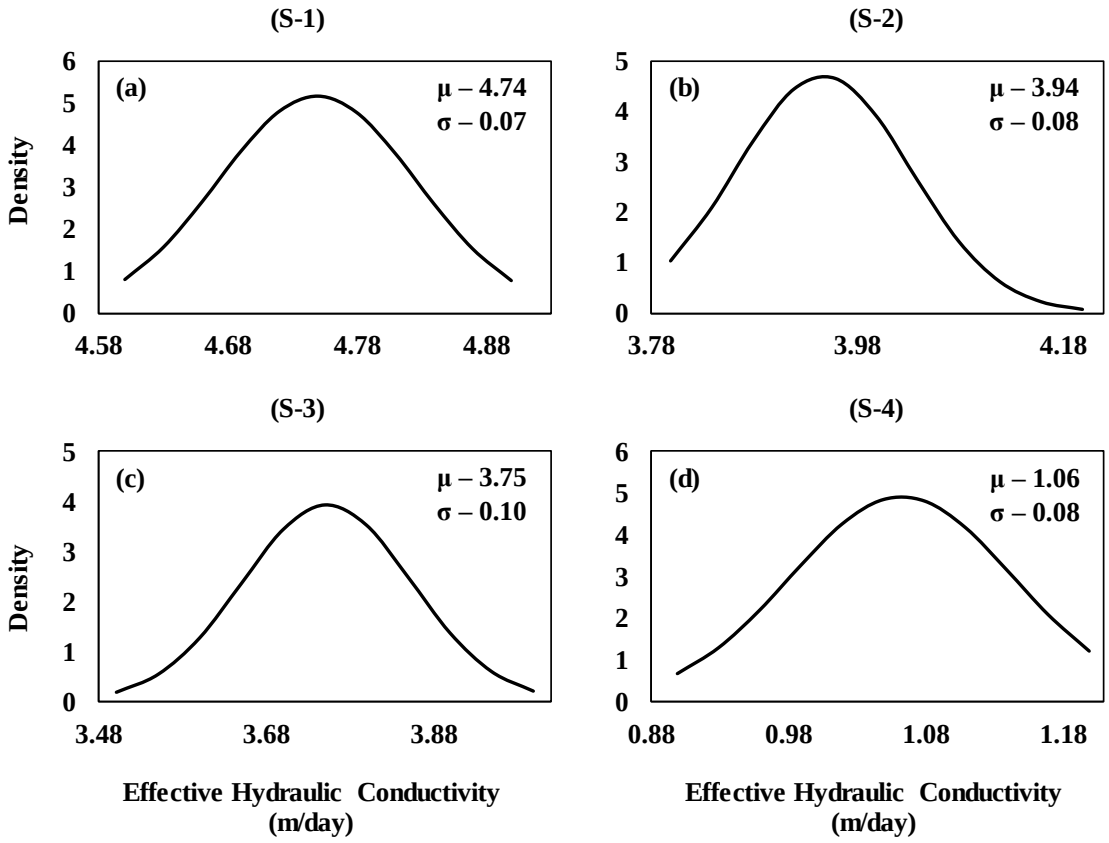

Figure 4.20: Normal distribution of Effective Hydraulic conductivity (K_{eff}) values in (a) Scenario 1(S1) (b) Scenario 2 (S2) (c) Scenario 3 (S3) (d) Scenario 4 (S4)

Note: μ indicates mean and σ indicates standard deviation

In the past, many researchers presented the Gaussian distribution for hydraulic conductivity, while other researchers presented with strong evidence of non-Gaussian distribution of hydraulic conductivity. Whereas, the findings of Lu et al. [2002] revealed that both the assumptions were correct depending on the heterogeneity structure [Meerschaert et al., 2013]. In this study, it is observed that K_{eff} of stratified soils followed normal distribution or Gaussian distribution in all the scenarios (Figure 4.20). In Scenario 1 (consists of Fine Sand I (FS I), Fine Sand II (FS II), Medium Sand (MS) at the top, middle and bottom respectively), fluid fluxes are observed to be higher than other scenarios. The reason for such behaviour is due to the placement of less permeable sand at top (Fine Sand

I), moderately permeable sand (FS II) in the middle layer, followed by highly permeable sand (MS) at the bottom. Furthermore, these higher fluxes caused to obtain higher K_{eff} values than the other three scenarios, ranging between 4.61-4.81 m/day with a standard deviation of 0.07 m/day (Figure 4.20(a)). In Scenario 2, as the fluxes obtained in the soil layers are less in comparison with S1, the K_{eff} values are also observed to be less in S2 than S1 (Figure 4.20(b)) with a range of 3.88-4.16 m/day (having a standard deviation of 0.08 m/day). The K_{eff} values are observed to be much lesser in S3 and S4 with a range of 3.56-3.89 m/day and 0.91-1.17 m/day respectively (Figure 20(c-d)). Table 4.22 shows calculated K_{eff} values of all the sixty-four experiments (sixteen experiments in each scenario) conducted in the sandbox. Whereas, Table 4.23 shows 10 percentile of K_{eff} (K_{eff-10}), 50 percentile of K_{eff} (K_{eff-50}) and 90 percentile of K_{eff} (K_{eff-90}) of the K_{eff} distribution of each scenario considered. These three different percentile values of K_{eff} in each scenario along with riverbed width and thickness are utilized to calculate riverbed conductance which is further utilized in groundwater modelling to assess river-aquifer exchange flux in chapter 5.

Table 4.22: Effective Hydraulic Conductivity (K_{eff}) of stratified soil for different cases of four different scenarios

Scenario 1	K_{eff} **(m/day)**	**Scenario 2**	K_{eff} **(m/day)**	**Scenario 3**	K_{eff} **(m/day)**	**Scenario 4**	K_{eff} **(m/day)**
S1-A1	4.61	S2-A1	3.88	S3-A1	3.56	S4-A1	0.91
S1-B1	4.64	S2-B1	3.94	S3-B1	3.60	S4-B1	0.96
S1-C1	4.66	S2-C1	3.96	S3-C1	3.63	S4-C1	0.96
S1-D1	4.67	S2-D1	3.97	S3-D1	3.67	S4-D1	0.97
S1-A2	4.69	S2-A2	3.92	S3-A2	3.64	S4-A2	1.01
S1-B2	4.72	S2-B2	3.92	S3-B2	3.66	S4-B2	1.05
S1-C2	4.76	S2-C2	3.93	S3-C2	3.70	S4-C2	1.06
S1-D2	4.75	S2-D2	3.94	S3-D2	3.72	S4-D2	1.06
S1-A3	4.76	S2-A3	3.98	S3-A3	3.73	S4-A3	1.08
S1-B3	4.79	S2-B3	4.01	S3-B3	3.75	S4-B3	1.08
S1-C3	4.81	S2-C3	4.05	S3-C3	3.79	S4-C3	1.10
S1-D3	4.83	S2-D3	4.09	S3-D3	3.81	S4-D3	1.13
S1-A4	4.80	S2-A4	4.06	S3-A4	3.82	S4-A4	1.14
S1-B4	4.81	S2-B4	4.09	S3-B4	3.87	S4-B4	1.16
S1-C4	4.84	S2-C4	4.12	S3-C4	3.89	S4-C4	1.16
S1-D4	4.86	S2-D4	4.16	S3-D4	3.89	S4-D4	1.17

.

Table 4.23: 10, 50 and 90 percentile of Effective Hydraulic Conductivity (Keff) of stratified soil for different cases of four different scenarios

PERCENTILE	K_{eff} (m/day)			
	S1	S2	S3	S4
10	4.62	3.83	3.55	0.93
50	4.74	3.99	3.75	1.05
90	4.86	4.15	3.95	1.17

To further analyze how the variables, ponding depth (D) and temperature gradients (T) affects the K_{eff} of stratified soils, three-dimensional responses are plotted (Figure 4.22). The variation of K_{eff} against ponding depth and temperature gradient of scenario 1 are presented in Figure 4.21(a). It showed that the variation of K_{eff} is less (around 4.60 m/day) at ponding depth of 10 cm and temperature gradient of 2°C and this similar response is seen up to the gradient of 4°C (4.68 m/day), while the ponding depth remained constant. Further, increase in temperature gradient by 2°C at constant ponding depth slightly increased the K_{eff} values (around 4.76 m/day) and the similar response is seen at gradients 6 and 8°C (4.76 and 4.79 m/day). At ponding depth of 11, 12 and 13 cm also, the increment in K_{eff} with an increment of temperature gradient is not significant or less variation. From these observations, it can be noted that the influence of increase in temperature gradient on K_{eff} is less or not significant while the ponding depth remains constant.

When the temperature gradient remains constant (2°C), the K_{eff} values did not show much variation for the increment of ponding depth from 10 to 13 cm (4.60-4.67 m/day). At temperature gradient of 4°C also, there is not much variation in K_{eff} (4.68-4.75 m/day) with increase in ponding depth. Similar observations are noted at 6 and 8°C with an increment of 4.76-4.82 m/day and 4.79-4.86 m/day as the ponding depth increased from 10 to 13 cm. With these observations, it can be noted that the effect of increasing ponding depth on K_{eff} is not significant or less while the temperature gradient remains constant. This analysis reveals that increase or change in ponding depth or temperature gradient has not much significant influence on K_{eff}. Although, there is not much influence of both the variables, the influence of temperature on K_{eff} is more over the influence of ponding depth. Also, as shown in the three-dimensional plot, the K_{eff} value is more effected at higher ponding depths (PD) and temperature gradients (TG) and this nature can be seen in all other scenarios (Figures (4.21(c-d)).

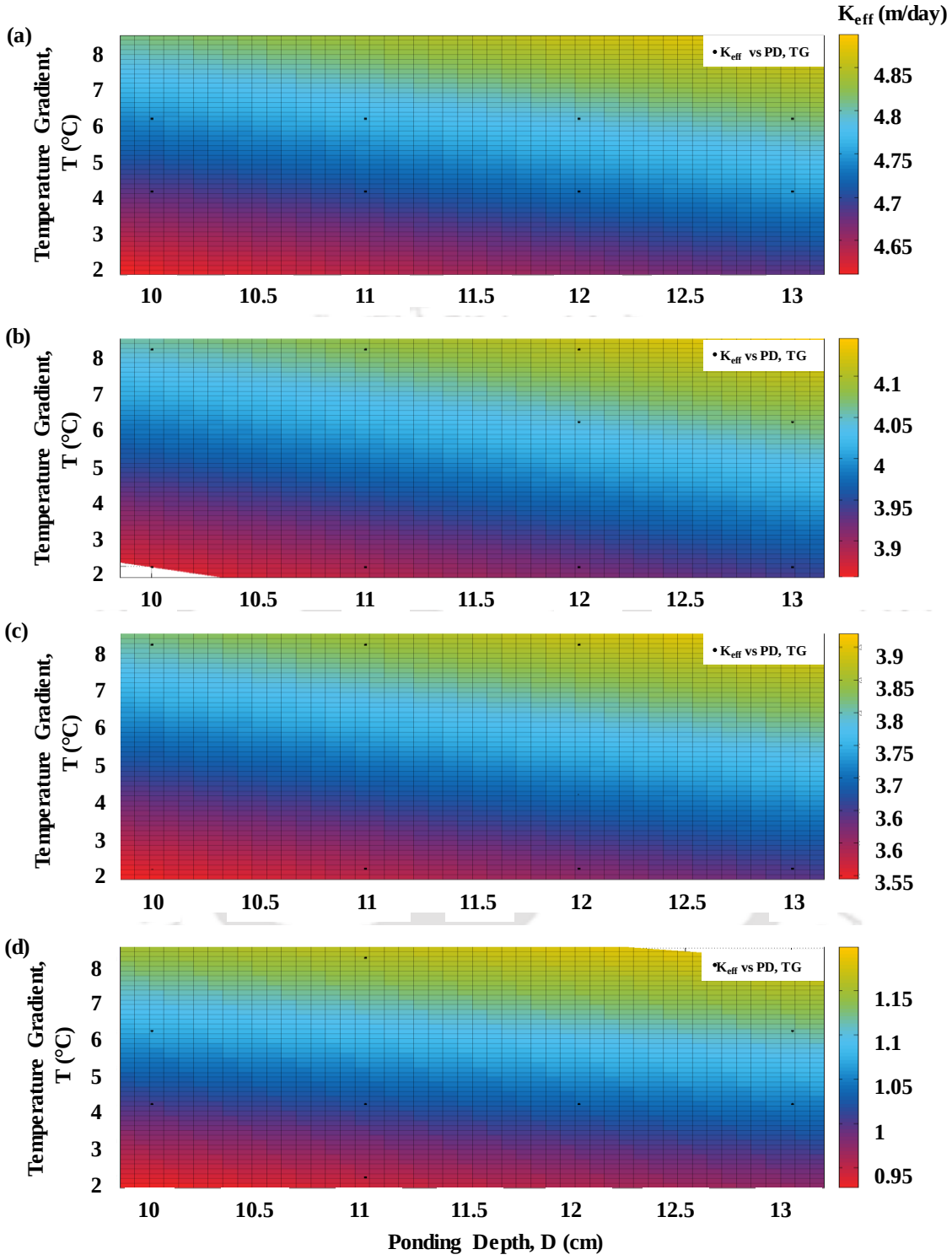

Figure 4.21: Three-dimensional plot between ponding depth (PD), Temperature gradient (TG) and Effective Hydraulic conductivity (K_{eff}) in (a) Scenario 1 (S1) (b) Scenario 2 (S2) (c) Scenario 3 (S3) (d) Scenario 4 (S4)

The calculated K_{eff} values in each scenario were used to obtain the empirical equation with polynomial 1st order function and its generalized form is given below as

$$K_{eff} = ax+by+c \quad (4.12)$$

Table 4.24 shows the empirical equation coefficients (a, b and c) obtained in each scenario along with R-square, RMSE and SSE.

Table 4.24: Empirical equations of K_{eff} for Scenario 1, 2, 3 and 4

Scenario	Type of fit and order	R-Square	RMSE	SSE	a	b	c
1	Polynomial 1st order	0.95	0.016	0.003	0.0224	0.0307	4.337
2	Polynomial 1st order	0.83	0.033	0.014	0.0263	0.0305	3.545
3	Polynomial 1st order	0.98	0.013	0.002	0.0301	0.0417	3.177
4	Polynomial 1st order	0.96	0.015	0.003	0.0144	0.0337	0.727

4.8 CONCLUSIONS

In the present study, heat was used as a natural tracer to estimate the fluid flux and riverbed hydraulic conductivity through the sediment-water interface based on laboratory experiments conducted in the sandbox. In order to understand the variation in fluid flux and hydraulic conductivity for different conditions, a series of experiments were conducted with four different scenarios (soil combinations, temperature gradients (gradient between hot water and normal water) and ponding depths. The conclusions from this chapter are listed as following:

Vertical thermal profiles were measured in soil column for different conditions (changing soil combination, varying ponding depth and temperature gradient) to estimate the fluid flux in different soil layers using four different analytical solutions i.e. Keery and Hatch Amplitude Ratio (AR) and Phase Difference (PD). Among these four methods, fluid fluxes estimated using Keery Amplitude Ratio method were observed to have good agreement with measured seepage velocity. The observed pattern could be due to the lack of consideration of dispersion term in Keery analytical method and violating the one-dimensional assumption.

Inter comparisons of four different scenarios showed that fluid fluxes were observed to be more in Scenario 1 (Fine Sand I at top, Fine Sand II at middle and Medium Sand at bottom layers) than other three scenarios. It is resulted due to the placing of highly

permeable media at bottom, moderately permeable soils at middle and less permeable media at top positions.

The influence of ponding depth and temperature gradient on fluid flux were analyzed using ANOVA (TukeyKramer HSD test at $P \leq 0.05$) by considering different cases i.e. varying temperature gradient while ponding depth remained constant and in other case, temperature was constant against varying ponding depth. This analysis revealed that ponding depth had a significant influence on fluid flux over temperature gradient in all the four scenarios considered.

Effective Hydraulic Conductivities (K_{eff}) calculated using hydraulic conductivities (estimated from the fluid fluxes) of different soil layers in all the four scenarios followed Gaussian distribution and the influence of ponding depth and temperature gradient on K_{eff} was observed to be not significant. However, the influence of temperature gradient was noted to be more over ponding depth. Furthermore, these K_{eff} values can be used in groundwater flow modelling of Kosi river basin to calculate riverbed conductance as the Kosi riverbed consists of similar type of sands those are used in the experimental study.

5

ASSESSMENT OF RIVER-AQUIFER INTERACTIONS

5.1 INTRODUCTION

River-aquifer interaction is a critical hydrological process and its investigation needs to be conducted at river reach scale [Winter et al., 1998]. Due to differences in total head of river water and groundwater, either a river loses water to a shallow aquifer (influent) or gains water from a shallow aquifer (effluent). This nature of losing or gaining may change over time and space with temporal changes of river stage and groundwater levels [Engeler et al., 2011]. The distribution of hydraulic head between river and aquifer as well as the distribution of hydraulic conductivity of the riverbed are the major factors that influence the river-aquifer exchange flux [Doppler et al., 2007]. In most of the basin systems, majority of the base flow during lean season comes from the groundwater flow through hyporheic zone although the water from lakes or glaciers contribute to base flows in some basin systems [Olsen and Young, 2009]. Understanding and quantifying the river-aquifer exchange flux is essential for effective groundwater management [Sophocleous, 2002].

Many researchers have recently focused on assessment of river-aquifer interaction at different spatial and temporal scales [Workman et al., 1997; Eikenberg et al., 2001; Miller et al., 2003; Rushton, 2007; Derx et al., 2010; Chitsazan et al. 2014; Bailey et al., 2016; Tang et al., 2017; Vrzel et al. 2018; Sahoo and Sahoo 2019]. New methodologies and approaches for understanding and quantification of river-aquifer exchange have been

practicing around the globe [Ward et al., 2013; McCallum et al., 2014; Rahman et al., 2016; Epting et al., 2018; Wen et al., 2019]. Water balancing method [Krause et al., 2007]; tracer test [Martinez et al., 2015; Xu et al., 2017], measuring streambed temperature profiles [Anibas et al., 2016; Essaid and Caldwell, 2017] and use of seepage meters [Brodie et al., 2009] are some of the field techniques. Whereas, numerical modelling approaches have been employed to quantify river-aquifer exchange flux at larger scales [Werner et al., 2006; Rushton, 2007; Sanz et al., 2011; Bailey et al., 2016; Kumar and Nagaraj, 2018]. The most commonly used numerical model to simulate surface water–groundwater interactions is MODFLOW [McDonald and Harbaugh, 1988; Barlow and Harbaugh, 2006; Furman, 2008]. In order to quantify these interactions, groundwater models need accurate inputs (recharge and evapotranspiration) and parameters (conductance, thickness and width of riverbed) [Brunner et al., 2017].

In this chapter, the study has focused on use of high-resolution remote sensing inputs (evapotranspiration) and surface water hydrological model inputs (recharge) along with riverbed parameters (riverbed hydraulic conductivity, width and thickness) to develop groundwater model for quantifying sptaio-temporal river-aquifer interaction exchange fluxes along the Kosi river, India.

5.2 STUDY AREA

In the present study, assessment of river-aquifer interactions was carried out in plain parts of the Kosi river basin using sub-surface hydrological flow model. Figure 5.1 shows the study area map of Kosi river basin, consist of seven sub-basins namely S-11, S-12, S-13, S-14, S-15, S-16 and S-17. Based on topography, these sub-basins were generated in the watershed delineation process of surface water hydrological modelling using SWAT. In the basin, the river has a length of 240 km reach from upstream (Kosi barrage) to downstream (conferencing point with the Ganga river) locations. Two observation well stations, Supaul and Jaynagar, located in sub-basins S-15 and S-12 were used to calibrate and validate the groundwater model. Furthermore, the details of the study area can be seen in the previous section (3.1).

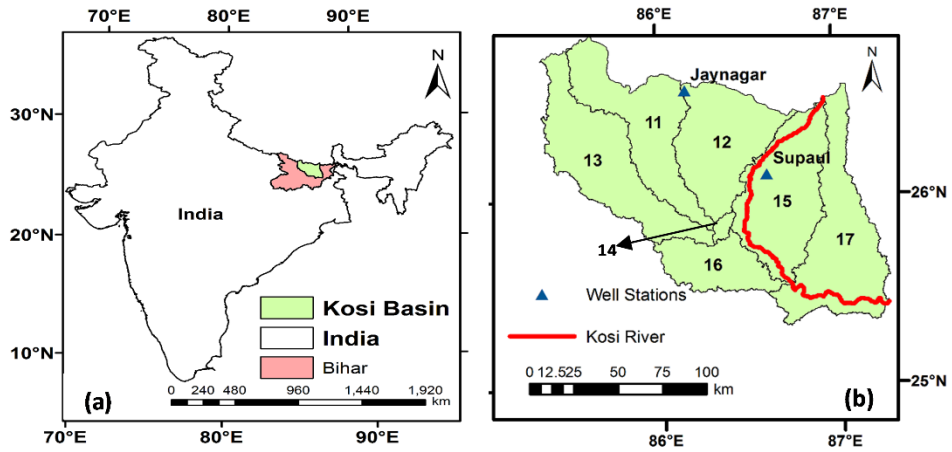

Figure 5.1: (a) Location of study area (b) Sub-basin map along with Kosi river reach and observed groundwater well stations

5.3 DATA USED

The assessment of river-aquifer interaction exchange flux was carried out using a transient sub-surface hydrological flow model (MODFLOW). In order to model the groundwater flow, MODFLOW needs the data such as topography, soil characteristics, aquifer characteristics, inflows and outflows into the groundwater system. Also, historical groundwater levels are required to calibrate and validate the flow model. The following data (obtained from various sources) were used in the study.

a) Digital Elevation Model: USGS, SRTM (Shuttle Radar Topography Mission) (90m spatial resolution).

b) **Aquifer Characteristics:** Aquifer characteristics such as hydraulic conductivity, specific storage, specific yield, and porosity have been obtained from Central Groundwater Board (CGWB), Patna and also from the past literature [Heath, 1983 and Ferris et al. 1962].

c) **Soil Characteristics:** Soil types in the study area have been obtained from Fence diagram map prepared by CGWB, Patna.

d) **Groundwater Recharge:** Monthly groundwater recharge estimated using the SWAT model and SWB method at the sub-basin scale (discussed in previous section 3.8).

e) **Evapotranspiration Estimates:** Evapotranspiration gridded data obtained from NOAA satellite data (8 km ×8 km) during 1996-2000 and MODIS Satellite data (1

km ×1 km) during 2000-2010 were used to construct the model [Bhattacharya et al. 2010; Mallick et al. 2007]

f) Historical Groundwater Level Information: Historical groundwater levels for four different periods i.e. pre-monsoon Rabi (January), pre-monsoon (April/May), monsoon (August) and post-monsoon Kharif (November) for the period 1996 to 2010 have been obtained from CGWB, Patna (http://www.india-wris.nrsc.gov.in/GWLevelApp.html?UType=R2VuZXJhbA==?UName=).

g) Riverbed Conductance: Riverbed conductance was calculated using the effective hydraulic conductivity of riverbed material (estimated using sandbox experiments), river bed width (mapped from google earth satellite images) and river bed thickness of 2m obtained from Sinha et al. [2019].

h) **River Stage**: River stage at Kosi barrage (upstream) and Baltara gauging station (downstream) were obtained from Central Water Commission (CWC), Patna.

5.4 METHODOLOGY

In the present study, the transient sub-surface hydrological modelling was carried out in Kosi river sub-basin with GMS-MODFLOW, version 10.2 (Modular Three-Dimensional Finite-Difference Ground-Water Flow Model) using available aquifer characteristics and other external stresses to predict spatio-temporal variations in groundwater levels and river-aquifer interaction exchange flux. For this purpose, two different cases were considered in sub-surface hydrological modelling. In the first case (case I), groundwater flow modelling was carried out with the estimated recharge (using the SWAT model), satellite-based evapotranspiration data, aquifer parameters, initial and boundary conditions. Whereas in the second case (case II), groundwater flow modelling was carried out with estimated recharge (using SWB method), satellite-based evapotranspiration data and other inputs (utilized in case I) remain unchanged. The transient model was calibrated and validated with observed groundwater heads for obtaining seasonal as well as groundwater level variations. MODFLOW-RIV (River) package was used to quantify river-aquifer exchange fluxes in the basin. Figure 5.2 shows the methodology adopted for studying river-aquifer interaction in the Kosi river basin.

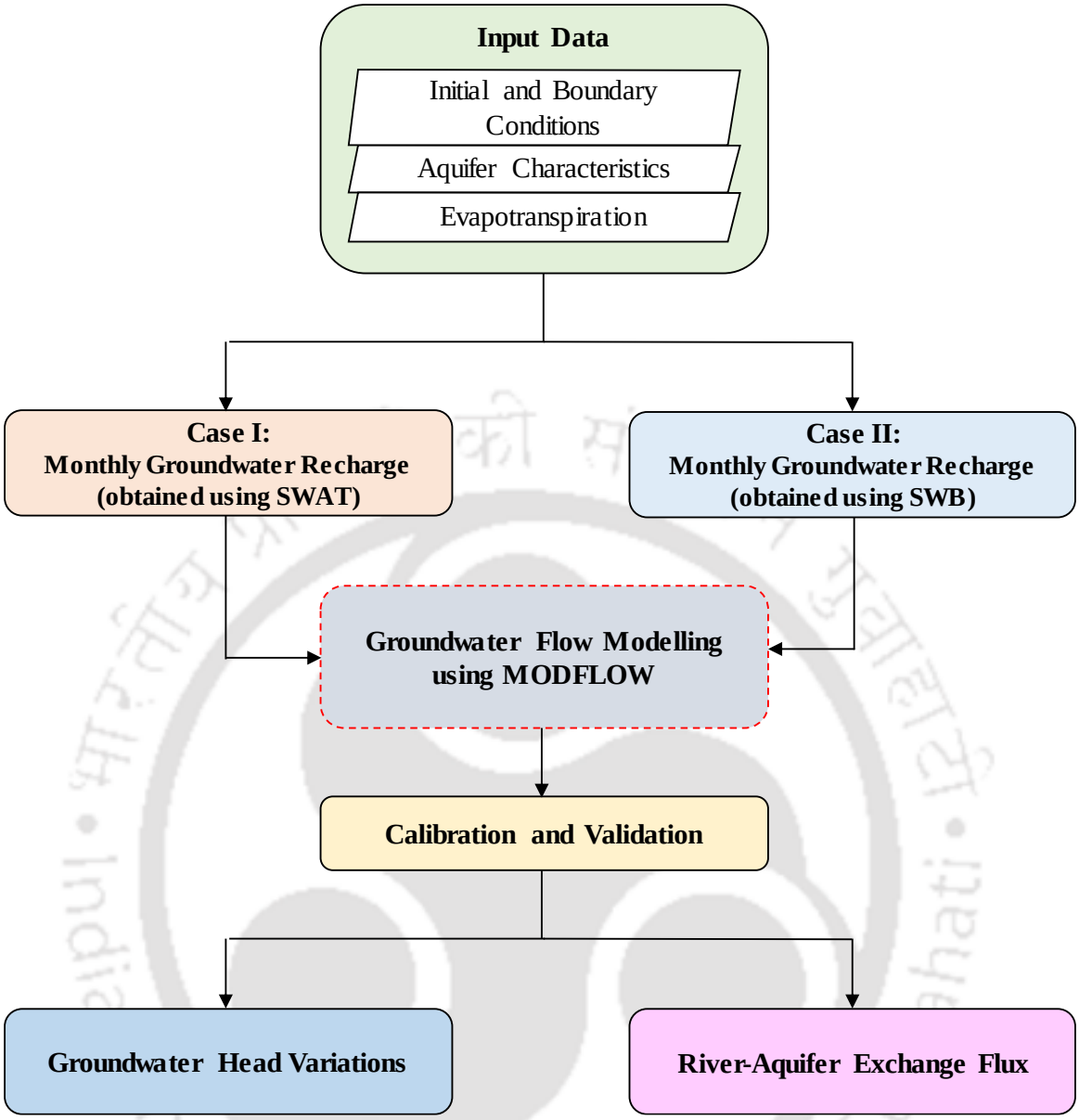

Figure 5.2: Methodology for studying river-aquifer interaction of the Kosi River with different input dataset

In order to quantify the exchange flux accurately, MODFLOW River package requires riverbed conductance values along the river reach. Estimation of this riverbed conductivity plays a vital role in the assessment of river-aquifer exchange flux [Boano et al., 2014] and chapter 4 (laboratory-based sandbox experimental study) focused on the estimation of Effective Hydraulic Conductivity (K_{eff}) of the riverbed. These K_{eff} values were utilized along with riverbed width and riverbed thickness to calculate riverbed conductance for four different scenarios (Scenario 1 (S1), Scenario 2 (S2), Scenario 3 (S3) and Scenario 4 (S4)) discussed in the previous section (4.14). Table 4.22 (section 4.4) provides the distribution of K_{eff} values in each scenario. Those distributions i.e. 10

percentile of K_{eff} (K_{eff-10}), 50 percentile of K_{eff} (K_{eff-50}) and 90 percentile of (K_{eff-90}) were used to calculate riverbed conductance for each scenario (i.e. three K_{eff} values were used to obtain three riverbed conductivities for each scenario). In both the cases of groundwater flow modelling, the simulations were carried out by incorporating these calculated riverbed conductance values of each scenario.

5.5 SUB-SURFACE HYDROLOGICAL MODELLING USING MODFLOW

MODLFOW is a three-dimensional finite-difference groundwater model. It was first developed in 1984. The model has a modular structure that allows it to be easily adjusted to adapt the code for a particular application. MODLFOW 2005 [Halford and Hanson, 2002; Harbaugh, 2005] simulates the steady and unsteady (transient) flow in irregularly shaped aquifer flow system. The aquifer may be of type confined, unconfined or combination of both. In this model, flow from external stresses such as areal recharge, evapotranspiration, flow to wells, flow to drains, flow through river beds can also be simulated. Boundary conditions can be applied using the specified head and specified flux boundary conditions [McDonald, 1994].

There are two approaches in MODFLOW to construct a model. One is grid approach and another one is conceptual approach. In the grid approach, the cell by cell basis calculations are made for 3D grids, sources/sinks and other model parameters. Whereas, the conceptual approach involves using the GIS tools in the Map module to construct the conceptual model. Sources/Sinks and other all parameters can be defined at the conceptual model. After specifying the grid size, all the parameters can be converted to grid model automatically by cell by cell basis. In this present study, groundwater flow modelling is being carried out to obtain groundwater level variations using GMS MODFLOW (10.2 version) with conceptual modelling approach.

5.5.1 Governing Equations used in MODFLOW

The governing flow equation to obtain simulated groundwater levels at each time step and the equation used in MODFLOW RIV package to obtain river-aquifer exchange flux are presented in the following section [McDonald and Harbaugh, 1988].

5.5.1.1 Groundwater Flow Equation

The partial-differential equation of three-dimensional movement of groundwater flow of constant density through porous earth material can be described as (by considering water is incompressible)

$$\frac{\partial}{\partial x}(K_{xx}\frac{\partial h}{\partial x})+\frac{\partial}{\partial y}(K_{yy}\frac{\partial h}{\partial y})+\frac{\partial}{\partial z}(K_{zz}\frac{\partial h}{\partial z})+W=S_s\frac{\partial h}{\partial t} \qquad (5.1)$$

where,

K_{xx}, K_{yy}, K_{zz} are the hydraulic conductivities along the x, y, z coordinate axes (L/T), respectively

h is the potentiometric head (L),

W is the volumetric flux per unit volume representing sources and or sinks of water (T^{-1}),

S_s is the specific storage of the porous material (L^{-1}),

t is the time (T).

In case of homogeneous aquifer, the equation 5.1 is simplified as

$$K_{xx}\frac{\partial^2 h}{\partial x^2}+K_{yy}\frac{\partial^2 h}{\partial y^2}+K_{zz}\frac{\partial^2 h}{\partial z^2}+W=S_s\frac{\partial h}{\partial t} \qquad (5.2)$$

In case of homogeneous isotopic aquifer,

$$K_{xx}=K_{yy}=K_{zz}=K \qquad (5.3)$$

hence,

$$K\frac{\partial^2 h}{\partial x^2}+K\frac{\partial^2 h}{\partial y^2}+K\frac{\partial^2 h}{\partial z^2}+W=S_s\frac{\partial h}{\partial t} \qquad (5.4)$$

For steady-state model, $\frac{\partial h}{\partial t}=0$

Hence, in the case of steady-state, groundwater flow equation for homogeneous isotropic aquifer is given by,

$$K\frac{\partial^2 h}{\partial x^2}+K\frac{\partial^2 h}{\partial y^2}+K\frac{\partial^2 h}{\partial z^2}+W=0 \qquad (5.5)$$

5.5.1.2 Flow between River and Groundwater

River may gain or loss water from the adjacent aquifer through riverbed depending on the head gradient between river and groundwater system. The rive-aquifer exchange flux rate can be quantified using MODFLOW RIV package using the following equation.

$$QRIV_{nb} = CRIV_{nb}(HRIV_{nb} - h_n) \qquad (5.6)$$

$$CRIV_{nb} = \frac{K_{nb} L_{nb} W_{nb}}{b} \qquad (5.7)$$

where,

$QRIV_{nb}$ is the flow between river and aquifer (L^3/T),

$CRIV_{nb}$ is the hydraulic conductance of the river-aquifer interaction (L^2T^{-1}),

$HRIV_{nb}$ is the water level in the river (L),

h_n is the head at the node in the cell underlying the river reach (L),

K_{nb} is the hydraulic conductivity of the riverbed material,

L_{nb} is the length of conductance block (L),

W_{nb} is the width of the river (L),

b_{nb} is the length of flow or thickness of riverbed (L) and

nb indicates boundary condition which is connected to cell n

5.6 GROUNDWATER FLOW MODELLING FOR KOSI RIVER BASIN

In order to assess the groundwater levels and river-aquifer exchange flux in Kosi river basin, a conceptual model was developed for the time period 1996-2010 using MODFLOW module of Groundwater Modelling Software (GMS- version 10.2). The modelling was carried out using the estimated recharge (discussed in chapter 3), observed evapotranspiration data, soil and aquifer characteristics data along with the calculated river bed conductance (discussed in chapter 4). The boundary conditions, initial conditions and all the information used in the model are explained below.

- **Boundary Conditions:** Specified head boundary condition (Dirichlet or first-type boundary conditions) was used along all sides of the boundary

- **Initial Heads or Starting Heads:** For constructing the groundwater flow model, initial or starting heads are required. For this purpose, observed averaged historical groundwater levels in the study area were used to start the model.
- **Aquifer Top Elevations:** SRTM 90 × 90 m gridded digital elevation model was used to obtain top elevations in the study area.

As a part of the conceptual model building process, a solid model (the stratigraphy at a site was modelled as a set of solids) was generated using borehole cross-section and topography data in which aquifer properties such as porosity, specific storage and hydraulic conductivities of different layers incorporated. This solid model was later utilized in the conceptual framework to read elevation and aquifer characteristics data through GIS environment.

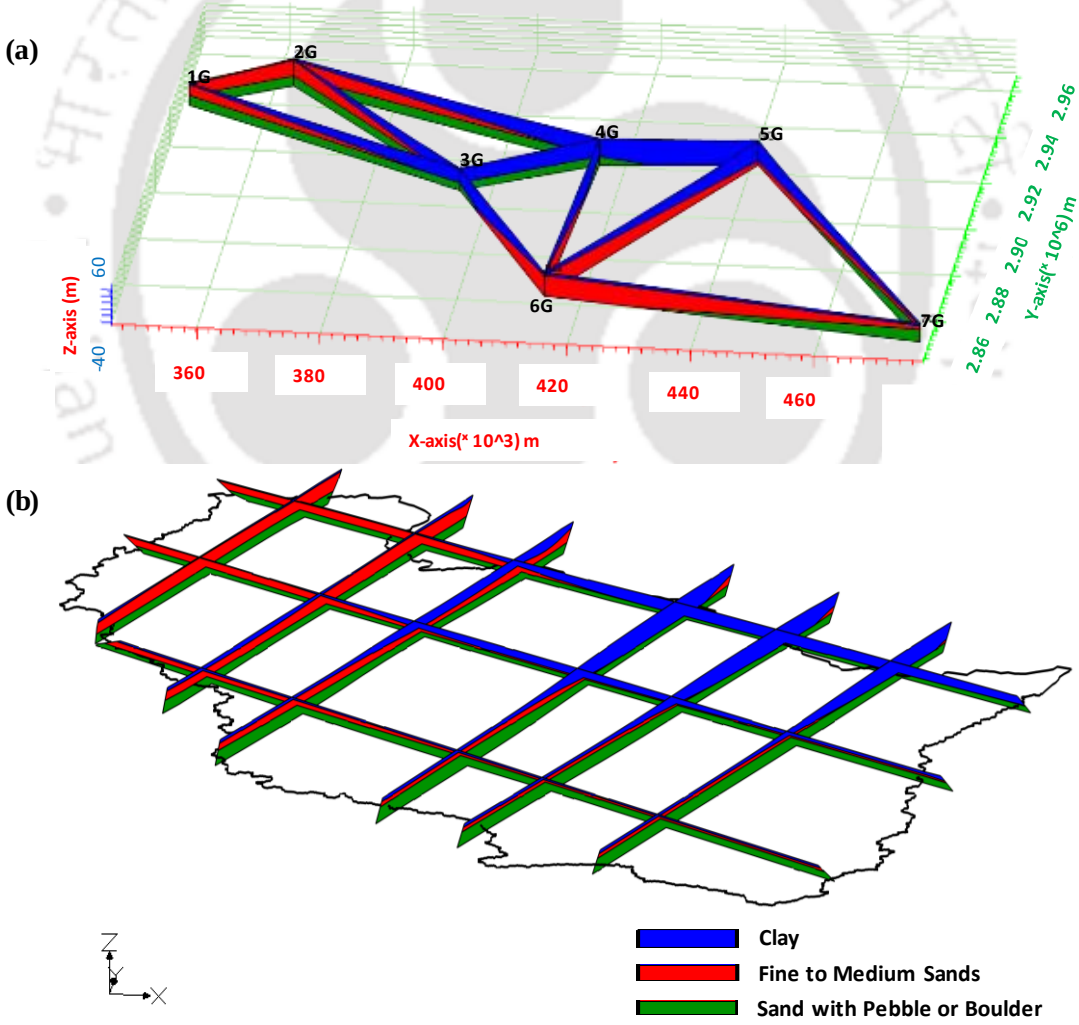

Figure 5.3: (a) Borehole cross-section (b) Fence diagram of the study area

Figure 5.3 shows the borehole cross-sections and fence diagram (lithology or soil stratification map) of the study area constructed using borehole data provided by CGWB, Patna. Detailed information of the fence diagram of the study area can be seen in Figure C.1 (Appendix C). The lithology map shows the study area consist of three different soils such as Clay, Fine to medium sands and Sands with pebble or boulder of varying depths.

In order to obtain the monthly groundwater level variations and river-aquifer exchange fluxes at the sub-basin scale, a transient groundwater flow modelling was considered and carried out using the conceptual approach from 1996 to 2010. For this purpose, the basin domain was discretized into 100 rows in latitude direction and 100 columns in longitudinal direction with a grid size of 2132 × 1907 km with three vertical layers in Z direction. Prior to transient flow modelling, a steady-state modelling was considered during the first month of simulation at10 daily time step. The developed conceptual model was calibrated and validated at two observed well locations Supaul and Jaynagar located in the districts of Supaul and Madhubani in Bihar state.

5.7 RESULTS AND DISCUSSION

Transient groundwater modelling was carried out in the plain parts of the Kosi river basin for the time period 1996-2010 to simulate monthly spatio-temporal groundwater head variations and river-aquifer interactions at sub-basin scale. Two different cases were considered for sub-surface hydrological modelling purpose i.e. groundwater flow modelling with recharge estimated using SWAT modelling (case I) and SWB method (case II) along with satellite-based evapotranspiration data, soil characteristics, aquifer parameters, river bed properties, initial and boundary conditions. For both the cases, the model was calibrated during 1997-2003 and validated during 2004-2010 at two well stations, Supaul and Jaynagar. These stations, Supaul and Jaynagar falls under sub-basins 15 (S-15) and 12 (S-12) respectively. The analysis of non-parametric SPI index (section 3.4) revealed that wet and dry years in the study period (1996-2010) were observed to be 2001 and 2005 in S-15 whereas 2007 and 2005 were observed to be wet and dry years in S-12. However, 1999 and 2005 were observed to be the wettest and driest years for the whole basin during the study period. Also, it was noted that 2005 onwards dry cycle was continued up to 2010. This information was used to compare the influence of wet and dry years on the results of groundwater modelling in both the cases.

5.7.1 Groundwater Flow Modelling with SWAT Model Recharge

The monthly sub-basin scale recharge obtained using SWAT model was used in the groundwater flow model along with satellite-based evapotranspiration data, aquifer characteristics, soil characteristics, initial and boundary conditions to predict spatio-temporal variations of groundwater levels and river-aquifer exchange flux.

5.7.1.1 Model Calibration and Validation at Supaul Well Station

(a) Calibration

Figure 5.4(a) shows the groundwater hydrograph variations between observed and simulated data at Supaul well station during the calibration period (1997-2003). In this period, i.e. during pre-monsoon Rabi season (January), the simulated groundwater levels varied between the ranges of 48.72-49.29 m whereas, the observed groundwater levels are noted to be in the range of 48.38-48.94 m that point toward the over-prediction of simulated groundwater levels from that of observed groundwater levels. During the pre-monsoon period (April) the simulated groundwater levels varied in the range of 48.48-48.73 m while the observed groundwater levels varied in the range of 48.05-48.50 m, also indicates the over-prediction of simulated groundwater levels. Similar observations are drawn during monsoon (August) and post-monsoon Kharif (November) seasons. The simulated groundwater levels in the months of August and November varied in the ranges of 49.83-51.45 m and 48.91-49.80 m whereas, observed groundwater levels varied in the range of 49.25-50.09 m and 48.68-49.28 m, respectively. It can be noted that irrespective of a season, the simulated values are observed to be over-predicted than that of the observed values. However, at a very few months (for example, in November, 2002) the simulated groundwater levels are observed to be under-predicted from that of observed groundwater levels. Figure 5.4(c) shows the scatter plot between observed and simulated groundwater levels during the calibration period. It is observed that the model can able to predict the groundwater levels during post-monsoon Kharif and pre-monsoon Rabi seasons. The coefficient of determination (R^2), Nash-Sutcliffe efficiency (NSE) root mean square error (RMSE) between observed and simulated groundwater levels are noted to be 0.71, 0.33, and 0.61 m respectively during the calibration period. In case I, hydraulic conductivity of 0.0004- 40 m/day and specific yield of 0.02-0.27 are found be the most sensitive calibration parameters

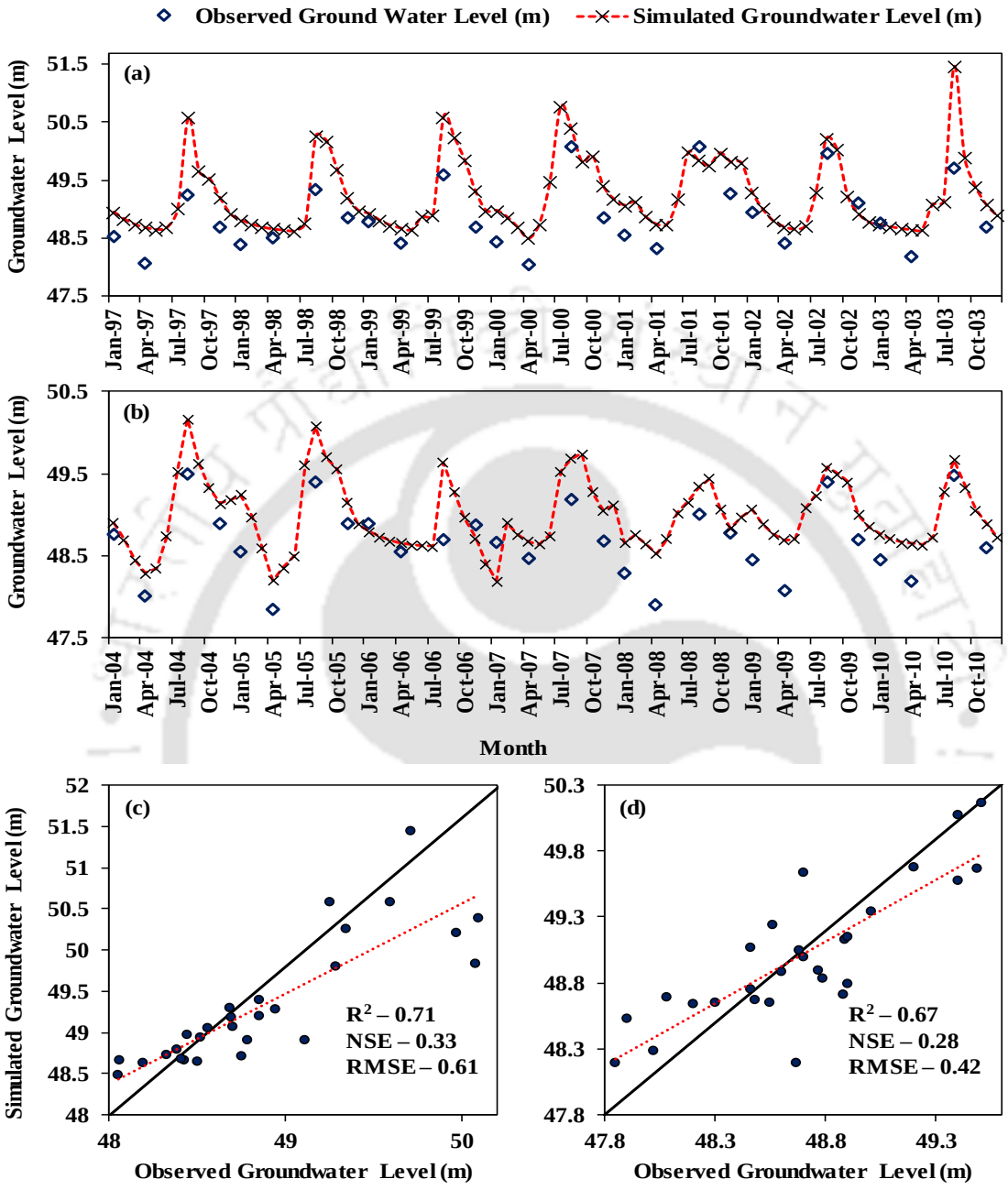

Figure 5.4: Observed and simulated groundwater level hydrograph variations at Supaul well station during (a) calibration period (b) validation period; scatter plot between observed and simulated groundwater levels during (c) calibration period (d) validation period.

(****Note***: Simulated groundwater levels were obtained using SWAT recharge; calibration period: 1997-2003; validation period 2004-2010)

(b) Validation

The groundwater hydrograph variation between observed and simulated data during the validation period (1997-2003) at Supaul well station is shown in Figure 5.4(b).

It can be noted that during pre-monsoon Rabi season (January), the simulated groundwater levels varied between the ranges of 48.19-49.24 m whereas, the observed groundwater levels varied in the range of 48.30-48.90 m. However, the simulated groundwater levels are found to be over-predicted than that of observed groundwater levels in few years. During pre-monsoon (April), the observed groundwater levels are observed to be varied in the range of 48.19-48.69 m whereas, simulated groundwater levels varied in the range of 47.85-48.55 m which indicates that the over-prediction of simulated groundwater levels than that of observed groundwater levels. The similar behavior can be observed during monsoon (August) and post-monsoon (November) seasons. The simulated groundwater levels varied between the ranges of 49.34-50.17 m and 48.71-49.15 m in August and November months whereas, observed groundwater levels remain in the range of 48.70-49.51 m and 48.60-48.90 m respectively. Similar to the calibration period, the simulated values in the validation period are found to be over-predicted than that of observed values irrespective of a season. Also, the scatter plot between observed and simulated groundwater levels (Figure 5.4(d)) indicates that the model predictions are not well captured by the model during validation period and R^2, NSE and RMSE between observed and simulated groundwater levels remain to be 0.67, 0.28, and 0.42 m respectively.

5.7.1.2 Model Calibration and Validation at Jaynagar Well Station

(a) Calibration

The model was also calibrated and validated at Jaynagar well station and the comparative plots are shown in Figure 5.5. The groundwater hydrograph variations between observed and simulated data of the calibration period (1997-2003) are shown in Figure 5.5(a). During pre-monsoon Rabi season (January), the simulated groundwater levels varied between the ranges of 64.14-64.93 m while, the observed groundwater levels varied in the range of 63.57-64.93 m. This difference indicates the over-prediction of simulated results from the observed groundwater levels. However, during the pre-monsoon period (April), the simulated groundwater levels varied between 63.54-64.26 m and the observed groundwater levels varied in the range of 63.56-65.22 m. It is to be noted that the

simulated results over-predict the observed ones during April except in few years. During the monsoon (August) and post-monsoon Kharif (November) seasons, a similar observation can be seen. It is found that in the month of August and November, the simulated groundwater levels varied in the ranges of 64.77-66.58 m and 64.26-65.39 m whereas, observed groundwater levels vary in the range of 63.87-67.04 m and 64.12-65.35 m respectively. It can be noted that similar to the observations at Supaul well station, the simulated values at Jaynagar station are found to be over-predicted than observed values irrespective of season. However, in some months (for example April month) the simulated groundwater levels are found to under-predict the observed groundwater levels. Scatter plot between observed and simulated groundwater levels during calibration period (Figure 5.5(c)) indicates better model performance in comparison with the results at Supaul well station with R^2 of 0.71, NSE of 0.56, and RMSE of 0.45 m respectively.

(b) Validation

Figure 5.5(b) shows the groundwater hydrograph variation between observed and simulated data during the validation period (1997-2003) at Jaynagar well station. During pre-monsoon Rabi season (January), the simulated groundwater levels varied in the range of 63.84-65.13 m whereas, the observed groundwater levels are noted to vary in the range of 63.59-65.53 m. However, the simulated groundwater levels closely matched the observed groundwater levels except in few years. During pre-monsoon (April), the simulated groundwater levels varied in the range of 62.87-64.31 m whereas, observed groundwater levels varied in the range of 62.92-64.62 m which also indicated close match with observed groundwater levels except in few years. Whereas, during monsoon (August), the simulated groundwater levels are found to vary between the ranges of 65.17-66.81 m while the observed groundwater levels varied between 64.51-66.17 m which indicates that over-prediction of simulated results. Similar to the observations found in pre-monsoon, the simulated groundwater levels (ranging between 64.45-66.04 m) are noted to have a close match with observed groundwater levels (ranging between 64.30-65.15 m) during post-monsoon Kharif (November) except in few years. Figure 5.4(d) shows the scatter plot of observed and simulated groundwater levels. It indicates the model performance in the validation period is similar to the calibration period, having R^2 of 0.69, NSE of 0.67 and RMSE of 0.51m. Overall, the simulated results of the groundwater flow model in Figure 5.3 and 5.4 indicates the simulated groundwater levels in case I are observed to be over-predicted than the observed groundwater levels except at few time periods.

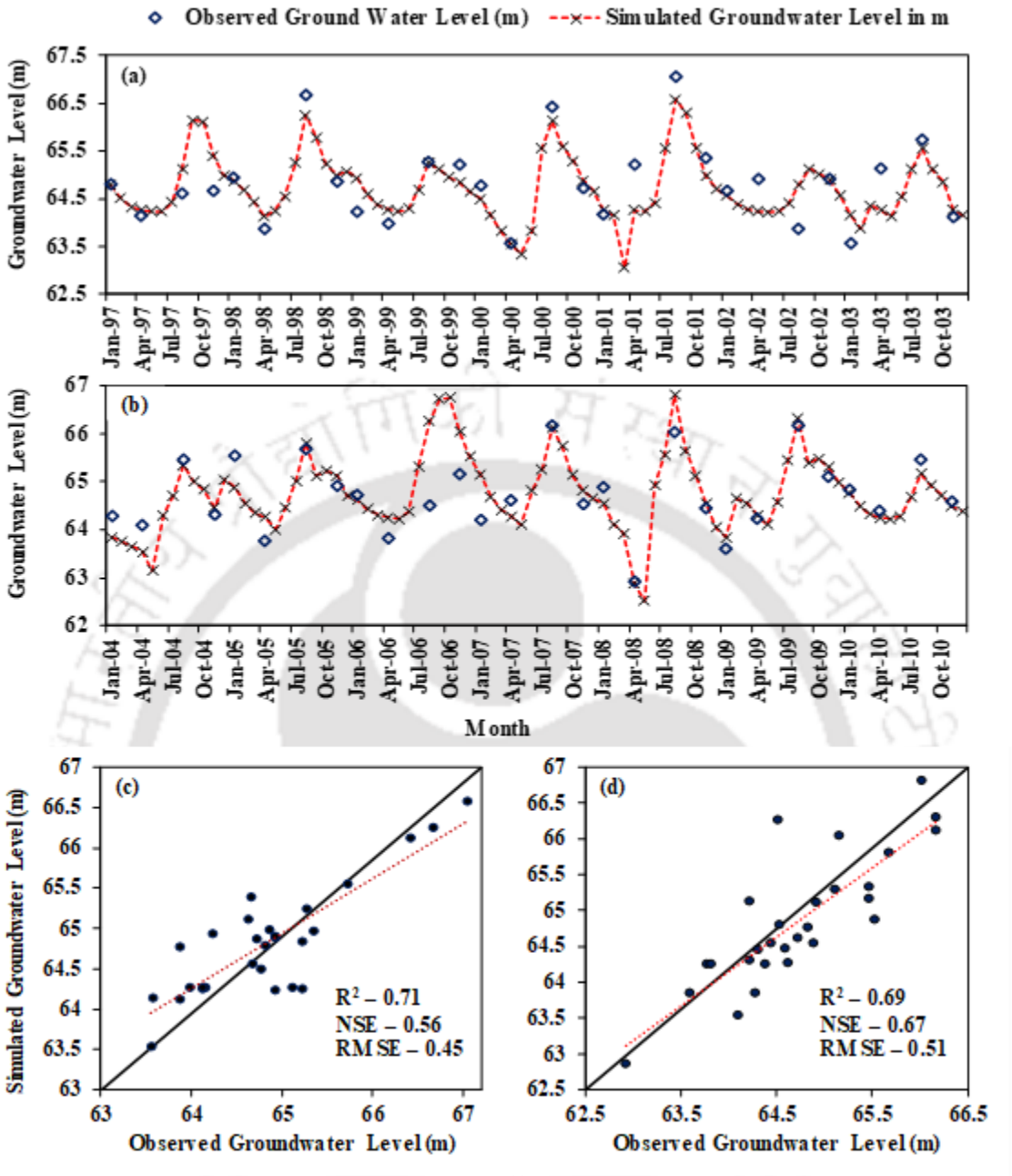

Figure 5.5: Observed and simulated groundwater level hydrograph variations at Jaynagar well station during (a) calibration period (b) validation period; scatter plot between observed and simulated groundwater levels during (c) calibration period (d) validation period.

(**Note*: Simulated groundwater levels were obtained using SWAT recharge; calibration period: 1997-2003; validation period 2004-2010)

Section 3.10 of chapter 3 revealed that the recharge obtained using SWAT model was observed to be over-predicted due to the underprediction of actual Evapotranspiration (AET) and the model was not able to capture the effects of wet and dry years during the study period. As the observed monthly groundwater recharge values were not available for

the study area at the sub-basin scale, the validation of groundwater recharge was not included at that point of discussion. The validation of these observations is attempted by incorporating the over-predicted recharge into the groundwater flow model in case I.

At Supaul station, it is observed that the simulated groundwater levels (varied in the range of 48.72 - 49.96 m) are found to be over-predicted slightly than that of observed groundwater levels (varied in the range of 48.32 - 50.08 m) during extremely wet year (2001) (Figure 5.4(a)). Also, during the extremely dry year (2005), the simulated groundwater levels (varied in the range of 48.18 - 50.08 m) are noted be over-predicted than that of the observed groundwater levels (varied in the range of 47.85 - 49.40 m) (Figure 5.4(b)). The comparison of simulated and observed values indicates the model is not able to capture the effects of wet and dry years. Similarly at Jaynagar station, the simulated groundwater levels (varied in the range of 64.10 - 66.12 m) are found to be slightly over-predicted than that of observed groundwater levels (varied in the range of 64.21 - 66.17 m) during extremely wet year (2007) (Figure 5.5(a)) Whereas, during extremely dry year (2005), the simulated groundwater levels (varied in the range of 64.01 - 65.81 m) are also found to be over-predicted than that of the observed groundwater levels (varied in the range of 63.76 - 65.67 m) during extremely dry year (2005) (Figure 5.5(b)). The comparison of simulated and observed values at Jaynagar also indicates the model is not able to capture the effects of wet and dry years. Overall, during calibration and validation period, the performance of the model (in case I) is found to be over-predicted (Figures 5.4 and 5.5) which indirectly reconfirms that the over-prediction of recharge by the SWAT model.

5.7.2 Groundwater Flow Modelling with SWB Method Recharge

In case II of groundwater flow modelling, the recharge obtained using SWB method was used to model the groundwater flow along with other inputs, parameters and initial boundary conditions to predict spatio-temporal variations of groundwater levels and river-aquifer exchange flux. Similar to case I, the model was calibrated and validated for the same time periods at the same well stations, Supaul and Jaynagar to compare both the cases.

5.7.2.1 Model Calibration and Validation at Supaul Well Station

(a) Calibration

During the calibration period (1997-2003), the groundwater hydrograph variations between observed and simulated data at Supaul well station are shown in Figure 5.6(a). It

is found that during pre-monsoon Rabi season (January), the simulated groundwater levels varied between the ranges of 48.39-49.19 m while the observed groundwater levels varied in the range of 48.38-48.94 m and showed that close match between simulated and observed values. During the pre-monsoon period (April), the simulated groundwater levels are observed to vary between 47.85-48.63 m while the observed groundwater levels varied in the range of 48.05-48.50 m. It's also shown that the simulated values are in good agreement with observed values. During the monsoon season (August), the simulated results varied in the range of 49.57-51.07 m while the observed values varied in the range of 49.25-50.09 m, indicates good agreement between simulated and observed values except in few years. Similar to the observations found in the monsoon period, the simulated groundwater levels (ranged between 48.83-49.42 m) during post-monsoon Kharif (November) are found to have a close match with observed groundwater levels (ranged between 48.68-49.28 m). Scatter plot (Figure 5.6(c)) shows the model predictions are found to have good agreement with observed groundwater levels during calibration period with R^2 of 0.83, NSE of 0.74 and RMSE of 0.38 m. Similar to case I, also hydraulic conductivity (0.0002-21 m/day) and specific yield (0.03-0.28) are found be most sensitive calibration parameters in case II.

(b) Validation

Figure 5.6(b) shows the groundwater hydrograph variations between observed and simulated data during the validation period (1997-2003) at Supaul station. During pre-monsoon Rabi season (January), the simulated groundwater levels varied in the ranges of 48.23-49.05 m whereas, the observed groundwater levels varied in the range of 48.30-48.90 m, indicates the close match between simulated and observed groundwater levels. In April (during pre-monsoon), the simulated groundwater levels are found to vary in the range of 47.86-48.62 m while the observed groundwater levels varied in the range of 47.85-48.55 m. This closeness again indicates good agreement between observed and simulated groundwater levels. The similar behaviour can be noted during monsoon (August) and post-monsoon (November) seasons. The simulated groundwater levels varied between the ranges of 49.06-49.72 m and 48.47-49.11 m in August and November months whereas,

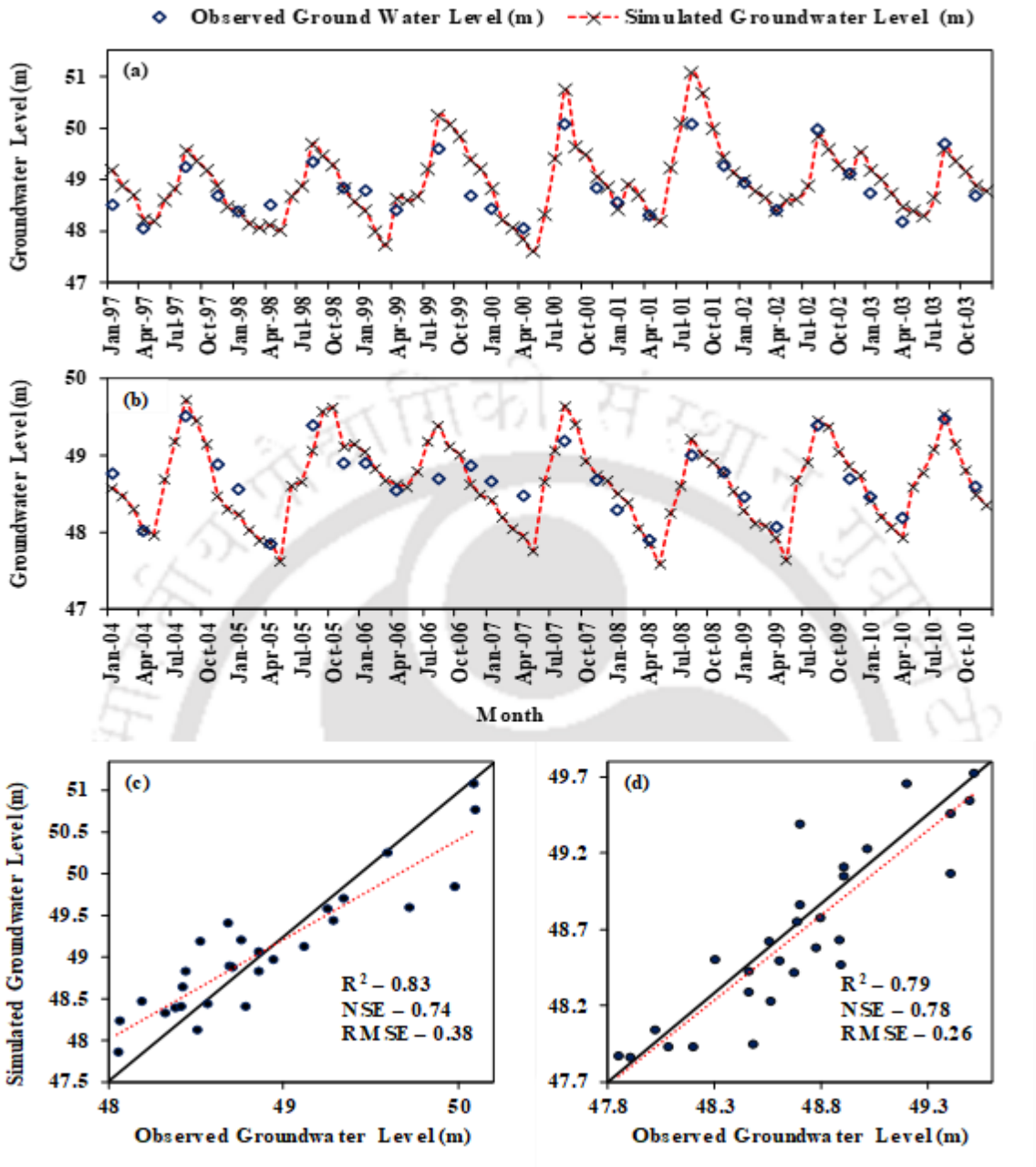

Figure 5.6: Observed and simulated groundwater level hydrograph variations at Supaul well station during (a) calibration period (b) validation period; scatter plot between observed and simulated groundwater levels during (c) calibration period (d) validation period.

(****Note***: Simulated groundwater levels were obtained using SWB recharge; calibration period: 1997-2003; validation period 2004-2010)

observed groundwater levels varied in the range of 48.70-49.51 m and 48.60-48.90 m respectively. The simulated values in the validation period are also found to have good agreement with observed values irrespective of season similar to the calibration period. Figure 5.6(d) shows scatter plot of observed and simulated groundwater levels, indicates

the predictions are well captured by the model during validation period having R^2 of 0.79, NSE of 0.78 and RMSE of 0.26 m. Overall, the groundwater levels simulated in case 1 are noted to be over-predicted except in few time periods whereas, the groundwater levels predicted in case 2, are found to have good agreement with observed groundwater levels at Supaul station.

5.7.2.2 Model Calibration and Validation at Jaynagar Well Station

(a) Calibration

Similar to case I, the groundwater model was also calibrated and validated at Jaynagar well station. Figure 5.7 shows the comparative plots of groundwater hydrographs during calibration and validation periods. During the calibration period (1997-2003), the groundwater level variations of observed and simulated values are shown in Figure 5.7(a). It is observed that during pre-monsoon Rabi season (January), the simulated groundwater levels varied between the ranges of 63.87-65.24 m whereas, the observed groundwater levels are noted to vary in the range of 63.57-64.93 m, indicates that the simulated groundwater levels are found to have good agreement with observed values. Similar behaviour is noticed during pre-monsoon, monsoon and post-monsoon Kharif seasons. The simulated groundwater levels varied between 63.85-64.79 m, 64.68-67.16 m and 64.48-65.40 m whereas, the observed groundwater levels varied in the range of 63.56-65.22 m, 63.87-67.04 m and 64.12-65.35 m in the months of April, August and November respectively. Similar to the observations at Supaul well station, the simulated values at Jaynagar station are found to have a close match with observed values irrespective of season. However, in few months (for example April month) the simulated groundwater levels are noted to be under-predicted than that of observed groundwater levels. Figure 5.7(c) shows the scatter plot of observed and simulated groundwater levels during the calibration period, indicates better model performance with R^2 of 0.80, NSE of 0.74, and RMSE of 0.39 m.

(b) Validation

The groundwater hydrograph variations between observed and simulated data during the validation period (1997-2003) at Jaynagar well station are shown in Figure 5.7(b). During pre-monsoon Rabi season (January), the simulated groundwater levels varied in the range of 64.09-65.08 m whereas, the observed groundwater levels are noted

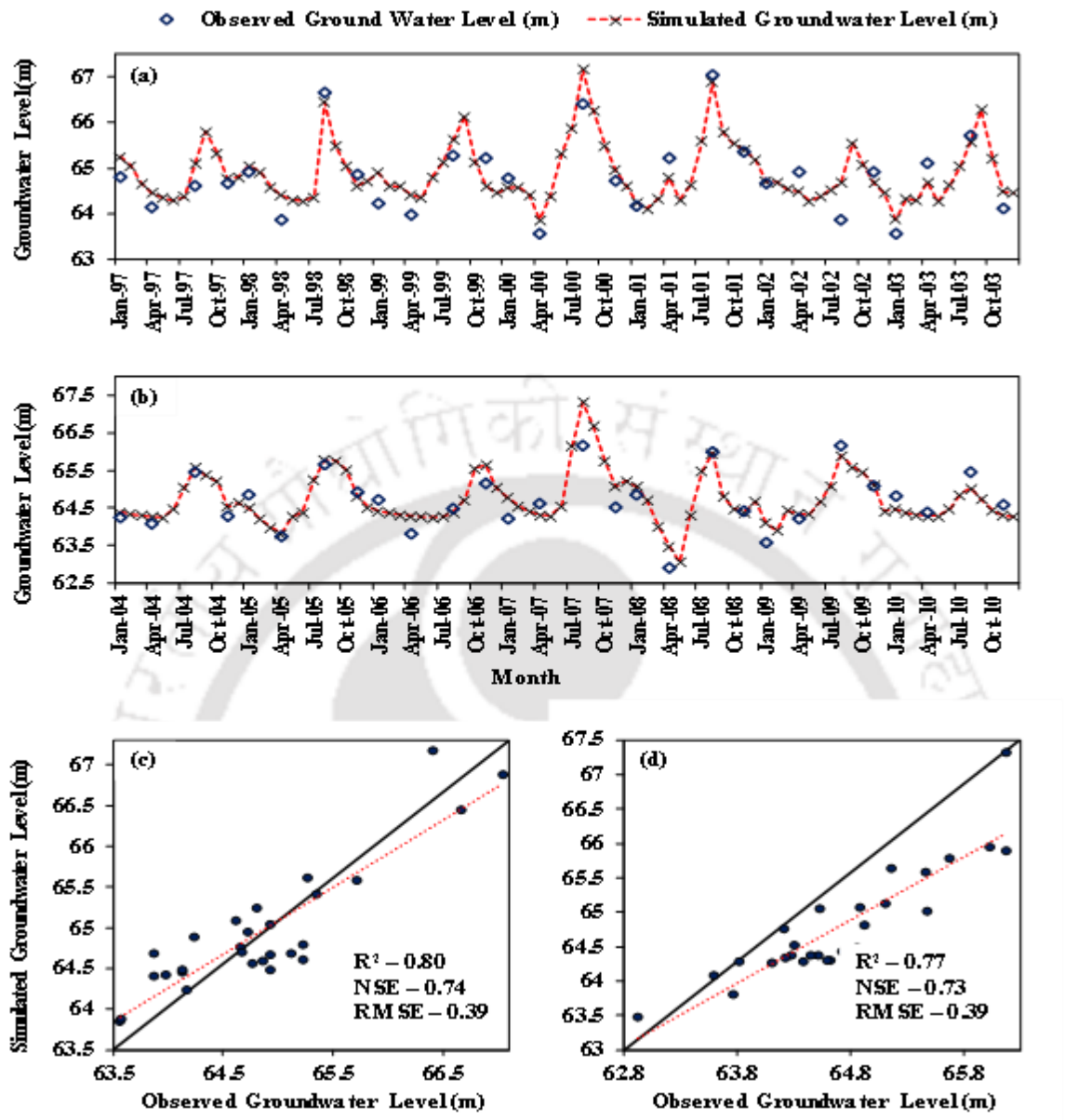

Figure 5.7: Observed and simulated groundwater level hydrograph variations at Jaynagar well station during (a) calibration period (b) validation period; scatter plot between observed and simulated groundwater levels during (c) calibration period (d) validation period.

(*_**Note**_: Simulated groundwater levels were obtained using SWB recharge; calibration period: 1997-2003; validation period 2004-2010)

to vary in the range of 63.59-65.53 m, indicates that the simulated groundwater levels are close match to the observed groundwater levels except at few years. Similar observations can be drawn during pre-monsoon (April), monsoon (August) and Post-monsoon Kharif (November). The simulated groundwater levels varied in the range of 63.49-64.34 m, 64.38-67.32, 64.30-65.64 m whereas the observed groundwater levels varied in the range of 62.92-64.62 m, 64.51-66.17 m and 64.30-65.15 m in April, August and November

months, respectively. Scatter plot (Figure 5.7(d)) of observed and simulated groundwater levels indicates the model performance in the validation period is similar to the performance in the calibration period, having R^2 of 0.77, NSE of 0.73 and RMSE of 0.39 m. Overall, the simulated results of the groundwater flow model showed in Figure 5.6 and 5.7 indicates that the simulated groundwater levels are found to have a good agreement with the observed groundwater levels except at few time periods.

Section 3.10 of chapter 3 revealed that the recharge obtained using SWB model was observed to be well predicted and also able to capture the effects of wet and dry years during the study period. As the observed monthly groundwater recharge was not available for the study area at the sub-basin scale, the validation of recharge was not included at that point of discussion. The validation of these observations is attempted by incorporating the recharge (estimated using SWB method) into the groundwater flow model in case II.

The simulated groundwater levels (varied in the range of 48.19 – 51.07 m) at Supaul station are noted to be in good agreement with observed groundwater levels (varied in the range of 48.32 - 50.08 m) during the extremely wet year (2001) except at few values (Figure 5.6(a)). Similarly, during the extremely dry year (2005), the simulated groundwater levels (varied in the range of 47.63- 49.63 m) are found be in good agreement with the observed groundwater levels (varied in the range of 47.85 - 49.40 m) (Figure 5.6(b)). These comparisons of simulated and observed values indicate that the model can able to capture the effects of wet and dry years. Similarly at Jaynagar station, the simulated groundwater levels (varied in the range of 64.28 – 67.23 m) are also found to be in good agreement with observed groundwater levels (varied in the range of 64.21 - 66.17 m) during extremely wet year (2007) except few values (Figure 5.7(a)) Whereas, during extremely dry year (2005), the simulated groundwater levels (varied in the range of 63.82 - 65.71 m) are also noted to be good agreement with the observed groundwater levels (varied in the range of 63.76 - 65.67 m) during extremely dry year (2005) (Figure 5.7(b)). It clearly indicates that the comparison of simulated and observed values has proven that the model is able to predict groundwater levels and capture the effects of wet and dry years. Overall, the performance of the model (in case II) during calibration and validation periods are observed to be well predicted (Figures 5.6 and 5.7), which indirectly reconfirms that the accurate estimation of recharge by the SWB method than SWAT model. Table 5.1 presents the evaluation statistics of the groundwater flow models for both the cases at the two well stations during calibration and validation periods.

Table 5.1: Evaluation statistics of Groundwater Model

Station Name	Groundwater Recharge used	Duration	R^2	NSE	RMSE (m)
Supaul	SWAT Recharge	Calibration	0.71	0.33	0.61
		Validation	0.67	0.38	0.43
	SWB Recharge	Calibration	0.83	0.85	0.36
		Validation	0.79	0.81	0.25
Jaynagar	SWAT Recharge	Calibration	0.71	0.56	0.45
		Validation	0.69	0.67	0.51
	SWB Recharge	Calibration	0.80	0.84	0.38
		Validation	0.77	0.80	0.37

5.7.3 River-Aquifer Exchange Flux

The calibrated groundwater flow model has been used to assess the river-aquifer exchange flux using MODFLOW RIV (River) package. Figure 5.8 shows the three-dimensional (3D) plot between distance (upstream to downstream), time period (month) and river leakage (exchange flux rate) along the river reach. In the 3-D plot, positive value of river leakage indicates the river losing water to the aquifer whereas negative value indicating river gaining water from the aquifer. Based on this exchange rate, the entire river reach can be divided into three critical zones and these zones can be seen in Figure 5.8. It can be observed that the river always loses water to the ground (as influent river) in Zone I (up to 80 km from upstream) while the Zone III (from 40 km above downstream to conferencing point) the river mostly gains water from river (as effluent river) throughout the study period (1996-2010) except in very few dry months. Whereas, in the middle reaches (Zone II), the river has a combination of both influent and effluent natures. Figure 5.8(a) shows the spatio-temporal variation of river-aquifer exchange flux along the Kosi river reach obtained in case I (groundwater modelling with recharge estimated using SWAT model and riverbed conductivity calculated using $K_{eff\text{-}10}$ value of Scenario 1 (S1) through sandbox experiments)). However, Figure 5.8(b) shows the spatio-temporal variation of river-aquifer exchange fluxes along the river reach in case II (groundwater modelling with recharge estimated using SWB method and riverbed conductivity calculated using $K_{eff\text{-}10}$ value of S1). Table 5.2 shows the zonal statistics of river-aquifer exchange flux obtained using both the cases.

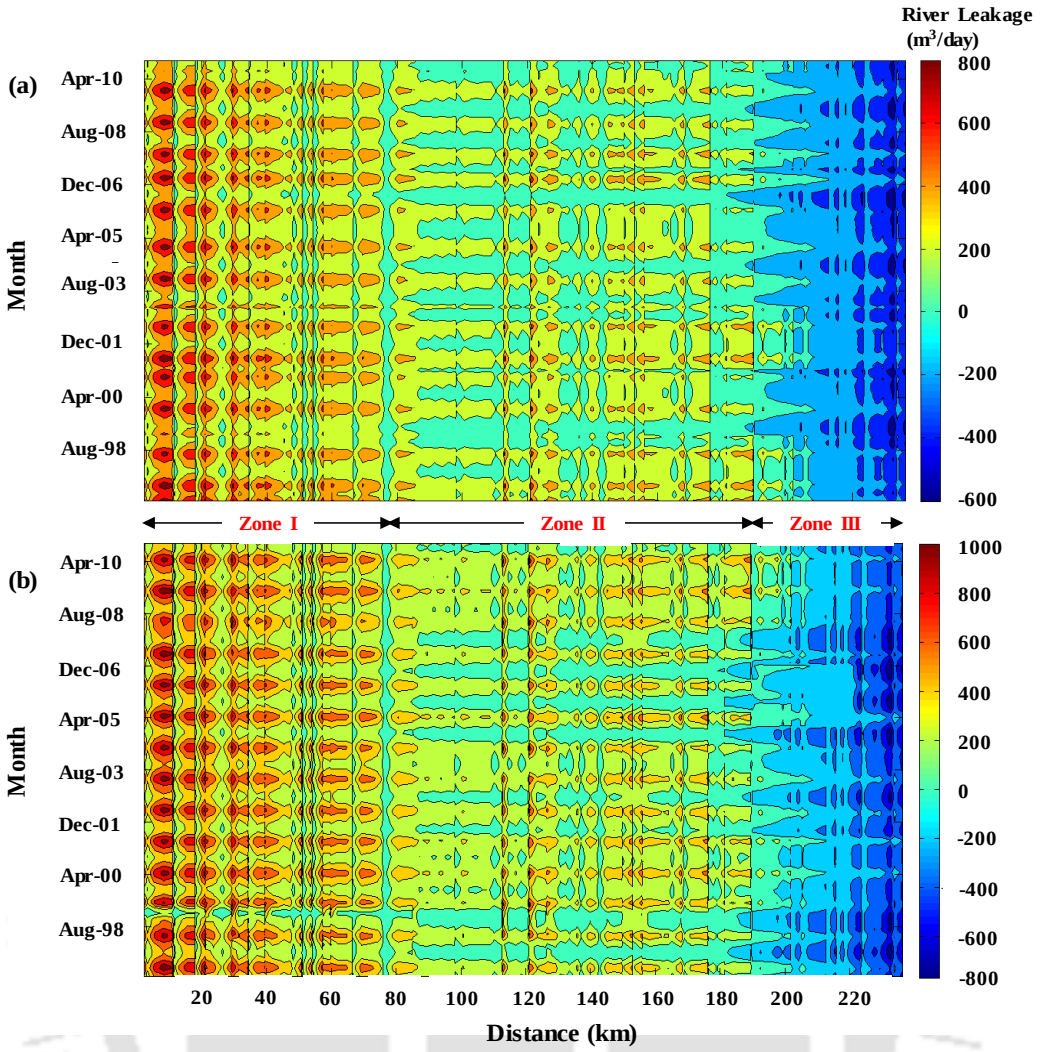

Figure 5.8: Spatio-temporal variations of River-Aquifer exchange flux along Kosi river reach (upstream to downstream) obtained using MODFLOW model with $K_{eff\text{-}10}$ value of Scenario 1 (S1) and recharge estimated by (a) SWAT model (case I) (b) SWB method (case II).

[**Note:* (1) Green to Red color indicates river losing state and blue color indicates river gaining state (2) Positive value of river leakage indicates the river is losing water to the aquifer whereas negative value indicates the river is gaining water from aquifer]

Table 5.2: Zonal statistics of river-aquifer exchange flux obtained using SWAT and SWB recharge

Case	Zone	River-Aquifer Exchange Flux (m^3/day)			
		Minimum	Average	Maximum	Standard Deviation
I	Zone I	1	292	794	191
	Zone II	-149	177	584	119
	Zone II	-597	-156	283	126
II	Zone I	33	433	979	211
	Zone II	-196	262	891	139
	Zone II	-768	-177	439	164

The observations from both the cases reveal that the losing rate is found be higher during the non-monsoon season than that in monsoon season throughout the study period. However, the gaining rate is observed to higher during monsoon season than that of non-monsoon season. Similar observation can be found in the study carried out on wetland-river interactions in Kosi river basin [Chembolu et al., 2019]. Their study also revealed that the flow was coming out of the river (losing) during monsoon period whereas the flow was leaving from the wetland (gaining) during non-monsoon season.

In comparison with case I and case II, the losing rates are noted to be lesser throughout Zone I and II in case I than case II. But, the gaining rates in case I are found to be higher in Zone III (falls in Sub-basin 17 (S-17)) in comparison with case II throughout the zone except the maximum values. It is resulted due to the incorporation of over-predicted recharge (section 3.10) into the groundwater model. However, the highest value of gaining rate (-769 m^3/day) is observed to be found in case II in comparison with the case I (-597 m^3/day). It has happened due to the highest value of recharge in S-17 (annual recharge of 67 cm per year) corresponding to the wettest year (1999) was obtained using SWB method against SWAT simulated recharge (24 cm per year), Also, the effect of wet and dry years on river-aquifer interaction is not well captured by the model in case I. For example, this behaviour can be clearly seen in zone III during wet and dry periods. The river is found to be significantly gaining water from the aquifer even during and after the dry cycle (2005 onwards) whereas the influence of the dry cycle can be seen in case II (2005 onwards) and the river is observed to lose water in comparison with the behaviour in early periods except in 2007. Also, the wet year influence can be clearly seen in case II than in case I. In comparison with case I (Figure 5.8(a)), the influence of wet year can be strongly seen throughout the stretch in zone III during wettest year (1999) in case II (Figure 5.8(b)). This inter-comparison between case I and case II clearly indicate that the groundwater modelling with SWB recharge can able to capture wet and dry year impacts on river-aquifer exchange fluxes than that of SWAT recharge-based modelling.

However, it can be observed that irrespective of case (I or II) considered for modelling, the river always loses water to aquifer (as influent River) at upstream and mostly gains water from aquifer (as effluent river) at downstream during wet and dry years which indicates that significant influence of topography on river-aquifer exchange flux. This influence of topography on river-aquifer exchange flux from Kosi barrage (upstream) to the point of conference with Ganga river (downstream) in different zones can be

represented through a conceptual diagram (Figure 5.9). It shows the spatial variation of the groundwater table along the river reach (from upstream to downstream) during wet and dry years. During wet and dry years, the groundwater levels at upstream (at higher ground elevations) always lie below the river water surface which causes the river to be behave influent in Zone I while the groundwater levels at downstream (at lower ground elevations) lie above the river water level which makes effluent river in Zone III. In Zone II, the groundwater levels rise above the river water levels during wet years which makes the river to behave as influent whereas falls below river water levels during dry years which makes the river to behave as effluent i.e. combination of influent and effluent nature can be seen in Zone II.

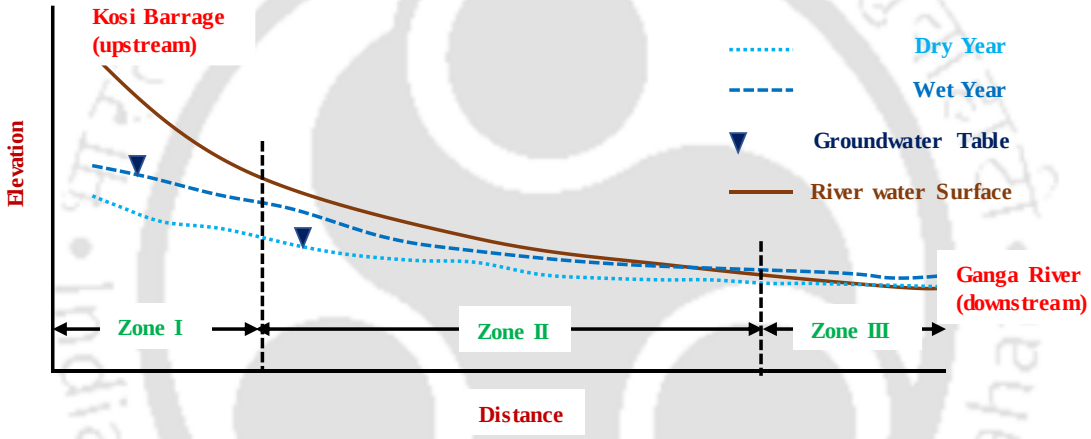

Figure 5.9: Conceptual diagram of groundwater table spatial variation along Kosi river reach (upstream to downstream) during wet and dry years

Overall, the groundwater modelling in case II (using SWB recharge) is found to have good agreement with observed groundwater levels and also able to capture the wet and dry year effects on river-aquifer interaction process in Kosi river basin. Like Kosi, Gandak river is also one of the major tributaries of Ganga river and the study on river-aquifer interaction in Gandak river revealed that the exchange rates varied in the range between -500 to 1000 m^3/day [Singh et al., 2018]. Similar to Gandak river, the river-aquifer exchange rates are found to vary in the range of -600 to 1000 m^3/day in Kosi river basin.

5.7.4 Inter-comparison of River-Aquifer Exchange Flux of Scenario 1 and 3

In order to see the influence of riverbed conductance on river-aquifer exchange flux, three different percentiles ($K_{eff\text{-}10}$, $K_{eff\text{-}50}$ and $K_{eff\text{-}90}$) (Section 4.4, Table 4.21) were used in riverbed conductance calculation which were further used in the groundwater flow modelling to assess the spatio-temporal variations of the exchange flux rate in the basin.

Figures 5.10 and 11 show the exchange flux spatio-temporal variations in the three-dimensional plot of case II modelling for Scenario 1 and 3 (S1 and S3) considered in the sandbox experiments. The variations of exchange flux obtained using SWB recharge and riverbed conductance calculated with $K_{eff\text{-}10}$ of S1 are shown in Figure 5.10(a). It can be noted that the river is observed to lose water (as influent) in Zone I with an average of 433 m^3/day, gain water (as effluent) in Zone III with an average of -177 m^3/day) whereas combination influent and effluent nature of river can be seen in Zone II with an average of 262 m^3/day. The losing rates are observed to vary between 33 and 979 m^3/day whereas, the gaining rates are found to vary in the range of -196 to -768 m^3/day respectively in the study area. It is observed that the river was significantly losing water to the aquifer after the dry cycle (2005 onwards) and this behaviour can be clearly seen in Zone III, whereas, the influence of the wet year can be strongly seen throughout the stretch in zone III during the wettest year (1999). Similar variations in the exchange rate are noted in case II groundwater modelling with riverbed conductance calculated with $K_{eff\text{-}50}$ and $K_{eff\text{-}90}$ values (Figures 5.10(b-c)). It can be found that there is not much significant difference in the exchange rates in the modelling outcomes with the variations of riverbed conductance value. This can be clearly seen with the statistics of river-exchange flux in all the three zones for S1 can be seen in Table 5.3.

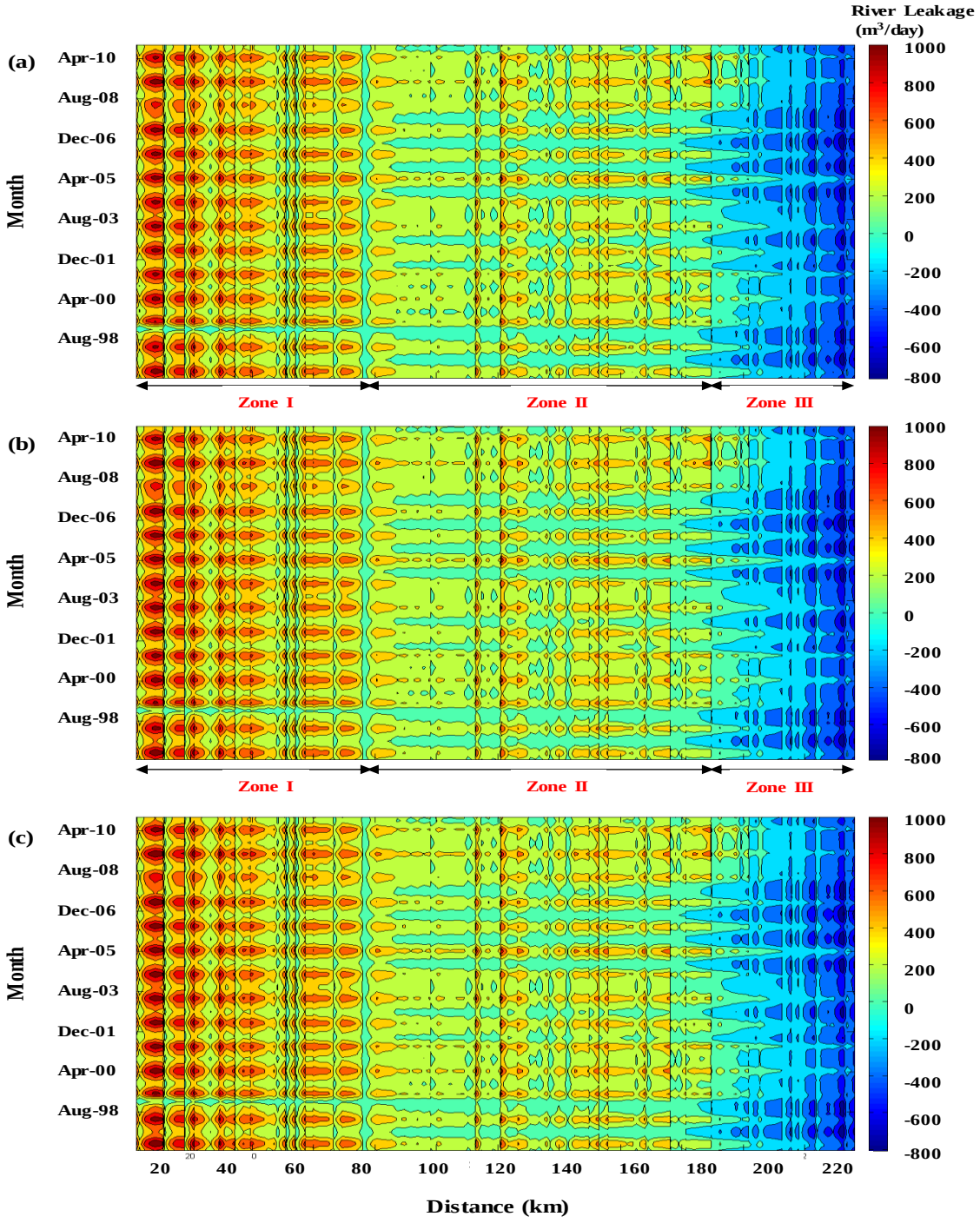

Figure 5.10: River-Aquifer exchange flux along Kosi river reach (upstream- downstream) obtained from case II groundwater modelling using SWB recharge and riverbed conductance calculated with (a) $K_{eff\text{-}10}$ (b) $K_{eff\text{-}50}$ (c) $K_{eff\text{-}90}$ values of Scenario 1 (S1)

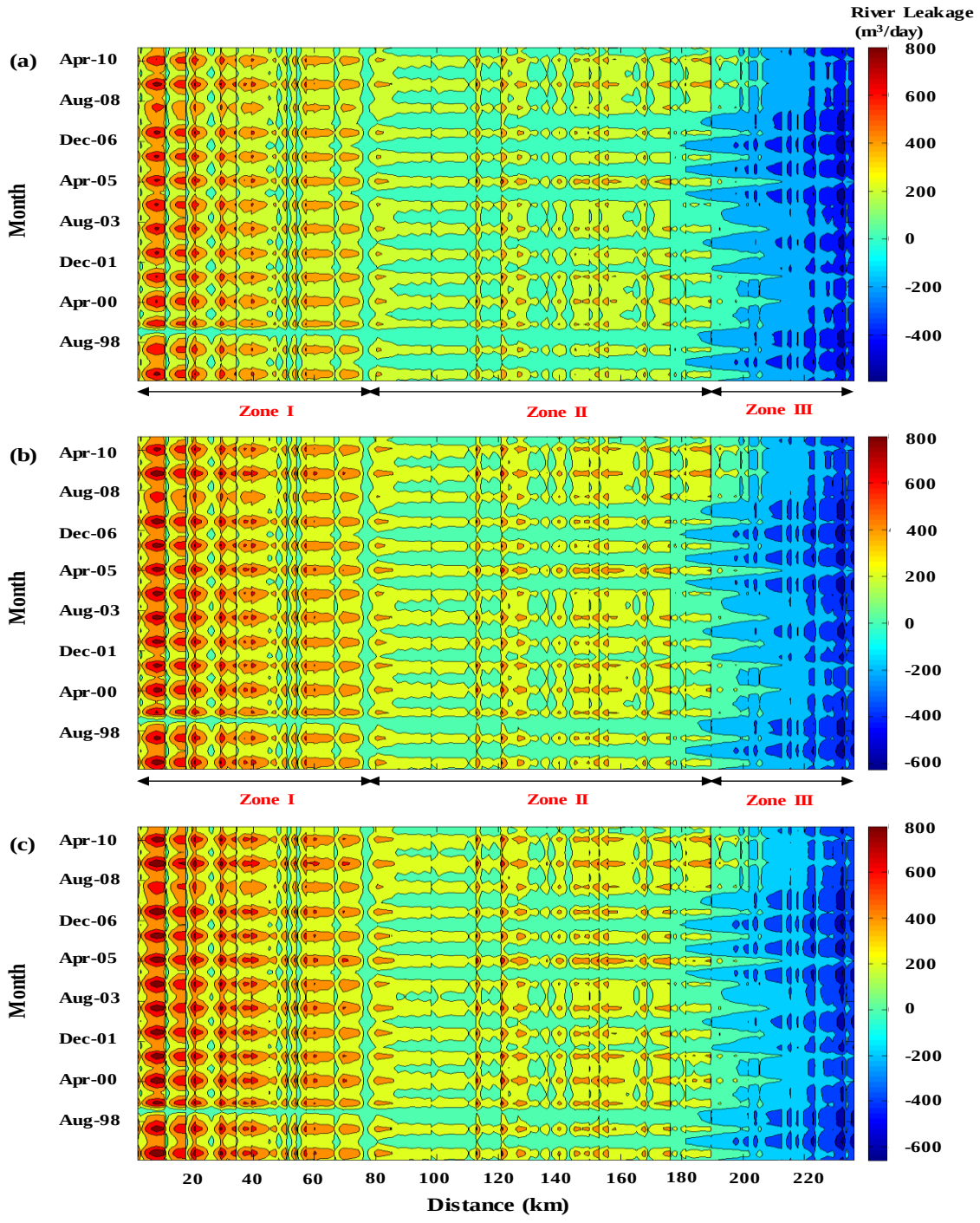

Figure 5.11: River-Aquifer exchange flux along Kosi river reach (upstream- downstream) obtained from case II groundwater modelling using SWB recharge and riverbed conductance calculated with (a) $K_{eff\text{-}10}$ (b) $K_{eff\text{-}50}$ (c) $K_{eff\text{-}90}$ values of Scenario 3 (S3)

Figure 5.11(a-c) shows the spatio-temporal variations of exchange flux obtained using case II modelling with riverbed conductance calculated using K_{eff} values of Scenario 3. Similar to the modelling with K_{eff} values of S1, the river is observed to be influent (losing river) in Zone I (with an average of 332 m^3/day), effluent in Zone III (with an average of -

137 m^3/day) and both influent and effluent in Zone II (with an average of 201 m^3/day) respectively. In the study area, the losing rates are found to vary with minimum and maximum of 26 and 756 m^3/day whereas, the gaining rates are observed to vary with a minimum and maximum of -149 and -573 m^3/day respectively. In comparison with the results obtained with S1, these exchange rates are noted be significantly decreased. Also, the wet and dry year behaviours are found to follow the similar trend observed (Figure 5.11) and there is not much significant difference in the exchange rates in the modelling results by varying riverbed conductance value. This can be clearly seen with the statistics of river-exchange flux in all the three zones for S3 (Table 5.3). From this study, it can be noted that variations in the riverbed conductance of a particular soil stratification combination does not have much significant effect on river-aquifer exchange flux. However, river -aquifer interaction is highly sensitive to different soil stratification.

Table 5.3: Zonal statistics of rive-aquifer exchange flux obtained using SWB recharge for Scenario 1 and 3

Scenario	K_{eff} Percentile	Zone	River-Aquifer Exchange Flux (m^3/day)			
			Minimum	Average	Maximum	Standard Deviation
S1	K_{eff-10}	Zone I	33	433	979	211
		Zone II	-196	262	891	139
		Zone II	-768	-177	439	164
	K_{eff-50}	Zone I	34	444	986	216
		Zone II	-201	268	902	142
		Zone II	-787	-182	446	168
	K_{eff-90}	Zone I	35	455	994	222
		Zone II	-206	275	908	146
		Zone II	-806	-186	455	172
S3	K_{eff-10}	Zone I	26	332	756	161
		Zone II	-149	201	683	106
		Zone II	-573	-137	338	127
	K_{eff-50}	Zone I	27	350	768	171
		Zone II	-158	212	721	112
		Zone II	-581	-145	357	134
	K_{eff-90}	Zone I	28	369	794	180
		Zone II	-166	223	760	118
		Zone II	-594	-152	376	141

Note: River-aquifer exchange flux was calculated using SWB recharge (case II) and riverbed conductance calculated with K_{eff-10}, K_{eff-50} and K_{eff-90} values of Scenario 1 (S1) and Scenario 3 (S3).

5.8 CONCLUSIONS

In the present study, assessment of spatio-temporal variation of river-aquifer interaction exchange flux of Kosi river was studied. For this purpose, fully distributed groundwater model (MODFLOW) was used along with remote sensing inputs (groundwater recharge and evapotranspiration), aquifer characteristics (hydraulic conductivity, porosity, specific storage) and riverbed conductance. Groundwater recharge incorporated in the groundwater modelling was estimated using two different methods using SWAT modelling and SWB method. In order to select the suitable recharge estimation method for groundwater modelling in Kosi river basin, groundwater modelling was carried out for two different cases, i) modelling with recharge estimated using SWAT model and ii) modelling with recharge estimated using SWB method. Also, the influence of riverbed conductance on river-aquifer interaction process was assessed by incorporating different riverbed conductance (calculated using K_{eff} values of different soil combinations considered in the sandbox experiments) values in the groundwater modelling. The following conclusions were drawn from this study.

1) Monthly groundwater levels simulated using SWAT recharge-based groundwater flow modelling (case I) did not correlate with observed groundwater levels and also was not able to capture the wet and dry year effects. However, simulated groundwater levels in the groundwater modelling with SWB based recharge were observed to have a better agreement with observed groundwater levels and also found to be captured the effects of wet and dry years.
2) Also, the effect of wet and dry year effect on river-aquifer exchange flux was not seen in case I modelling whereas case II model was able to capture the effects of wet and dry years on the exchange process.
3) Three different interaction zones were identified from upstream (Kosi barrage) to downstream (conferencing point with Ganga river) in the study reach. It is observed that the river always loses water to the aquifer (as influent) in Zone I (80 km from upstream) and the river mostly gains water from the aquifer (as effluent) in Zone III (40 km above downstream). Whereas, in the middle reaches (Zone II), the river has a combination of both influent and effluent natures.
4) At the upstream, the river always loses water to the aquifer and mostly gains water from the aquifer at downstream during wet and dry years indicates that significant influence of topography on river-aquifer exchange flux.

5) The results obtained in case II modelling with different riverbed conductance values indicate that the river-aquifer interactions are highly sensitive to the riverbed conductance with different soil layer strata. Whereas, these interactions are found to be less sensitive to the variations in riverbed conductance values (10, 50, 90 percentiles) for a soil layer strata.

Overall, this inter-comparison of groundwater modelling results indicates, remote sensing inputs (recharge and evapotranspiration used in SWB method for estimating recharge) along with estimated riverbed conductance values can improve the assessment and understanding river-aquifer interaction process in Kosi river basin.

6

SUMMARY AND FUTURE SCOPE

6.1 SUMMARY

The present research aimed to understand the river-aquifer interaction process and its assessment along the reaches of Kosi river basin, India. The river basin consists of agricultural lands and relies on a groundwater-based irrigation system. The study attempted to investigate river-aquifer interaction exchange process by determining the input parameters required for sub-surface hydrological model such as groundwater recharge and riverbed hydraulic conductivity. For this purpose, the plain parts of Kosi river basin (excluding the hilly Nepal and Tibet regions) that falls in India was considered as the study area. The groundwater recharge estimations techniques using remote sensing inputs, tracer techniques using heat flux measurements and, sub-surface hydrological models were used for achieving the objectives. The following sub-sections are the brief summary of the work carried out and observations made in the present research.

6.1.1 Estimation of Groundwater Recharge

In this objective, monthly and seasonal groundwater recharge was estimated for Kosi river basin, India using four different methods namely, Water Table Fluctuation (WTF), Rainfall Infiltration Factor Method (RIF), Soil and Water Assessment Tool (SWAT) and Soil Water Balance (SWB) methods. The results provided insights in groundwater recharge estimation using different methods for effective groundwater management in highly groundwater irrigation dominated region. The results of the study lead to the following observations.

(a) **Analysis of rainfall variations** indicated that there was an average of six-year cyclic period for the wet year and nine-year cyclic period for the dry year over the 29 years of the analysis period (1982-2010).

(b) **LULC change analysis** for the year 1985-2005 indicated that there was no significant change in the LULC in the study region, which was mostly dominated by agricultural lands (90%).

(c) **Spatio-temporal variations of evapotranspiration** (ET) showed that there was a shift of one month in the cropping pattern from October to September during the study period (1982-2010).

(d) The **seasonal groundwater estimation** results showed that WTF method considered the fluctuations in groundwater levels and RIF method simply followed the rainfall patterns. But both the methods were not able to capture the wet and dry year impacts on groundwater recharge.

(e) **Surface water hydrological model** (SWAT) was calibrated and validated with the observed monthly discharge time series to get the monthly groundwater recharge at sub-basin scale. Groundwater delay and shallow groundwater storage were found to be the most sensitive calibration parameters.

(f) SWAT model also over-predicted the recharge and also not able to capture wet and dry year effects on groundwater recharge due to the under-prediction of simulated Actual Evapotranspiration (38% of observed AET).

(g) **SWB method** (in which high resolution remote sensing-based satellite datasets such as precipitation, actual evapotranspiration (ground truth validated) and soil moisture along with runoff obtained from calibrated SWAT model were considered) improved the monthly groundwater recharge estimations and also captured wet and dry year effects on groundwater recharge in the study zone.

6.1.2 Estimation of Fluid Flux and Hydraulic Conductivity

In this objective, heat was used as a natural tracer to estimate the fluid flux and bed hydraulic conductivity through the sediment-water interface based on laboratory experiments conducted in a sandbox. In order to understand the variation in fluid flux and hydraulic conductivity under different conditions, a series of laboratory experiments were conducted with four different scenarios (soil combinations, temperature gradients (gradient between hot water and normal water) and ponding depths). The following conclusions were drawn from this study

1. Vertical thermal profiles were measured in soil column for different conditions to estimate the fluid flux in different soil layers using four different analytical solutions i.e. Keery and Hatch Amplitude Ratio (AR) and Phase Difference (PD). Among these four methods, fluid fluxes estimated using Keery AR method were observed to have a good agreement with measured seepage velocity. It might be due to the lack of consideration of dispersion term in Keery analytical method and violating the one-dimensional assumption.
2. Inter-comparison of four different scenarios show that fluid fluxes were observed to be higher values in Scenario 1 (Fine Sand I at top, Fine Sand II at middle and Medium Sand at bottom layers) than other three scenarios. It is resulted due to the placing of highly permeable media at bottom, moderately permeable soils at middle and less permeable media at the top layers.
3. The influence of ponding depth and temperature gradient on fluid flux were analyzed using ANOVA (TukeyKramer HSD test at $P \leq 0.05$) by considering different cases i.e. varying temperature gradient while ponding depth remained constant and in other case, temperature was constant against varying ponding depth. This analysis revealed that ponding depth had a significant influence on fluid flux over temperature gradient in all the four scenarios considered.
4. Effective Hydraulic Conductivities (K_{eff}) calculated using hydraulic conductivities (estimated from the fluid fluxes) of different soil layers in all the four scenarios followed Gaussian normal probability distribution and the influence of ponding depth and temperature gradient on K_{eff} was observed to be not significant. However, the influence of temperature gradient was noted to be slightly more compared to ponding depth.

6.1.3 Assessment of River-Aquifer Interaction

The objective aimed the assessment of spatio-temporal variation of river-aquifer interaction exchange flux of Kosi river. For this purpose, a fully distributed groundwater model (MODFLOW) was used along with remote sensing inputs (groundwater recharge and evapotranspiration), aquifer characteristics (hydraulic conductivity, porosity, and specific storage) and riverbed conductance. Groundwater recharge incorporated in the groundwater modelling was estimated using two different methods using SWAT modelling and SWB method. In order to understand the best accurate recharge estimation method for groundwater modelling in Kosi river basin, groundwater modelling was carried out for two

cases, i) modelling with recharge estimated using SWAT model and ii) modelling with recharge estimated using SWB method. Also, the influence of riverbed conductance on river-aquifer interaction process was assessed by incorporating different riverbed conductance (calculated using K_{eff} values of different soil combinations considered in the sandbox experiments) in the groundwater modelling. The major observations in the study lead to the following conclusions.

First, monthly groundwater levels simulated using SWAT recharge-based groundwater flow modelling (case I) did not correlate with observed seasonal groundwater levels and also was not able to capture the wet and dry year effects. However, simulated groundwater levels in the groundwater modelling with SWB based recharge were observed to have a better agreement with observed groundwater levels and also found to be captured the effects of wet and dry years. In addition, the model was able to capture the effects of wet and dry years on the exchange process. Second, three different interaction zones were identified from upstream (Kosi barrage) to downstream (conferencing point with Ganga river) in the study reach. It is observed that the river always loses water to the aquifer (as influent) in Zone I (80 km from upstream) and the river mostly gains water from the aquifer (as effluent) in Zone III (40 km above downstream). However, in the middle reaches (Zone II), the river has a combination of both influent and effluent natures. Third, at the upstream, the river always loses water to the aquifer and mostly gains water from the aquifer at downstream during wet and dry years which indicates significant influence of topography on river-aquifer exchange flux. Fourth, the results obtained in case II modelling with different riverbed conductance values of different scenarios (soil combinations) indicate that the river-aquifer interactions are the most sensitive to the riverbed conductance.

From this study, it can be concluded that use of satellite remote sensing inputs (recharge and evapotranspiration used in SWB method for estimating recharge) and estimated river bed conductance based on laboratory sandbox experiments improved the assessment and understanding river-aquifer interaction process in an alluvial River basin.

6.2 Limitations of the Study

Although, this study helps to improve the understanding and assessment of river-aquifer interaction, there are few limitations in the study to be addressed.

- In SWB method, SWAT simulated discharge is used to estimate the monthly groundwater recharge due to non-availability of observed discharge data. The

presence of real observed discharge data can provide better estimation of recharge values.

- In the sandbox experiments, representative soil samples of Kosi basin are used to estimate the fluid flux and riverbed conductivity. Collection and use of real field soil samples can improve the experimental results.
- In this study, hydraulic conductivity of aquifer and riverbed are obtained from literature. Real field data of these parameters will improve the modelling results.

6.3 FUTURE SCOPE

The present research has provided better insights to understand the river-aquifer interaction process in an alluvial River. However, there are many other important aspects to be looked in detail for process-form based understanding of this river basin. The present work can be extended further with prime focus to following aspects

- A detailed study in the hilly region of Kosi basin needs to be considered for better-understanding river-aquifer interactions throughout the basin.
- In order to validate the river-aquifer interactions simulated using groundwater model, a simple and cost-effective field investigations need to be carried out by measuring thermal profiles inside the riverbeds.
- Assessment of river-aquifer interactions with groundwater model can be further improved by incorporating high-resolution evapotranspiration and groundwater pumping data into the model.
- Groundwater model performance can be further validated with GRACE (Gravity Recovery Climate Experiment) data.
- Long-term simulations of groundwater model with climate change data for future scenarios can be studied in detail for groundwater sustainable management.
- Groundwater model performance can be improved further by considering heterogeneity in the aquifer parameters.
- For detailed understanding of the input parameters that govern aquifer/groundwater recharging process, models such as DRASTIC can be used.
- The results of the MODFLOW can be compared with other groundwater models such as DRAINMOD.

6.4 DECISION SUPPORT SYSTEM OF THE STUDY

Around the globe, many countries are facing severe water crisis and this critical problem can be addressed with proper sustainable water management. For effective management of water resources, the watershed mangers have to focus on each and every component of the hydrological cycle. However, all the site scale observations of components are not available in many developing countries. In order to address this, the present study focused on estimation of few important components of hydrological cycle (i.e. surface runoff, groundwater recharge and the river-aquifer exchange) in an ungauged, alluvial river basin using suitable methods and available data.

Assessment of river-aquifer interaction is the main objective of this study in an agriculturally dominated basin of Kosi river, India. In order to obtain spatio-temporal variations of this component, a numerical modelling technique is proposed. However to use this sophisticated model, accurate input parameters are required. Groundwater recharge, evapotranspiration, riverbed and aquifer characteristics are major input parameters to the model. For this basin, high resolution remote sensing based AET is available to represent the irrigation dominated basin properties. But, monthly ground recharge and riverbed hydraulic conductivity values of this basin are not available at field scale which are highly sensitive parameters of the model. Hence, this study is aimed to estimate these parameters initially using hydrological model, remote sensing inputs (to estimate recharge) and heat as natural tracer (to estimate riverbed hydraulic conductivity). Estimated quantities of these two components along with AET and aquifer properties improved and helped to assess river-aquifer interaction at reach scale. This similar approach used in the study can be followed for similar type of ungauged river basins to manage water resources.

REFERENCES

Agarwal, A., Babel, M.S., Maskey, S., Shrestha, S., Kawasaki, A. and Tripathi, N.K., 2016. Analysis of temperature projections in the Koshi River Basin, Nepal. International Journal of Climatology, 36(1), pp.266-279.

Aladaileh, H., Al Qinna, M., Karoly, B., Al-Karablieh, E. and Rakonczai, J., 2019. An Investigation into the Spatial and Temporal Variability of the Meteorological Drought in Jordan. Climate, 7(6), p.82.

Al-Bassam, A.M. and Al-Rumikhani, Y.A., 2003. Integrated hydrochemical method of water quality assessment for irrigation in arid areas: application to the Jilh aquifer, Saudi Arabia. Journal of African Earth Sciences, 36(4), pp.345-356.

Al-Dousari, A., Milewski, A., Din, S.U. and Ahmed, M., 2010. Remote sensing inputs to SWAT model for groundwater recharge estimates in Kuwait. Advances in Natural and Applied Sciences, 4(1), pp.71-77.

Ali, M.H., Mubarak, S., Islam, M.A. and Biswas, P., 2017. Comparative evaluation of various empirical methods for estimating groundwater recharge. Archives of Current Research International, pp.1-10.

Allen, R.G., Pereira, L.S., Raes, D. and Smith, M., 1998. Crop evapotranspiration-Guidelines for computing crop water requirements-FAO Irrigation and drainage paper 56. Fao, Rome, 300(9), p.D05109.

Almas, A.A. and Scholz, M., 2006. Agriculture and water resources crisis in Yemen: Need for sustainable agriculture. Journal of Sustainable Agriculture, 28(3), pp.55-75.

Amitha, K., 2000. Estimation of natural ground water recharge. LAKE 2000: National Conference, Indian Institute of Science, Bangalore, November, pp. 27-29.

Anand, J., Gosain, A.K. and Khosa, R., 2018. Prediction of land use changes based on Land Change Modeler and attribution of changes in the water balance of Ganga basin to land use change using the SWAT model. Science of the total environment, 644, pp.503-519.

Andersen, J., Dybkjaer, G., Jensen, K.H., Refsgaard, J.C. and Rasmussen, K., 2002. Use of remotely sensed precipitation and leaf area index in a distributed hydrological model. Journal of Hydrology, 264(1-4), pp.34-50.

Anderson, M.P., 2005. Heat as a ground water tracer. Groundwater, 43(6), pp.951-968.

Anibas, C., Buis, K., Verhoeven, R., Meire, P. and Batelaan, O., 2011. A simple thermal mapping method for seasonal spatial patterns of groundwater–surface water interaction. Journal of Hydrology, 397(1-2), pp.93-104.

Anibas, C., Fleckenstein, J.H., Volze, N., Buis, K., Verhoeven, R., Meire, P. and Batelaan, O., 2009. Transient or steady- state? Using vertical temperature profiles to quantify groundwater–surface water exchange. Hydrological Processes: An International Journal, 23(15), pp.2165-2177.

Anibas, C., Schneidewind, U., Vandersteen, G., Joris, I., Seuntjens, P. and Batelaan, O., 2016. From streambed temperature measurements to spatial- temporal flux quantification: using the LPML method to study groundwater–surface water interaction. Hydrological Processes, 30(2), pp.203-216.

Arnold, J.G., Srinivasan, R., Muttiah, R.S. and Williams, J.R., 1998. Large area hydrologic modeling and assessment part I: model development 1. JAWRA Journal of the American Water Resources Association, 34(1), pp.73-89.

Arnold, J.G., Muttiah, R.S., Srinivasan, R. and Allen, P.M., 2000. Regional estimation of base flow and groundwater recharge in the Upper Mississippi river basin. Journal of Hydrology, 227(1-4), pp.21-40.

Arriaga, M.A. and Leap, D.I., 2006. Using solver to determine vertical groundwater velocities by temperature variations, Purdue University, Indiana, USA. Hydrogeology Journal, 14(1-2), pp.253-263.

Awan, U.K. and Ismaeel, A., 2014. A new technique to map groundwater recharge in irrigated areas using a SWAT model under changing climate. Journal of Hydrology, 519, pp.1368-1382.

Baalousha, H.M., 2012. Characterisation of groundwater–surface water interaction using field measurements and numerical modelling: a case study from the Ruataniwha Basin, Hawke's Bay, New Zealand. Applied Water Science, 2(2), pp.109-118.

Bailey, R.T., Wible, T.C., Arabi, M., Records, R.M. and Ditty, J., 2016. Assessing regional- scale spatio-temporal patterns of groundwater–surface water interactions using a coupled SWAT- MODFLOW model. Hydrological processes, 30(23), pp.4420-4433.

Bajjali, W., 2006. Recharge mechanism and hydrochemistry evaluation of groundwater in the Nuaimeh area, Jordan, using environmental isotope techniques. Hydrogeology Journal, 14(1-2), pp.180-191.

Banks, E.W., Simmons, C.T., Love, A.J. and Shand, P., 2011. Assessing spatial and temporal connectivity between surface water and groundwater in a regional catchment: Implications for regional scale water quantity and quality. Journal of Hydrology, 404(1-2), pp.30-49.

Baker, T.J. and Miller, S.N., 2013. Using the Soil and Water Assessment Tool (SWAT) to assess land use impact on water resources in an East African watershed. Journal of hydrology, 486, pp.100-111.

Barlow, P.M. and Harbaugh, A.W., 2006. USGS directions in MODFLOW development. Groundwater, 44(6), pp.771-774.

Bartsch, S., Frei, S., Ruidisch, M., Shope, C.L., Peiffer, S., Kim, B. and Fleckenstein, J.H., 2014. River-aquifer exchange fluxes under monsoonal climate conditions. Journal of hydrology, 509, pp.601-614.

Baskaran, S., Brodie, R.S., Ransley, T. and Baker, P., 2009. Time-series measurements of stream and sediment temperature for understanding river–groundwater interactions: Border Rivers and Lower Richmond catchments, Australia. Australian Journal of Earth Sciences, 56(1), pp.21-30.

Batelaan, O., Wang, Z.M. and De Smedt, F., 1996. An adaptive GIS toolbox for hydrological modelling. IAHS Publications-Series of Proceedings and Reports-Intern Assoc Hydrological Sciences, 235, pp.3-10.

Baxter, C., Hauer, F.R. and Woessner, W.W., 2003. Measuring groundwater–stream water exchange: new techniques for installing minipiezometers and estimating hydraulic conductivity. Transactions of the American Fisheries Society, 132(3), pp.493-502.

Bazuhair, A.S. and Wood, W.W., 1996. Chloride mass-balance method for estimating ground water recharge in arid areas: examples from western Saudi Arabia. Journal of Hydrology, 186(1-4), pp.153-159.

Bhat, T.A., 2014. An analysis of demand and supply of water in India. Journal of Environment and Earth Science, 4(11), pp.67-72.

Bhattacharya, B.K., Mallick, K., Patel, N.K. and Parihar, J.S., 2010. Regional clear sky evapotranspiration over agricultural land using remote sensing data from Indian geostationary meteorological satellite. Journal of Hydrology, 387(1-2), pp.65-80.

Bhuiyan, C., Singh, R.P. and Flügel, W.A., 2009. Modelling of ground water recharge-potential in the hard-rock Aravalli terrain, India: a GIS approach. Environmental Earth Sciences, 59(4), p.929.

Biswas, S.P., 1996. Global water scarcity: issues and implications with special reference to India. Internationale Vereinigung für theoretische und angewandte Limnologie: Verhandlungen, 26(1), pp.115-121.

Boano, F., Harvey, J.W., Marion, A., Packman, A.I., Revelli, R., Ridolfi, L. and Wörman, A., 2014. Hyporheic flow and transport processes: Mechanisms, models, and biogeochemical implications. Reviews of Geophysics, 52(4), pp.603-679.

Bravo, H.R., Jiang, F. and Hunt, R.J., 2002. Using groundwater temperature data to constrain parameter estimation in a groundwater flow model of a wetland system. Water Resources Research, 38(8), pp.28-1.

Bredehoeft, J.D. and Papaopulos, I.S., 1965. Rates of vertical groundwater movement estimated from the Earth's thermal profile. Water Resources Research, 1(2), pp.325-328.

Brodie, R.S., Baskaran, S., Ransley, T. and Spring, J., 2009. Seepage meter: progressing a simple method of directly measuring water flow between surface water and groundwater systems. Australian Journal of Earth Sciences, 56(1), pp.3-11.

Brunner, P., Simmons, C.T., Cook, P.G. and Therrien, R., 2010. Modeling surface water- groundwater interaction with MODFLOW: some considerations. Groundwater, 48(2), pp.174-180.

Brunner, P., Therrien, R., Renard, P., Simmons, C.T. and Franssen, H.J.H., 2017. Advances in understanding river- groundwater interactions. Reviews of Geophysics, 55(3), pp.818-854.

Cai, J., Taute, T., Hamann, E. and Schneider, M., 2015. An Integrated Laboratory Method to Measure and Verify Directional Hydraulic Conductivity in Fine- to- Medium Sandy Sediments. Groundwater, 53(1), pp.140-150.

Carter, A., 2000. How pesticides get into water-and proposed reduction measures. Pesticide Outlook, 11(4), pp.149-156.

Chandra, R., Jain, SK., Singh, AK., 2018. Assessment of ground water resources for irrigation in Nalanda district of South Bihar, India. Journal of current microbiology and applied sciences, 7(2), pp 1223-1232.

Chapman, T.G. and Malone, R.W., 2002. Comparison of models for estimation of groundwater recharge, using data from a deep weighing lysimeter. Mathematics and Computers in Simulation, 59(1-3), pp.3-17.

Chaturvedi, R.S., 1973. A note on the investigation of ground water resources in western districts of Uttar Pradesh. Annual Report, UP Irrigation Research Institute, 1973, pp.86-122.

Chembolu, V., Dubey, A.K., Gupta, P.K., Dutta, S. and Singh, R.P., 2019. Application of satellite altimetry in understanding river–wetland flow interactions of Kosi river. Journal of Earth System Science, 128(4), p.89.

Chen, N.S., Hu, G.S., Deng, W., Khanal, N., Zhu, Y.H. and Han, D., 2013. On the water hazards in the trans-boundary Kosi River basin. Natural Hazards and Earth System Sciences, 13(3), pp.795-808.

Chen, X., 2000. Measurement of streambed hydraulic conductivity and its anisotropy. Environmental Geology, 39(12), pp.1317-1324.

Chen, X., 2004. Streambed hydraulic conductivity for rivers in South- Central Nebraska 1. JAWRA Journal of the American Water Resources Association, 40(3), pp.561-573.

Chen, X., Zhang, Z.C., Zhang, X.N., Chen, Y.Q., Qian, M.K. and Peng, S.F., 2008. Estimation of groundwater recharge from precipitation and evapotranspiration by lysimeter measurement and soil moisture model. Journal of Hydrologic Engineering, 13(5), pp.333-340.

Cheng, C. and Chen, X., 2007. Evaluation of methods for determination of hydraulic properties in an aquifer–aquitard system hydrologically connected to a river. Hydrogeology Journal, 15(4), pp.669-678.

Cheong, J.Y., Hamm, S.Y., Kim, H.S., Ko, E.J., Yang, K. and Lee, J.H., 2008. Estimating hydraulic conductivity using grain-size analyses, aquifer tests, and numerical modeling in a riverside alluvial system in South Korea. Hydrogeology Journal, 16(6), p.1129.

Chitsazan, M., Faryabi, M. and Zarrasvandi, A.R., 2014. Evaluation of river–aquifer interaction in the north part of Dezful–Andimeshk district, SW of Iran. Arabian Journal of Geosciences, 8(9), pp.7177-7189.

Cho, J., Mostaghimi, S. and Kang, M.S., 2010. Development and application of a modeling approach for surface water and groundwater interaction. Agricultural water management, 97(1), pp.123-130.

Chung, I.M., Sophocleous, M.A., Mitiku, D.B. and Kim, N.W., 2016. Estimating groundwater recharge in the humid and semi-arid African regions. Geosciences Journal, 20(5), pp.731-744.

Constantz, J., 2008. Heat as a tracer to determine streambed water exchanges. Water Resources Research, 44(4).

Crosbie, R.S., Binning, P. and Kalma, J.D., 2005. A time series approach to inferring groundwater recharge using the water table fluctuation method. Water Resources Research, 41(1).

Crosbie, R.S., Peeters, L.J., Herron, N., McVicar, T.R. and Herr, A., 2017. Estimating groundwater recharge and its associated uncertainty: Use of regression kriging and the chloride mass balance method. Journal of Hydrology, 561, pp.1063-1080.

Darcy, H.P.G., 1856. Les Fontaines publiques de la ville de Dijon. Exposition et application des principes à suivre et des formules à employer dans les questions de distribution d'eau, etc. V. Dalamont.

Dawoud, M.A. and Ismail, S.S., 2013. Saturated and unsaturated River Nile/groundwater aquifer interaction systems in the Nile Valley, Egypt. Arabian journal of geosciences, 6(6), pp.2119-2130.

Delin, G.N., Healy, R.W., Lorenz, D.L. and Nimmo, J.R., 2007. Comparison of local-to regional-scale estimates of ground-water recharge in Minnesota, USA. Journal of Hydrology, 334(1-2), pp.231-249.

Derx, J., Blaschke, A.P. and Blöschl, G., 2010. Three-dimensional flow patterns at the river–aquifer interface—a case study at the Danube. Advances in Water Resources, 33(11), pp.1375-1387.

Dhungel, R. and Fiedler, F., 2016. Water balance to recharge calculation: Implications for watershed management using systems dynamics approach. Hydrology, 3(1), p.13.

Doble, R.C. and Crosbie, R.S., 2017. Current and emerging methods for catchment-scale modelling of recharge and evapotranspiration from shallow groundwater. Hydrogeology journal, 25(1), pp.3-23.

Doppler, T., Franssen, H.J.H., Kaiser, H.P., Kuhlman, U. and Stauffer, F., 2007. Field evidence of a dynamic leakage coefficient for modelling river–aquifer interactions. Journal of Hydrology, 347(1-2), pp.177-187.

Dripps, W.R. and Bradbury, K.R., 2007. A simple daily soil–water balance model for estimating the spatial and temporal distribution of groundwater recharge in temperate humid areas. Hydrogeology Journal, 15(3), pp.433-444.

Duque, C., Calvache, M.L. and Engesgaard, P., 2010. Investigating river–aquifer relations using water temperature in an anthropized environment (Motril-Salobreña aquifer). Journal of Hydrology, 381(1-2), pp.121-133.

Eikenberg, J., Tricca, A., Vezzu, G., Stille, P., Bajo, S. and Ruethi, M., 2001. 228Ra/226Ra/224Ra and 87Sr/86Sr isotope relationships for determining interactions between ground and river water in the upper Rhine valley. Journal of environmental radioactivity, 54(1), pp.133-162.

Eilers, V.H.M., Carter, R.C. and Rushton, K.R., 2007. A single layer soil water balance model for estimating deep drainage (potential recharge): An application to cropped land in semi-arid North-east Nigeria. Geoderma, 140(1-2), pp.119-131.

Engeler, I., Franssen, H.H., Müller, R. and Stauffer, F., 2011. The importance of coupled modelling of variably saturated groundwater flow-heat transport for assessing river–aquifer interactions. Journal of Hydrology, 397(3-4), pp.295-305.

Epting, J., Huggenberger, P., Radny, D., Hammes, F., Hollender, J., Page, R.M., Weber, S., Bänninger, D. and Auckenthaler, A., 2017. Spatiotemporal scales of river-groundwater interaction–The role of local interaction processes and regional groundwater regimes. Science of the total environment, 618, pp.1224-1243.

Essaid, H.I. and Caldwell, R.R., 2017. Evaluating the impact of irrigation on surface water–groundwater interaction and stream temperature in an agricultural watershed. Science of the total environment, 599, pp.581-596.

Evers, M., 2016. Integrative river basin management: challenges and methodologies within the German planning system. Environmental Earth Sciences, 75(14), p.1085.

Ferris, J.G., Knowles, D.B., Brown, R.H. and Stallman, R.W., 1962. Theory of aquifer tests Denver, Colorado: US Geological Survey, pp. 69-174.

Finch, J.W., 1998. Estimating direct groundwater recharge using a simple water balance model–sensitivity to land surface parameters. Journal of Hydrology, 211(1-4), pp.112-125.

Finch, J.W., 2001. Estimating change in direct groundwater recharge using a spatially distributed soil water balance model. Quarterly Journal of Engineering Geology and Hydrogeology, 34(1), pp.71-83.

Fleckenstein, J.H., Krause, S., Hannah, D.M. and Boano, F., 2010. Groundwater-surface water interactions: New methods and models to improve understanding of processes and dynamics. Advances in Water Resources, 33(11), pp.1291-1295.

Fleckenstein, J.H., Niswonger, R.G. and Fogg, G.E., 2006. River- aquifer interactions, geologic heterogeneity, and low- flow management. Groundwater, 44(6), pp.837-852.

Frohlich, K., Frohlich, W. and Wittenberg, H., 1994. Determination of groundwater recharge by baseflow separation: regional analysis in northeast China. IAHS Publications-Series of Proceedings and Reports-Intern Assoc Hydrological Sciences, 221, pp.69-76.

Furman, A., 2008. Modeling coupled surface–subsurface flow processes: A review. Vadose Zone Journal, 7(2), pp.741-756.

Gao, X., Wang, Y., Wu, P. and Guo, Q., 2010. Trace elements and environmental isotopes as tracers of surface water–groundwater interaction: a case study at Xin'an karst water system, Shanxi Province, Northern China. Environmental Earth Sciences, 59(6), p.1223.

Gaye, C.B. and Edmunds, W.M., 1996. Groundwater recharge estimation using chloride, stable isotopes and tritium profiles in the sands of northwestern Senegal. Environmental Geology, 27(3), pp.246-251.

Gebreyohannes, H.G., 2008. Groundwater recharge modelling a case study in the central Veluwe, The Netherlands. Dissertation, Wageningen University, The Netherlands.

Gleick, P.H., Ed., 1996. Water resources in Encyclopedia of Climate and Weather. Oxford University Press, ed. S.H. Shneider. (2), pp.817-823.

Gemitzi, A., Ajami, H. and Richnow, H.H., 2017. Developing empirical monthly groundwater recharge equations based on modeling and remote sensing data–Modeling future groundwater recharge to predict potential climate change impacts. Journal of Hydrology, 546, pp.1-13.

Gerhart, J.M., 1986. Ground- water recharge and its effects on nitrate concentration beneath a manured field site in Pennsylvania. Groundwater, 24(4), pp.483-489.

Goroshi, S., Pradhan, R., Singh, R.P., Singh, K.K. and Parihar, J.S., 2017. Trend analysis of evapotranspiration over India: Observed from long-term satellite measurements. Journal of Earth System Science, 126(8), p.113.

Groundwater Estimation Committee, 1997. Report of the Groundwater Resource Estimation methodology, Ministry of Water Resources, Govt. of India.

Gyamfi, C., Ndambuki, J.M., Anornu, G.K. and Kifanyi, G.E., 2017. Groundwater recharge modelling in a large scale basin: an example using the SWAT hydrologic model. Modeling Earth Systems and Environment, 3(4), pp.1361-1369.

Haldar, R., Singla, S., Singla, R., Rajeev, R. and Khosa, R., 2014. Hydrologic Modeling for the Gandak Basin Using SWAT with Sensitivity Considerations. International Journal of Earth Sciences and Engineering, 7(2), pp.448-455.

Halford, K.J. and Hanson, R.T., 2002. User guide for the drawdown-limited, multi-node well (MNW) package for the US Geological Survey's modular three-dimensional finite-difference ground-water flow model, versions MODFLOW-96 and MODFLOW-2000. US Department of the Interior, US Geological Survey, 2(293).

Halford, K.J. and Mayer, G.C., 2000. Problems associated with estimating ground water discharge and recharge from stream- discharge records. Groundwater, 38(3), pp.331-342.

Harbaugh, A.W., 2005. MODFLOW-2005, The US Geological Survey modular ground-water model: the ground-water flow process, US Department of the Interior, US Geological Survey, pp. 6-A16.

Harlen, W. and Holroyd, C., 1997. Primary teachers' understanding of concepts of science: Impact on confidence and teaching. International journal of science education, 19(1), pp.93-105.

Hatch, C.E., Fisher, A.T., Revenaugh, J.S., Constantz, J. and Ruehl, C., 2006. Quantifying surface water–groundwater interactions using time series analysis of streambed thermal records: Method development. Water Resources Research, 42(10), pp.1-14.

Healy, R.W. and Cook, P.G., 2002. Using groundwater levels to estimate recharge. Hydrogeology journal, 10(1), pp.91-109.

Hearne, G.A. and Dewey, J.D., 1988. Hydrologic analysis of the Rio Grande basin north of Embudo, New Mexico, Colorado and New Mexico (Vol. 86, No. 4113). Department of the Interior, US Geological Survey.

Heath, R.C., 1983. Basic ground-water hydrology: US Geological Survey Water-Supply Paper 2220, 84 p. 1984. Ground-water regions of the United States: US Geological Survey Water-Supply Paper, 2242, p.78.

Irvine, D.J., Cranswick, R.H., Simmons, C.T., Shanafield, M.A. and Lautz, L.K., 2015a. The effect of streambed heterogeneity on groundwater- surface water exchange fluxes inferred from temperature time series. Water Resources Research, 51(1), pp.198-212.

Irvine, D.J., Lautz, L.K., Briggs, M.A., Gordon, R.P. and McKenzie, J.M., 2015b. Experimental evaluation of the applicability of phase, amplitude, and combined methods to determine water flux and thermal diffusivity from temperature time series using VFLUX 2. Journal of Hydrology, 531, pp.728-737.

Isiorho, S.A. and Meyer, J.H., 1999. The effects of bag type and meter size on seepage meter measurements. Groundwater, 37(3), pp.411-413.

Islam, S., Singh, R.K. and Khan, R.A., 2015. Methods of Estimating Ground water Recharge. International Journal of Engineering Associates, 5(2), pp.6-13.

Ivkovic, K.M., 2009. A top–down approach to characterise aquifer–river interaction processes. Journal of Hydrology, 365(3-4), pp.145-155.

Izady, A., Davary, K., Alizadeh, A., Ziaei, A.N., Akhavan, S., Alipoor, A., Joodavi, A. and Brusseau, M.L., 2015. Groundwater conceptualization and modeling using distributed SWAT-based recharge for the semi-arid agricultural Neishaboor plain, Iran. Hydrogeology journal, 23(1), pp.47-68.

Jain, S.K., 2019. Water resources management in India–challenges and the way forward. Current Science, 117(4), pp.569-576.

Jassas, H. and Merkel, B., 2014. Estimating Groundwater Recharge in the Semiarid Al-Khazir Gomal Basin, North Iraq. Water, 6(8), pp.2467-2481.

Jiménez-Martínez, J., Skaggs, T.H., Van Genuchten, M.T. and Candela, L., 2009. A root zone modelling approach to estimating groundwater recharge from irrigated areas. Journal of Hydrology, 367(1-2), pp.138-149.

Johnson, A.N., Boer, B.R., Woessner, W.W., Stanford, J.A., Poole, G.C., Thomas, S.A. and O'Daniel, S.J., 2005. Evaluation of an inexpensive small- diameter temperature logger for documenting ground water–river interactions. Groundwater Monitoring & Remediation, 25(4), pp.68-74.

Kahil, M.T., Ward, F.A., Albiac, J., Eggleston, J. and Sanz, D., 2016. Hydro-economic modeling with aquifer–river interactions to guide sustainable basin management. Journal of Hydrology, 539, pp.510-524.

Kalbus, E., Reinstorf, F. and Schirmer, M., 2006. Measuring methods for groundwater? surface water interactions: a review. Hydrology and Earth System Sciences Discussions, 10(6), pp.873-887.

Kalbus, E., Schmidt, C., Molson, J.W., Reinstorf, F. and Schirmer, M., 2009. Influence of aquifer and streambed heterogeneity on the distribution of groundwater discharge. Hydrology and Earth System Sciences, 13(1), pp.69-77.

Kambhammettu, B.V.N.P., James, P., King, J.P. and Praveena, A., 2011. Evaluation of mountain-front recharges estimation techniques for Southern New Mexico basins. International Journal of Water Resources and Environmental Engineering, 3(3), pp.66-72.

Katz, B.G., Coplen, T.B., Bullen, T.D. and Davis, J.H., 1997. Use of chemical and isotopic tracers to characterize the interactions between ground water and surface water in mantled karst. Groundwater, 35(6), pp.1014-1028.

Kaur, T., Bhardwaj, R. and Arora, S., 2017. Assessment of groundwater quality for drinking and irrigation purposes using hydrochemical studies in Malwa region, southwestern part of Punjab, India. Applied Water Science, 7(6), pp.3301-3316.

Keery, J., Binley, A., Crook, N. and Smith, J.W., 2007. Temporal and spatial variability of groundwater–surface water fluxes: development and application of an analytical method using temperature time series. Journal of Hydrology, 336(1-2), pp.1-16.

Kendy, E., Gérard- Marchant, P., Todd Walter, M., Zhang, Y., Liu, C. and Steenhuis, T.S., 2003. A soil-water- balance approach to quantify groundwater recharge from irrigated cropland in the north China plain. Hydrological Processes, 17(10), pp.2011-2031.

Kendy, E. and Bredehoeft, J.D., 2006. Transient effects of groundwater pumping and surface-water-irrigation returns on streamflow. Water Resources Research, 42(8), pp. 1-11.

Khadri, S.F.R. and Moharir, K., 2015. Hydrogeology investigation and water level fluctuation in hard rock of the Man River Basin, Akola and Buldhana Districts, Maharashtra, India. American Journal of Geophysics, Geochemistry and Geosystems, 1(3), pp.92-99.

Kim, N.W., Chung, I.M., Won, Y.S. and Arnold, J.G., 2008. Development and application of the integrated SWAT–MODFLOW model. Journal of hydrology, 356(1-2), pp.1-16.

King, A.C., Raiber, M., Cox, M.E. and Cendón, D.I., 2017. Comparison of groundwater recharge estimation techniques in an alluvial aquifer system with an intermittent/ephemeral stream (Queensland, Australia). Hydrogeology Journal, 25(6), pp.1759-1777.

Koeniger, P., Gaj, M., Beyer, M. and Himmelsbach, T., 2016. Review on soil water isotope- based groundwater recharge estimations. Hydrological Processes, 30(16), pp.2817-2834.

Krause, S., Boano, F., Cuthbert, M.O., Fleckenstein, J.H. and Lewandowski, J., 2014. Understanding process dynamics at aquifer- surface water interfaces: An introduction to the special section on new modeling approaches and novel experimental technologies. Water Resources Research, 50(2), pp.1847-1855.

Krause, S., Bronstert, A. and Zehe, E., 2007. Groundwater–surface water interactions in a North German lowland floodplain–implications for the river discharge dynamics and riparian water balance. Journal of hydrology, 347(3-4), pp.404-417.

Kumar Pradhan, R., Srivastava, P.K., Maurya, S., Kumar Singh, S. and Patel, D.P., 2018. Integrated framework for soil and water conservation in Kosi River Basin. Geocarto International, pp.1-20.

Kumar, C.P. and Seethapathi, P.V., 2002. Assessment of natural groundwater recharge in upper ganga canal command area. Journal of Applied Hydrology, 15(4), pp.13-20.

Kumar, S.H. and Nagaraj, M.K., 2018. Assessment of Interactions between River and Aquifer in the Gowri-hole Sub-catchment. Journal of the Geological Society of India, 92(4), pp.435-440.

Kumar, U.S., Sharma, S. and Navada, S.V., 2008. Recent studies on surface water–groundwater relationships at hydro-projects in India using environmental isotopes. Hydrological Processes: An International Journal, 22(23), pp.4543-4553.

Landon, M.K., Rus, D.L. and Harvey, F.E., 2001. Comparison of instream methods for measuring hydraulic conductivity in sandy streambeds. Groundwater, 39(6), pp.870-885.

Lautz, L.K. and Siegel, D.I., 2006. Modeling surface and ground water mixing in the hyporheic zone using MODFLOW and MT3D. Advances in Water Resources, 29(11), pp.1618-1633.

Lautz, L.K., 2010. Impacts of nonideal field conditions on vertical water velocity estimates from streambed temperature time series. Water Resources Research, 46, pp.1-14.

Lee, C.H., Chen, W.P. and Lee, R.H., 2006. Estimation of groundwater recharge using water balance coupled with base-flow-record estimation and stable-base-flow analysis. Environmental Geology, 51(1), pp.73-82.

Lekula, M. and Lubczynski, M.W., 2019. Use of remote sensing and long-term in-situ time-series data in an integrated hydrological model of the Central Kalahari Basin, Southern Africa. Hydrogeology Journal, 27(5), pp.1541-1562.

Li, Y., Zhang, Q., Lu, J., Yao, J. and Tan, Z., 2018. Assessing surface water–groundwater interactions in a complex river-floodplain wetland-isolated lake system. River Research and Applications, 35(1), pp.25-36.

Lu, C., Chen, S., Zhang, Y., Su, X. and Chen, G., 2017. Heat tracing to determine spatial patterns of hyporheic exchange across a river transect. Hydrogeology Journal, 25(6), pp.1633-1646.

Lu, S., Molz, F.J., Fogg, G.E. and Castle, J.W., 2002. Combining stochastic facies and fractal models for representing natural heterogeneity. Hydrogeology Journal, 10(4), pp.475-482.

Lu, X., Jin, M., van Genuchten, M.T. and Wang, B., 2011. Groundwater recharge at five representative sites in the Hebei Plain, China. Groundwater, 49(2), pp.286-294.

Maheswaran, R., Khosa, R., Gosain, A.K., Lahari, S., Sinha, S.K., Chahar, B.R. and Dhanya, C.T., 2016. Regional scale groundwater modelling study for Ganga River basin. Journal of Hydrology, 541, pp.727-741.

Mallick, K., Bhattacharya, B.K., Chaurasia, S., Dutta, S., Nigam, R., Mukherjee, J., Banerjee, S., Kar, G., Rao, V.U.M., Gadgil, A.S. and Parihar, J.S., 2007. Evapotranspiration using MODIS data and limited ground observations over selected agroecosystems in India. International Journal of Remote Sensing, 28(10), pp.2091-2110.

Mallick, K., Bhattacharya, B.K., Rao, V.U.M., Reddy, D.R., Banerjee, S., Venkatesh, H., Pandey, V., Kar, G., Mukherjee, J., Vyas, S.P. and Gadgil, A.S., 2009. Latent heat flux estimation in clear sky days over Indian agroecosystems using noontime satellite remote sensing data. Agricultural and Forest Meteorology, 149(10), pp.1646-1665.

Manoj, S., Thirumurugan, M. and Elango, L., 2019. Hydrogeochemical modelling to understand the surface water–groundwater interaction around a proposed uranium mining site. Journal of Earth System Science, 128(3), p.49.

Martinez, J.L., Raiber, M. and Cox, M.E., 2015. Assessment of groundwater–surface water interaction using long-term hydrochemical data and isotope hydrology: Headwaters of the Condamine River, Southeast Queensland, Australia. Science of the Total Environment, 536, pp.499-516.

McCallum, A.M., Andersen, M.S., Rau, G.C. and Acworth, R.I., 2012. A 1- D analytical method for estimating surface water–groundwater interactions and effective thermal diffusivity using temperature time series. Water Resources Research, 48(11), pp.1-8.

McCallum, A.M., Andersen, M.S., Rau, G.C., Larsen, J.R. and Acworth, R.I., 2014. River- aquifer interactions in a semiarid environment investigated using point and reach measurements. Water Resources Research, 50(4), pp.2815-2829.

McDonald, M.C., 1994. MODFLOW-USGS three-dimensional finite-difference groundwater flow model. Reston, Virginia.

McDonald, M.G., and Harbaugh, A.W., 1988. A modular three-dimensionalfinite-difference ground-water flow model, U.S. Geological SurveyTechniques of Water-Resources Investigations, Book 6, Chap. A1.

McKee, T. B, N. J. Doeskin, and J. Kleist, 1995. Drought Monitoring with Multiple Time Scales. Proc. 9th Conf. on Applied Climatology, American Meteorological Society, Boston, Massachusetts, pp. 233-236.

McNally, R. and Tognetti, S., 2002. Tackling poverty and promoting sustainable development: Key lessons for integrated river basin management. WWF-UK.

Meerschaert, M.M., Dogan, M., Van Dam, R.L., Hyndman, D.W. and Benson, D.A., 2013. Hydraulic conductivity fields: Gaussian or not?. Water resources research, 49(8), pp.4730-4737.

Mileham, L., Taylor, R.G., Todd, M., Tindimugaya, C. and Thompson, J., 2009. The impact of climate change on groundwater recharge and runoff in a humid, equatorial catchment: sensitivity of projections to rainfall intensity. Hydrological sciences journal, 54(4), pp.727-738.

Miller, S.A., Johnson, G.S., Cosgrove, D.M. and Larson, R., 2003. Regional scale modeling of surface and ground water interaction in the Snake river basin1. JAWRA Journal of the American Water Resources Association, 39(3), pp.517-528.

Mohanty, S., Jha, M.K., Kumar, A. and James, B.K., 2010. Characterization of stream-aquifer system and dynamics of stream-aquifer interaction in kathajodi river basin, Orissa. J. Indian Water Resour. Soc. Vol, 30(3).

Moon, S.K., Woo, N.C. and Lee, K.S., 2004. Statistical analysis of hydrographs and water-table fluctuation to estimate groundwater recharge. Journal of Hydrology, 292(1-4), pp.198-209.

Moyer, J.W., Saporito, L.S. and Janke, R.R., 1996. Design, construction, and installation of an intact soil core lysimeter. Agronomy Journal, 88(2), pp.253-256.

Munz, M., Oswald, S.E. and Schmidt, C., 2011. Sand box experiments to evaluate the influence of subsurface temperature probe design on temperature based water flux calculation. Hydrology and Earth System Sciences, 15(11), pp.3495-3510.

Mutiti, S. and Levy, J., 2010. Using temperature modeling to investigate the temporal variability of riverbed hydraulic conductivity during storm events. Journal of Hydrology, 388(3-4), pp.321-334.

Naganna, S.R., Deka, P.C., Ch, S. and Hansen, W.F., 2017. Factors influencing streambed hydraulic conductivity and their implications on stream–aquifer interaction: a conceptual review. Environmental Science and Pollution Research, 24(32), pp.24765-24789.

Najmuddin, O., Rasul, G., Hussain, A., Molden, D., Wahid, S. and Debnath, B., 2018. Low Water Productivity for Rice in Bihar, India—A Critical Analysis. Water, 10(8), p.1082.

Neitsch, S.L., Arnold, J.G., Kiniry, J.R., Srinivasan, R. and Williams, J.R., 2002. Soil and Water Assessment Tool user's manual, version 2000, Grassland. Soil and Water Research Laboratory, Agricultural Research Service and Blackland Research Center, Texas Agricultural Experiment Station, Temple, Texas.

Neitsch, S.L., Arnold, J.G., Kiniry, J.R., Srinivasan, R. and Williams, J.R., 2004. Soil and water assessment tool input/output file documentation, version 2005. US Department of Agriculture-Agricultural Research Service, Grassland Soil and Water Research Laboratory, Temple, Texas.

Niswonger, R.G., 2003. Modeling heat as a tracer to estimate streambed seepage and hydraulic conductivity. Heat as a tool for studying the movement of ground water near streams, pp.81-89.

Oke, M.O., Martins, O., Idowu, O.A. and Aiyelokun, O., 2015. Comparative analysis of groundwater recharge estimation Value obtained using empirical methods in Ogun and Oshun river basins. Ife Journal of Science, 17(1), pp.53-63.

Olsen, D.A. and Young, R.G., 2009. Significance of river–aquifer interactions for reach-scale thermal patterns and trout growth potential in the Motueka River, New Zealand. Hydrogeology Journal, 17(1), pp.175-183.

Paces, J.B. and Wurster, F.C., 2014. Natural uranium and strontium isotope tracers of water sources and surface water–groundwater interactions in arid wetlands–Pahranagat Valley, Nevada, USA. Journal of hydrology, 517, pp.213-225.

Partington, D., Brunner, P., Simmons, C.T., Werner, A.D., Therrien, R., Maier, H.R. and Dandy, G.C., 2012. Evaluation of outputs from automated baseflow separation methods against simulated baseflow from a physically based, surface water-groundwater flow model. Journal of Hydrology, 458, pp.28-39.

Penman, H.L., 1948. Natural evaporation from open water, bare soil and grass. Proceedings of the Royal Society of London. Series A. Mathematical and Physical Sciences, 193(1032), pp.120-145.

Pérez-Martín, M.A., Estrela, T., Andreu, J. and Ferrer, J., 2014. Modeling water resources and river-aquifer interaction in the Júcar River Basin, Spain. Water resources management, 28(12), pp.4337-4358.

Pozdniakov, S.P., Wang, P. and Lekhov, M.V., 2016. A semi-analytical generalized Hvorslev formula for estimating riverbed hydraulic conductivity with an open-ended standpipe permeameter. Journal of Hydrology, 540, pp.736-743.

Pradhan, R.K., Srivastava, P.K., Maurya, S., Kumar Singh, S. and Patel, D.P., 2018. Integrated framework for soil and water conservation in Kosi River Basin. Geocarto International, pp.1-20.

Prasad, Y.S. and Rao, B.V., 2018. Groundwater depletion and groundwater balance studies of Kandivalasa river sub basin, Vizianagaram district, Andhra Pradesh, India. Groundwater for Sustainable Development, 6, pp.71-78.

Ragab, R., Finch, J. and Harding, R., 1997. Estimation of groundwater recharge to chalk and sandstone aquifers using simple soil models. Journal of Hydrology, 190(1-2), pp.19-41.

Rahman, M.M., Thompson, J.R. and Flower, R.J., 2016. An enhanced SWAT wetland module to quantify hydraulic interactions between riparian depressional wetlands, rivers and aquifers. Environmental Modelling & Software, 84, pp.263-289.

Rai, P.K., Chandel, R.S., Mishra, V.N. and Singh, P., 2018. Hydrological inferences through morphometric analysis of lower Kosi river basin of India for water resource management based on remote sensing data. Applied water science, 8(1), p.15.

Rai, S.N. and Singh, R.N., 1995. Two-dimensional modelling of water table fluctuation in response to localised transient recharge. Journal of Hydrology, 167(1-4), pp.167-174.

Rajbhandari, R., Shrestha, A.B., Nepal, S., Wahid, S. and Ren, G.Y., 2017. Extreme climate projections over the transboundary Koshi River Basin using a high resolution regional climate model. Advances in Climate Change Research, 8(3), pp.199-211.

Rangarajan, R., Mondal, N.C., Singh, V.S. and Singh, S.V., 2009. Estimation of natural recharge and its relation with aquifer parameters in and around Tuticorin town, Tamil Nadu, India. Current Science, pp.217-226.

Rassam, D.W., Pagendam, D.E. and Hunter, H.M., 2008. Conceptualisation and application of models for groundwater–surface water interactions and nitrate attenuation potential in riparian zones. Environmental Modelling & Software, 23(7), pp.859-875.

Ravazzani, G., Curti, D., Gattinoni, P., Della Valentina, S., Fiorucci, A. and Rosso, R., 2016. Assessing groundwater contribution to streamflow of a large alpine river with heat tracer methods and hydrological modelling. River Research and Applications, 32(5), pp.871-884.

Reddy, C.S., Rangaswamy, M. and Jha, C.S., 2008. Monitoring of spatio-temporal changes in part of Kosi River Basin, Bihar, India using remote sensing and geographical information system. Research Journal of Environmental Sciences, 2(1), pp.58-62.

Ren, J., Wang, X., Shen, Z., Zhao, J., Yang, J., Ye, M., Zhou, Y. and Wang, Z., 2018. Heat tracer test in a riparian zone: laboratory experiments and numerical modelling. Journal of Hydrology, 563, pp.560-575.

Rolls, R.J., Leigh, C. and Sheldon, F., 2012. Mechanistic effects of low-flow hydrology on riverine ecosystems: ecological principles and consequences of alteration. Freshwater Science, 31(4), pp.1163-1186.

Rolls, R.J. and Bond, N.R., 2017. Environmental and ecological effects of flow alteration in surface water ecosystems. Water for the Environment, pp. 65-82.

Rosenberry, D.O., 2000. Unsaturated- zone wedge beneath a large, natural lake. Water Resources Research, 36(12), pp.3401-3409.

Rosenberry, D.O., 2008. A seepage meter designed for use in flowing water. Journal of Hydrology, 359(1-2), pp.118-130.

Rukundo, E. and Doğan, A., 2019. Dominant Influencing Factors of Groundwater Recharge Spatial Patterns in Ergene River Catchment, Turkey. Water, 11(4), p.653.

Rushton, K., 2007. Representation in regional models of saturated river–aquifer interaction for gaining/losing rivers. Journal of Hydrology, 334(1-2), pp.262-281.

Rushton, K.R. and Ward, C., 1979. The estimation of groundwater recharge. Journal of Hydrology, 41(3-4), pp.345-361.

Sahoo, S. and Sahoo, B., 2019. A geomorphology- based integrated stream–aquifer interaction model for semi- gauged catchments. Hydrological Processes, 33(9), pp.1362-1377.

Sangrey, D.A., Harrop-Williams, K.O. and Klaiber, J.A., 1984. Predicting ground-water response to precipitation. Journal of geotechnical engineering, 110(7), pp.957-975.

Sanz, D., Castaño, S., Cassiraga, E., Sahuquillo, A., Gómez-Alday, J.J., Peña, S. and Calera, A., 2011. Modeling aquifer–river interactions under the influence of groundwater abstraction in the Mancha Oriental System (SE Spain). Hydrogeology journal, 19(2), pp.475-487.

Scanlon, B.R., Healy, R.W. and Cook, P.G., 2002. Choosing appropriate techniques for quantifying groundwater recharge. Hydrogeology journal, 10(1), pp.18-39.

Schmidt, C., Bayer-Raich, M. and Schirmer, M., 2006. Characterization of spatial heterogeneity of groundwater-stream water interactions using multiple depth streambed temperature measurements at the reach scale. Hydrology and Earth System Sciences Discussions, 3(4), pp.1419-1446.

Schmidt, C., Conant Jr, B., Bayer-Raich, M. and Schirmer, M., 2007. Evaluation and field-scale application of an analytical method to quantify groundwater discharge using mapped streambed temperatures. Journal of Hydrology, 347(3-4), pp.292-307.

Schornberg, C., Schmidt, C., Kalbus, E. and Fleckenstein, J.H., 2010. Simulating the effects of geologic heterogeneity and transient boundary conditions on streambed temperatures—Implications for temperature-based water flux calculations. Advances in Water Resources, 33(11), pp.1309-1319.

Semiromi, M.T. and Koch, M., 2019. Analysis of spatio-temporal variability of surface–groundwater interactions in the Gharehsoo river basin, Iran, using a coupled SWAT-MODFLOW model. Environmental earth sciences, 78(6), pp.201.

Shamsuddin, M.K.N., Sulaiman, W.N.A., Ramli, M.F. and Kusin, F.M., 2019. Vertical hydraulic conductivity of riverbank and hyporheic zone sediment at Muda River riverbank filtration site, Malaysia. Applied Water Science, 9(1), pp.1-22.

Sharma, M.L., 1986. Measurement and prediction of natural groundwater recharge—an overview. Journal of Hydrology (New Zealand), pp.49-56.

Shrestha, A.B., Bajracharya, S.R., Sharma, A.R., Duo, C. and Kulkarni, A., 2017. Observed trends and changes in daily temperature and precipitation extremes over the Koshi river basin 1975–2010. International Journal of Climatology, 37(2), pp.1066-1083.

Shrestha, M.L., 2000. Interannual variation of summer monsoon rainfall over Nepal and its relation to Southern Oscillation Index. Meteorology and Atmospheric Physics, 75(1-2), pp.21-28.

Sibanda, T., Nonner, J.C. and Uhlenbrook, S., 2009. Comparison of groundwater recharge estimation methods for the semi-arid Nyamandhlovu area, Zimbabwe. Hydrogeology Journal, 17(6), pp.1427-1441.

Siddiq, E. A. 2006. Field crops: Rice. In Handbook of Agriculture, Indian Council of Agricultural Research, New Delhi, pp. 817–844.

Simmers, I. 1988. Estimation of Natural Groundwater Recharge. NATO ASI Series C 222. Dordrecht, The Netherlands: Reidel.

Singh, V., Raj, C. and Chakraborty, B., 2018. River Aquifer Interaction in Lower Gandak Command Area in Bihar, India. In IOP Conference Series: Earth and Environmental Science, 150(1), pp. 1-8.

Sinha, R. and Friend, P.F., 1994. River systems and their sediment flux, Indo- Gangetic plains, Northern Bihar, India. Sedimentology, 41(4), pp.825-845.

Sinha, R., Gupta, A., Mishra, K., Tripathi, S., Nepal, S., Wahid, S.M. and Swarnkar, S., 2019. Basin-scale hydrology and sediment dynamics of the Kosi river in the Himalayan foreland. Journal of hydrology, 570, pp.156-166.

Sinha, R., Gupta, S. and Nepal, S., 2018. Groundwater dynamics in North Bihar plains. Current Science, 114(12), pp.2482-2493.

Sinha, R., Tandon, S.K., Gibling, M.R., Bhattacharjee, P.S. and Dasgupta, A.S., 2005. Late Quaternary geology and alluvial stratigraphy of the Ganga basin. Himalayan Geology, 26(1), pp.223-240.

Smith, J.W.N., Bonell, M., Gibert, J., McDowell, W.H., Sudicky, E.A., Turner, J.V. and Harris, R.C., 2008. Groundwater–surface water interactions, nutrient fluxes and ecological response in river corridors: Translating science into effective environmental management. Hydrological Processes: An International Journal, 22(1), pp.151-157.

Soľáková, T., De Michele, C. and Vezzoli, R., 2014. Comparison between parametric and nonparametric approaches for the calculation of two drought indices: SPI and SSI. Journal of Hydrologic Engineering, 19(9), p.04014010-11.

Sophocleous, M., 2002. Interactions between groundwater and surface water: the state of the science. Hydrogeology journal, 10(1), pp.52-67.

Srinivasan, R., Ramanarayanan, T.S., Arnold, J.G. and Bednarz, S.T., 1998. Large area hydrologic modeling and assessment part II: model application 1. Journal of the American Water Resources Association, 34(1), pp.91-101.

Stallman, R.W., 1965. Steady one- dimensional fluid flow in a semi- infinite porous medium with sinusoidal surface temperature. Journal of geophysical Research, 70(12), pp.2821-2827.

Stellato, L., Petrella, E., Terrasi, F., Belloni, P., Belli, M., Sansone, U. and Celico, F., 2008. Some limitations in using 222 Rn to assess river–groundwater interactions: the case of Castel di Sangro alluvial plain (central Italy). Hydrogeology journal, 16(4), pp.701-712.

Subyani, A.M., 2004. Use of chloride-mass balance and environmental isotopes for evaluation of groundwater recharge in the alluvial aquifer, Wadi Tharad, western Saudi Arabia. Environmental Geology, 46(6-7), pp.741-749.

Sun, H. and Cornish, P.S., 2005. Estimating shallow groundwater recharge in the headwaters of the Liverpool Plains using SWAT. Hydrological Processes: An International Journal, 19(3), pp.795-807.

Sun, X., Bernard- Jannin, L., Garneau, C., Volk, M., Arnold, J.G., Srinivasan, R., Sauvage, S. and Sánchez-Pérez, J.M., 2015. Improved simulation of river water and groundwater exchange in an alluvial plain using the SWAT model. Hydrological processes, 30(2), pp.187-202.

Suzuki, S., 1960. Percolation measurements based on heat flow through soil with special reference to paddy fields. Journal of Geophysical Research, 65(9), pp.2883-2885.

Swanson, T.E. and Cardenas, M.B., 2011. Ex-Stream: A MATLAB program for calculating fluid flux through sediment–water interfaces based on steady and transient temperature profiles. Computers & geosciences, 37(10), pp.1664-1669.

Szucs, P., Madarasz, T. and Civan, F., 2009. Remediating over-produced and contaminated aquifers by artificial recharge from surface waters. Environmental Modeling & Assessment, 14(4), pp.511-520.

Tang, Q., Kurtz, W., Schilling, O.S., Brunner, P., Vereecken, H. and Franssen, H.J.H., 2017. The influence of riverbed heterogeneity patterns on river-aquifer exchange fluxes under different connection regimes. Journal of hydrology, 554, pp.383-396.

Taniguchi, M., 1993. Evaluation of vertical groundwater fluxes and thermal properties of aquifers based on transient temperature- depth profiles. Water Resources Research, 29(7), pp.2021-2026.

Thornthwaite, C.W. and Mather, J.W., 1955. The water balance. Centerton, Drexel Institute of Technology, Laboratory of Climatology, 8(1), pp.1 104.

Thornthwaite, C.W., 1948. An approach toward a rational classification of climate. Geographical review, 38(1), pp.55-94.

Ting, C.S., Kerh, T. and Liao, C.J., 1998. Estimation of groundwater recharge using the chloride mass-balance method, Pingtung Plain, Taiwan. Hydrogeology Journal, 6(2), pp.282-292.

Tiwari, A.K., Lavy, M., Amanzio, G., De Maio, M., Singh, P.K. and Mahato, M.K., 2017. Identification of artificial groundwater recharging zone using a GIS-based fuzzy logic approach: a case study in a coal mine area of the Damodar Valley, India. Applied Water Science, 7(8), pp.4513-4524.

Touhami, I., Andreu, J.M., Chirino, E., Sánchez, J.R., Moutahir, H., Pulido- Bosch, A., Martínez- Santos, P. and Bellot, J., 2012. Recharge estimation of a small karstic aquifer in a semiarid Mediterranean region (southeastern Spain) using a hydrological model. Hydrological Processes, 27(2), pp.165-174.

Turcotte, D.L. and Schubert, G., 2002. Geodynamics. Cambridge university press.

Van Tonder, G.J. and Kirchner, J., 1990. Estimation of natural groundwater recharge in the Karoo aquifers of South Africa. Journal of Hydrology, 121(1-4), pp.395-419.

Varma, V.S., Shabtay, A., Yishay, M., Mizrahi, I., Shterzer, N., Freilich, S., Medina, S., Agmon, R. and Laor, Y., 2018. Diet supplementation with pomegranate peel extract altered odorants emission from fresh and incubated calves' feces. Frontiers in Sustainable Food Systems, 2, p.33.

Varni, M., Comas, R., Weinzettel, P. and Dietrich, S., 2013. Application of the water table fluctuation method to characterize groundwater recharge in the Pampa plain, Argentina. Hydrological Sciences Journal, 58(7), pp.1445-1455.

Vasiliev, O.F., 1987. System modelling of the interaction between surface and ground waters in problems of hydrology. Hydrological sciences journal, 32(3), pp.297-311.

Venetis, C., 1969. A study on the recession of unconfined acquifers. International Association of Scientific Hydrology. Bulletin, 14(4), pp.119-125.

Vrzel, J., Solomon, D.K., Blaženka, Ž. and Ogrinc, N., 2018. The study of the interactions between groundwater and Sava River water in the Ljubljansko polje aquifer system (Slovenia). Journal of Hydrology, 556, pp.384-396.

Wakode, H.B., Baier, K., Jha, R. and Azzam, R., 2018. Impact of urbanization on groundwater recharge and urban water balance for the city of Hyderabad, India. International Soil and Water Conservation Research, 6(1), pp.51-62.

Walker, D., Parkin, G., Schmitter, P., Gowing, J., Tilahun, S.A., Haile, A.T. and Yimam, A.Y., 2019. Insights From a Multi- Method Recharge Estimation Comparison Study. Groundwater, 57(2), pp.245-258.

Waltemeyer, S.D., 2001. Estimates of mountain-front streamflow available for potential recharge to the Tularosa Basin, New Mexico (Vol. 1, No. 4013). US Department of the Interior, US Geological Survey.

Ward, A.S., Payn, R.A., Gooseff, M.N., McGlynn, B.L., Bencala, K.E., Kelleher, C.A., Wondzell, S.M. and Wagener, T., 2013. Variations in surface water- ground water interactions along a headwater mountain stream: Comparisons between transient storage and water balance analyses. Water Resources Research, 49(6), pp.3359-3374.

Wen, J., Tang, C., Cao, Y., Li, X. and Chen, Q., 2019. Assessment of trace metals in an aquifer with river-groundwater interaction: The influence of colloidal redistribution and porous matrix change on the migration of metals. Chemosphere, 223, pp.588-598.

Werner, A.D., Gallagher, M.R. and Weeks, S.W., 2006. Regional-scale, fully coupled modelling of stream–aquifer interaction in a tropical catchment. Journal of Hydrology, 328(3-4), pp.497-510.

White, P.A., Hong, Y.S., Murray, D.L., Scott, D.M. and Thorpe, H.R., 2003. Evaluation of regional models of rainfall recharge to groundwater by comparison with lysimeter measurements, Canterbury, New Zealand. Journal of Hydrology (New Zealand), pp.39-64.

Winter, T.C., 1995. Recent advances in understanding the interaction of groundwater and surface water. Reviews of Geophysics, 33(S2), pp.985-994.

Winter, T.C., Harvey, J.W., Franke, O.L. and Alley, W.M., 1998. Ground water and surface water: a single resource. U.S. Geol. Surv. Circular 1139.

Wittenberg, H. and Sivapalan, M., 1999. Watershed groundwater balance estimation using streamflow recession analysis and baseflow separation. Journal of hydrology, 219(1-2), pp.20-33.

Wojnar, A. 2008. Investigating Riverbed Hydraulic Conductivity at Several Well Fields along the Great Miami River, Southwest Ohio. Thesis, Geology Department, Miami University, Oxford, OH, 35.

Wojnar, A.J., Mutiti, S. and Levy, J., 2013. Assessment of geophysical surveys as a tool to estimate riverbed hydraulic conductivity. Journal of hydrology, 482, pp.40-56.

Woodbury, A.D. and Smith, L., 1988. Simultaneous inversion of hydrogeologic and thermal data: 2. Incorporation of thermal data. Water Resources Research, 24(3), pp.356-372.

Workman, S.R., Serrano, S.E. and Liberty, K., 1997. Development and application of an analytical model of stream/aquifer interaction. Journal of Hydrology, 200(1-4), pp.149-163.

Xie, Y., Cook, P.G., Shanafield, M., Simmons, C.T. and Zheng, C., 2016. Uncertainty of natural tracer methods for quantifying river–aquifer interaction in a large river. Journal of hydrology, 535, pp.135-147.

Xu, W., Su, X., Dai, Z., Yang, F., Zhu, P. and Huang, Y., 2017. Multi-tracer investigation of river and groundwater interactions: a case study in Nalenggele River basin, northwest China. Hydrogeology Journal, 25(7), pp.2015-2029.

Yagbasan, O., 2016. Impacts of climate change on groundwater recharge in Küçük Menderes River Basin in Western Turkey. Geodinamica Acta, 28(3), pp.209-222.

Young, R.A. and Haveman, R.H., 1985. Economics of water resources: a survey. In Handbook of natural resource and energy economics (2), pp. 465-529.

Zhang, B., Song, X., Zhang, Y., Han, D., Tang, C., Yu, Y. and Ma, Y., 2012. Hydrochemical characteristics and water quality assessment of surface water and groundwater in Songnen plain, Northeast China. Water research, 46(8), pp.2737-2748.

Zhang, J., Song, J., Long, Y., Kong, F., Wang, L., Zhang, Y., Li, Q., Wang, Y. and Hui, Y., 2018. Seasonal variability of hyporheic water exchange of the Weihe River in Shaanxi Province, China. Ecological Indicators, 92, pp.278-287.

Zhang, L., Dawes, W.R., Hatton, T.J., Reece, P.H., Beale, G.T.H. and Packer, I., 1999. Estimation of soil moisture and groundwater recharge using the TOPOG_IRM model. Water Resources Research, 35(1), pp.149-161.

Zhao, D., Wang, G., Liao, F., Yang, N., Jiang, W., Guo, L., Liu, C. and Shi, Z., 2018. Groundwater-surface water interactions derived by hydrochemical and isotopic (222Rn, deuterium, oxygen-18) tracers in the Nomhon area, Qaidam Basin, NW China. Journal of hydrology, 565, pp.650-661.

Zhu, M., Wang, S., Kong, X., Zheng, W., Feng, W., Zhang, X., Yuan, R., Song, X. and Sprenger, M., 2019. Interaction of Surface Water and Groundwater Influenced by Groundwater Over-Extraction, Waste Water Discharge and Water Transfer in Xiong'an New Area, China. Water, 11(3), p.539.

WEB REFERENCES

APHORDITE Rainfall Data (Accessed on October, 2018)

http://www.chikyu.ac.jp/precip/english/downloads.html

Princeton University Global Forcing (PGF) Temperature and Weather Data (Accessed October, 2018)

http://hydrology.princeton.edu/data.pgf.php

Landuse/landcover Data (for SWAT modelling) (Accessed August, 2015)

https://modis.gsfc.nasa.gov/data/dataprod/mod12.php

NBSS & LUP Soil Data (n.d) (no date)

http://gisserver.civil.iitd.ac.in/grbmp/

Topography SRTM Data (Accessed November, 2014)

http://srtm.csi.cgiar.org/srtmdata/

CWC Discharge Data ((n.d) (no date)

http://www.cwc.gov.in/get-hydrological-data

Observed Groundwater levels Data (Accessed May, 2017)

http://www.india-wris.nrsc.gov.in/GWLevelApp.html?UType=R2VuZXJhbA==?UName=

GLDAS Soil Moisture Data (Accessed on February, 2018)

https://disc.gsfc.nasa.gov/datasets/GLDAS_VIC10_M_V001/summary?keywords=GLDAS

NOAA Evapotranspiration Data (n.d) (no date)

ftp://disc1.gsfc.nasa.gov/data/avhrr/global_8 km/

MODIS Evapotranspiration Data (n.d) (no date)

https://modis.gsfc.nasa.gov/data/dataprod/mod16.php

Decdal Landue/landcover Data (for LULC Change Analysis) (Accessed on March, 2017)

https://daac.ornl.gov/VEGETATION/guides/Decadal_LULC_India.html

APPENDIX A

A.1 SEMI-DISTRIBUTED HYDROLOGICAL MODELLING (SWAT)

SWAT is river based, or watershed, scale model and developed to predict the impact of land management practices on water, sediment, and agricultural chemical yields in large, complex watersheds with varying soils, land use, and management conditions over a long period of time. The model is physically based and computationally efficient.

A.1.1 Water Balance Equation

The hydrological cycle simulated in SWAT model uses the following water balance equation.

$$SW_t = SW_0 + \Sigma (R_i - Q_i - Et_i - P_i - QR_i) \qquad (A.1)$$

Where, SW_t = the soil water content (mm)

SW_0 = the soil water content available for plants uptake, defined as the initial soil water content minus the permanent wilting point water content (mm)

t= time in days

R_i= amount of precipitation (mm)

Q_i =amount of surface runoff (mm)

Et_i= amount of evaporation (mm)

P_i = amount of percolation (mm)

QR_i= amount of return flow (mm)

A.1.2 SCS Runoff Equation

The SCS runoff equation is an empirical equation model. The model was developed for providing a consistent basis to estimate the amounts of runoff under varying land use and soil types.

The SCS curve number equation is (SCS 1972)

$$Q_{surf} = \frac{R_{day} - I_a^{\,2}}{R_{day} - I_a + S} \qquad (A.2)$$

Where, Q_{surf} = Runoff depth (mm)

R_{day} = Rainfall (mm)

S = Maximum retention after runoff begins (mm)

I_a = Initial abstraction

The initial abstraction includes water captured by vegetation, depression storage, evaporation, and infiltration. For any P, this abstraction must be satisfied before any runoff is possible. The universal default for the initial abstraction is given by the equation:

$$I_a = 0.2\ S \qquad (A.3)$$

The ratio, 0.2, is rarely, if ever, modified.

The potential maximum retention after runoff begins, S, is related to the soil and land use/vegetative cover characteristics of the watershed by the equation:

$$S = 28.4\left(\frac{100}{CN} - 10\right) \qquad (A.3)$$

Where the runoff curve number is developed by coincidental tabulation of soil/land use extents in the weighted runoff curve number parameter, CN.

A.1.3 Development of SWAT Model

In order to simulate monthly discharge and groundwater recharge at sub-basin scale, SWAT modelling was through the ArcSWAT interface (Version, 2012: 10_1.4) for the period 1970-2010. For this purpose, global weather data along with geospatial data are used to build up the model (Table 3.1). Whereas, the default watershed conservation practice data like, channel input, reservoir input, manning's n used in the model are mentioned in Neitsch et al. [2004]. The model divided the watershed into seventeen sub-basins to represent the spatial heterogeneity. Further, these sub-basin are discretized into hydrologic response units (HRU). SWAT model works at this HRU level to compute all the water balance components. Using SCS curve number technique, surface runoff was simulated and this simulated discharge was calibrated and validated with observed CWC discharge data. While, monthly groundwater recharge is obtained using this simulated SWAT model.

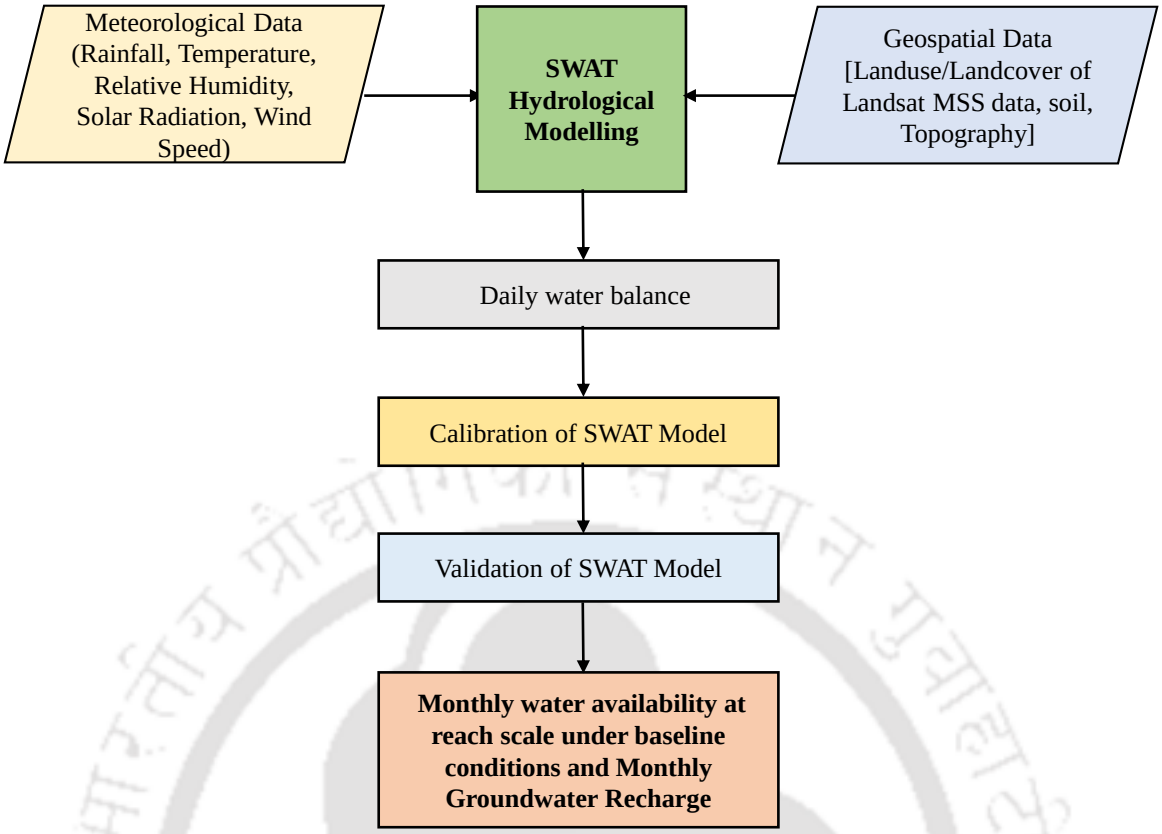

Figure A.1: Methodology of SWAT model

A.2 Non-Parametric SPI Index

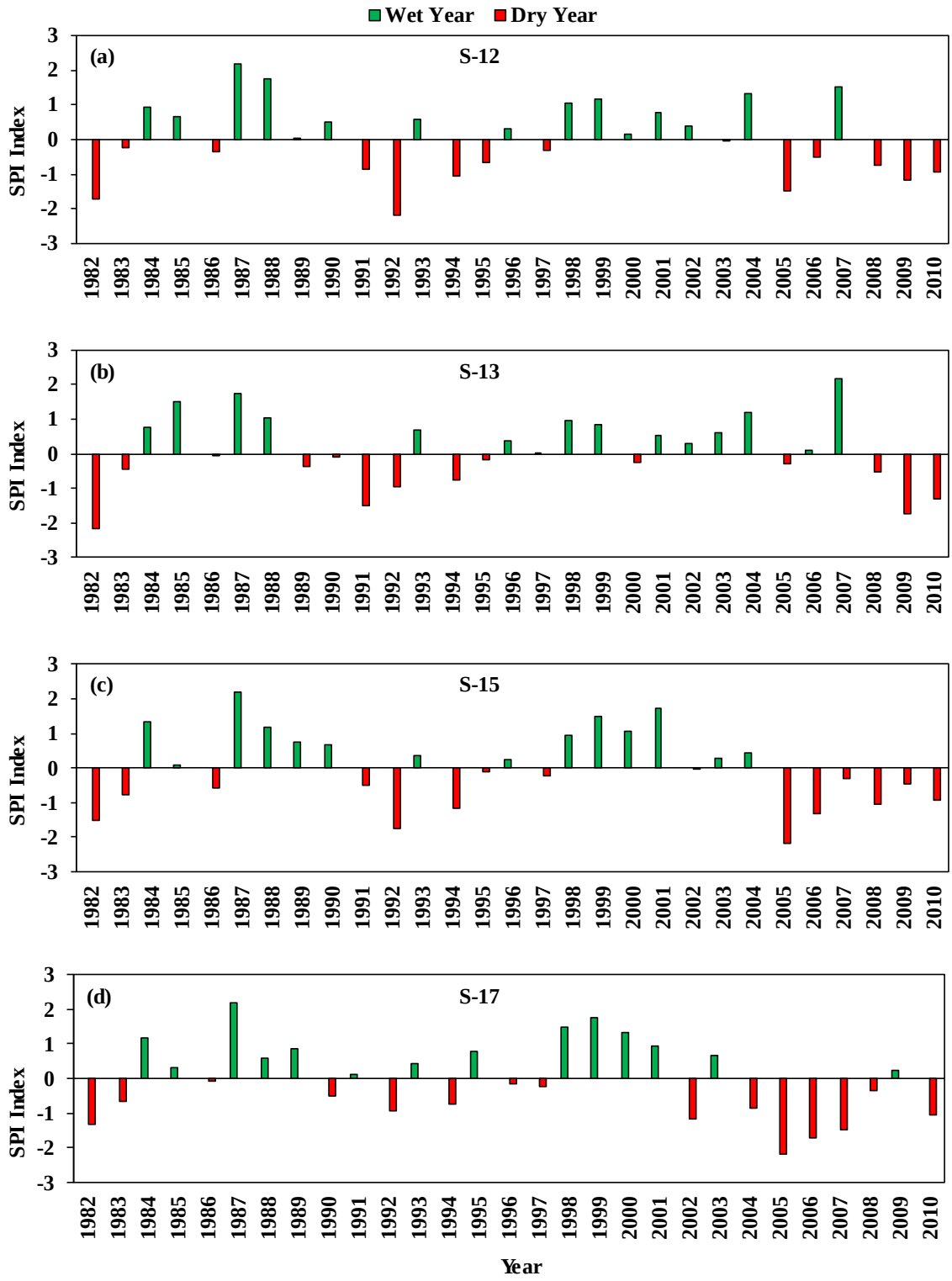

Figure A.2: 12-month non-parametric SPI index from 1982-2010 in (a) S-12 (b) S-13 (c) S-15 (d) S-17

APPENDIX B

B.1 Effective Hydraulic Conductivity of Soil Strata

Effective hydraulic conductivity (K_{eff}) of stratified soils can be estimated using the concept of flow orthogonal to plane of stratification as

$$K_{eff} = H\left[\sum_{i=1}^{n}\left(H_i / k_i\right)\right]^{-1} \quad (4.11)$$

where

K_{eff} - Effective Hydraulic Conductivity of soil strata (m/day)

H – Thickness of soil strata (m)

H_i – Thickness of layer i (m)

k_i – hydraulic conductivity of layer I (m/day)

B.2 River and groundwater temperature variation

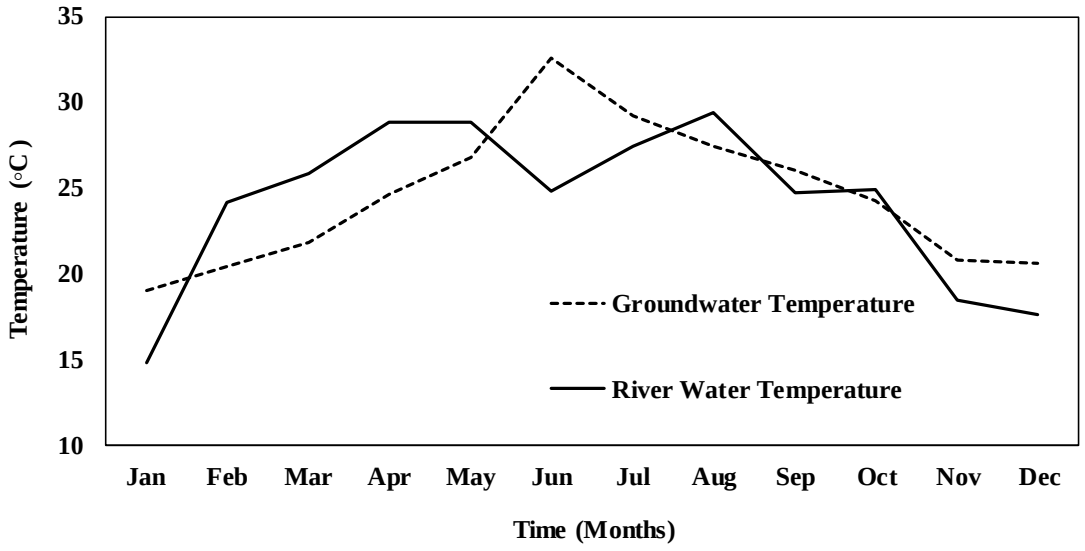

Figure B.1: Kosi river water temperature (2003) and groundwater temperature variations

B.3 Particle distribution Curve

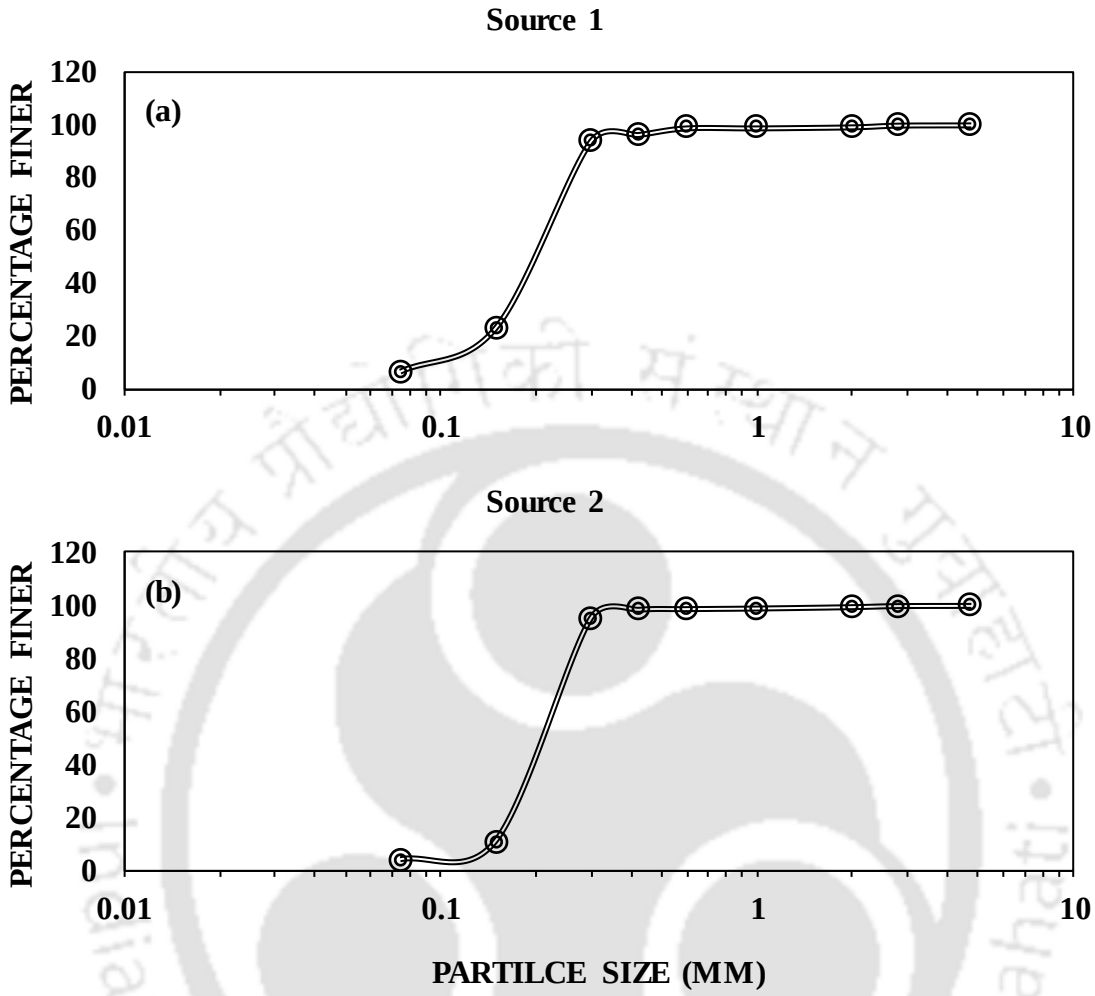

Figure B.2: Particle size distribution curve of (a) Source 1 (b) Source 2

Table B.1: Soil physical properties

Source	D50	C_u	C_c
Source 1	0.20	2.51	1.39
Source 2	0.22	1.59	1.01

B.4 Assumptions

- Fluid flow is parallel to z-axis and along z-axis, the fluid velocity is assumed to be steady and uniform,
- With respect to space and time, the heat characteristics of fluid and medium are assumed to be constant.
- All the components of fluid and heat flow occur along only z-axis.

APPENDIX C

C.1 Fence Diagram of Bihar, India

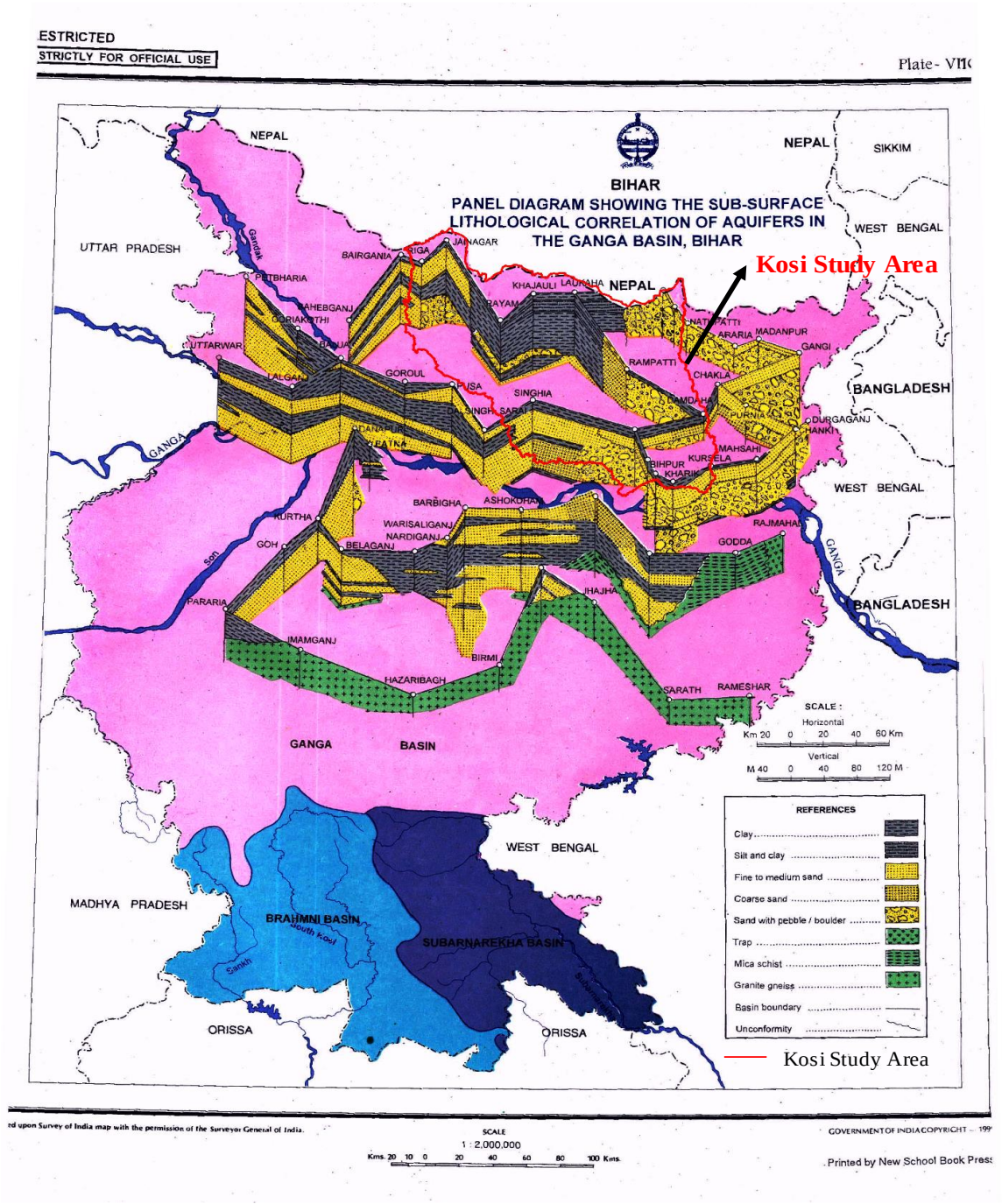

Figure C.1: Fence Diagram of Bihar state include study area

APPENDIX D

PUBLICATIONS

A.1 UNDER PREPARATION

- Satish L.N.V., Dutta, S., Kartha S.A. Estimation of Groundwater Recharge and Extractions using Satellite Based Evapotranspiration Data in Kosi River Basin (To be Submitted)
- Satish L.N.V., Dutta, S., Kartha S.A. Estimation of Fluid Flux through Sediment - Water Interface using Heat as Tracer based on Laboratory Experiments. (Under Preparation)
- Satish L.N.V., Dutta, S., Kartha S.A. River-Aquifer interactions in Kosi river basin, India. (Under Preparation)

A.2 CONFERENCES

- Satish L.N.V., Dutta, S., Kartha S.A. (2017). Effects of Landuse/landcover Changes on Surface Water and Groundwater Interactions in Kosi River Basin, India. International Conference of 14th Annual meeting of Aisa Oceania Geosciences Society, Singapore, 6-11, August, 2017.
- Satish L.N.V., Dutta, S., Kartha S.A. (2018). Surface Water and Groundwater Interactions in Kosi River Basin using Surface and Subsurface Hydrological Modelling. International Conference on SWAT 2018, Indian Institute of Technology Madras, 10-12 Janurary, 2018.
- Satish L.N.V., Dutta, S., Kartha S.A. (2019). Groundwater recharge estimation with remote sensing inputs in Kosi basin. National symposium on Innovation in Geospatial Technology for Sustainable Development with special emphasis on NER, Shillong, 20-22, November, 2019.